NOTICE

The quality of this microform is heavily dependent upon the quality of the original thesis submitted for microfilming. Every effort has been made to ensure the highest quality of reproduction possible.

If pages are missing, contact the university which granted the degree.

Some pages may have indistinct print especially if the original pages were typed with a poor typewriter ribbon or if the university sent us an inferior photocopy.

Reproduction in full or in part of this microform is governed by the Canadian Copyright Act, R.S.C. 1970, c. C-30, and subsequent amendments.

AVIS

La qualité de cette microforme dépend grandement de la qualité de la thèse soumise au microfilmage. Nous avons tout fait pour assurer une qualité supérieure de reproduction.

S'il manque des pages, veuillez communiquer avec l'université qui a conféré le grade.

La qualité d'impression de certaines pages peut laisser à désirer, surtout si les pages originales ont été dactylographiées à l'aide d'un ruban usé ou si l'université nous a fait parvenir une photocopie de qualité inférieure.

La reproduction, même partielle, de cette microforme est soumise à la Loi canadienne sur le droit d'auteur, SRC 1970, c. C-30, et ses amendements subséquents.

^{31}P AND ^{2}H SOLID-STATE NUCLEAR MAGNETIC RESONANCE STUDIES OF THE HEADGROUP CONFORMATION OF PHOSPHONOLIPIDS IN BIOLOGICAL AND MODEL MEMBRANES

by

Marie-Rose Van Calsteren, M.Sc.

Thesis presented to the
School of Graduate Studies – University of Ottawa
in partial fulfillment of requirements for the degree of
Doctor of Philosophy

Ottawa, Ontario
May, 1990

ISBN 0-315-67997-2

Canada

UNIVERSITÉ D'OTTAWA
UNIVERSITY OF OTTAWA

ABSTRACT

Solid-state nuclear magnetic resonance (NMR) techniques were applied to the study of the phase behavior and to the determination of the headgroup conformation of phosphonolipids, both natural and synthetic. The results are compared with those for analogous phospholipids in biological and model membranes.

^{31}P NMR was used to characterize the phase behavior of phospho- and phosphonolipids present in polar and total lipid extracts of the protozoa *Tetrahymena thermophila*. The ^{31}P NMR spectra of aqueous dispersions of polar and total lipids consist in the partial superposition of two powder patterns, one for each phosphorus-containing lipid class. At low temperature, both lipid extracts give rise to lineshapes characteristic of the lamellar structure. Spectra of the polar lipids show that between 15 and 40°C, a broad, reversible transition from bilayer to hexagonal phase takes place. On the other hand, the phase behavior for total lipids is different: no hexagonal phase is formed, the lipids remain in the bilayer phase at a higher temperature, and a transition to an isotropic phase occurs between 35 and 40°C, which is not easily reversible. A large proportion of ethanolamine-containing lipids, both phosphate and phosphonate analogs, is responsible for the hexagonal phase formation observed with the polar lipids. When neutral lipids are present with the polar lipids, the bilayer is stabilized up to a higher temperature. One of the neutral lipid components, tetrahymanol, a pentacyclic triterpenoid, is believed to be responsible for this stabilization.

The absolute value of the ^{31}P NMR chemical shift anisotropy $\Delta\sigma$ is smaller for phosphonolipids than for phospholipids. The trace of the chemical shift tensor for phosphonolipids is smaller than that for phospholipids, reflecting the lower electron density around the phosphorus atom in the phosphonate. At 0°C, the values for the phosphonolipids are $\Delta\sigma = -31$ ppm and $\sigma_i = -20.1$ ppm, and for the phospholipids $\Delta\sigma = -48$ ppm and $\sigma_i = 1.2$ ppm. Without the knowledge of the complete chemical shielding tensor for the phosphonate moiety, it is impossible to determine the individual contributions of electronic, geometrical and motional factors on the difference in $\Delta\sigma$.

For this reason, the symmetric part of the ^{31}P NMR chemical shielding tensor was determined in a single crystal of 2-aminoethylphosphonic acid (AEP). The principal values, relative to 85% H_3PO_4 are $\sigma_{11} = -87.1$, $\sigma_{22} = -15.6$ and $\sigma_{33} = 47.5$ ppm. Four orientations of the chemical shielding tensor on the molecule are possible, but only one of them shows correlation with the bond directions. The two most shielded components of the tensor lie almost in the plane containing the two P=O bonds, with σ_{22} approximately bisecting the O–P–O angle and σ_{33} roughly along the O–O connecting vector, leaving the phosphorus relatively deshielded in the perpendicular σ_{11} direction. The results can be correlated with the electron density distribution around the phosphorus atom, as determined by the bonding pattern of the phosphonate.

Since ^{31}P NMR is not sufficient to completely determine the headgroup conformation of a phosphonolipid, deuterium was used as a probe for the higher part of the headgroup. The synthesis of deuterated 1,2-di-*O*-hexadecyl-*sn*-glycero-3-(2-aminoethyl)phosphonate specifically labelled in five positions of the headgroup, *i.e.* *sn*-1, *sn*-2 and *sn*-3 of the glycerol moiety and positions 1 and 2 of the headgroup, was carried out. The headgroup was prepared via the Arbuzov reaction

from triethyl phosphite and 1,2-dibromoethane (available fully deuterated), followed by hydrolysis of the diethyl ester to give 2-bromoethylphosphonic acid. Because of its molecular symmetry corresponding to two glycerol units linked tail to tail, D-mannitol was used as a precursor for the glycerol moiety. D-[1,1,6,6–$^2H_4$]Mannitol was obtained by reduction with NaB^2H_4 of the dilactone of D-mannaric acid, itself synthesized by oxidation of D-mannitol. Reduction of β-D-fructose with sodium borodeuteride gave D-[2–^{2}H]mannitol. The following steps were carried out for the preparation of 1,2-di-*O*-hexadecyl-*sn*-glycerol. D-Mannitol was converted to its 1,2:3,4:5,6-tri-*O*-isopropylidene derivative, which gave 3,4-*O*-isopropylidene-D-mannitol by selective hydrolysis. The ether chains were introduced at this stage by reaction with 1-hexadecyl methanesulfonate under strongly basic conditions, followed by hydrolysis of the isopropylidene protecting group. The resulting 1,2,5,6-tetra-*O*-hexadecyl-D-mannitol was split into two identical glyceraldehyde molecules with periodic acid. Reduction with $NaBH_4$ or NaB^2H_4 afforded the desired compound which, after esterification with 2-bromoethylphosphonic acid and amination with ammonia, gave the complete phosphonolipid.

Differential scanning calorimetry thermograms demonstrated that 1,2-di-*O*-hexadecyl-*sn*-glycero-3-(2-aminoethyl)phosphonate dispersed in excess buffer undergoes two endothermic transitions. The main transition from gel to liquid crystal is centered at 70.2°C, and the second transition at 84.5°C is attributed to the lamellar-to-hexagonal phase transition.

The principal components of the ^{31}P NMR chemical shielding tensor were measured on a powder of the synthetic phosphonolipid and found to be $\sigma_{11} = -94$, $\sigma_{22} = -27$ and $\sigma_{33} = 61$ ppm. The ^{31}P and ^{2}H NMR spectra were obtained as a function of temperature for 1,2-di-*O*-hexadecyl-*sn*-glycero-3-(2-aminoethyl)phosphonate and its analogs deuterated in positions 1 and 2 of the

headgroup and in position 3 of the glycerol moiety. Both techniques confirm the phase behavior determined previously. The absolute value of the ^{31}P NMR chemical shift anisotropy decreased slightly between 28 and 75°C, while above the bilayer-to-hexagonal phase transition temperature the magnitude of it dropped by a factor of two with a change of sign. In the gel phase, no ^{2}H NMR quadrupolar splittings could be measured because of a featureless lineshape; the splittings were more or less constant through the liquid crystalline phase and their value was halved in the hexagonal phase. These NMR spectral parameters, together with the full ^{31}P NMR chemical shielding tensor for the phosphonolipid – the principal components coming from the powder spectrum and the principal directions being those of AEP – were used to determine the headgroup conformation in the liquid crystal and hexagonal phases. A simple model for headgroup reorientation, which involves rapid transitions between two enantiomeric conformations of the headgroup and free rotation about the glycerol C2–C3 bond direction, was used to calculate possible torsion angles. The results show that the conformation of the headgroup up to the phosphorus atom is very similar in phospho- and phosphonolipids, *i.e.* the C2–C3–O–P torsion angle is nearly *trans* and the C3–O–P–C1 angle variable over the range of values investigated, with a bend at the phosphorus atom. Contrary to the phosphodiester moiety in analogous phospholipids which adopts a gauche-gauche conformation, two solutions for the next torsion angle O–P–C1–C2 were found around 100 and 130°. The last segment P–C1–C2–N is nearly *trans*, whereas the corresponding O–C1–C2–N segment in phospholipids is gauche. Despite the differences in the torsion angle values, the overall appearance of the headgroup is similar for both phospho- and phosphonolipids. The headgroup first extends out of the bilayer plane, bending at the phosphorus atom and the terminal portion lies nearly parallel to the membrane surface.

REMERCIEMENTS

Je tiens tout d'abord à exprimer ma gratitude à mon directeur de thèse, le docteur Ian C.P. Smith, pour m'avoir accueillie dans son laboratoire, pour sa constante bonne humeur, sa générosité, et aussi pour son opiniâtreté à toujours vouloir s'exprimer en français avec moi.

Je remercie également le docteur John K. Saunders qui m'a transmis son amour de la spectroscopie par résonance magnétique nucléaire, des défis qu'elle permet de relever, et qui m'a indiqué la possibilité de faire des études doctorales dans ce laboratoire.

Mes sincères remerciements vont à mes collègues étudiants, particulièrement Erick J. Dufourc pour m'avoir souvent défiée intellectuellement, Michèle Auger pour son amitié et son assistance et Sylvain Lareau pour son aide et son support durant plusieurs années. Je dis également merci à Kim Francoeur, étudiante sous-graduée, et à Dr Danielle Carrier, qui a fait des recherches post-doctorales dans le même laboratoire.

Je tiens aussi à souligner l'assistance technique occasionnelle mais indispensable fournie par Hector Séguin et Thérèse Kroft.

Je suis tout particulièrement reconnaissante envers le docteur J.R. Jocelyn Paré, qui a cru en mes possibilités et m'a offert le poste de spectroscopiste de la résonance magnétique nucléaire à Saint-Hyacinthe, ce qui m'a permis de terminer mes études tout en étant rémunérée. Tous les membres de

l'équipe sont également remerciés chaleureusement, soit les docteurs Jacqueline M.R. Bélanger et François Lamarche, ainsi que Jacques Lapointe, Michel Sigouin, Lise St-Onge Sigouin, Louise Guérette et tout particulièrement Richard R. Laing, qui m'a épaulée lors de la rédaction de cette thèse.

Je dois au Conseil national de recherches du Canada et au Centre de recherches alimentaires de Saint-Hyacinthe d'Agriculture Canada la possibilité d'utiliser de l'équipement moderne, de très haute qualité.

Finalement, je remercie le Conseil de recherches en sciences naturelles et en génie du Canada et l'Université d'Ottawa pour leur aide financière sans laquelle ce travail n'aurait jamais été entrepris.

ACKNOWLEDGEMENTS

First, I wish to express my gratitude to Dr. Irena H. Ekiel, without whom I would still be a novice in the field of nuclear magnetic resonance spectroscopy, both high-resolution and solid-state.

My appreciation goes to Dr. Harold C. Jarrell for his advice on synthetic procedures and mathematical calculations, to Drs. Jerzy B. Giziewicz and David B. Moir for their insights and suggestions on many reaction steps and general working technique, and to Dr. Robin J. Hill who taught me basic techniques in cell culture and lipidology, but without success in converting me to biology.

I want to sincerely thank Dr. George I. Birnbaum who performed x-ray diffraction and unit cell axis orientation determination on my so-called "big" crystal, although an even bigger one would have been very appreciated for the nuclear magnetic resonance experiments. Many thanks are given to Jean-Pierre Dumont and John Lynn for building the goniometer and to Margaret E. Pippy for help with the ORTEP program.

I am indebted to Dr. R. Andrew Byrd for his patience in answering numerous questions about the theory and practice of nuclear magnetic resonance, to Dr. Keith W. Butler for help with the differential scanning calorimetry and to Dr. Richard J. Buist, as well as Leo Turner and Anthony Wessel, for technical assistance with the spectrometers and computers.

Finally, I also wish to thank my fellow graduate students, namely Eric C. Kelusky, Laura C. Stewart, Janet H. Johns, John E. Baenziger, Myrna A. Monck, Eva J. Princz and Beatrice G. Winsborrow.

TABLE OF CONTENTS

page

LIST OF TABLES

LIST OF FIGURES

page

LIST OF SCHEMES

LIST OF ABBREVIATIONS

AEP	2-aminoethylphosphonic acid
AEPL	2-aminoethylphosphonolipid
APT	attached proton test
ATP	adenosine triphosphate
CAEP	ceramide 2-aminoethylphosphonate
CL	cardiolipin
CNAEP	ceramide *N*-methyl-2-aminoethylphosphonate
CPMG	Carr-Purcell-Meiboom-Gill
DANTE	Delays Alternating with Nutations for Tailored Excitation
DCC	dicyclohexylcarbodiimide
DEPT	distortionless enhancement by polarization transfer
DHPE	di-*O*-hexadecylphosphatidylethanolamine
DLPE	dilauroylphosphatidylethanolamine
DMAP	*N*,*N*-dimethyl-4-aminopyridine
DMPC	dimyrystoylphosphatidylcholine
DMF	*N*,*N*-dimethylformamide
DMSO	dimethylsulfoxide
DMSO-d_6	deuterated dimethylsulfoxide
DPPC	dipalmitoylphosphatidylcholine
DPPE	dipalmitoylphosphatidylethanolamine
DSC	differential scanning calorimetry

EDTA	ethylenediaminetetraacetic acid
FID	free induction decay
GPnL	glycerophosphonolipid
Im	imaginary
lit.	literature
MOPS	3-(*N*-morpholino)propanesulfonic acid
M. p.	Melting point
NMR	nuclear magnetic resonance
PA	phosphatidic acid
PC	phosphatidylcholine
PE	phosphatidylethanolamine
PE-Me	*N*-methylphosphatidylethanolamine
PE-diMe	*N*,*N*-dimethylphosphatidylethanolamine
PG	phosphatidylglycerol
PGP	phosphatidylglyceryl phosphate
PI	phosphatidylinositol
ppm	part per million
PS	phosphatidylserine
Re	real
rf	radiofrequency
rpm	rotation per minute
SM	sphingomyelin
TFA	trifluoroacetic acid
THF	tetrahydrofuran
TLC	thin-layer chromatography
TMS	tetramethylsilane
Tris	2-amino-2-(hydroxymethyl)-1,3-propanediol

CHAPTER 1

INTRODUCTION

1.1 Biological membranes

All living organisms possess at least one essential membrane, which permits distinction between the inside from the outside world, the plasma membrane. Eucaryotes also have a variety of more specialized membranes such as those of mitochondria, chloroplasts, endoplasmic reticulum, Golgi apparatus, vacuoles, peroxisomes, lysosomes or nuclei. The cell membrane has many functions. It provides a permeability barrier between the interior and the exterior of the cell; it is also a working apparatus that assures the relative constancy of the cellular interior. Membranes contain enzymes which develop chemical potential gradients by utilizing high-energy compounds such as adenosine triphosphate (ATP). In addition, plasma membranes contain specific receptors for external stimuli that may result in such varied responses as oriented movement of the cell, stimulation of membrane-bound enzymes, or generation of chemical or electrical signals. The plasma membrane plays an important role in processes such as phagocytosis, pinocytosis and secretion. It is also the locus of cell-specific antigens. Proteins and specific enzymes concerned with ion and metabolite transport across the membrane barrier are also localized in this structure. Enzymes of the mitochondrial membranes are involved in the electron transport chain and in oxidative phosphorylation to generate the ATP required for most cellular functions.

In all membranes, two major components are found: lipids and proteins. These two components play complementary roles in the control of membrane permeability. Its impermeability lies in the lipid core which, being hydrophobic, does not allow the passage of water or charged molecules. Membrane proteins serve as carriers, channels and receptors.

In this work, the structural aspects of the lipids will be considered. Lipids are universal components of biomembranes. In order to understand how they contribute to membrane function, it is necessary to know which lipids are actually found in membranes and to be able to correlate the specific molecular configuration of these lipids with specific physiological functions of the membranes in which they are found.

1.2 Lipids[1]

Lipids are defined as substances that are insoluble in water, soluble in organic solvents, contain long hydrocarbon chains in their molecules and are present in or derived from living organisms. This definition covers a wide range of compounds and includes simple compounds such as long-chain hydrocarbons, alcohols, aldehydes and fatty acids, and derivatives such as glycerides, wax esters, phospholipids, glycolipids, sphingolipids and others. Also included are the fat-soluble vitamins and their derivatives, as well as carotenoids and sterols and their fatty acid esters, because they are usually associated with membranes and are obtained together with the phospholipids and neutral lipids when cells or tissues are extracted.

---

[1] Taken from Kates (1).

1.2.1 Neutral lipids

Hydrocarbons form the simplest types of lipids. The chains can be normal and saturated – general formula $CH_3(-CH_2)_n-CH_3$ –, monobranched of the *iso*-series – general formula $(CH_3-)_2CH(-CH_2)_n-CH_3$ – or *anteiso*-series – general formula $(CH_3-CH_2-)(CH_3-)CH(-CH_2)_n-CH_3$ – multibranched (isopranes), mono- or polyunsaturated – the double bonds are usually *cis* –, or can contain various combinations of branching and unsaturations (*e.g.* carotenoids).

Long-chain alcohols form another class. Primary alcohols are most common. Again they can be normal and saturated, mono- or multibranched (isopranols), unsaturated, or possess a combination of branches and double bonds (terpenols). Sterols are widely distributed in animals (zoosterols) and in plants (phytosterols). Scheme 1–1 illustrates the structure of cholesterol, one of the major sterols found in animals. Members of the fat-soluble vitamins A (retinol), D (calciferol) and E (tocopherol) are closely related. Long-chain amino alcohols, usually homologues of sphingosine (Scheme 1–2), occur largely in complex form as sphingolipids: ceramides, cerebrosides, sphingosyl phosphatides and gangliosides.

Long-chain aldehydes occur in free form, but also in the form of alk-1-enyl ether (plasmalogen analogs of glycerides and phosphatides). Normal saturated and unsaturated, as well as isoprenoid aldehydes (*e.g.* retinal) are found in nature.

Long-chain carboxylic acids (fatty acids) occur in many forms, with variations in degree and kind of branching, number of double bonds, presence of other functional groups, and chain length. Table 1–1 presents the most common

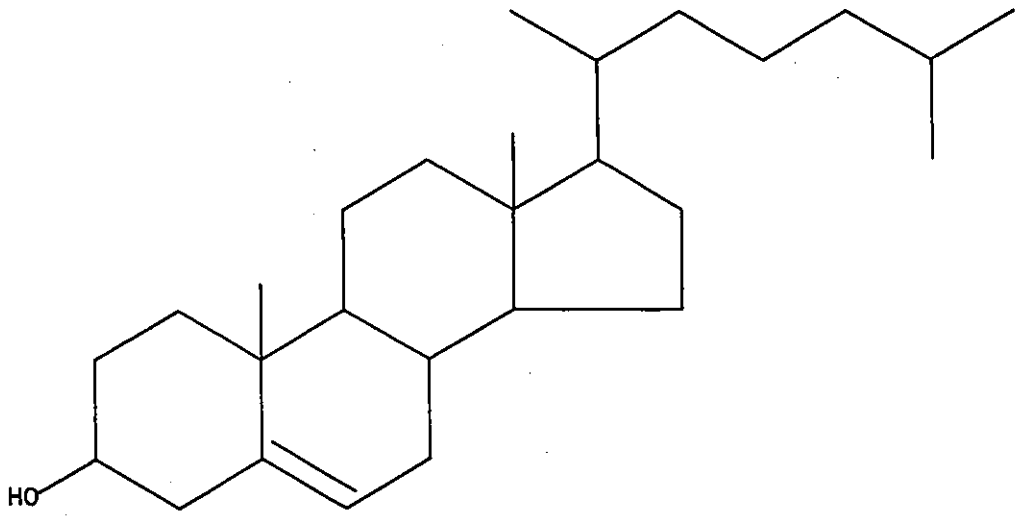

Scheme 1–1. Structure of cholesterol, cholest-5-en-3β-ol.

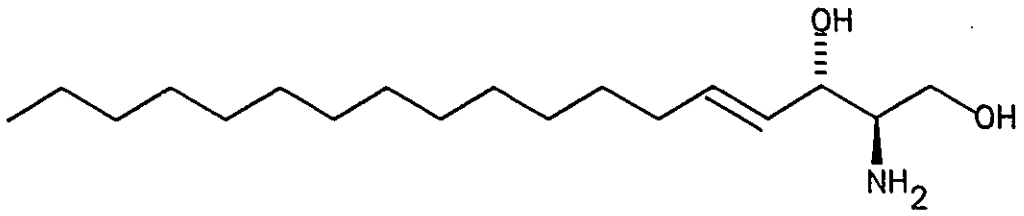

Scheme 1–2. Structure of sphingosine or *trans*-4-sphingenine, (2*S*,3*R*,4*E*)-2-amino-4-octadecen-1,3-diol.

Table 1–1. Some natural fatty acids.

Symbol	Structure[a]	Systematic name	Trivial name
12:0	$CH_3(-CH_2)_{10}-COOH$	dodecanoic	lauric
14:0	$CH_3(-CH_2)_{12}-COOH$	tetradecanoic	myristic
16:0	$CH_3(-CH_2)_{14}-COOH$	hexadecanoic	palmitic
$16:1^{\Delta 9}$	$CH_3(-CH_2)_5-CH=CH(-CH_2)_7-COOH$	9-hexadecenoic	palmitoleic
18:0	$CH_3(-CH_2)_{16}-COOH$	octadecanoic	stearic
$18:1^{\Delta 9}$	$CH_3(-CH_2)_7-CH=CH(-CH_2)_7-COOH$	9-octadecenoic	oleic
$18:2^{\Delta 9,12}$	$CH_3(-CH_2)_3(-CH_2-CH=CH)_2(-CH_2)_7-COOH$	9,12-octadecadienoic	linoleic
$18:3^{\Delta 9,12,15}$	$CH_3(-CH_2-CH=CH)_3(-CH_2)_7-COOH$	9,12,15-octadecatrienoic	α-linolenic
$18:3^{\Delta 6,9,12}$	$CH_3(-CH_2)_3(-CH_2-CH=CH)_3(-CH_2)_4-COOH$	6,9,12-octadecatrienoic	γ-linolenic
20:0	$CH_3(-CH_2)_{18}-COOH$	icosanoic	arachidic
$20:4^{\Delta 5,8,11,14}$	$CH_3(-CH_2)_3(-CH_2-CH=CH)_4(-CH_2)_3-COOH$	5,8,11,14-icosatetraenoic	arachidonic
22:0	$CH_3(-CH_2)_{20}-COOH$	docosanoic	behenic

[a] All double bonds are *cis*.

fatty acids. A symbol has been assigned to each fatty acid and is composed of the chain length, number of double bonds and their position. Fatty acids are found largely in esterified form, *e.g.* as waxes, glycerides, phosphatides, etc.

The simple lipids described above usually combine to form derivatives. Waxes are fatty acid esters of fatty alcohols. Sterols and vitamin alcohols also form esters with fatty acids. Acylglycerols (neutral fats) are fatty acid esters of glycerol. This class includes monoacylglycerols, which exist in two isomeric forms, *sn*-1-[2] and 2-isomers, diacylglycerols which also occur in two isomeric forms, *sn*-1,2- and 1,3-isomers, and finally triacylglycerols, where the acids may be all alike, two alike, or all different. Two general classes of glycerol ethers are known: alkyl ethers and alk-1-enyl ethers (plasmalogens). Alkyl ethers take the form of monoalkyl ethers – only the *sn*-1-isomer has been found in nature –, and dialkyl ethers (*i.e.* the *sn*-2,3-isomer of the branched-chain alcohol phytanol). Glyceryl ethers of other configurations have been synthesized but so far have not been found in nature. The alkyl ethers of glycerol occur as mono– and diacyl derivatives. The aldehydo enol ethers of glycerol occur naturally, with the alk-1-enyl linkage in the *cis* configuration, in the form of esterified derivatives such as phospholipids (plasmalogens) and neutral lipids (neutra. plasmalogens). Only the *sn*-1-isomer has been found in nature. Ceramides are *N*-acyl derivatives of long-chain bases.

---

2 For asymmetrically substituted glycerol derivatives, the stereospecific numbering (*sn*) system of nomenclature is used to distinguish between the two primary alcohol groups. If the secondary hydroxyl group in glycerol is oriented to the left of C2 in the Fischer projection, the carbon atom above C2 is designated C1 and the one below C3. The use of this stereospecific numbering is indicated by the prefix *sn* before the stem-name of the compound (2, 3).

1.2.2 Polar lipids

Phospholipids are constituents of cell membranes and may be classified into two main groups: glycerophosphatides and sphingosylphosphatides. The glycerophosphatides consist of derivatives of 1,2-diradyl-*sn*-glycero-3-phosphate or phosphatidic acid (PA). The phosphate is usually esterified with an amino alcohol (nitrogenous base) or a polyol. Nitrogenous bases include serine, ethanolamine and its *N*-methyl, *N*,*N*-dimethyl and *N*,*N*,*N*-trimethyl (choline) derivatives. Polyols include glycerol, glycerol phosphate, inositol and inositol phosphates. Diphosphatidylglycerol or cardiolipin (CL) is also encountered. Variations in the chain substitution include structures such as 1,2-diacyl-, 1-alk-1-enyl-2-acyl- (plasmalogens), 1-alkyl-2-acyl-, 2,3-dialkyl-, 1-acyl- (lyso) and 1-alkyl- forms. Scheme 1–3 gives the structures of some phospholipids.

The most common lipid in the sphingosyl phosphatide class is sphingomyelin (SM), the phosphocholine ester of an *N*-acylsphingosine (ceramide). Other classes of polar lipids include glycolipids, which consist of mono–, di– or trisaccharides linked glycosidically to the hydroxyl group of a diradylglycerol, glycophospholipids, phosphoglycolipids, cerebrosides, which are glycosides of ceramides, gangliosides, which are complex cerebrosides containing sialic acid, and sulfolipids.

1.3 Phosphonates

1.3.1 Occurrence of phosphonates in living systems

All phosphorus accessible to living organisms occurs in phosphate minerals as orthophosphates. The phosphorus atom occurs at the +5 level of

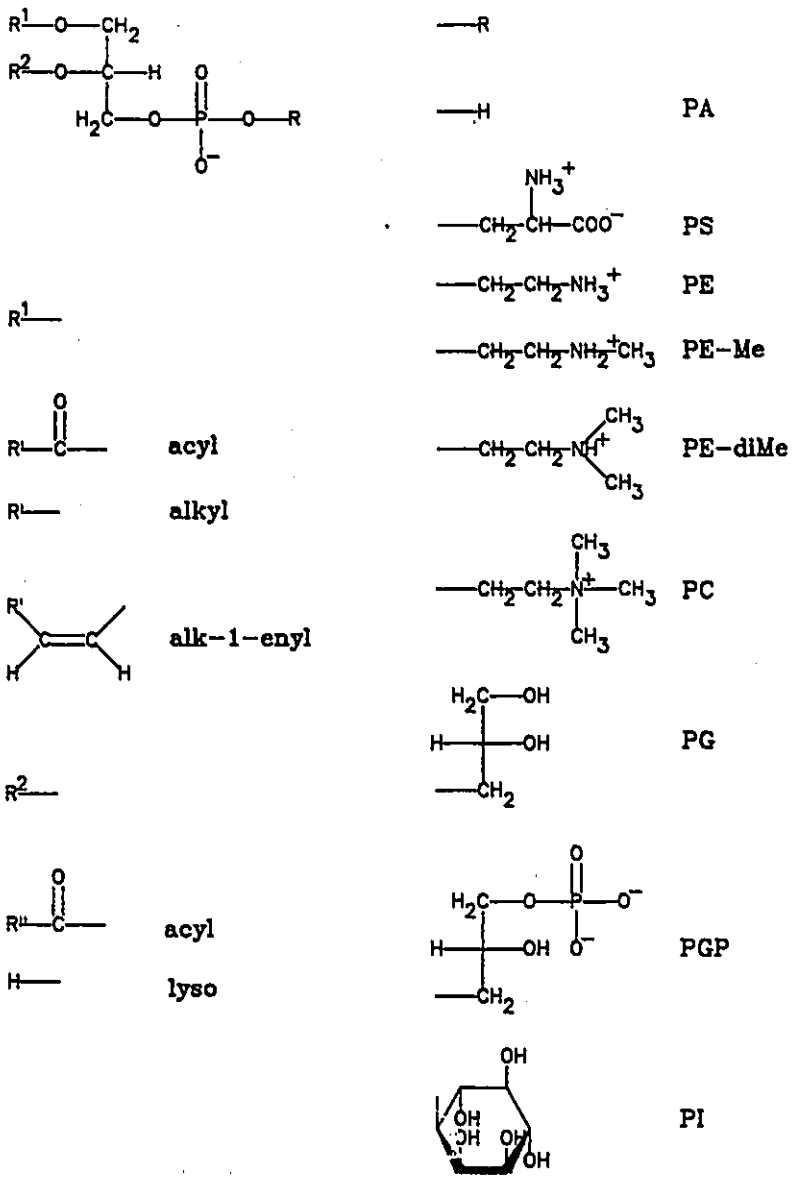

Scheme 1–3. Structure of some phospholipids. PA, phosphatidic acid; PS, phosphatidylserine; PE, phosphatidylethanolamine; PE-Me, *N*-methylphosphatidylethanolamine; PE-diMe, *N*,*N*-dimethylphosphatidylethanolamine; PC, phosphatidylcholine; PG, phosphatidylglycerol; PGP, phosphatidylglycerophosphate; PI, phosphatidylinositol. R' and R" represent long alkyl chains.

oxidation with four oxygen atoms bonded to the phosphorus in a tetrahedral structure. The organophosphates which occur naturally in a living system are usually oxygen esters, diesters, or anhydrides of phosphoric acid. There are rather infrequent exceptions to this bonding of phosphates in living systems. One exception is the natural occurrence of the carbon-phosphorus bond in the phosphonate class of organophosphates (4).

The actual identification of a naturally occurring phosphonate came in 1959 by Horiguchi and Kandatsu (5), who identified 2-aminoethylphosphonic acid (AEP) in an amino acid extract from an hydrolysate of rumen protozoal lipids. Phosphonates have subsequently been shown to occur naturally in a variety of phyla in the animal kingdom, in lower plants and in some bacteria (6). AEP has been found as a free molecule, in lipids and in macromolecular material. The lipids containing AEP are analogs of phospholipids and are both glycerophosphonolipids (Scheme 1–4) and sphingophosphonolipids (Scheme 1–5). Although the C–P bond could theoretically occur at the position of either of the two phosphate ester bonds in the phospholipid, the known naturally occurring materials contain the C–P bond only in the position it is found in AEP. The macromolecular materials are proteoglycan type materials and may contain fatty acids. These phosphonate molecules may make up a significant proportion of the phospholipids which occur in a given organism or tissue.

1.3.1.1 Glycerophosphonolipids

AEP was found to be bound to glycerol in lipids of *Anthopleura elegantissima* (7). Kittredge *et al.* (8) isolated and characterized *N*-methyl-AEP and *N,N,N*-trimethyl-AEP from *A. xanthogrammica*. These derivatives were then identified in phospholipid fractions other than sphingolipids, which would

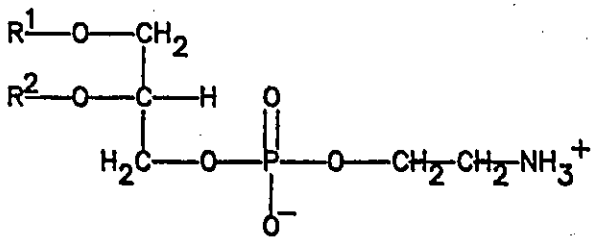

1,2–diradylglycero–3–(2–aminoethyl)phosphate

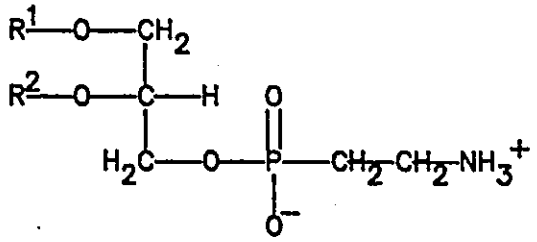

1,2–diradylglycero–3–(2–aminoethyl)phosphonate

Scheme 1–4. Phospho– and phosphono– analogs of PE.

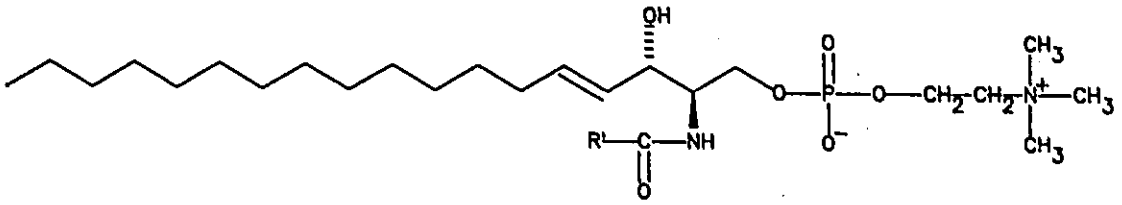

sphingomyelin (SM)

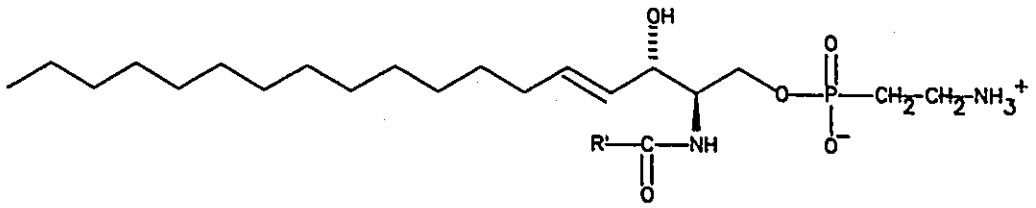

ceramide 2–aminoethylphosphonate

Scheme 1–5. Structure of two naturally occurring ceramide derivatives.

presumably indicate their presence as glycerophosphonolipids. Liang and Rosenberg (9) identified diacylglyceryl-AEP, the AEP analog of PE, in lipid extracts of the protozoan *Tetrahymena pyriformis*. Thompson (10) found that a large percentage of this phosphonolipid contained an alkyl ether bond at carbon 1 of the glycerol. Later work has shown that the major component of the ciliary lipids of *T. pyriformis* is glycerophosphonolipids. These phosphonate-containing analogs seem to be enriched in ciliary lipids over the remainder of the protozoal lipids (11, 12). Since that time, diacylglyceryl-AEP and diacylglyceryl-*N*,*N*,*N*-trimethyl-AEP, which is the phosphonate analog of PC, have been isolated from bovine liver (13) and bile (14).

1.3.1.2 Sphingophosphonolipids

Ceramide AEP was first identified as a component of the lipids of the sea anemone *A. elegantissima* by Rouser *et al.* (15). Simon and Rouser (16) then elucidated the structure of the ceramide AEP and found the base to be sphingosine with the AEP esterified to the first hydroxyl group and an *N*-acyl group at the second carbon. The fatty acids were predominantly saturated and had chain lengths from 14 to 18 carbons. Ceramide AEP has been identified in a variety of other species. These ceramides contain sphingosine or closely related derivatives as long-chain bases. More complex sphingolipids, containing both a phosphonate and a carbohydrate moiety, have also been characterized. Cerebrosides containing AEP or *N*-methyl-AEP, palmitic acid, galactose, and a long-chain base have been isolated from viscera and muscle of *Turbo cornutus* (17–19).

1.3.2 Role of phosphonates

The discovery of AEP has led to investigations on the distribution, metabolic pathways, chemical properties and biological significance of naturally occurring phosphonates. The answers to many of the questions concerning phosphonates have proven to be elusive. Of increasing importance are the questions concerning the role of the unusual materials in the intact organism and the explanation for their existence. Since there is no documented role for free AEP, the role of the aminophosphonates *in vivo* consists of two interrelated aspects: first, the role of the aminophosphonates in the structure and function of the molecule into which it is incorporated and, second, the role of that macromolecule in the structure and function of the organism in which it is found. The first aspect must be addressed by examining the aminophosphonates and the molecules into which they are incorporated naturally. The molecular properties involved include effects on the *p*I, solubility, and steric relationships. Secondary effects such as change in structural conformation of macromolecules may result from the primary effects. All of these factors have the capability of imposing metabolic or functional restrictions on the phosphonate-containing molecules or of imparting a unique function to the materials. Many phosphonate-containing molecules have been observed to be resistant to enzymatic hydrolysis (12, 20). This property may be observed at the C—P bond or at other parts of the molecule as well. Rosenthal and Pousada (21) have investigated the effects of phosphonates on phospholipases. The enzymes most effectively inhibited by phosphonates are those that would hydrolyze an ester at the location of the C—P bond. They also found that the phosphonate analog of PC was a weak inhibitor of phospholipase C from *Clostridium perfringens*. Thompson (22) has also noted that the presence of incorporated AEP prevents the degradation of phosphonolipids by phospholipases. Thus, the presence of a C—P bond can impart resistance to a variety of hydrolytic enzymes. In addition to the

resistance to enzymatic hydrolysis, there are some structural considerations of importance. The presence of an alkyl ether in the glycerophosphonolipids imparts an inert character to the molecule but does not disturb the normal lipid interaction. The presence of AEP together with sphingosine may provide a molecule of even more inert character in the hydrocarbon backbone than the glycerophosphonolipids.

The second aspect of the role which the phosphonate molecule plays in the organism is directly related to the properties of the molecule itself. The inert character of the phosphonate-containing molecules may be used to generate membranes or structural components which are resistant to oxidation, hydrolysis, or metabolic processes. Whether there is an actual biological requirement for these resistant structures is not known. The nonrandom incorporation of AEP into anatomic structures in *T. pyriformis* (11, 12) and other organisms is indicative of a unique function. It has been proposed that in *T. pyriformis* the AEP was incorporated into structural material and conferred resistance to enzymatic hydrolysis on the cell membrane. This AEP-containing material is apparently not metabolized further, is necessary for structural integrity and is synthesized only during cell growth. Thus, phosphonates may be a storage mechanism for phosphorus in a phosphorus-deficient environment. This phosphonate phosphorus may then be utilized as required for the structural integrity of membranes (12, 20), since it is apparently not available metabolically. It is apparent that structures and functions involving phosphonates are intimately related.

1.4 Cell and model membranes

The model presently universally accepted to represent the structure of biological membranes is that originally proposed by Singer and Nicolson (23). In

this model, the basic matrix is constituted of a relatively fluid phospholipid bilayer in which are imbedded mainly globular amphiphilic proteins (Figure 1–1). From a thermodynamic point of view, two types of noncovalent interactions are thus maximized: hydrophobic and hydrophilic. Nonpolar fatty acid chains are embedded inside the bilayer, whereas polar or ionic groups of phospholipids are in direct contact with the aqueous phase located on both sides of the membrane. Furthermore, nonpolar amino acid residues of proteins are imprisoned as much as possible inside the membrane, out of water contact, and their polar or ionic residues, as well as oligosaccharides, are in contact with the surrounding aqueous medium. The individual molecules in the lipid-protein mosaic are able to diffuse with respect to each other. The bilayer acts as a two-dimensional liquid through which the lipids and proteins may move laterally.

Due to the complexity of natural membranes, it is often difficult to localize specific interactions occurring in biological membranes. In order to simplify the system, model membranes are often used. As a consequence of the combination of a polar and an apolar part in the same molecule, membrane lipids spontaneously form aggregates when they are dispersed in water. The molecular organization of such aggregates is dependent on the molecular shape of the constituting molecules (24). Lipids which have a good balance between the size of the polar headgroup and that of the hydrophobic part easily form bilayer structures (*e.g.* PC, PG and SM). They consist of concentric multilamellar dispersions or liposomes of variable sizes. Each lamella is a bilayer similar to that formed by the lipids of natural membranes. Bilayers of lipids and water layers alternate in the multilamellar dispersion.

Most discussions of lipids in membranes have presumed the dominance of a bilayer structure, in either the highly ordered and immobile gel

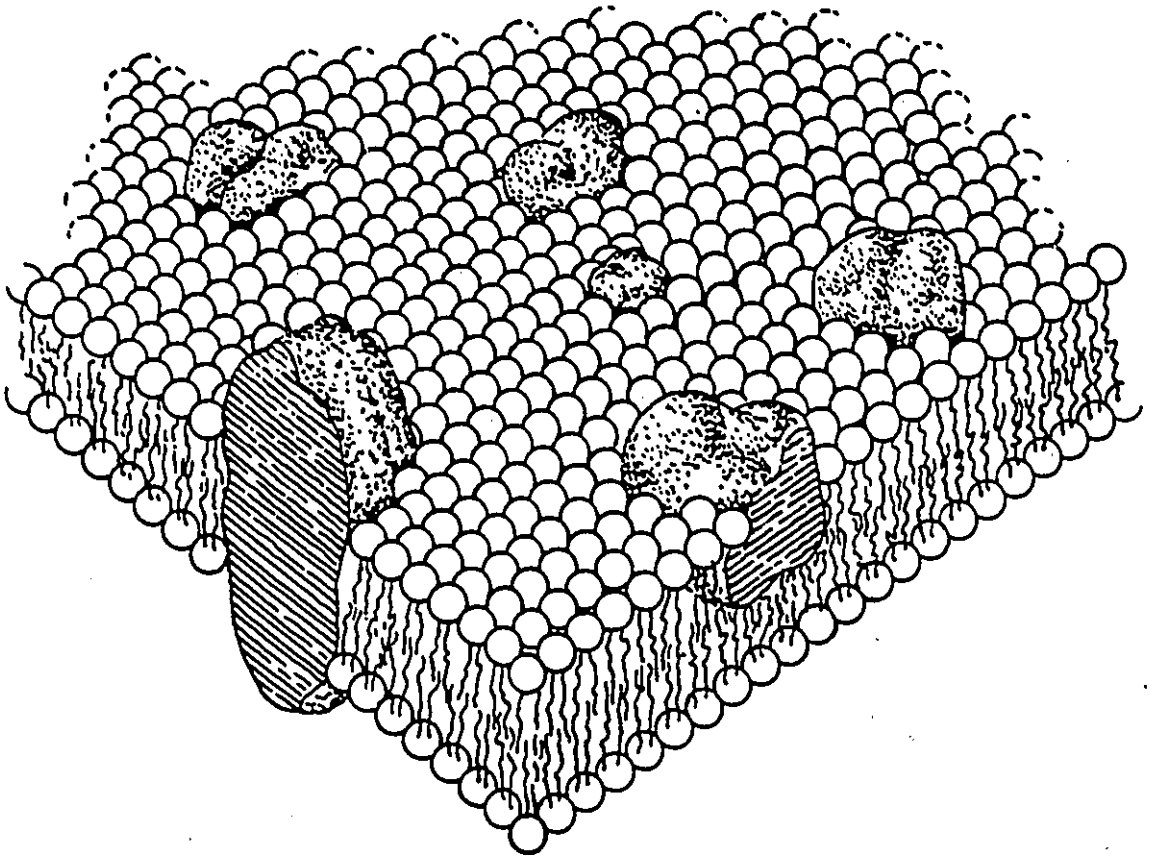

Figure 1–1. The fluid mosaic model of membrane structure. The membrane consists of a fluid lipid bilayer, in which globular proteins are embedded on one side or another, or span the entire membrane thickness. Phospholipids are represented by a polar or ionic headgroup (spheres) and hydrophobic fatty acid chains (wavy lines). The solid bodies with hatched section represent integral globular proteins. From Singer and Nicholson (23).

phase, or the less ordered and mobile liquid crystalline phase. Various studies have suggested the possible existence of two other morphological states of the lipids, an inverted hexagonal (H_{II}) phase and an isotropic phase. The hexagonal phase has been characterized by x-ray studies on model systems (25). It consists of long cylinders of phospholipids where the polar headgroups surround an inner aqueous channel. Lipid molecules with a polar headgroup of limited size and hydration (*e.g.* unsaturated PE) prefer this arrangement (24). When the polar headgroups are dominating in lipid molecules (*e.g.* lysoPC), a reversed hexagonal (H_I) organization is formed upon hydration with a limited amount of water, which is converted into a system of globular micelles in excess water.

1.5 Nuclear magnetic resonance spectroscopy

Phospholipid membranes can be examined from two points of view. In the first, the membrane is considered as a collection of phospholipids with particular macroscopic properties, *e.g.* thermodynamic properties such as phase behavior and transitions. The second is a molecular or microscopic one, which examines the structural and motional properties of the various parts of the phospholipid molecule. Nuclear magnetic resonance (NMR) techniques have been applied to both types of studies. It has been useful in demonstrating the presence of the phases mentioned above in many different lipid systems and biological membranes (24). NMR can also provide information about the local environment in a very small, submolecular region of the membrane, in fact, at the level of individual atoms. Different techniques of NMR apply to studies of static or averaged structural and dynamic parameters. ^{1}H, ^{2}H, ^{13}C, ^{14}N, ^{15}N and ^{31}P NMR can provide different types of information on the same membrane structure (26, 27). Solid-state NMR studies (28) of biomembranes have been carried out mostly with deuterium and phosphorus–31.

1.5.1 ^{2}H NMR

^{2}H NMR spectroscopy has been of great help in the study of the physical state of the hydrocarbon chain region of phospholipid bilayers (29, 30). This requires the synthesis of specifically deuterated phospholipids. These lipids are then dispersed in water; proteins or other membrane components may be incorporated if required.

The ^{2}H NMR signal has a symmetric appearance (Figure 1–2). The separation between the two maxima $\Delta\nu_Q$ is called the quadrupolar splitting and an order parameter can be calculated directly from it. This order parameter is a well-defined physical parameter and is suited for describing membrane lipid properties; it is the C$-^2$H vector angular fluctuation average over the time scale of the deuterium NMR experiment ($\approx 10^{-5}$ s) (31). The quadrupolar splitting can be measured only in dispersed preparations, since in small vesicles the interactions of interest are completely motionally averaged, resulting in a single line. The signals can be assigned in a straightforward manner and there are no complications from naturally occurring deuterium. Since ^{2}H NMR relaxation proceeds by only one mechanism (quadrupole relaxation), spin lattice relaxation time (T_1) measurements provide a good indication of motion in a phospholipid system.

1.5.2 ^{31}P NMR

A great deal of insight into the phase behavior of lipids in membranes and into the degree of organization of lipid headgroups has been gained by ^{31}P NMR. Many of the details of the method are given in Seelig (32) and Cullis and de Kruijff (24). The relatively high sensitivity of this nucleus is an advantage. ^{31}P NMR has been applied to membrane studies mainly for the detection of phase changes. Hydrated phospholipids may adopt a variety of conformations according

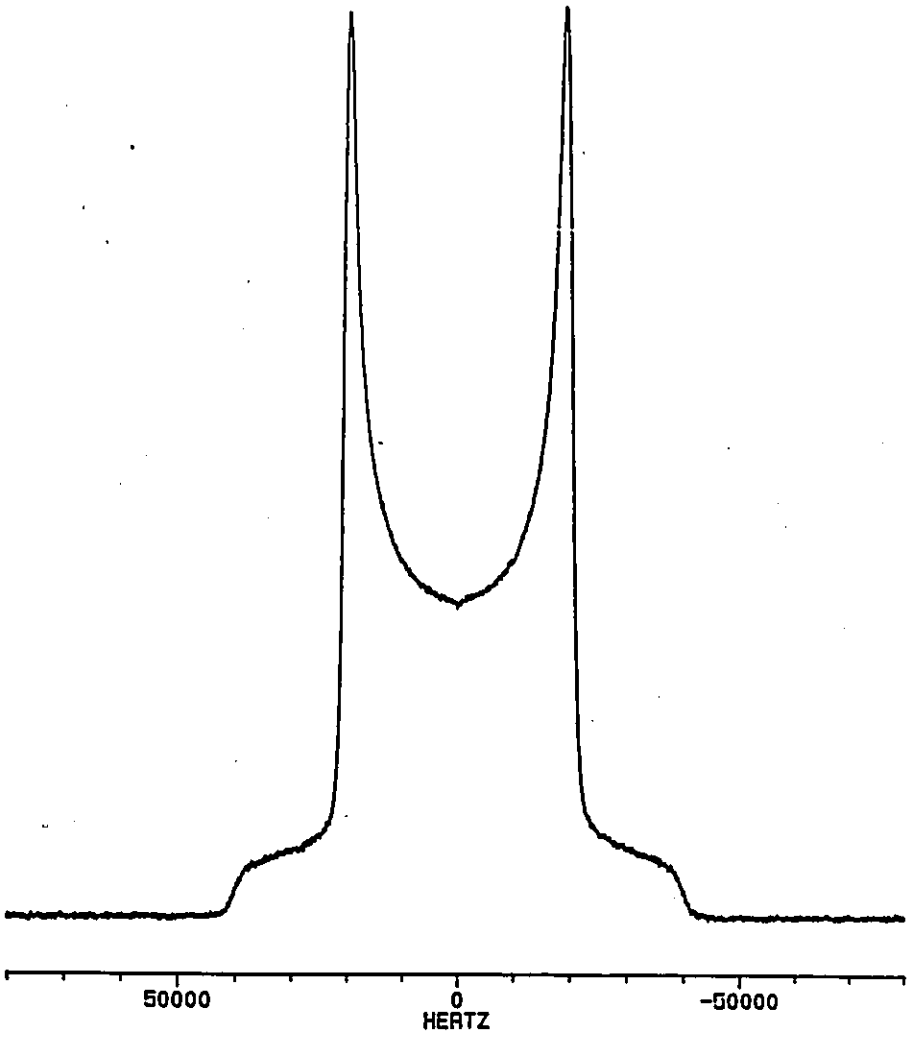

Figure 1–2. Example of a solid-state ^2H NMR spectrum. The sample is a fine powder of L-alanine-3,3,3-d_3 and the spectrometer frequency 46.1 MHz. The quadrupole splitting $\Delta\nu_Q$ is easily measured as the separation of the two peaks.

to the nature of the lipid, the amount of water, the presence of ions, the *p*H, the temperature, etc. Two of these dispositions are depicted in Figure 1–3, the so-called bilayer and hexagonal H_{II} arrangements; other phases such as cubic, micellar and inverted micellar are also possible. Classically, the various phases have been distinguished by means of x-ray diffraction; however, ^{31}P NMR can be used instead, and often advantageously (32, 24).

The technique is based on the large chemical shift anisotropy exhibited by lipid phosphorus. In the presence of proton decoupling, the anisotropy results in characteristically broad spectra whose shape and width depend on phospholipid motion; in turn, this is related to the lipid phase. In large bilayer structures (radius greater than 200 nm), as is the case for most biomembrane preparations, the only possibility of motion at the NMR time scale is the rotation of the phospholipid molecules about their long axis. The result is a very broad spectrum with a low-field shoulder and a high-field peak (Figure 1–3). In the hexagonal (H_{II}) phase, lipids experience additional motion averaging, because of the lateral diffusion around the small aqueous channels. As a result, ^{31}P NMR lineshapes occur with reversed asymmetry as compared to the bilayer spectra, and with about half their width. Finally, in the case of small sonicated liposomes, or in micellar configurations, effective isotropic motion occurs, and lateral diffusion succeeds in averaging all orientations, leading to narrow symmetric ^{31}P NMR spectrum, as shown in Figure 1–3. A detailed up-to-date review of the application of ^{31}P NMR to membrane studies may be found in Smith and Ekiel (34).

1.5.3 Headgroup conformation

Many techniques have given a picture of the headgroups of PC and PE. The conformation of the PC headgroup in a membrane is now widely accepted

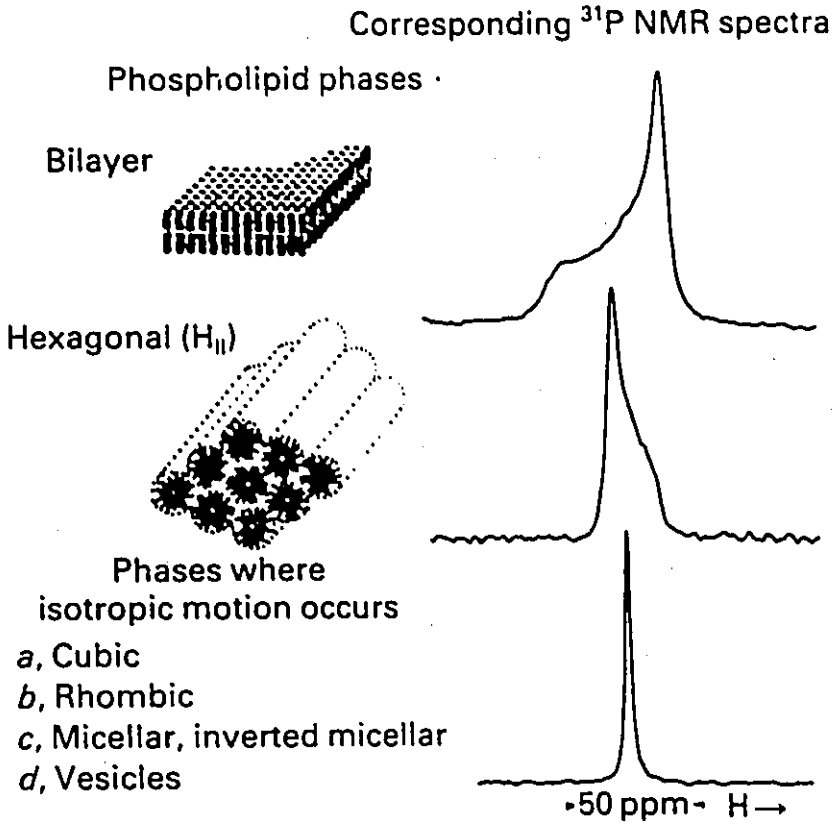

Figure 1–3. Polymorphic phases available to hydrated liquid-crystalline phospholipids and the corresponding ^{31}P NMR spectra. The bilayer spectrum was obtained from aqueous dispersions of egg yolk phosphatidylcholine; the hexagonal spectrum corresponds to soybean phosphatidylethanolamine; the "isotropic motion" spectrum was obtained from a mixtureof 85 mol% soya phosphatidylethanolamine and 15 mol% phosphatidylcholine. The spectra were obtained at 30°C in the presence of broadband proton decoupling. From Cullis and Hope (33).

to be approximately that shown in Figure 1–4. The headgroup is seen to lie parallel to the membrane surface with the quaternary amine function directed upwards. The most direct evidence for this conformation comes from crystal structure of dimyristoylphosphatidylcholine (DMPC) (35). The orientation of the PE headgroup is also parallel to the bilayer surface. Figure 1–4 shows the crystal structure of dilauroylphosphatidylethanolamine (DLPE) (36, 37). A gauche-gauche conformation is almost always found for the O—P—O ester linkage, whether in phospholipids, small model compounds or nucleic acids (38). This conformation introduces a bend already at the phosphorus, probably imparting an orientational preference. Steric factors would then place further limits on the available conformations.

^{2}H NMR in combination with ^{31}P NMR has been proven useful in the analysis of headgroup structure and these data are compatible with the crystal structure, although they can be interpreted in terms of other conformations (39–41).

1.6 Aim of the research

The conformation and motional properties of the polar headgroup region of phospho– and phosphonolipids are of considerable interest. This attention is well deserved, since it is at the level of the headgroup that the bilayer interacts with its environment, the surrounding water. The presence of the phosphorus-carbon bond in phosphonolipids might confer to them a different headgroup conformation which could be responsible for a special function. In this work, NMR techniques were applied to the study of biological and model membrane systems containing phosphonolipids.

The aim of the research was to determine the headgroup conformation of phosphonolipids using NMR techniques, and to compare it with that of

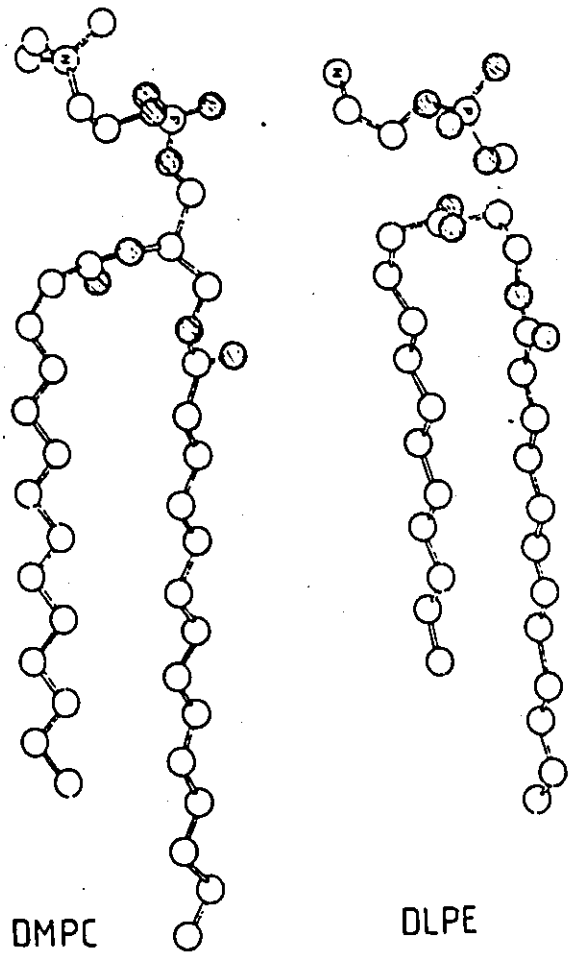

Figure 1–4. Crystal structures of dimyristoylphosphatidylcholine (DMPC) (35) and dilauroylphosphatidylethanolamine (DLPE) (36, 37). Oxygen atoms are shaded. From Browning (27).

phospholipids. To achieve this goal, the work was divided into several parts. The protozoa *Tetrahymena thermophila* possess a large proportion of phosphonolipids in its various membranes. In the first part, the lipids of this organism were studied by ^{31}P NMR. The technique was useful mainly to determine the phase behavior or phospho– and phosphonolipids in polar and total lipid extracts. For a quantitative interpretation of the ^{31}P NMR data obtained for phosphonates, the chemical shift tensor is required. In the second part, the principal values of the ^{31}P NMR chemical shielding tensor and their orientation were measured on single crystals of AEP, which was used as a model compound. Phosphonolipids selectively labelled in the headgroup were then synthesized in the third part, in preparation for the model membrane studies. Finally, in the fourth part, ^{2}H and ^{31}P NMR parameters were measured and, by analogy with previous studies on phospholipids (39–41), were used to calculate possible headgroup conformations for a synthetic phosphonolipid.

1.7 Outline of the thesis

The next chapter (Chapter 2) presents a general outline of the theory of nuclear magnetic resonance together with the particular applications of ^{2}H and ^{31}P NMR to membrane studies. Chapter 3 is devoted to the study of the lipids of *Tetrahymena thermophila*, mainly the use of ^{31}P NMR to examine the phase behavior of phospho– and phosphonolipids in mixtures of polar and total lipids extracted from this organism. The complete ^{31}P NMR chemical shielding tensor of 2-aminoethylphosphonic acid has been determined (Chapter 4). The synthesis of headgroup-deuterated phosphonolipids is described in Chapter 5. In Chapter 6, using a simple model for headgroup reorientation, possible headgroup conformations for a synthetic phosphonolipid were calculated from ^{31}P and ^{2}H NMR

spectral parameters. Finally, the main conclusions of the thesis research together with suggestions for future work are presented in the last chapter (Chapter 7).

1.8 References

1. M. Kates, in *Laboratory Techniques in Biochemistry and Molecular Biology*, Vol. 3, Part 2, edited by R.H. Burdon and P.H. van Knippenberg (Elsevier, Amsterdam, 1986), Chap. 1, pp. 1–79.

2. IUPAC-IUB Commission on Biochemical Nomenclature, *Lipids* **12**, 455–468 (1977).

3. IUPAC-IUB Commission on Biochemical Nomenclature, *Eur. J. Biochem.* **79**, 11–21 (1977).

4. R.L. Hilderbrand and T.O. Henderson, in *The role of phosphonates in living systems*, edited by R.L. Hilderbrand (CRC Press, Boca Raton, Florida, 1983), Chap. 2, pp. 5–29.

5. M. Horiguchi and M. Kandatsu, *Nature* **184**, 901–902 (1959).

6. T. Hori and Y. Nozawa, in *Phosphonolipids*, edited by J.N. Hawthorne and G.B. Ansell (Elsevier Biomedical Press, Amsterdam, 1982), Chap. 3, pp. 95–128.

7. J.S. Kittredge, E. Roberts and D.G. Simonsen, *Biochemistry* **1**, 624–628 (1962).

8. J.S. Kittredge, A.F. Isbell and R.R. Hughes, *Biochemistry* **6**, 289–295 (1967).

9. C.R. Liang and H. Rosenberg, *Biochim. Biophys. Acta* **125**, 548–562 (1966).

10. G.A. Thompson, Jr., *Biochemistry* **6**, 2015–2022 (1967).

11. J.D. Smith, W.R. Snyder and J.H. Law, *Biochem. Biophys. Res. Commun.* **39**, 1163–1169 (1970).

12. K.E. Kennedy and G.A. Thompson, Jr., *Science* **168**, 989–991 (1970).

13. S. Hasegawa, M. Tamari and M. Kametaka, *J. Biochem.* **80**, 531–535 (1976).

14. M. Tamari, M. Ogawa, S. Hasegawa and M. Kametaka, *Agric. Biol. Chem.* **40**, 2057–2062 (1976).

15. G. Rouser, G. Kritchevsky, D. Heller and E. Lieber, *J. Am. Oil Chem. Soc.* **40**, 425–454 (1963).

16. G. Simon and G. Rouser, *Lipids* **2**, 55–59 (1967).

17. A. Hayashi and F. Matsuura, *Biochim. Biophys. Acta* **248**, 133–136 (1971).

18. A. Hayashi and F. Matsuura, *Chem. Phys. Lipids* **22**, 9–23 (1978).

19. F. Matsuura, *Chem. Phys. Lipids* **19**, 223–242 (1977).

20. J.S. Kittredge and E. Roberts, *Science* **164**, 37–42 (1969).

21. A.F. Rosenthal and M. Pousada, *Biochim. Biophys. Acta* **164**, 226–237 (1968).

22. G.A. Thompson, Jr., *Biochim. Biophys. Acta* **176**, 330–338 (1969).

23. S.J. Singer and G.L. Nicolson, *Science* **175**, 720–731 (1972).

24. P.R. Cullis and B. de Kruijff, *Biochim. Biophys. Acta* **559**, 399–420 (1979).

25. V. Luzatti and A. Tardieu, *Ann. Rev. Phys. Chem.* **25**, 79–94 (1974).

26. I.C.P. Smith and R. Deslauriers, in *Structural Molecular Biology: Methods and Applications*, edited by D.B. Davies, W. Saenger and S.S. Danyluk (Plenum Press, New York, 1983), pp. 113–159.

27. J.L. Browning, in *Liposomes: From Physical Structure to Therapeutic Applications*, edited by C.G. Knight (Elsevier/North-Holland, Amsterdam, 1981), Chap. 7, pp. 189–242.

28. R.G. Griffin, *Methods Enzymol.* **72**, 108–174 (1981).

29. I.C.P. Smith, *Bull. Magn. Reson.* **3**, 120–133 (1981).

30. I.C.P. Smith, in *Biomembranes*, Volume 12, edited by M. Kates and L.A. Manson (Plenum Press, New York, 1984), Chap. 4, pp. 133–168.

31. J. Seelig, *Q. Rev. Biophys.* **10**, 353–418 (1977).

32. J. Seelig, *Biochim. Biophys. Acta* **515**, 105–140 (1978).

33. P.R. Cullis and M.J. Hope, *Nature* **271**, 672–674 (1978).

34. I.C.P. Smith and I.H. Ekiel, in *Phosphorus–31 NMR, Principles and Applications*, edited by D.G. Gorenstein (Academic Press, Orlando, Florida, 1984), Chap. 15, pp. 447–475.

35. R. Pearson and I. Pascher, *Nature* **281**, 499–501 (1979).

36. P.B. Hitchcock, R. Mason, K.M. Thomas and G.G. Shipley, *Proc. Natl. Acad. Sci.* **71**, 3036–3040 (1974).

37. M. Elder, P. Hitchcock, R. Mason and G.G. Shipley, *Proc. Roy. Soc. London* **A354**, 157–170 (1977).

38. M. Sundaralingam, *Ann. N.Y. Acad. Sci.* **195**, 324–355 (1972).

39. J. Seelig, H.-U. Gally and R. Wohlgemuth, *Biochim. Biophys. Acta* **467**, 109–119 (1977).

40. J. Seelig and H.-U. Gally, *Biochemistry* **15**, 5199–5204 (1976).

41. R. Skarjune and E. Oldfield, *Biochemistry* **18**, 5903–5909 (1979).

CHAPTER 2

THEORY OF NUCLEAR MAGNETIC RESONANCE AND APPLICATIONS TO MEMBRANE STUDIES

2.1 Introduction

High-resolution nuclear magnetic resonance (NMR) spectroscopy has been widely used to determine molecular structures and conformations and to study dynamic chemical processes in solution. For samples constrained to be examined in the solid state, either for solubility reasons or because sample properties are modified in solution, conventional liquid-state NMR techniques have not been very useful.

Essentially the same interactions are responsible for liquid- and solid-state NMR spectra. The major difference is that molecular tumbling averages these interactions in liquids while in solids such motion is either absent or considerably reduced, and this gives rise to additional complexities in the spectrum.

2.2 The NMR experiment[1]

Nuclei with odd mass or charge possess the property of spin. The spin angular momentum vector $I\hbar$ is measured in units of $\hbar$, where $\hbar$ is Planck's constant divided by 2π. The value of the spin quantum number I is an integral multiple of $^1/_2$. The possession of both spin and charge confers on the nucleus a magnetic moment $\underline{\mu}$ which is proportional to the magnitude of the spin:

$$\underline{\mu} = \gamma \hbar \underline{I}, \qquad [2\text{–}1]$$

where γ, the magnetogyric ratio, is a constant which varies from one type of nucleus to another.

The magnetic moments $\underline{\mu}$ of nuclei having a net spin will normally be randomly oriented, but when placed in a static magnetic field they will align with the lines of force of the field. The interaction between the applied field $\boldsymbol{B_0}$ and the nuclear moment generates a torque which causes the latter to precess about the direction of the field. For a given field strength, each nucleus precesses at its own characteristic angular frequency $\underline{\omega_0}$, and this is determined by the Larmor relationship:

$$\underline{\omega_0} = 2\pi \underline{\nu_0} = -\gamma \boldsymbol{B_0}. \qquad [2\text{–}2]$$

Quantum theory demands that the allowable nuclear spin states are quantized; the spin quantum number m_I, which is the component of the nuclear spin vector in any given direction, can only take up one of a set of $2I + 1$ discrete values which are: $I, I - 1, \ldots, -I + 1, -I$. The energy of the different levels is given by:

---

1 Taken from Carrington and McLachlan (1), Lynden-Bell and Harris (2), Farrar and Becker (3) and Müllen and Pregosin (4).

$$E = -\underline{\mu} \cdot \boldsymbol{B_0} = -\gamma h m_I B_0. \qquad [2\text{–}3]$$

For nuclei with $I = {}^1/_2$, only two orientations of the magnetic moments – parallel and antiparallel to the field – are quantum mechanically allowed. Since the two orientations have slightly different energies, a small excess of nuclei in the lower energy state (parallel if a positive value of γ is assumed) results. The population ratio N_B/N_A of the two states (B upper and A lower) depends on the absolute temperature T, the strength of the magnetic field and the nuclear magnetic moment according to the Boltzmann relation:

$$N_B/N_A = \exp(-\gamma h B_0/kT), \qquad [2\text{–}4]$$

where k is Boltzmann constant. A consequence of the excess population in the lower spin state is the existence of a net macroscopic equilibrium magnetization $\boldsymbol{M_0}$ directed along $\boldsymbol{B_0}$ (by convention the z axis). This represents the resultant effect or weighted average of all the individual magnetic moments of the nuclear species in the sample.

If this net magnetization is subjected to a second field $\boldsymbol{B_1}$ placed at right angles to the static field $\boldsymbol{B_0}$ and made to rotate at a frequency $\underline{\omega}_0$, then the magnetization vector $\boldsymbol{M}$ experiencing the resultant of the two fields will be tipped away from the original z direction by an angle $\underline{\alpha}$ which is dependent on the strength $\boldsymbol{B_1}$ and duration t of this second field according to:

$$\underline{\alpha} = -\gamma \boldsymbol{B_1} t. \qquad [2\text{–}5]$$

A common simplification is to view the spin system from a rotating frame where the entire coordinate system is taken as rotating about $\boldsymbol{B_0}$ at the precession frequency of $\boldsymbol{M_0}$. Since both the observer and the magnetic moment rotate around together, the tipping of $\boldsymbol{M}$ appears as a simple rotation of $\boldsymbol{M}$ about an apparently stationary

field B_1. In practice this displacement of M is achieved by surrounding the sample with a transmitter coil connected to a source of radio-frequency (rf) power which when pulsed creates a rotating magnetic field component in the *xy* plane.

Immediately after M is tipped away from the *z* direction and the applied pulse is discontinued the resultant magnetization will have a rotating component in the *xy* plane which can be detected by the decaying sinusoidal voltage it induces in a receiver coil placed in this plane. This signal is called a free induction decay (FID).

The tipping of the magnetization M corresponds to the absorption of energy as some nuclei undergo transition from the lower to the higher energy state. In a typical NMR experiment, a pulse which rotates M_0 by 90° (termed a 90-degree pulse) usually lasts a few microseconds. This pulse is of such power and encompasses a range of frequencies $\Delta\nu$ to simultaneously tip the magnetizations of many dissimilar nuclei in a molecule (3-dB attenuation):

$$\Delta\nu = 3.79/\pi t_{90°}. \qquad [2\text{–}6]$$

Thus, multiple energy absorptions take place and the FID consists of superimposed sine waves each with its characteristic frequency resulting in a complex interference pattern. To abstract the individual frequency domain spectrum (a plot of energy absorption versus frequency), Fourier transformation, a mathematical operation, is required.

The absorption of energy (resonance) occurs when the sample is irradiated with electromagnetic energy at a frequency corresponding to the precessing macroscopic moment M_0. In fact, both absorption and emission of energy are stimulated when a nucleus is in resonance. The probability of a particular transition, however, is proportional to the population of the energy state from which it occurs.

To determine the spectra of low-receptivity nuclei, *i.e.* those with small magnetogyric ratio or low natural abundance, a series of repetitive pulses with signal acquisition between pulses is necessary to develop a strong FID. The successive free induction decays are automatically digitized and accumulated in a computer prior to Fourier transformation into the conventional spectrum.

The utility of NMR as an analytical method stems directly from the fact that for a given nuclear species the resonance frequency is very sensitive to small variations in molecular structure as well as to much larger changes in going from one nuclear species to another. In complex molecules, the magnetic field is subtly and nonuniformly altered in the vicinity of some nuclei as a result of shielding currents associated with neighboring electronic orbitals. The resonance magnetic field in Equation [2–2] must be replaced by an effective field slightly different from $\boldsymbol{B_0}$. The internally created secondary fields shield nuclei from the applied field to different extents, giving rise to a range of chemical shifts or resonance frequencies for nuclei in different molecular environments. Molecules possessing more than one magnetic nucleus frequently give NMR spectra showing that the magnetic moments of different nuclei interact with each other, the nature of the interaction again being characteristic of the molecular environment of the nuclei.

Some nuclei with spins $I > {}^1/_2$ also possess an electric quadrupole moment Q which occurs because the distribution of electric charge density inside the nucleus is ellipsoidal rather than spherical. Nuclei with quadrupole moments tend to orient themselves in the strongly nonuniform electric fields produced by valence electrons in a molecule and this produces various complications in NMR spectra.

2.3 Relaxation[2]

2.3.1 Spin-lattice relaxation

When the excitation pulse is discontinued the individual nuclei begin to undergo relaxation by releasing the absorbed rf energy to the surrounding lattice causing primarily increased molecular translations and rotations. In this manner, the original thermal equilibrium Boltzmann population of nuclear spins is re-established. The relaxation time T_1 is characteristic of the time required for the magnetization to realign itself along the z axis and depends on the mechanisms available for the transfer of energy. Although there are several mechanisms by which this transfer can occur, the common feature of all spin-lattice relaxation processes is that they depend on the existence of some molecular motion to generate a randomly varying magnetic field or electric field gradient which will have a local field component fluctuating at the Larmor frequency of the nucleus to be relaxed. It is important to note that T_1 is determined by molecular motions. Temperature and viscosity influence translational and tumbling motions whereas molecular size, shape and viscosity determine rotational motions. In solution large polymeric molecules tumble at rates comparable to the precessional frequencies providing effective relaxation mechanisms and leading to short relaxation times. Small molecules undergo rotational reorientation at rates considerably faster and T_1 is found to be long, several seconds or more, because the transfer of energy is inefficient. In solids, where atomic and molecular motions are severely restricted, T_1 can last for hours. Lattice vibrations are ineffective in providing the appropriate fluctuating internal magnetic fields because their frequencies are much higher than the usual Larmor frequencies.

---

[2] Taken from Carrington and McLachlan (1), Farrar and Becker (3) and Shaw (5).

The optimum pulse angle in a Fourier transform NMR experiment can easily be determined with the knowledge of the spin-lattice relaxation time. It is given by the Ernst angle α_E (6), where:

$$\cos\alpha_E = \exp(-T/T_1), \qquad [2\text{–}7]$$

and T is the repetition time, *i.e.* the time between successive excitation pulses.

The longitudinal relaxation time T_1 can be measured with the inversion recovery pulse sequence: $(T-180°_x-\tau-90°_x-\mathrm{FID})_n$, where the subscript after a pulse represents the phase of the pulse. The T delay establishes or re-establishes the Boltzmann equilibrium between the populations. A first $180°_x$ pulse inverts the magnetization vector towards the $-z$ axis. Since no component of this vector lies in the xy plane, the return to equilibrium is governed by the relaxation time T_1 only. After a variable time τ, a $90°_x$ pulse brings the magnetization on the $\pm y$ axis. The FID can then be detected and its initial amplitude is proportional to M_z at the time τ.

The return to equilibrium of M_z is given by the differential equation:

$$dM_z/dt = -(M_z - M_0)/T_1, \qquad [2\text{–}8]$$

which gives after integration:

$$M_z = M_0[1 - 2\exp(-\tau/T_1)]. \qquad [2\text{–}9]$$

In practice, to account for pulse imperfections and nonequilibrium conditions, the data is fitted to the following equation:

$$A(\tau) = c_2 + c_3\exp(-\tau/c_1), \qquad [2\text{–}10]$$

where $A(\tau)$ represents the amplitude of the signal following the $90°_x$ pulse at time τ. From Equation [2–9], the delay T between each pulse sequence must be at least $5T_1$ to allow for the complete return of the magnetization to the $+z$ axis.

2.3.2 Spin-spin relaxation

A second process called spin-spin relaxation T_2 can take place during the NMR experiment. The NMR signal detected in the *xy* plane, the FID, exponentially decreases with time. If when the excitation pulse ends all the nuclei in the sample were experiencing the identical field strength, then the individual nuclear moments would continue to precess in phase and the rotating component in the *xy* plane would disappear at a rate governed by T_1, which reflects the return alignment of $\boldsymbol{M}$ along the *z* axis. In a typical sample where molecular diffusion and reorientation are occurring, the precessing nuclei experience varying internuclear magnetic fields. With nuclei distributed over a range of field strengths, the individual moments begin to precess at different frequencies causing dephasing, cancellation and diminishing intensity of the signal. It is worth noting that this spin-spin or transverse relaxation time T_2 can be shorter than T_1 but never longer. For liquids T_2 can be as long as several seconds and tends to be not too different from T_1, but for solids T_2 is much smaller with values falling in the microsecond range.

Moreover, since the fields created by real magnets are not uniform over the entire volume of the sample, this inhomogeneity also contributes to the dephasing of the magnetic vectors, causing the FID to decay faster than it would if the field were perfectly homogeneous. The true molecular relaxation time T_2 is inversely related to the natural linewidth and is distinguished from the time constant T_2^*, which is characteristic of the rate of decay of the signal in an imperfect field.

The spectral resolution as measured by the linewidth at half-height $\Delta\nu_{1/2}$ is essentially governed by T_2^* according to:

$$\Delta\nu_{1/2} = 1/\pi T_2^*. \qquad [2\text{–}11]$$

By the application of appropriate pulse sequences it is possible to identify and cancel contributions from field inhomogeneities and determine the sample intrinsic T_2 value. The pulse sequence used to measure T_2 is the spin echo: $(T-90°_x-\tau-180°_x-\tau-\text{echo})_n$. The first $90°_x$ pulse brings the magnetization vector along the $+y$ axis. During the time τ, the individual components of the magnetization vector precess at different frequencies in the xy plane, since they each experience a different value of the field. A dephasing of the different component vectors follows, which can be inverted after a time τ by a $180°_x$ pulse. The vectors, which diverged previously, now converge at the same relative frequency with respect to the rotating frame and are all aligned along the $-y$ axis after another time τ.

The amplitude of the magnetization vector M_y at the time 2τ depends on T_2 according to:

$$dM_y/dt = -M_y/T_2, \qquad [2\text{–}12]$$

which gives after integration:

$$M_y = M_0\exp(-2\tau/T_2). \qquad [2\text{–}13]$$

In practice, an equation of the form of Equation [2–10] is used.

For the vectors to converge exactly along the $-y$ axis in the spin echo method, each nucleus must experience the same magnetic field during the time 2τ. This is not always the case, since nuclei diffuse from one part of the field to another.

The effects of diffusion can be reduced with the Carr-Purcell technique. The sequence is: $T-90°_x-\tau-180°_x-\tau-\text{echo}-\tau-180°_x-\tau-\text{echo}-\tau-...$, where τ is made small enough for the diffusion to be negligible. The difference with the spin echo sequence is that, after vector dephasing, another $180°_x$ pulse is applied at a time 3τ after the initial $90°_x$ pulse, which brings the vectors back into phase again along the $+y$ axis at 4τ. Successive $180°_x$ pulses at 5τ, 7τ, etc. cause echos at 6τ, 8τ, etc., which are alternately positive and negative.

A modification of the above sequence, the Carr-Purcell-Meiboom-Gill (CPMG) technique allows the reduction of the cumulative effects caused by pulse length misadjustments in the multipulse sequence. The CPMG sequence is: $T-90°_x-\tau-180°_y-\tau-\text{echo}-\tau-180°_y-\tau-\text{echo}-\tau-...$, where the phase of the 180° pulses is shifted by 90° with respect to the initial 90° pulse. Only positive echos are obtained with this sequence. If the first $180°_y$ pulse is slightly too short, the magnetization vectors will rephase above the $+y$ axis, reducing the echo amplitude. However, the next $180°_y$ pulse will be just long enough to bring back the vectors exactly in the xy plane. Thus, the second echo and all even echos have the good amplitude; odd echos are less intense, but in a noncumulative way.

2.3.3 Relaxation mechanisms

Local magnetic fields can be generated in many ways. Some of the important mechanisms that contribute to the spin-lattice and spin-spin relaxation processes are: internal dipole-dipole interaction, spin rotation, chemical shift anisotropy, scalar coupling and quadrupolar interaction. Table 2–1 summarizes the mathematical form of these various magnetic fields and the appropriate molecular correlation time. The expected form of any equations describing nuclear relaxation resulting from random molecular motion will be:

Table 2–1. Summary of relaxation mechanisms[a].

Mechanism	$<b_{loc}^2>^b$	Correlation time
Dipole-dipole		
nuclear-nuclear	$\mu_0^2\gamma_I^2\gamma_S^2\hbar^2I(I+1)/16\pi^2r_{IS}^6$	reorientational
electron-nuclear		translational
Spin rotation[c]	$2I'kT(2C_\perp^2 + C_\parallel^2)/3\hbar^2$	angular momentum
Chemical shift anisotropy[c]	$\gamma^2B_0^2(\sigma_\parallel - \sigma_\perp)^2$	reorientational
Scalar coupling	$^2/_3S(S+1)(2\pi J)^2$	exchange or excited state lifetime
Quadrupolar	$[(2I+3)/I^2(2I-1)](1+\eta^2/3)(e^2qQ/4\pi\epsilon_0\hbar)^2$	reorientational

[a] From Shaw (5).

[b] Symbols: $\hbar$, Planck's constant divided by 2π; k, Boltzmann constant; e, charge of the electron; μ_0, permeability of vacuum; ϵ_0, permittivity of vacuum; T, absolute temperature; I', moment of inertia; B_0, applied magnetic field; I, nuclear spin; S, coupled spin; r_{IS}, distance between spins I and S; γ, magnetogyric ratio; Q, quadrupole moment; $C_\parallel$ and $C_\perp$, parallel and perpendicular components of the spin rotation tensor; $\sigma_\parallel$ and $\sigma_\perp$, parallel and perpendicular components of the chemical shielding tensor; J, spin-spin coupling constant; q, electric field gradient; η, asymmetry parameter of the electric field gradient; $<b_{loc}^2>$, mean square average of the interaction.

[c] Assuming axial symmetry.

$$2\pi/T_1 = <b_{loc}^2>[c_1\tau_c/(1 + \omega^2\tau_c^2)], \quad [2\text{–}14]$$

$$2\pi/T_2 = <b_{loc}^2>[c_2\tau_c + c_3\tau_c/(1 + \omega^2\tau_c^2)], \quad [2\text{–}15]$$

where $<b_{loc}^2>$ is the mean square average of the local field at the nucleus expressed in rad^2/s^2 and τ_c the correlation time for the process.

2.3.3.1 Internuclear dipole-dipole interaction

Two neighboring magnetic nuclei will experience not only the external magnetic field but also the local fields produced by each other the strength and direction of which depends on their respective magnetic moments, internuclear separation and orientation in the field. Constantly changing orientations of the two nuclear spins generates fluctuating local fields which stimulate relaxation of nuclei. This is the most important mechanism for spin $I = {}^1/_2$ nuclei.

Another case of this interaction is where the relaxing field has its origin with an electron spin rather than a nuclear spin, *e.g.* from any paramagnetic species present in the sample. Since the magnetic moment of the electron is roughly three orders of magnitude greater than nuclear moments, the fields are correspondingly more intense. When modulated by molecular tumbling, such fields can then induce very efficient relaxation.

2.3.3.2 Spin rotation

The next most important relaxation mechanism for spin $I = {}^1/_2$ nuclei, especially in small molecules, is spin rotation. A freely rotating molecule or molecular segment has associated with it a constant molecular magnetic moment which fluctuates when collision with other molecules occurs. The mechanism is most efficient for small symmetrical molecules at high temperatures and is very

significant when dealing with molecules in the gas phase. Nuclei relaxed partially by spin rotation show a nonlinear behavior in relaxation time as a function of temperature.

2.3.3.3 Chemical shift anisotropy

Electrons in a molecule produce an auxiliary field the direction and magnitude of which depends on the spatial disposition of the electronic orbitals with respect to the static field. Fluctuating local fields are generated when the molecule moves in the field. The mechanism can be detected by its dependence on the square of the operating field.

2.3.3.4 Scalar coupling

If a nucleus *I* is spin-spin coupled with a second nucleus *S*, it is possible for *S* to provide a fluctuating magnetic field, and hence a relaxation mechanism, at the first nucleus via scalar interactions involving the bonding electrons. Fluctuations can occur from two sources, firstly from any time dependence of their spin coupling constant, and secondly from the time dependence of the excited state of spin *S*.

2.3.3.5 Quadrupolar interaction

For a nucleus with a quantum number greater than $^1/_2$, there is an additional relaxation process available which occurs via interactions with a fluctuating electric field, as opposed to magnetic field. A spin $I = {}^1/_2$ nucleus has a spherical nuclear charge distribution; for nuclei with a higher quantum number, the charge distribution is nonspherical, resulting in their having a quadrupole moment *Q*. Quadrupolar nuclei do not have an electric dipole moment, hence their energy is

independent of orientation in a uniform electric field. However, in the presence of an electric field gradient, they precess about the net electric field, and in doing so provide a relaxation mechanism.

2.4 Basic nuclear spin interactions in solids[3]

This section summarizes the basic nuclear spin interactions which occur in solids. The notation will be in tensorial form throughout to emphasize the anisotropy of these interactions.

First, nuclear spin interactions between external fields ($\boldsymbol{B_0}$ and $\boldsymbol{B_1}$) and internal fields are distinguished. The total spin Hamiltonian H is thus given by:

$$H = H_{ext} + H_{int}, \qquad [2\text{–}16]$$

where

$$H_{ext} = H_0 + H_1. \qquad [2\text{–}17]$$

H_0 and H_1 are the Hamiltonians for the Zeeman interaction with the external fields $\boldsymbol{B_0}$ and $\boldsymbol{B_1}$, respectively. The spin interaction of two different types of spins $\boldsymbol{I}$ and $\boldsymbol{S}$ with internal fields may be written as:

$$H_{int} = H_S + H_D + H_J + H_Q, \qquad [2\text{–}18]$$

where H_S is the shielding Hamiltonian, H_D and H_J the direct and indirect interactions among spins $\boldsymbol{I}$ and $\boldsymbol{S}$, and H_Q the quadrupole interaction Hamiltonian.

---

[3] Taken from Mehring (7).

Table 2–2 gives the form of the Hamiltonian for the interactions with internal fields. All Hamiltonians are expressed in angular frequency units for convenience. It is assumed that the symmetry of the solid is such that all the spin interactions can be represented by second-rank Cartesian tensors. Coupling of the spin I to the external fields is expressed as:

$$H_{0I} = \boldsymbol{I} \cdot \boldsymbol{Z} \cdot \boldsymbol{B_0}, \qquad [2\text{–}19]$$

$$H_{1I} = \boldsymbol{I} \cdot \boldsymbol{Z} \cdot \boldsymbol{B_1}, \qquad [2\text{–}20]$$

where

$$\boldsymbol{B_0} = (B_x, B_y, B_z), \qquad [2\text{–}21]$$

$$\boldsymbol{B_1} = 2(B_{1x}(t).\, B_{1y}(t), B_{1z}(t))\cos\omega t, \qquad [2\text{–}22]$$

$$\boldsymbol{Z} = -\gamma \mathbf{1}, \qquad [2\text{–}23]$$

and $\mathbf{1}$ is the unit matrix.

2.5 NMR in solids

2.5.1 Chemical shift anisotropy

In liquids, rapid and random molecular tumbling occurs and the frequencies are averaged to the isotropic value that is observed as a narrow line. As the rigidity of the sample lattice increases, this motional averaging diminishes.

In polycrystalline samples or amorphous powders some molecules will be aligned parallel to the field, some perpendicular, and others will assume the full range of possible orientations between these limits. The interaction between the

Table 2–2. Spin Hamiltonians for interactions with internal fields[a].

Interaction	Form of the Hamiltonian[b]
Chemical shift	$H_S/h = \gamma \boldsymbol{I} \cdot \underline{\sigma} \cdot \boldsymbol{B_0}$
Dipole-dipole	$H_D/h = \Sigma_{i<j} (\mu_0 h \gamma_i \gamma_j / 4\pi r_{ij}^3)[\boldsymbol{I}_i \cdot \boldsymbol{I}_j - 3(\boldsymbol{I}_i \cdot \boldsymbol{r}_{ij})(\boldsymbol{I}_j \cdot \boldsymbol{r}_{ij})/r_{ij}^2]$
	$H_D/h = \Sigma_{i=j} \boldsymbol{I}_i \cdot \boldsymbol{D} \cdot \boldsymbol{I}_j$
	$D_{\alpha\beta} = (\mu_0 h \gamma_i \gamma_j / 4\pi r_{ij}^3)(\delta_{\alpha\beta} - 3e_\alpha e_\beta)$
	$\alpha, \beta = x, y, z$
Spin-spin coupling	$H_J/h = 2\pi \Sigma_{i \neq j} \boldsymbol{I}_i \cdot \boldsymbol{J} \cdot \boldsymbol{I}_j$
Quadrupole	$H_Q/h = [eQ/2I(2I - 1)h] \boldsymbol{I} \cdot \boldsymbol{V} \cdot \boldsymbol{I}$

[a] From Mehring (7).

[b] Symbols: h, Planck's constant divided by 2π; e, charge of the electron; γ, magnetogyric ratio; Q, quadrupole moment; δ, Kroenecker symbol; e_α, α-component of the unit vector along $\boldsymbol{r}_{ij}$; $\boldsymbol{I}$, spin angular momentum; $\boldsymbol{B_0}$, applied magnetic field; $\boldsymbol{r}$, internuclear vector; $\underline{\sigma}$, chemical shielding tensor; $\boldsymbol{D}$, dipolar coupling tensor; $\boldsymbol{J}$, spin-spin coupling tensor; $\boldsymbol{V}$, electric field gradient tensor.

electrons surrounding a nucleus and the applied field produces an effective field at each nuclear site which depends on the orientation of the molecule in the applied field. Thus, even chemically identical nuclei in different molecules may be shielded from the external field to varying extents and the powder patterns that result reflect the three-dimensional nature of this chemical shielding anisotropy.

2.5.2 Dipolar broadening

The dominant forces acting on dilute nuclei arise from the direct nuclear dipole-dipole interaction between the rare nuclei and their nearby abundant neighbors (usually protons). The strength of this interaction and the local field $\boldsymbol{B}_{loc}$ produced by the abundant nucleus at the rare nucleus site vary inversely with the third power of the distance vector $\boldsymbol{r}$ between the two nuclei and with θ, the angle between the internuclear vector and the static magnetic field $\boldsymbol{B}_0$. This relationship may be expressed as:

$$\boldsymbol{B}_{loc} \sim \pm(3\cos^2\theta - 1)/2r^3. \qquad [2\text{–}24]$$

The effective field $\boldsymbol{B}_{loc}$ at the nucleus is either greater or less than the static field $\boldsymbol{B}_0$, depending on whether the neighboring dipole is aligned with or against the field. Since the probabilities of these two alignments are almost equal, the rare spin resonance is split into a characteristic doublet the width of which is a function of θ. For a polycrystalline sample, each nucleus is dipolar coupled to many neighboring rare spins each with somewhat different values of r and θ. The result is the overlap of the various dipolar splittings to give the broadline spectrum.

A relation known as Van Vleck's formula (1) gives the second moment. For the heteronuclear case, its has the form:

$$(2\pi\Delta\nu)^2 = (\mu_0{}^2/60\pi^2)\gamma_I{}^2\gamma_S{}^2\hbar^2(1/n)S(S+1)\Sigma_i{}^n(1/r_i{}^6), \qquad [2\text{–}25]$$

and for the homonuclear case:

$$(2\pi\Delta\nu)^2 = (3\mu_0{}^2/80\pi^2)\gamma_I{}^4\hbar^2(1/n)I(I+1)\Sigma_i{}^n(1/r_i{}^6). \qquad [2\text{–}26]$$

2.5.3 High-power decoupling

Heteronuclear proton dipolar contributions to the rare nucleus linewidths can be removed by an alternative approach. If while the spectrum is recorded the sample is simultaneously irradiated at the proton resonance frequency the result is that rapid transitions between the two proton spin states are induced effectively eliminating the dipolar field created by the protons at the rare nuclei. Since the strength of this dipolar interaction is substantial, a powerful decoupling field is required.

2.5.4 Cross polarization[4]

In most chemically interesting solids containing two nuclear species, it is usually the proton that is the abundant magnetic nucleus and the other is considered the rare nucleus. The rarity may be due to low natural abundance as with ^{13}C and ^{15}N, or it may be due to high magnetic dilution as in the case with isotopes such as ^{31}P and ^{14}N which frequently occur in a lattice rich in nonmagnetic nuclei (*e.g.* ^{16}O and ^{12}C). In one respect, this is a fortunate situation because it lessens the complications that might otherwise arise from homonuclear dipolar interactions which are not removed by proton decoupling.

Although concentration dependence is important, the more serious difficulty hampering NMR measurements on rare nuclei is the exceedingly long

---

[4] From Pines *et al.* (8) and Yannoni (9).

spin-lattice relaxation times. Fortunately, cross-polarization techniques overcome the problem of low sensitivity in the detection of the rare nucleus.

The concept of spin temperature is useful in discussing the cross-polarization strategy. For rare nuclei in a static field the difference in energy between two spin alignments is $\Delta E = \gamma \hbar B_0$. The ratio of the populations in the two spin states is given by the Boltzmann relation:

$$N_B/N_A = \exp(-\Delta E/kT_S), \qquad [2\text{–}27]$$

where A and B refer to the lower and upper states, respectively. Here T_S is defined as the spin temperature and this does not necessarily correspond to the situation in which the spin system is in thermal equilibrium with its lattice environment. Since the net magnetization available for detection in an NMR experiment is proportional to the population difference $N_A - N_B$, a low rare nucleus spin temperature, implying a large polarization of the magnetic moments, is desirable. To achieve this, advantage is taken of the fact that the abundant protons surrounding the rare nuclei usually undergo spin lattice relaxation much faster than the rare nuclei and under appropriate conditions magnetization can be transferred from the protons to the rare nuclei.

A typical cross-polarization experiment viewed from a rotating frame of reference begins with the application of a 90° pulse that tips the net proton magnetization into a plane perpendicular to the static field $\boldsymbol{B_0}$. Immediately following the pulse while continuing the proton irradiation, the phase of the driving rf field $\boldsymbol{B_1}$ is shifted by 90° so that it is collinear with the magnetization and the two are spin locked to each other. Thermodynamically, this nonequilibrium condition is equivalent to a lowering of the proton spin temperature in this rotating frame. The large magnetization that originally corresponded to and was locked along $\boldsymbol{B_0}$ at the

beginning of the experiment is now locked along the effective field B_1. This field is perpendicular to the external field B_0 and is several orders of magnitude less.

During the spin lock period, the rare nucleus transmitter is turned on and thermal contact is made between the cooled protons and the warm dilute nuclei. In the spin temperature sense, thermal contact means that two spins exchange energy as one undergoes a transition from a lower to a higher spin state and the other makes the opposite transition. For identical nuclei in a uniform field the same quantum of energy is involved in the two transitions, but this is not the case for dissimilar nuclei. To establish the cross-polarization transfer of magnetization between abundant—rare spin pairs requires having the two nuclei simultaneously under the influence of different effective fields so that their Larmor frequencies in the rotating frame become equal and the Hartmann-Hahn condition

$$\gamma_I B_I = \gamma_S B_S \qquad [2\text{–}28]$$

is satisfied. This is accomplished by the adjustment of both the proton (B_S) and rare nucleus (B_I) rf power levels. The oscillating field seen at one nucleus due to another will then have the correct frequency to induce mutual spin transitions.

The Hartmann-Hahn condition is maintained for a short period so that cross-polarization can occur causing a build-up of rare nucleus magnetization which is proportional to the proton magnetization previously developed. In the final step, proton irradiation is maintained while the rare nucleus FID is observed in the usual manner.

The cross-polarization technique affords two significant benefits. One is that the rare signal is enhanced by the abnormally large rare nucleus spin polarization that has been created and this can be as much as γ_S/γ_I that obtained by a single pulse excitation. The other is that the cross-polarization process is more

efficient than the normal rare nucleus spin lattice relaxation process permitting the pulse repetition rate to be increased because the interpulse delay is now governed by the shorter proton relaxation rate.

2.6 NMR of membranes

Membranes are ordered fluids and because of this have a number of properties in common with liquid crystals. Most important, the normal to the surface of the lipid bilayer constitutes an axis of motional averaging. From an optical point of view, the membrane therefore behaves like an uniaxial crystal with the bilayer normal as the optical axis. This unique axis of the fluid bilayer is also called the director. If the phospholipids constituting the bilayer are represented by rigid rods and the movements of the individual molecules are followed over a long enough period of time, the most probable orientation of the rods will be parallel to the director axis. However, due to thermal energy, the molecules will continuously execute angular excursions around this preferred orientation. As a quantitative measure for the angular excursions and fluctuations around the director, the concept of order parameters has been introduced (10). If δ is the instantaneous angle between the rod-like molecule and the director, then the order parameter is defined as:

$$S = {}^1/_2 < 3\cos^2\delta - 1 >, \qquad [2\text{-}29]$$

where the brackets denote a time average. This is actually a rather simplified representation of the order parameter formalism. It is fortunately valid for ^{2}H NMR, where it provides a physically unambiguous description of the average orientation of the C$-^2$H bond vector. Due to symmetry of the electric field gradient around the C$-^2$H bond vector, one order parameter is sufficient to specify the average orientation of a C$-^2$H bond. However, there are many spectroscopic problems

where more than one order parameter is needed, in fact, the most general case would require a 3 × 3 ordering matrix (10).

2.6.1 ^{2}H NMR[5]

Deuterium NMR has proven to be particularly useful for determining the motional anisotropies in membranes. A few unique features of this method should be pointed out. The first step is the selective deuteration of the molecule of interest. This may be achieved either by chemical synthesis or by biochemical incorporation. One of the obvious advantages of selective deuteration is the fact that the replacement of hydrogen by deuterium does not perturb the system. A second advantage is the ease of assignment of the deuterium resonances. The natural abundance of deuterium is low, and in a selectively deuterated membrane the observed signal can be assigned unambiguously. The magnetic moment of the nuclear spin of the deuterium nucleus is by a factor 6.5 smaller than that of the hydrogen, which decreases the sensitivity of the measurements. However, dipolar couplings are also reduced by the same factor. The dominant relaxation mechanism in ^{2}H NMR is quadrupolar relaxation.

2.6.1.1 ^{2}H NMR of liquid crystalline systems

The main asset of ^{2}H NMR is the possibility to detect and quantitate anisotropic motions in microscopically ordered systems such as bilayers or hexagonal lipid phases. A macroscopic ordering of these systems is not necessary; it is possible to work with random dispersions of lipid bilayers.

---

[5] From Smith and Mantsch (11) and Smith (12).

Deuterium is a spin $I = 1$ nucleus and as such has a quadrupolar moment. In a magnetic field $\boldsymbol{B}_0$, there are three allowed spin orientations as indicated in Figure 2–1. The magnetic energy levels are equally spaced and the $m_I = +1 \rightarrow m_I = 0$ and $m_I = 0 \rightarrow m_I = -1$ transitions are therefore degenerate. In isotropic solutions, only a single absorption line is observed. However, in anisotropic systems, there is an additional perturbation due to the quadrupolar interaction. This interaction of the electric quadrupole moment of the deuterium nucleus with the surrounding bonding electrons leads to a first order perturbation of the magnetic energy levels shifting them to different extent. The singlet is split into a doublet with the frequency separation of the two resonances being called the quadrupole splitting $\Delta\nu_Q$.

When the electric field gradient tensor is symmetric, the quadrupole splitting is given by:

$$\Delta\nu_Q(\theta) = {}^3/_4(e^2qQ/4\pi\epsilon_0 h)\,|3\cos^2\theta - 1|, \qquad [2\text{–}30]$$

where $e^2qQ/4\pi\epsilon_0 h$ is the quadrupole coupling constant and θ the angle between the principal axis of the electric field gradient tensor – usually the C–^{2}H bond direction – and the applied magnetic field. If in a sample all orientations are equally probable, as in a polycrystalline sample, there will be a continuum of doublets covering all values of θ. The case of a multilamellar lipid dispersion is illustrated in Figure 2–2. The separation between the two most intense peaks in the spectrum is given by:

$$\Delta\nu_Q(90°) = {}^3/_4(e^2qQ/4\pi\epsilon_0 h). \qquad [2\text{–}31]$$

In subsequent discussions, the term quadrupole splitting will refer to that for the angle $\theta = 90°$.

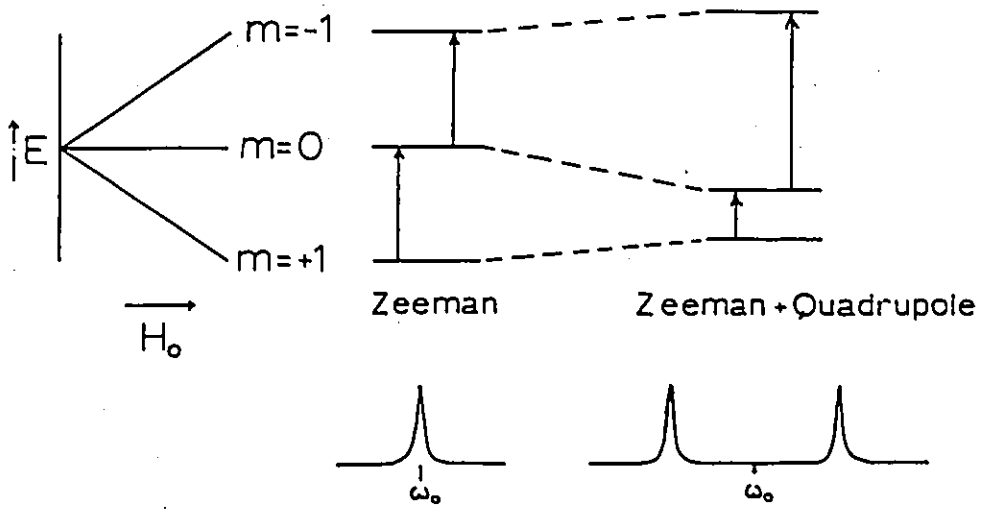

Figure 2–1. Effect of the quadrupolar interaction on the Zeeman energy levels of a spin $I = 1$ nucleus with axial symmetry. I is the total spin, m its component and θ the angle between the applied magnetic field and the principal axis of the electric field gradient tensor. Adapted from Smith and Mantsch (11).

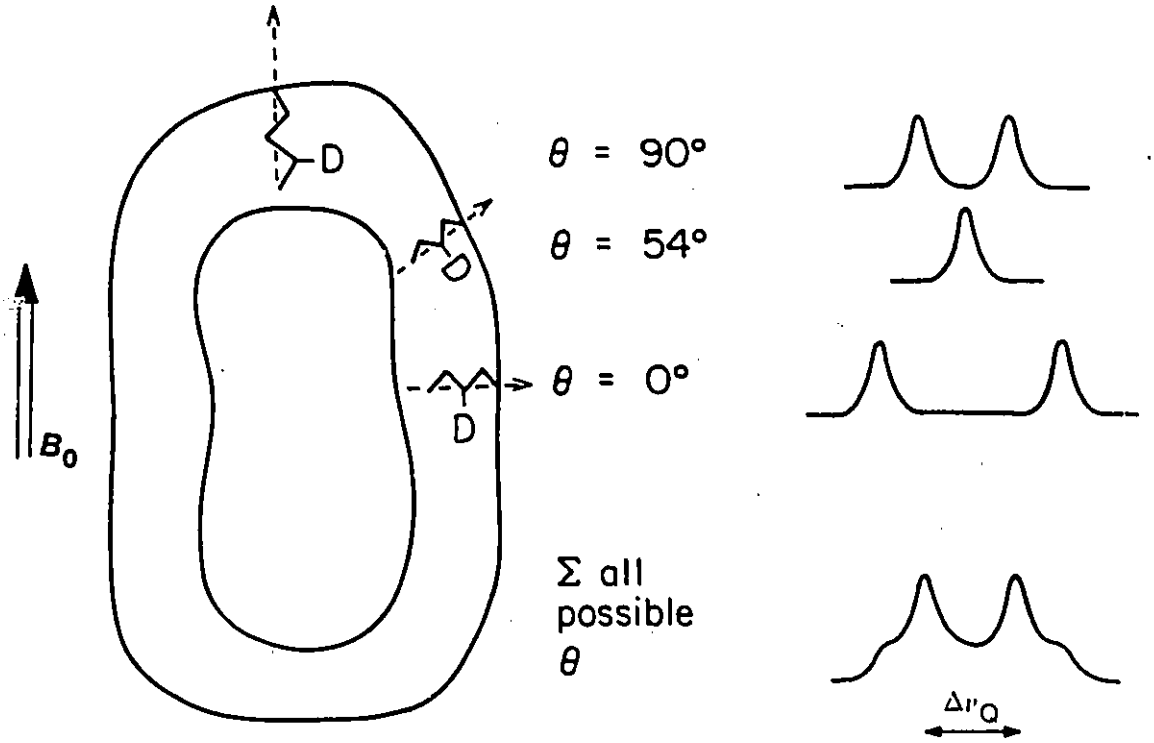

Figure 2–2. Origin of the powder-type ^2H NMR spectra observed for membranes. Different angles between the magnetic field B_0 and the axis of motional averaging (dashed arrows) lead to different quadrupole splittings. Since membranes rotate slowly on the timescale of ^2H NMR splittings, all these subspectra will contribute to the observed powder spectrum. The quadrupolar splitting $\Delta\nu'_Q$ corresponds to the separation observed for $\theta = 90°$ and leads to a simple measure of the order parameter. Adapted from Smith (12).

In liquid crystals, molecules are not static but fluctuate anisotropically in the sample. The average over this fluctuation is expressed by the order parameter S_{C-^2H} according to:

$$S_{C-^2H} = {}^1/_2 < 3\cos^2\beta - 1 >, \qquad [2\text{–}32]$$

where β is the time-varying angle between the major axis of the electric field gradient and the director. Thus, in multilamellar dispersions or any similar systems, the quadrupole splitting of Equation [2–31] is effectively reduced by a factor S_{C-^2H}:

$$\Delta\nu_Q = {}^3/_4(e^2qQ/4\pi\epsilon_0 h)|S_{C-^2H}|. \qquad [2\text{–}33]$$

The relation between the order parameter of the long molecular axis S and that of the $C-^2H$ bond S_{C-^2H} is given by:

$$S_{C-^2H} = {}^1/_2 < 3\cos^2\alpha - 1 > S, \qquad [2\text{–}34]$$

where α is the angle between the long axis of the molecule and the $C-^2H$ bond direction. For a rigid molecule, the angular brackets can be removed and a molecular order parameter can be calculated directly from the quadrupolar splitting.

2.6.1.2 Instrumental techniques

Special instrumental techniques are required to observe ^2H NMR spectra of membranes. Strong radiofrequency pulses must be used to cover wide spectral ranges, since all components must be equally excited to avoid distorsions. In other words, the Zeeman interaction with the applied rf field must dominate the quadrupole interaction across the entire spectrum. High sensitivity can be achieved by the use of high magnetic fields and special probe design. Wide spectral windows are obtained with high-speed analog-to-digital converters. This is also necessary to provide adequate time resolution of the rapidly decaying ^2H NMR

signals. The principal drawback in early ^2H NMR studies of membranes was this very fast signal decay. Figure 2–3 gives a view of the problem. Excitation of the spin system also excites the detection coil and the probe circuitry. This hardware excitation decays with a characteristic time determined by probe design. If observed, it introduces spurious signals into the detector. To avoid this aberration, a delay is usually inserted between the pulse and the start of data acquisition. If this delay is comparable to the decay time of the NMR signal, very poor baselines and a weak distorted NMR signal are obtained. These problems can be circumvented by the use of the quadrupole echo technique (13) (Figure 2–3) and a phase-altered acquisition sequence (14) (Figure 2–4). The quadrupole echo sequence involves two successive 90° rf pulses, differing in phase by 90°, and separated by a delay τ. When a residual quadrupole splitting is present in the system, the second 90° pulse leads to formation of an echo after another delay τ. If τ can be adjusted to be longer than the hardware ringdown time, no interference from the spurious signal occurs, and the full intensity of the echo may be utilized. With appropriate care to Fourier transform the echo from its maximum, spectral distortion is minimized.

In earlier use of quadrature detection to observe this type of spectrum, it was common to zero the data in one of the two quadrature channels before Fourier transformation. If the channels were perfectly orthogonal and properly balanced and phased, the pulses exactly 90°, and the transmitter on resonance, this situation would occur naturally. The overall effect of zeroing the second channel is to fold the spectrum about the transmitter frequency. This increases the signal-to-noise ratio by $2^{1/2}$ but has the potential of yielding artefacts in the transformed spectrum. The preferred way to acquire the echo is via a phase-alternated sequence, such as the CYCLOPS sequence shown in Figure 2–4. This has the effect of averaging out differences in channel response, achieving orthogonality of the channels, and removing any residual baseline distortions due to hardware

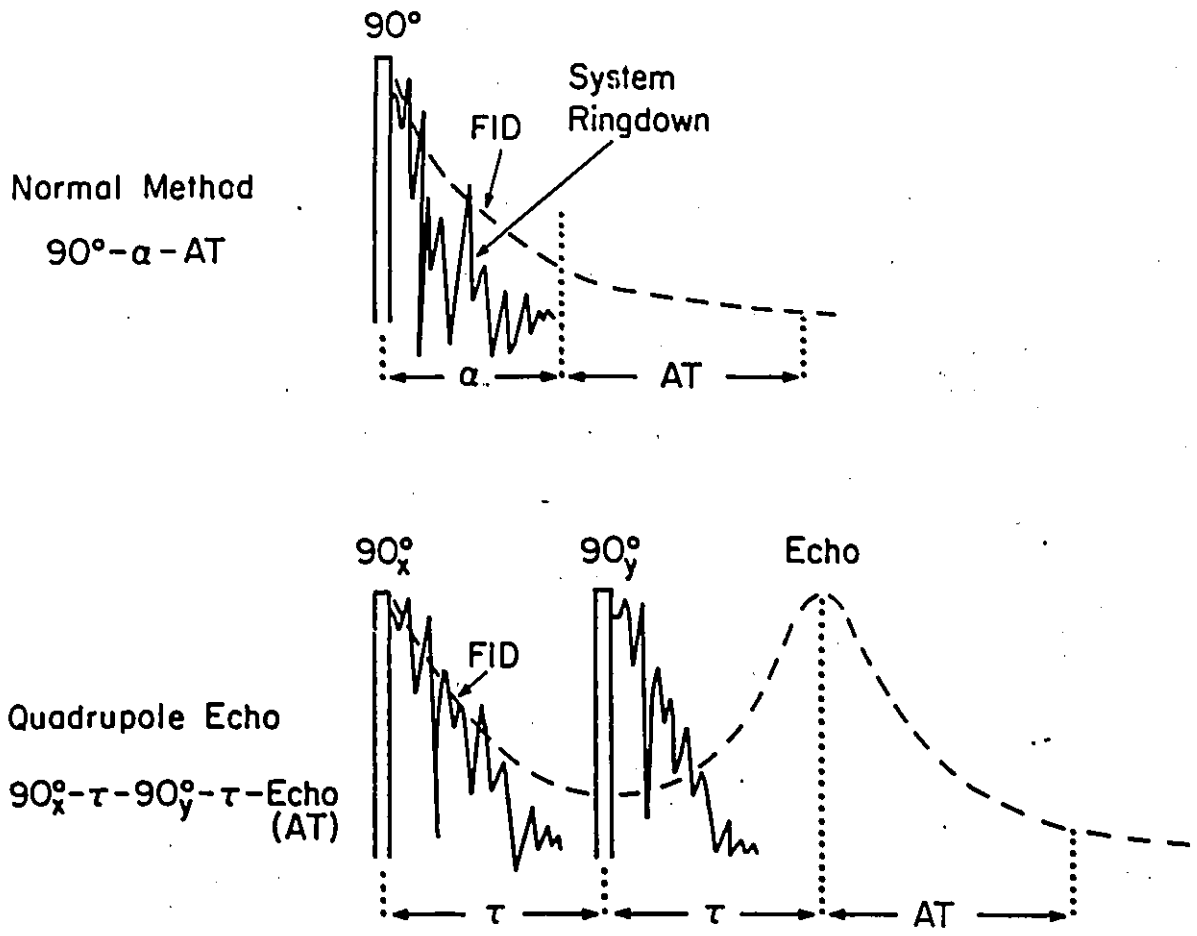

Figure 2–3. Schematic of the NMR behavior of a rapidly relaxing spin system with finite ringdown time of the receiver network after a normal 90° pulse and after a quadrupole echo sequence (13). AT represents the time during which data are digitized for Fourier transformation. Use of the echo sequence minimizes acquisition of any signal due to system ringdown. From Smith (12).

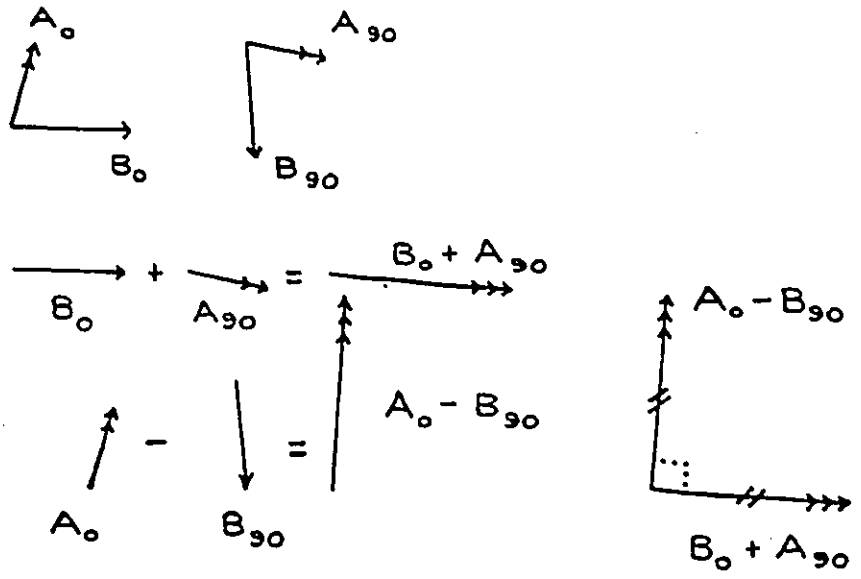

TRANSMITTER	CHANNEL 1	CHANNEL 2
0	+B	+A
90	+A	-B
180	-B	-A
270	-A	+B

Figure 2–4. Schematic of the CYCLOPS pulse sequence (14) employed to minimize the effects of amplitude imbalance and nonorthogonality of the two receiver channels (A and B) used for quadrature detection. Only the first two elements of the sequence (transmitter phase 0° and 90° are shown). Successive additions, in two separate channels of the computer, of signals according to the scheme at the bottom of the figure leads to an effectively balanced and phased situation. From Smith (12).

ringdown. Any phasing that is still required may be done on the time domain spectra. The final result is a spectrum of high fidelity with a very flat baseline.

2.6.2 ^{31}P NMR[6]

The natural abundance of ^{31}P is 100% and no synthetic labelling is necessary. ^{31}P has a nuclear spin $I = {}^1/_2$ and in an external magnetic field $\boldsymbol{B_0}$ only two spin orientations with the magnetic quantum numbers $m_I = +{}^1/_2$ and $m_I = -{}^1/_2$ are allowed. The complete Hamiltonian for the interaction of the nuclear spin and the magnetic field is the sum of the Zeeman and the chemical shielding interactions:

$$H = -\gamma\hbar(1 - \underline{\sigma})\boldsymbol{B_0}, \qquad [2\text{–}35]$$

where $\underline{\sigma}$, the chemical shielding tensor, is a measure of the screening of the applied field $\boldsymbol{B_0}$ via the bonding electrons. Considering the bonding pattern around a tetrahedral PO_4 segment in more detail, it is obvious that the electronic screening must be dependent on the orientation of the magnetic field with respect to the molecular coordinate system of the phosphate group.

2.6.2.1 ^{31}P NMR of membranes

The ^{31}P NMR chemical shift of a rigid phosphodiester, such as that found in membrane lipids, depends on its orientation with respect to the magnetic field $\boldsymbol{B_0}$. The three principal components of the chemical shift tensor are labelled σ_{11}, σ_{22} and σ_{33} (Figure 2–5). Knowledge of the principal components and the

---

[6] From Smith and Ekiel (15) and Seelig (16).

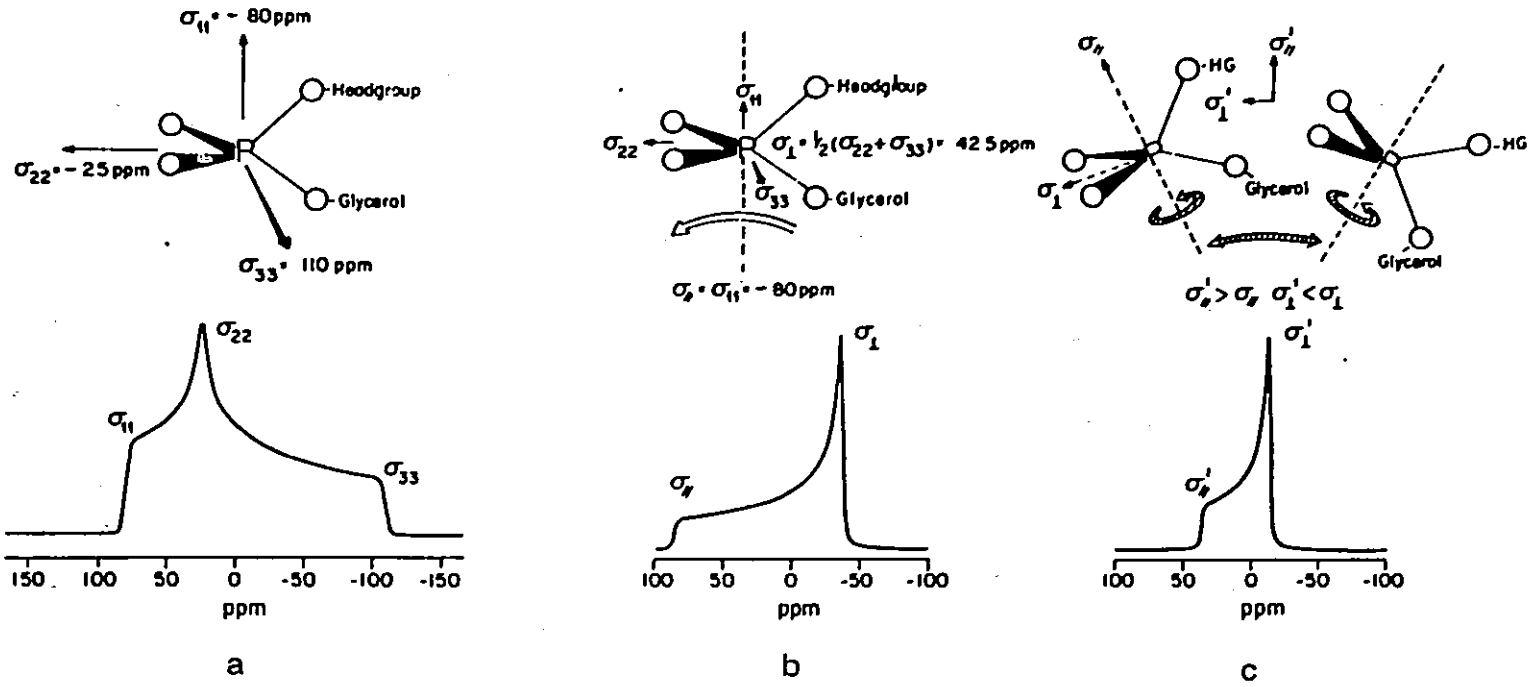
σ11 = −80ppm
Headgroup
σ22 = −25ppm
Glycerol
σ33 = 110 ppm
σ22
σ11
σ33
150 100 50 0 -50 -100 -150
ppm
a
σ11
Headgroup
σ22
σ1 = ½(σ22+σ33) = 42.5ppm
σ33
Glycerol
σ// = σ11 = −80ppm
σ1
σ//
100 50 0 -50 -100
ppm
b
σ//
HG
σ//'
σ1'
σ1
Glycerol
HG
Glycerol
σ//' > σ// σ1' < σ1
σ1'
σ//'
100 50 0 -50 -100
ppm
c

orientation of the principal axis system is required to calculate the chemical shift expected for any orientation:

$$\sigma = \sigma_{11}\cos^2\theta_1 + \sigma_{22}\cos^2\theta_2 + \sigma_{33}\cos^2\theta_3, \qquad [2\text{–}36]$$

where θ_i is the angle between the i^{th} principal axis of the chemical shielding tensor and the direction of $\boldsymbol{B_0}$.

For a microcrystalline sample, all angles between the applied magnetic field and the principal axes are populated. The ^{31}P NMR spectrum is thus the sum of spectra for all possible orientations. The resulting powder spectrum has distinctive features: σ_{11} and σ_{33} define the outermost edges and σ_{22} leads to a peak. The principal values of the tensor can be estimated directly from the spectrum, as shown in Figure 2–5(a). The directions of the principal axes in the molecular system can be found by studying a single crystal of known structure.

In membranes, rapid anisotropic motion that can average some of the components of the chemical shift tensor are allowed. For simplicity, motion about the 1 axis is supposed, thus averaging σ_{22} and σ_{33}:

$$\sigma_{\parallel} = \sigma_{11}, \qquad [2\text{–}37]$$

$$\sigma_{\perp} = (\sigma_{22} + \sigma_{33})/2. \qquad [2\text{–}38]$$

Thus, the chemical shift will have the same value for the field anywhere in the 23 plane, but a different value when the field is perpendicular to the plane; the tensor becomes axially symmetric, as shown in Figure 2–5(b). If rapid motion of limited amplitude of the 1 axis of the phosphodiester moiety is also allowed, the 1 axis moves in a cone and there is partial averaging of the former $\sigma_{\parallel}$ and $\sigma_{\perp}$ to yield new effective values $\sigma_{\parallel}'$ and $\sigma_{\perp}'$. This is represented in Figure 2–5(c). The effective tensor still has axial symmetry, but the total chemical shift anisotropy

$\Delta\sigma = \sigma_{\parallel}' - \sigma_{\perp}'$ is reduced. The amount by which it is reduced is related to the allowed amplitude of the motion. In solution, the motion is unrestricted and the pattern collapses to a single line. With a constant molecular geometry, the chemical shift anisotropy represents a measure of the degree of order of the phosphate group, but the shape and the width of the pattern depend critically on the orientation of the axis of motional averaging with respect to the principal components of the chemical shift tensor (17).

2.6.2.2 Types of phases

Figure 2–6 illustrates the bilayer and hexagonal arrangements of lipids, and the origin of the difference in the chemical shielding anisotropy. The cylinders in a hexagonal (H_{II}) phase have a very small radius, and therefore lateral diffusion about the cylinder axis can cause further averaging of the tensor components as compared with the bilayer-type spectrum. The unique axis of the system now becomes the axis of the cylinder and is labelled $\sigma_{\parallel}^{H}$. Along this axis, the field would be roughly normal to the fatty acyl chains, the value for $\sigma_{\parallel}^{H}$ would be equal to $\sigma_{\perp}^{L}$. On the other hand, owing to rapid motion around the cylinder axis, $\sigma_{\perp}^{H}$ will be an average of $\sigma_{\perp}^{L}$ and $\sigma_{\parallel}^{L}$:

$$\sigma_{\parallel}^{H} = \sigma_{\perp}^{L}, \qquad [2\text{–}39]$$

$$\sigma_{\perp}^{H} = (\sigma_{\parallel}^{L} + \sigma_{\perp}^{L})/2, \qquad [2\text{–}40]$$

$$\Delta\sigma^{H} = -\Delta\sigma^{L}/2. \qquad [2\text{–}41]$$

The net result is that the ^{31}P NMR powder pattern for the hexagonal phase has a $\Delta\sigma$ roughly half that of a corresponding lamellar phase and an opposite sidedness. When x-ray data is available, the ^{31}P NMR spectra can be properly interpreted. However, if this is not the case, some caution is necessary because the chemical

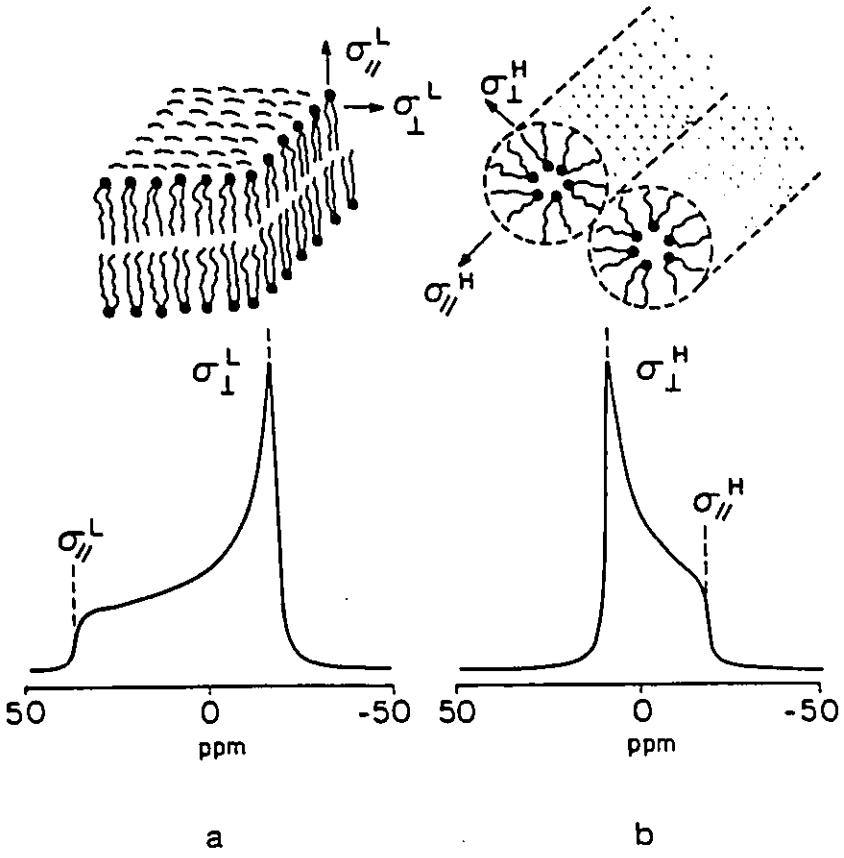

Figure 2–6. Representation of the bilayer (a) and hexagonal (b) phases formed by membrane lipids and their expected ^{31}P NMR spectra. From Smith and Ekiel (15).

shift anisotropy is also dependent on the geometry of the phosphate headgroup within the bilayer. A tilting of the headgroup out of a parallel conformation into a more perpendicular orientation can lead to a much smaller $\Delta\sigma$, or even to a change of its sign. In such cases, the phosphorus spectrum could appear identical to that of lipids in isotropic or hexagonal phases, respectively (17).

2.6.2.3 Instrumental considerations

As for ^2H NMR, the powder patterns for ^{31}P NMR can be quite broad, T_2 values can be quite short and T_1 values quite long. The first problem arising from the spectral width is circumvented by using short pulses which excite equally the nuclei contributing to all frequencies within the powder spectrum. A second problem arises from the long ringdown time after application of the rf pulse, as compared with the short T_2 values expected in these spectra. By analogy with the quadrupolar echo used in solid-state ^2H NMR spectroscopy, Rance and Byrd (18) reported the use of the analogous Hahn echo based on residual chemical shift anisotropy. A schematic of the behavior of the magnetization in the real (Re) and imaginary (Im) channels of a quadrature spectrometer is shown in Figure 2–7. A 90° (θ_1) pulse excites magnetization in the Re channel that decays in amplitude according to T_2. A 180° pulse (θ_2) after a delay τ results in a refocusing of this magnetization to reach an echo maximum in the Re channel after a further time τ. When the echo reaches a maximum in the Re channel, the magnetization in the Im channel passes through zero; this condition can be used to adjust the phase relationship between the quadrature channels using the time-domain signals. If the exact maximum of the echo can be determined and a Fourier transform done on half the echo starting from the time of maximum amplitude, no first-order phase correction should be required on the transformed signal. Extensive phase cycling of the two pulses serves to minimize other aberrations owing to errors in pulse length

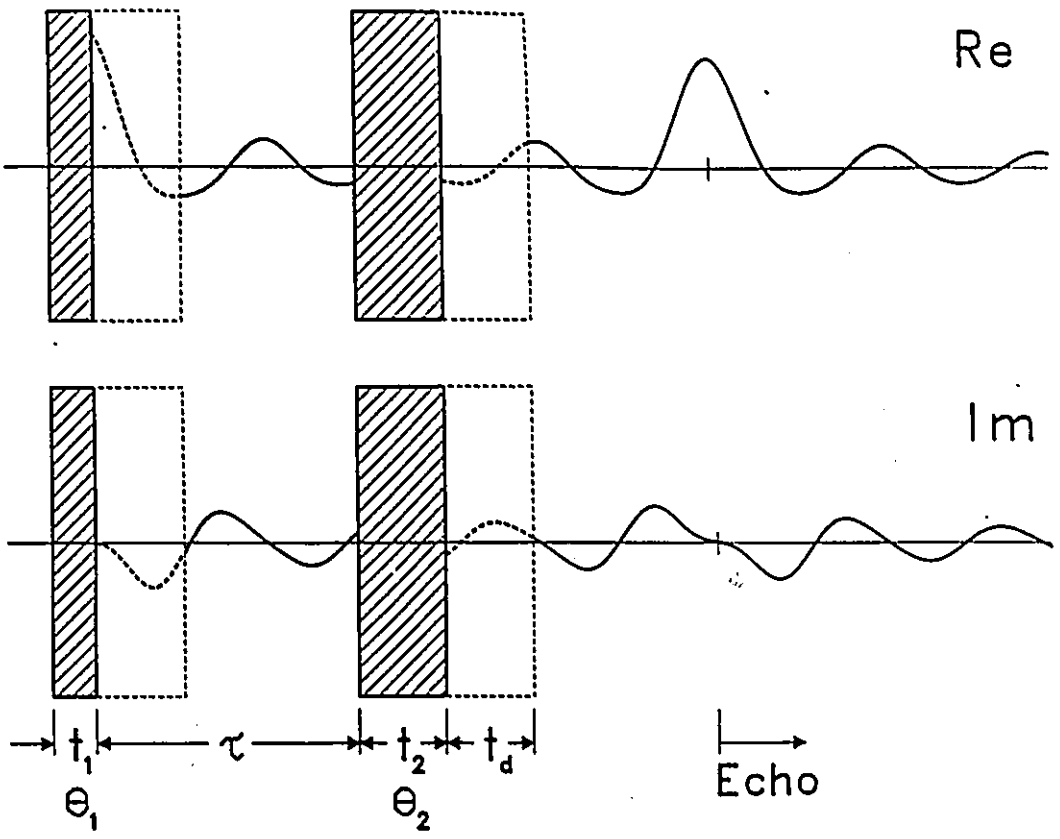

Figure 2–7. Schematic diagram of the events during a two-pulse Hahn echo sequence. Re and Im refer to the so-called real and imaginary NMR signal components, that is the two channels of the quadrature phase-sensitive detector. Ideally, $\theta_1 = 90°$ and $\theta_2 = 180°$, with phase cycling of θ_1 and θ_2. The dashed regions of NMR signals following the pulses represent the deadtime t_d of the receiver. From Rance and Byrd (18).

and channel imbalance. To avoid saturation effects, some estimate of the T_1 values of the system must be made and an appropriate recycling time employed. Alternatively, cross polarization could be used to gain in sensitivity and total experiment time.

2.7 References

1. A. Carrington and A.D. McLachlan, *Introduction to Magnetic Resonance with Applications to Chemistry and Chemical Physics* (Harper and How, New York, New York, 1967).

2. R.M. Lynden-Bell and R.K. Harris, *Nuclear Magnetic Resonance Spectroscopy* (Nelson, London, 1969), Chap. 1.

3. T.C. Farrar and E.D. Becker, *Pulse and Fourier Transform NMR: Introduction to Theory and Methods* (Academic Press, New York, New York, 1971), Chap. 1.

4. K. Müllen and P.S. Pregosin, *Fourier Transform NMR Techniques: A Practical Approach* (Academic Press, London, 1976).

5. D. Shaw, *Fourier Transform N.M.R. Spectroscopy*, second edition (Elsevier, Amsterdam, 1984).

6. R.R. Ernst and W.A. Anderson, *Rev. Sci. Instrum.* **37**, 93–102 (1966).

7. M. Mehring, *Principles of High Resolution NMR in Solids*, Second Edition (Springer-Verlag, Berlin-Heidelberg, 1983), Chap. 2, pp. 8–62.

8. A. Pines, M.G. Gibby and J.S. Waugh, *J. Chem. Phys.* **59**, 569–590 (1973).

9. C.S. Yannoni, *Acc. Chem. Res.* **15**, 201–208 (1982).

10. A. Saupe, *Angew. Chem. Intl. Ed. Engl.* **7**, 97–112 (1968).

11. I.C.P. Smith and H.H. Mantsch, in *NMR Spectroscopy: New Methods and Applications*, edited by G.C. Levy, *ACS Symposium Series* **191**, Chap. 6, pp. 97–117 (1982).

12. I.C.P. Smith, in *Biomembranes*, Vol. 12, edited by M. Kates and L.A. Manson (Plenum Press, New York, New York, 1984), Chap. 4, pp. 133–168.

13. J.H. Davis, K.R. Jeffrey, M. Bloom, M.I. Valic and T.P. Higgs, *Chem. Phys. Lett.* **42**, 390–394 (1976).

14. D.I. Hoult and R.E. Richards, *Proc. Roy. Soc. London* **A344**, 311–340 (1975).

15. I.C.P. Smith and I.H. Ekiel, in *Phosphorus–31 NMR, Principles and Applications*, edited by D.G. Gorenstein (Academic Press, Orlando, Florida, 1984), Chap. 15, pp. 447–475.

16. J. Seelig, *Biochim. Biophys. Acta* **515**, 105–140 (1978).

17. A.M. Thayer and S.J. Kohler, *Biochemistry* **20**, 6831–6834 (1981).

18. M. Rance and R.A. Byrd, *J. Magn. Reson.* **52**, 221–240 (1983).

CHAPTER 3

STUDIES OF *TETRAHYMENA THERMOPHILA* LIPIDS

3.1 Introduction

The naturally occurring phosphonic acid, 2-aminoethylphosphonic acid (AEP), has been the subject of much research since it was first reported as a natural product (1). The primary organism used for the study of the biochemistry of this compound is the protozoan *Tetrahymena*, which has the highest known content of AEP (2). While some of the AEP exists in soluble form, 95% of it is found at the lipid level, in 1,2-diacyl-*sn*-glycero-3-(2-aminoethyl)phosphonate, the analog of phosphatidylethanolamine (PE) (2). Biochemical investigations have centered on two aspects of AEP: its biosynthesis (2) and the role of phosphonolipids in membrane structure and function (3, 4).

The free-living, unicellular, ciliated protozoan *Tetrahymena* is widely recognized as an organism well suited for biochemical investigations, because it furnishes the key advantages offered by bacteria with respect to rapid growth and easy manipulation. Especially for biological membrane studies, *Tetrahymena* is a potentially convenient model system. Since it is eukaryotic, *Tetrahymena* contains most of the subcellular organelles found in higher animal cells. Thus it combines the experimental conveniences of a unicellular organism with the physiological makeup of a higher animal cell. *Tetrahymena* cells are most commonly pear-shaped,

average 60 μm in length and approximately 20 μm in width, and have many cilia on the cell surface. The subcellular membrane components include nuclei, mitochondria, lysosomes, endoplasmic reticulum, cilia, pellicles, oral apparatus and food vacuoles.

As mentioned above, organisms of the *Tetrahymena* genus possess in their membrane lipids of an unusual type: phosphonolipids. They differ from the phospholipids normally found in the membranes by the presence of a direct carbon-phosphorus bond in their headgroups. The exact role of these lipids in the membranes is still unknown. As a matter of fact, although the presence of phosphonolipids nas been detected in several types of organisms, mainly molluscs, crustaceans and protozoa, very few studies have been oriented towards their characterization, as much from the point of view of the three-dimensional structure in the membrane as physico-chemical and dynamic.

^{31}P nuclear magnetic resonance (NMR) can be used to probe the headgroup environment and the phase behavior of phosphorus-containing lipids in membranes and aqueous dispersions (5). In this study, the technique was applied to examine the phase behavior of the polar and total lipids of *T. thermophila*.

3.2 Review of the literature

3.2.1 Phospholipid composition

Most of the studies on phospholipid composition in *Tetrahymena* have been carried out using the different strains of *T. pyriformis*. Many of these studies were performed more than fifteen years ago. Important differences are observed in

the results, which do not seem to depend only upon the strain used. This section presents a review of the most important studies on the subject.

Liang and Rosenberg (2) were the first to identify diacylglyceroaminoethylphosphonate, the AEP analog of PE, in lipid extracts of the protozoan *Tetrahymena pyriformis*. They presented evidence for the pathway for its synthesis.

From a qualitative point of view, Smith *et al.* (6) detected the presence of cardiolipin (CL), 2-aminoethylphosphonolipid (AEPL), phosphatidylethanolamine (PE), lysoAEPL and phosphatidylcholine (PC). The relative proportions of these different components varied from one organelle to the other. For example, the phosphonolipid content in cilia was at least twice that of whole cells, whereas other organelles contained more PC, PE and CL.

One of the most important studies on lipid composition in *Tetrahymena pyriformis* was performed by Nozawa and Thompson (7) on the WH–14 strain. Table 3–1 summarizes the results. The major constituents were PE, PC and AEPL or glycerophosphonolipid (GPnL). A high level of phosphonolipids was observed in cilia membranes.

Also of interest is the presence of ether derivatives of glycerol. Thompson (10) was the first to analyze the lipids of *T. pyriformis* for the ether linkage content. Alkylglycerols, almost exclusively 1-*O*-hexadecyl-*sn*-glycerol, occur in phospholipids containing choline and ethanolamine. The ether derivatives represent 60 mol% of the choline fraction and 22 mol% of the ethanolamine fraction. This last fraction includes AEP analogs. A more detailed analysis of this mixed fraction revealed an obvious preference for the association between ether and AEP derivatives of glycerol. Diacylphospholipids contain only 12–20 mol% AEP and

Table 3–1. Phospholipid composition of various membrane fractions from *T. pyriformis* WH–14 cells[a].

Membrane fractions	Phosphonate (% of total lipid phosphorus)	Composition (mol% of total phospholipids)[b]						Tetrahymanol (mol/mol lipid phosphorus)	Glyceryl ether (mol/100 mol lipid phosphorus)
		GPnL	PE	PC	Lyso PC	Lyso GPnL and Lyso PE	CL		
Whole cells	29	23	37	33	2	0	5	0.057	29.7
Cilia	67	47	11	28	1	9	1	0.30	52.6
Ciliary supernatant	44	35	16	19	8	13	1	0.16	23.1
Pellicles	42	30	34	25	5	3	2	0.084	32.8
Mitochondria	26	18	35	35	2	0	10	0.048	24.7
Nuclear envelopes	–	23	26	31	6	6	3	0.036	–
Microsomes	33	23	34	35	1	3	1	0.041	18.3
Post-microsomal supernatant	26	22	30	34	5	4	2	0.016	27.4

[a] Data from Nozawa and Thompson (7) and Thompson *et al.* (8). From Hori and Nozawa (9).

[b] Abbreviations: GPnL, glycerophosphonolipid; PE, phosphatidylethanolamine; PC, phosphatidylcholine; CL, cardiolipin.

alkylacylphospholipids 70–80 mol%. Finally, Thompson (10) found no trace of plasmalogens in *Tetrahymena*.

Using two-dimensional thin-layer chromatography, Jonah and Erwin (11) detected the presence of four major components: PE, AEPL, PC and CL (Table 3–2). Lyso analogs of PE and AEPL were also found. It should be noted that the reported compositions are slightly different from those found by Nozawa and Thompson (7).

Berger *et al.* (12) separated the lipids of *T. pyriformis* W by silica gel chromatography. The major phospholipids are PE (64%) and PC (22%). Other components identified are cardiolipin and a ceramide aminoethylphosphonate (CAEP). The PE fraction contains 30% of the phosphonate and 70% of the phosphate analog. The phosphonate fraction is composed of 75% 1-*O*-hexadecyl-2-acyl-*sn*-glycero-3-(2-aminoethyl)phosphonate and 25% 1,2-diacyl-*sn*-glycero-3-(2-aminoethyl)phosphonate. The PC fraction contains two major components: 1-*O*-hexadecyl-2-acyl-*sn*-glycero-3-phosphocholine (60%) and 1,2-diacyl-*sn*-glycero-3-phosphocholine. No phosphonate was detected in this fraction.

Sugita *et al.* (13) isolated two sphingophosphonolipids from lipids of the WH–14 strain. The first one is ceramide 2-aminoethylphosphonate (CAEP) and the second, found in lesser amounts, ceramide *N*-methyl-2-aminoethylphosphonate (CMAEP).

In another study, Ramesha and Thompson (14) divided the ceramides into two fractions: ceramide 2-aminoethylphosphonate and ceramide 2-aminoethylphosphate. Significant quantities appear to be present in the cilia membrane.

Table 3–2. Glycerophospholipids from membranes of whole cells, cilia and mitochondria isolated from *T. pyriformis*[a].

Ciliate lipid	% of total lipid phosphorus[b]		
	Whole cells	Cilia	Mitochondria
Glyceryl 2-aminoethyl phosphonolipid	31.7 ± 1.7	56.2 ± 8.1	16.1 ± 1.6
Phosphatidyl ethanolamine	19.9 ± 1.2	14.7 ± 1.9	19.4 ± 2.4
Cardiolipin	8.7 ± 0.8	0	16.2 ± 1.7
Phosphatidyl choline	21.2 ± 4.3	8.6 ± 2.4	30.2 ± 2.9
Total lysophospholipids plus trace components	17.6 ± 2.2	20.1 ± 4.1	17.1 ± 5.3

[a] From Jonah and Erwin (11).

[b] Values are means (5–8 determinations) ± deviation from the mean.

3.2.2 Fatty acid distribution

According to Erwin and Bloch (15), saturated fatty acids are present in *T. pyriformis* II–1 in relatively small proportions, the major ones being myristic (14:0) and palmitic (16:0) acids. Linoleic ($18:2^{\Delta 9,12}$) and γ-linolenic ($18:3^{\Delta 6,9,12}$) acids are the major unsaturated fatty acids and represent more than 50% of all fatty acids of the cilia (Table 3–3). As the culture ages, the ratio of monounsaturated to saturated fatty acids decreases, while the relative content of dienoic and trienoic fatty acids remains constant. An increase in incubation temperature gives the same effect on young cultures.

Jonah and Erwin (11) carried out a similar study, but found a greater proportion of saturated fatty acids (Table 3–4). Moreover, the fatty acid composition in each phospholipid class characterized was determined (Table 3–5). The results show that phosphonolipids and PC contain a greater proportion of polyunsaturated fatty acids.

3.2.3 Neutral lipids

Jonah and Erwin (11) analyzed the subcellular membrane fractions of *T. pyriformis* II–1 for their neutral lipid composition. They found that triglycerides were the principal neutral lipids of whole cells. Substantial amounts of the pentacyclic triterpenoid tetrahymanol (Scheme 3–1), which in this organism replaces sterols, and tetrahymanol ester were also present. These two components were the major neutral lipids of both cilia and mitochondria, while neither organelle contained triglycerides. Fatty acids were found to be only minor components of this fraction in both whole cells and isolated organelles.

Table 3–3. Fatty acid composition of *Tetrahymena pyriformis* II–1 grown at 25°C[a].

Fatty acid		Relative composition (%)
lauric	(12:0)	1.9
myristic	(14:0)	6.5
isopentadecanoic	(i15:0)	2.5
palmitic	(16:0)	4.8
palmitoleic	($16:1^{\Delta 9}$)	11.5
oleic	($18:1^{\Delta 9}$)	8.7
linoleic	($18:2^{\Delta 9,12}$)	17.9
γ-linolenic	($18:3^{\Delta 6,9,12}$)	37.7

[a] Data taken from Erwin and Bloch (15).

Table 3–4. Fatty acid composition of the total lipids extracted from various isolated membranous organelles of *T. pyriformis*[a].

Ciliate fatty acid	Composition (weight %)		
	Whole cells	Cilia	Mitochondria
14:0	22.7	7.0	0.3
16:0	14.0	12.2	5.2
$16:1^{\Delta 9}$	11.5	5.6	3.1
18:0	2.2	3.1	2.1
$18:1^{\Delta 9}$	4.2	22.4	6.1
$18:2^{\Delta 9,12}$	15.8	15.5	30.4
$18:3^{\Delta 6,9,12}$	25.6	22.8	47.7
Minor acids[b]	4.1	11.5	5.2

[a] From Jonah and Erwin (11).

[b] Minor fatty acids consisted of: 12:0, 15:0, 17:0, 17:1, i15:0, i16:0 and several unsaturated eicosenoic acids.

Table 3–5. Fatty acid composition of individual glycerophospholipids extracted from various isolated membranous organelles of *T. pyriformis*[a].

Ciliate fatty acid	Composition (weight %)[c]								
	Whole cells				Cilia	Mitochondria			
	PnE	PE	Car	PC	PnE + PE	PnE	PE	Car	PC
14:0	0.7	0	1.5	0	–	0	0	2.6	0
16:0	2.3	3.1	15.7	3.0	8.2	0	2.7	5.4	1.3
$16:1^{\Delta 9}$	3.2	2.3	9.5	2.5	5.2	0	2.0	1.4	0.8
18:0	0.5	4.6	7.0	0	1.9	0	0	1.8	1.1
$18:1^{\Delta 9}$	5.5	37.6	10.2	0	9.4	3.2	7.4	3.6	3.6
$18:2^{\Delta 9,12}$	33.1	33.6	22.3	34.5	27.8	24.9	38.5	44.1	44.1
$18:3^{\Delta 6,9,12}$	50.4	12.7	23.5	56.8	33.3	67.9	48.7	38.7	38.7
Minor acids[b]	4.5	6.2	10.5	3.2	13.6	3.9	0.7	5.4	5.4

[a] From Jonah and Erwin (11).

[b] Minor fatty acids consisted of: 12:0, 15:0, 17:0, 17:1, i15:0, i16:0 and several unsaturated eicosenoic acids.

[c] Abbreviations: PnE, glyceryl 2-aminoethyl phosphonolipid; PE phosphatidyl ethanolamine; Car, cardiolipin; PC, phosphatidyl choline.

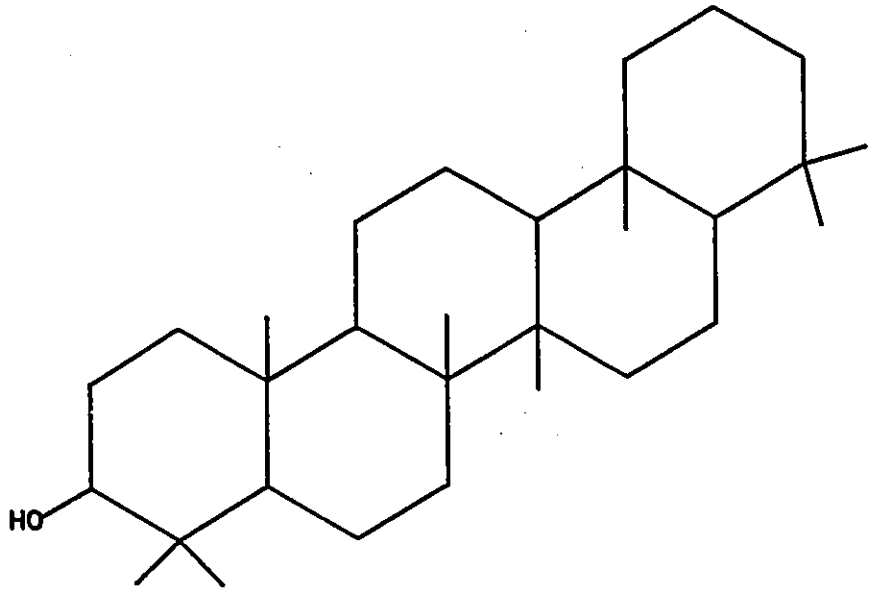

Scheme 3–1. Structure of tetrahymanol.

The results gathered by Nozawa and Thompson (7) were similar. The tetrahymanol content is clearly much higher in relation to phospholipid level in ciliary membranes than in other organelles.

3.2.4 Effect of temperature

In studying the thermotolerant strain NT–1, Fukushima *et al.* (16) detected a few changes in the lipid composition of membranes for cultures grown at different temperatures. Thus, the degree of unsaturation increased at low temperatures (Table 3–6), and the same was true for the content in ether derivatives. A decrease in the amount of PE was also observed, with a proportional increase in the AEPL levels (Table 3–7).

Ramesha and Thompson (14) obtained similar results with respect to degree of unsaturation and phospholipid composition (Tables 3–8 and 3–9), and observed also that the relative proportions of ceramide 2-aminoethylphosphonate and ceramide 2-aminoethylphosphate vary inversely with temperature.

Watanabe *et al.* (17) determined the fatty acid composition of two components, 1,2-diacyl-*sn*-glycero-3-(2-aminoethyl)phosphonate and 1-*O*-alkyl-2-acyl-*sn*-glycero-3-(2-aminoethyl)phosphonate, according to their position (*sn*–1 or *sn*–2) on the glycerol skeleton (Table 3–10). At low temperature a large proportion of cilienic ($18{:}2^{\Delta 6,11}$) acid could be observed in ether derivatives.

Finally, Maruyama *et al.* (18) found that at the 1 position, the content of palmitate in diacyl-PE, PC and AEPL decreased progressively after a temperature shift from 39 to 15°C, while γ-linolenate increased in a complementary fashion, in mitochondria and microsomes of the thermotolerant strain NT–1. The increase in the percentage of γ-linolenate was compensated by the decrease in oleate at the 2

Table 3–6. Fatty acid composition of total phospholipids from *Tetrahymena* grown at different temperatures[a].

Component	Retention time (min)	Composition (weight %)[b]					
		15°C [6(4)]		24°C [6]	39.5°C [5(4)]		
12:0	1.4	0.6±0.3	(1.5±0.4)	1.0±0.5	0.9±0.3	(1.4±0.3)
14:0	2.7	6.9±0.7	(7.7±0.8)	6.6±0.9	6.5±1.0	(10.5±2.5)
anteiso 15:0	3.2	1.5±0.3	(1.0±0.4)	1.5±0.3	3.4±0.4	(4.4±0.4)
15:0	3.7	<0.5	(<0.5)	0.8±0.4	1.2±0.1	(1.5±0.3)
16:0	5.1	8.9±0.5	(9.4±1.0)	10.4±1.2	12.6±1.6	(13.8±1.4)
16:1	6.0	8.7±0.9	(10.2±1.9)	8.9±0.8	8.7±1.1	(12.2±1.8)
16:2 + 17:0	7.1	2.2±0.2	(3.1±0.6)	3.3±0.4	4.4±0.3	(4.7±1.1)
17:1	8.1	0.8±0.4	(1.2±0.4)	1.2±0.2	1.4±0.2	(0.7±0.4)
?		0.9±0.3	(2.4±0.8)	0.9±0.2	1.2±0.3	(1.5±0.4)
18:0	9.9	0.6±0.3	(0.9±0.2)	1.4±0.7	2.1±0.4	(2.0±0.8)
?		1.3±0.4	(<0.5)	1.5±0.1	1.1±0.2	(<0.5)
18:1	11.2	9.6±1.6	(7.8±5.1)	7.4±0.6	10.6±3.9	(7.4±2.9)
?	13.3	7.0±0.3	(7.7±1.1)	5.1±0.4	3.4±1.0	(1.2±0.8)
18:2	13.9	20.2±1.6	(16.8±1.6)	18.2±1.6	14.5±0.9	(13.0±1.5)
18:3	16.3	31.1±0.9	(28.4±0.2)	32.6±2.0	24.5±2.4	(22.4±3.2)
19:0	19.2	<0.5	(0.8±0.3)	<0.5	2.6±2.2	(1.1±0.1)
20:1	21.0	<0.5	(<0.5)	<0.5	<0.5	(<0.5)
?	22.7	<0.5	(<0.5)	<0.5	<0.5	(0.9±0.6)

[a] From Fukushima *et al.* (16).

[b] Values represent averages ± standard deviations, the number of separate experiments being shown in brackets. Values in parentheses represent data from a different group.

Table 3–7. Lipid composition of *Tetrahymena* whole cells adapted to different temperatures[a].

Lipid	Composition (weight %)[b]		
	15°C	24°C	39.5°C
Lipid phosphorus (μmol/10^6 cells)	0.14 ± 0.01	0.13 ± 0.02	0.14 ± 0.01
Tetrahymanol/phosphorus (molar ratio)	0.081	0.078	0.083
Alkyl ether (mol% of phospholipids)	27.1 ± 6.6	–	20.9 ± 2.8
Individual phospholipids (mol%)			
Cardiolipin	5.2 ± 0.6	5.6 ± 0.4	7.8 ± 1.9
	(5.0 ± 0.8)	(7.3 ± 1.0)	(7.4 ± 0.9)
2-Aminoethylphosphonolipid	29.0 ± 0.6	25.4 ± 2.0	15.6 ± 1.7
	(24.1 ± 1.9)	(18.9 ± 0.6)	(12.2 ± 3.0)
Ethanolamine glycerophosphatides	25.6 ± 4.4	34.4 ± 1.6	42.5 ± 1.3
	(35.7 ± 3.8)	(34.7 ± 0.7)	(46.5 ± 4.2)
Lysophosphatidylethanolamine,	8.3 ± 0.6	5.4 ± 0.9	2.7 ± 1.0
lyso-2-aminoethylphosphonolipid,	(4.2 ± 2.2)	(4.2 ± 2.1)	(2.7 ± 1.1)
ceramide aminoethylphosphonate			
Choline glycerophosphatides	27.2 ± 1.3	26.2 ± 0.5	26.8 ± 3.4
	(26.4 ± 3.2)	(27.7 ± 1.5)	(26.5 ± 1.9)
Lysophosphatidylcholine	2.8 ± 1.9	2.6 ± 1.8	2.8 ± 1.6
	(1.5 ± 1.7)	(1.4 ± 1.9)	(2.2 ± 0.4)

[a] From Fukushima *et al.* (16).

[b] Values represent averages ± standard deviations of three or more experiments. Values in parentheses represent data from a different group.

Table 3–8. Overall fatty acid composition of ciliary phospholipids of *Tetrahymena* grown at different temperatures[a].

Fatty acid	Composition[b]	
	39°C-grown	15°C-grown
14:0	14.9 ± 3.3	7.3 ± 0.1
iso 15:0	4.9 ± 0.5	0.9 ± 0.2
15:0	1.8 ± 0.3	< 0.5
16:0	16.3 ± 0.5	14.9 ± 1.8
16:1	11.5 ± 1.5	6.5 ± 0.5
16:2 + 17:0 + 17:1	3.8 ± 0.4	2.9 ± 0.5
18:0	1.9 ± 0.4	2.5 ± 0.2
18:1	5.0 ± 0.9	4.8 ± 0.6
$18:2^{\Delta 6,11}$	2.5 ± 0.3	17.3 ± 0.5
$18:2^{\Delta 9,12}$	8.6 ± 1.0	5.5 ± 0.7
18:3	27.9 ± 2.6	37.0 ± 5.5

[a] From Ramesha and Thompson (14).

[b] Values are expressed as mol percent and are mean ± standard deviation of three or more experiments. Values are not corrected for the presence of ether side chains.

Table 3–9. Phospholipid composition of cilia from 39 and 15°C-grown *Tetrahymena*[a].

Phospholipid	Composition[b]	
	39°C-grown	15°C-grown
2-Aminoethylphosphonolipid	40.0 ± 2.2	42.8 ± 1.2
Phosphatidylethanolamine	18.4 ± 2.0	9.9 ± 1.2
Phosphatidylcholine	15.7 ± 3.7	3.1 ± 0.6
Ceramide aminoethylphosphonate	3.0 ± 1.7	37.4 ± 2.2
Ceramide aminoethylphosphate	22.8 ± 1.5	6.8 ± 1.3
Phospholipid/tetrahymanol (molar ratio)	2.56 ± 0.36	4.23 ± 0.23

[a] From Ramesha and Thompson (14).

[b] Values are expressed as mol percent and are mean ± standard deviation from four or more analyses.

Table 3–10. Fatty acid composition of 1,2-diacyl- and 1-*O*-alkyl-2-acyl-glycero-3-(2-aminoethyl) phosphonate in *T. pyriformis* NT–1 cells grown at 39.5 or 15°C[a].

Fatty acids	1,2-diacylglycerophosphonolipid						1-*O*-alkyl-2-acyl-glycerophosphonolipid	
	Overall composition[b]		1-position		2-position		Overall composition (2-position)	
	39.5°C	15°C	39.5°C	15°C	39.5°C	15°C	39.5°C	15°C
14:0	15.2	10.4	26.0	20.1	4.5	1.1	0.4	0.3
16:0	19.3	10.9	39.1	23.4	0.5	–	1.3	0.9
16:1	19.8	12.8	7.8	14.6	31.6	11.0	5.9	1.0
16:2 + 17:0	8.0	4.5	3.2	3.7	12.8	5.2	3.6	0.7
18:1	8.3	9.3	0.8	3.3	15.8	15.4	4.1	3.3
$18:2^{\Delta 6,11}$	tr	3.8	0.7	3.8	–	3.9	10.9	39.5
18:2	9.1	24.5	0.8	5.9	17.4	43.1	9.2	5.5
18:3	8.0	18.4	3.7	18.6	12.3	18.3	58.0	47.6
Unsaturation index[c]	71	135	23	93	121	177	239	237
$\Sigma U/\Sigma S$[d]	0.9	2.5	0.2	0.9	3.9	13.5	16.8	50.0

[a] From Watanabe *et al.* (17).

[b] Values are expressed as mol% of total fatty acids.

[c] Definition: (number of double bonds per fatty acid) × (percentage of the fatty acid).

[d] Ratio of unsaturated to saturated fatty acids.

position of 1,2-diacylphospholipids. On the other hand, a marked increment in γ-linolenate occurred with a decline of oleate and linoleate at the 2 position of 1-*O*-alkyl-2-acyl-PC, but no significant alterations were seen at the 2 position of 1-*O*-alkyl-2-acyl-AEPL.

3.2.5 NMR studies

Jarrell *et al.* (19) examined the phase behavior of a synthetic phosphonolipid, 1,2-dipalmitoyl-*sn*-glycero-3-(2-aminoethyl)phosphonate, alone and in the presence of dipalmitoylphosphatidylcholine (DPPC) and dipalmitoyl-phosphatidylethanolamine (DPPE). When mixed with PC, the phosphonolipid possess a lamellar organization, whereas with PE the hexagonal (H_{II}) phase is preferred. The chemical shift anisotropy is considerably smaller for AEPL than for the analogous phospholipid. On the other hand, total lipids extracted from *Tetrahymena* sp. contain phospho– and phosphonolipids organized as bilayers between −20 and 20°C.

Following this study, Deslauriers *et al.* (20) examined the phase behavior of total lipids from *Tetrahymena* sp. as a function of temperature. Above 25°C, phospho– and phosphonolipids undergo a transition from the lamellar to the hexagonal phase and, moreover, an isotropic component appears on the ^{31}P NMR spectra. Both ^{2}H and ^{14}N NMR spectra of lipids mixed with 10% egg yolk 2-[14,14–$^{2}H_2$]palmitoylphosphatidylcholine show an isotropic peak superimposed on the normal powder pattern at 25°C, the latter disappearing by 40°C. This observation supports the hypothesis that an isotropic phase is formed at elevated temperatures.

Ferguson *et al.* (21) isolated PE and AEPL from membranes of *T. pyriformis* W. Using ^{31}P NMR spectroscopy, it was shown that the PE occurs in

a hexagonal phase above 10°C, that the transition temperature between the lamellar and hexagonal phases is around 30°C for AEPL, and that a mixture of these two components shows a powder pattern characteristic of the H_{II} phase for each at 30°C. Small amounts of PC appeared to stabilize AEPL in a bilayer form up to *ca.* 50°C, temperature where peaks indicative of an isotropic phase show up.

Hill *et al.* (22) studied the properties of cilia of *T. thermophila* by ^{31}P NMR. In the case of cilia and membranes isolated from them, two powder patterns, corresponding to phospho– and phosphonolipids, were observed, on which were superimposed two isotropic peaks. In contrast, lipids isolated from cilia did not give rise to these isotropic resonances, suggesting that they arise from nonlipid components of membranes. At higher temperatures, the spectra of ciliary preparations showed an increased proportion of these isotropic components. However, an hexagonal phase could not be detected at any temperature, despite the high PE and AEPL content of the ciliary membrane. The authors suggested that this could be due to the stabilizing effect of sphingolipids or ether derivatives of glycerol.

3.3 Experimental part

3.3.1 Cell culture and harvesting

Tetrahymena thermophila, B1868, Chx–2/Chx–2 (cysen, IV) is grown in a medium containing 1% bacteriological peptone (Oxoid L37), 0.1% yeast extract (Oxoid L21) and 36 μM $FeCl_3$ (23). The strain is maintained at room temperature by weekly transfer.

Cultures are started with a 10% inoculum in 500-ml erlenmeyer flasks containing 100 ml medium. After a 24-hour incubation period at 30°C under rotary agitation at 100 rpm, the erlenmeyer contents are transferred to a 2-l Fernbach flask containing 1 l medium. Incubation is continued for 24 hours at the same temperature, under agitation at 60 rpm. Cell density is determined before harvesting by counting on a hemacytometer. Cells are fixed by adding an equal volume of 4% (v/v) formaldehyde to an aliquot of culture. For harvest, cultures are cooled on ice and centrifuged at 4°C at 1200 × g_{av} for 8 minutes. The cell pellets are resuspended in a volume of distilled water corresponding to half the volume of the culture and centrifuged at the same speed for 6 minutes. All pellets are then combined, washed in a small volume of water and recentrifuged as above. Cells are then dispersed in a small amount of water and lyophilized.

Cultures in fermentors are performed by adding the content of a Fernbach flask to a New Brunswick Microferm fermentor (New Brunswick, New Jersey) containing 11 l medium. Cultures are grown to late log phase (36 h) at 30°C with aeration at 3.5 l/min and vane rotation at 30 rpm. Dow Corning Antifoam A (100 μl) is added per 12 l medium to prevent excessive foaming. A Coulter counter, model ZM, fitted with a 100-μm orifice is used for counting. Duplicate 2-ml samples of cells are fixed with 38 ml of a solution — which is iso-osmotic to the culture medium — containing 1% formaldehyde and 1.4 g/l NaCl prior to counting. Batches (24 l) of cells are cooled on ice and harvested at 500 ml/min by continuous-flow centrifugation at 1700 × g_{av} at a rotor temperature of −10°C. The resultant cell pellets are transferred to a round-bottom flask and lyophilized.

3.3.2 Lipid extraction

All solvents were purified by simple distillation. The lyophilized cellular residue was extracted for 20 minutes at about 40°C under a nitrogen atmosphere with 30 volumes (ml/g solid) of a $CHCl_3-CH_3OH$ 2:1 mixture. The extract was filtered by suction on a sintered glass funnel and the cellular debris extracted once more with 15 volumes $CHCl_3-CH_3OH$. After a second filtration, followed by a washing with 5 volumes of the same mixture, the solvent was removed on a rotary evaporator (24).

Sephadex chromatography was performed to eliminate the nonlipid components present in the preparation (25). Sephadex G-25 fine (Pharmacia, Uppsala) was first swollen for 24 hours in 4 volumes (ml/g) of the upper phase of the mixture $CHCl_3-CH_3OH-H_2O$ 8:4:3 described by Folch *et al.* (26). For 200 mg of extract, the Sephadex suspension was poured into a 1-cm diameter column to a height of 10 cm. The column was washed with one volume of upper phase, followed by one volume of lower phase. The extract was dissolved in about 2 ml of lower phase, filtered if necessary to eliminate the insoluble residue, and applied to the column, which was eluted with about 2 volumes of lower phase. The nonlipid components, soluble in the aqueous phase inside the Sephadex beads, are retained on the column, while the lipids are eluted in the void volume. The organic solvents were evaporated on a rotary evaporator and the residue put in a high vacuum to eliminate all traces of water.

3.3.3 Fractionation of neutral and polar lipids

Total lipids can be fractionated into neutral and polar lipids by chromatography on silica gel (27). For each gram of total lipids, a column was prepared with 40 g Bio Sil A (Bio-Rad, Mississauga, Ontario) suspended in $CHCl_3$.

After washing with $CHCl_3$, the lipids dissolved in the same solvent were applied to the column. Neutral lipids were eluted with 20 volumes (ml/g silica gel) $CHCl_3$ and polar lipids with 20 volumes CH_3OH.

3.3.4 Thin-layer chromatography

Thin-layer chromatography of lipids was carried out using 0.25-mm thickness Silica gel 60 plates (E. Merck, Darmstadt) with no fluorescent indicator. Polar lipids were separated with the system $CHCl_3-CH_3COOH-CH_3OH-H_2O$ 75:25:5:2.2, which allows the proper separation of AEPL and PE (7). Neutral lipids were chromatographed with the solvent system petroleum ether–ethyl ether–acetic acid 70:30:1 (7).

Different stains were used for the detection of the spots corresponding to different lipids. Iodine is a nonspecific stain that enables the visualization of compounds containing double bonds (28). Rhodamine 6G is a universal lipid stain (28, 29) that colors neutral as well as polar lipids. Under a UV light, lipids appear as blue spots on a fluorescent pink background. Phosphorus-containing lipids were revealed with phosphate stain (30, 31), which gives blue spots on a white background. Ninhydrin (28, 32) was used for the detection of lipids that contain a primary amine function. With gentle heating, these lipids adopt a red color, while the background remains white. It was possible to reveal choline-containing lipids with the Dragendorff reagent (32), which gives orange spots on a yellow background. Finally, the hypochlorite–benzydine reagent (33) was used to develop sphingolipids (and secondary amines), which give blue spots on a white background.

3.3.5 ^{31}P NMR studies

The preparation of lipid samples for NMR was as follows. A lipid sample (*ca.* 150 mg) dissolved in chloroform–methanol was evaporated to dryness under vacuum, then under a stream of N_2. It was then put in a high vacuum for several hours to eliminate all traces of solvent. Lipids were then dispersed in about 1.2 ml water or buffer with the use of a Vortex mixer. Several cycles of freezing, thawing and mixing were often required to obtain homogeneity. The preparation was purged with nitrogen and transferred to a 10-mm NMR tube.

^{31}P NMR spectra were acquired with a high-power probe tuned to 121.5 MHz in a Bruker CXP–300 NMR spectrometer. The spectral width was 50 kHz and the number of points 4096. Temperature was controlled to $\pm 1°C$. A spin echo sequence with complete phase cycle (34) and quadrature detection were used. High-power broadband proton decoupling was applied and gated off during the recycling delay. Acquisition was started before the echo and the points to the left of it discarded. Line broadening (*ca.* 50 Hz) was introduced by exponential multiplication before Fourier transformation to increase the signal-to-noise ratio. Spin lattice relaxation time T_1 measurements were carried out by the inversion-recovery method combined with the Hahn echo.

Selective saturation of ^{31}P resonances was achieved using a DANTE (Delays Alternating with Nutations for Tailored Excitation) pulse sequence (35). The duration of the saturation was chosen to be long relative to molecular reorientation, via tumbling or lateral diffusion, but less than or comparable to the T_1 of the saturated resonance.

Chemical shifts are reported in ppm relative to an external reference of 85% H_3PO_4 assuming positive values for resonances at higher frequencies. The

sign convention for chemical shielding tensor components is the opposite of that for chemical shifts.

3.3.6 Silica gel chromatography

A column was prepared with 10 g Bio Sil A (Bio-Rad, Mississauga, Ontario) suspended in $CHCl_3$. After washing with $CHCl_3$, 80 mg of lipids dissolved in the same solvent were applied to the column. Chloroform was used for the elution of neutral lipids. The polar lipids were eluted with a gradient containing increasing proportions of CH_3OH in $CHCl_3$. At each gradient step, two volumes of solvent were passed on the column. Fractions were collected in test tubes and immediately purged with N_2 before analysis by TLC.

To separate AEPL from PE, the lipid sample (10 mg/g adsorbent) was applied to a silica gel column prepared in chloroform. Elution was carried out with chloroform–acetic acid–water mixtures (30:20:1 or 75:25:1) as described by Kapoulas (36). The fractions were treated as above.

3.3.7 Hydrolysis with phospholipase D

The procedure for the purification of phospholipase D was adapted from Davidson and Long (37). The yellow and green internal leaves of a fresh Savoy cabbage (550 g) were cut into small pieces and homogenized in a blender with 725 ml water for 5 min. The suspension was filtered through cheesecloth. The filtrate (*ca.* 1 l) was then centrifuged at 13000 × g_{av} for 30 min. The supernatant was brought to *p*H 6.5 with 1 N NaOH and heated at 55°C for 5 min. After cooling in ice, a precipitate formed which was centrifuged off as above. The solution was again cooled in ice, then 2 l acetone cooled to −15°C added, and centrifugation performed again. The pellet was dissolved in 15 ml H_2O and a final centrifugation

carried out under the same conditions. The supernatant which contains the purified enzyme was lyophilized and stored at −20°C under nitrogen.

For the hydrolysis, 1 g enzyme was dissolved in 100 ml 0.1 M sodium acetate buffer, 0.1 M $CaCl_2$, *p*H 5.6. The lipids (3.7 g) dissolved in 100 ml ether were added and the mixture agitated vigorously. The reaction was followed by TLC and stopped by adding a 50 mM ethylenediaminetetraacetic acid (EDTA) solution.

3.4 Results and discussion

3.4.1 Thin-layer chromatography

3.4.1.1 Polar lipids

The chemical characteristics of the phosphate and phosphonate analogs are so similar that only specific chromatographic procedures (36) allow adequate separation for unequivocal identification (6). By thin-layer chromatography using a solvent system suitable for the separation of polar lipids (7), some lipids present in *Tetrahymena* could be identified. This was done by revealing the plates with different stains more or less selective and also by comparison with standards. Among the stains employed, some did not work as well as expected. Thus, Rhodamine 6G (28, 29) effectively colors lipids, but the spots must be visualized under UV light, and they disappear quite rapidly. The protocol for staining with the Dragendorff reagent (32) had to be slightly modified to make choline-containing lipids visible. Finally, staining with the hypochlorite–benzidine reagent (33) was not successful, using either a 6% hypochlorite solution, Javex or Romco bleach.

Figure 3–1 shows a typical thin-layer chromatogram obtained with *Tetrahymena* lipids. Most of the lipids known to be present in this organism were found. Thus, CL, AEPL, PE and PC have been positively identified. These components were assigned to specific spots either by comparing their migration distance with that of standards or by specific staining. Other spots were tentatively assigned to lysoAEPL, lysoPE and sphingolipids, compounds assumed to be present in *Tetrahymena*. The assignments are in this case uncertain but probable, based on the migration of some standards, specific coloration of certain spots and literature data.

The TLC results show that separation of AEPL from PE is easily achieved using a solvent mixture that contains a large proportion of acetic acid (36). The methanol in the eluent has to be used to achieve separation of PE from the more polar phospholipids (36). The spots for AEPL and PE are doubled due to a different migration of 1-*O*-alkyl-2-acyl and 1,2-diacyl derivatives, the latter having a lower retention factor R_f (6).

3.4.1.2 Neutral lipids

Figure 3–2 illustrates a thin-layer chromatogram of *Tetrahymena* total lipids developed with the solvent system petroleum ether–ethyl ether–acetic acid 70:30:1 (7). The identified components are, in decreasing order of polarity: 1-*O*-alkyldiacylglycerol, triacylglycerol, different fatty acids, probably 1-*O*-alkyl-2-acylglycerol, 1,2-diacylglycerol and tetrahymanol, 1-*O*-alkylglycerol and 1-acylglycerol, and finally the polar lipids which stay at the origin.

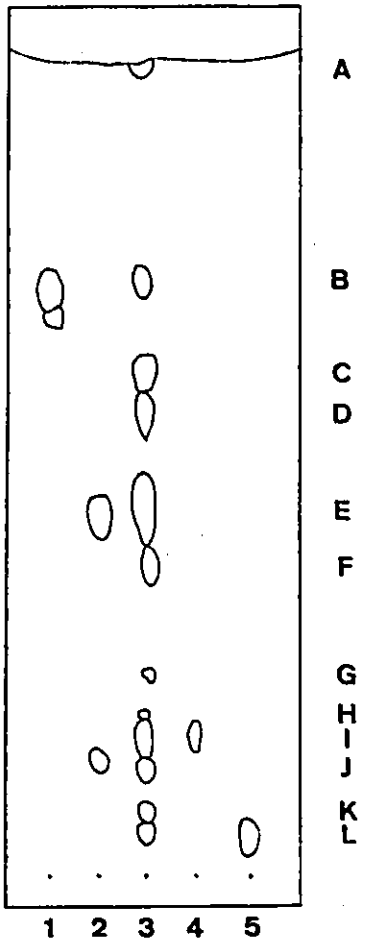

Figure 3–1. Thin-layer chromatography on Silica gel 60 of the total lipids of *Tetrahymena thermophila* with the system $CHCl_3-CH_3COOH-CH_3OH-H_2O$ 75:25:5:2.2. Samples: 1, CL; 2, egg yolk PE and lysoPE; 3, lipids *of T. thermophila*; 4, egg yolk PC; 5, sphingomyelin (SM). Tentative identification of spots: A, neutral lipids; B, CL; C and D, AEPL; E and F, PE; G, lysoAEPL; H, unknown; I, PC and unknown; J, lysoPE; K and L, sphingolipids. Spots stained with I_2: A, B, C, E and I; phosphate spray: B, C, D, E, F, G, H, I, J and L; ninhydrin: C, D, E, F, G, H, I, J and K; Dragendorff: I; hypochlorite–benzydine: none.

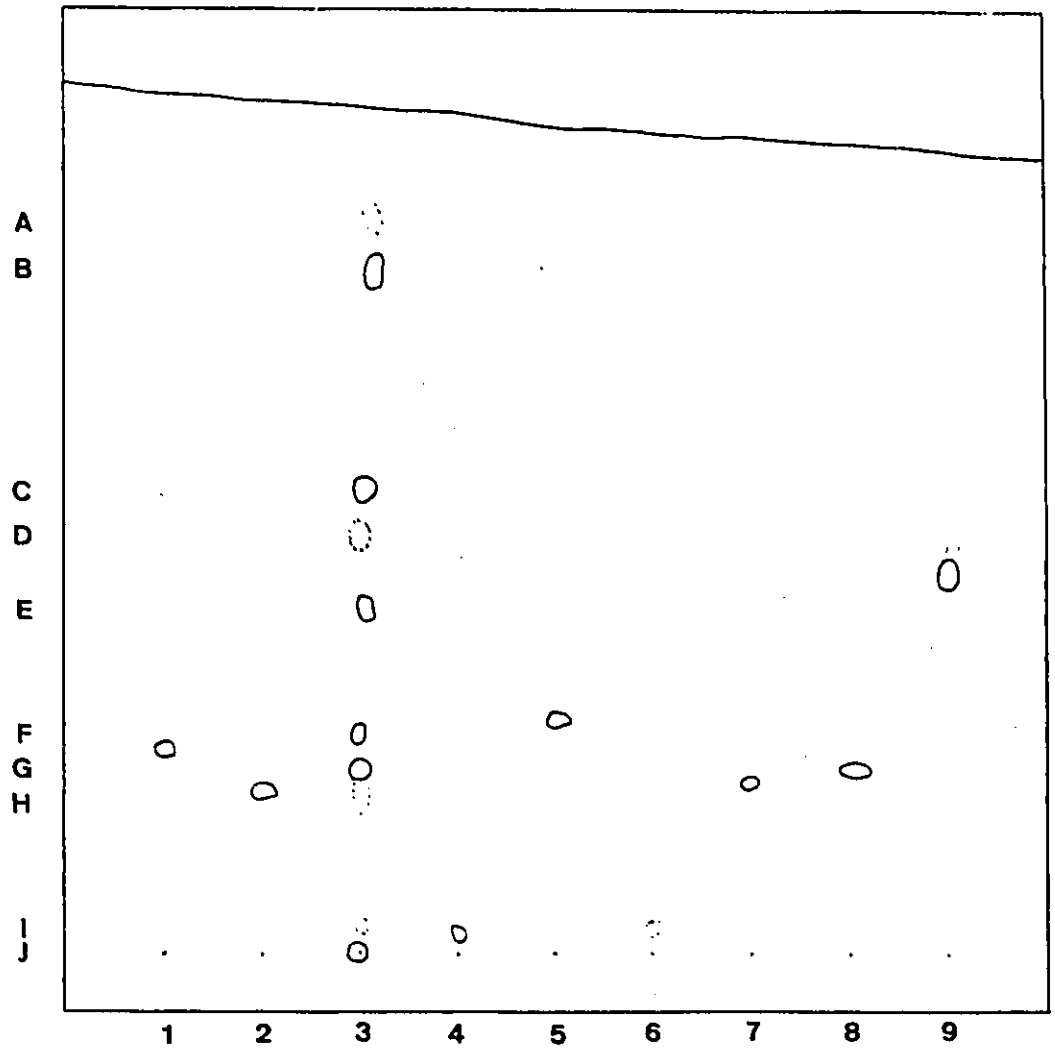

Figure 3–2. Thin-layer chromatography on Silica gel 60 of the neutral lipids of *T. thermophila* using the solvent system petroleum ether—ethyl ether—acetic acid 70:30:1. Samples: 1, 1,3-dipalmitoylglycerol; 2, 1,2-dipalmitoylglycerol; 3, lipids of *T. thermophila*; 4, 1-palmitoylglycerol; 5, 1-hexadecanol; 6, 1-*O*-hexadecyl-*sn*-glycerol; 7, cholestanol; 8, cholesterol; 9, stearic acid. Tentative identification of spots: A, 1-*O*-alkyldiacylglycerol; B, triacylglycerol; C, D and E, fatty acids; F, 1-*O*-alkyl-2-acylglycerol; G, 1,2-diacylglycerol; H, tetrahymanol; I, 1-*O*-alkyl-glycerol and 1-acylglycerol; J, polar lipids. The spots were revealed with iodine.

3.4.2 ^{31}P NMR studies

3.4.2.1 Preliminary results

To choose a suitable aqueous medium for the NMR experiments, the lipids were dispersed in water, in a 150 mM NaCl solution, in a buffer composed of 25 mM 3-(*N*-morpholino)propanesulfonic acid (MOPS), 2 mM EDTA, *p*H 7.15, and in a 25 mM MOPS, 2 mM EDTA, 150 mM NaCl, *p*H 7.15 buffer. In suspensions containing salt, lipids precipitated after a few hours. In those containing MOPS, lipids apparently degraded more rapidly than in water, as judged by the suspension color and the fact that ^{31}P NMR spectra changed with time. A physiological buffer containing phosphate cannot be used for ^{31}P NMR experiments because a large narrow resonance would interfere with the lipid powder spectrum. Since a defined *p*H is necessary to ensure identical conditions from one preparation to the next, and the presence of EDTA required (see T_1 measurements below), the buffer 25 mM 2-amino-2-(hydroxymethyl)-1,3-propanediol (Tris), 2 mM EDTA, *p*H 7.0, *i.e.* that used by Jarrell *et al.* (19) and Deslauriers *et al.* (20) was finally chosen and used with no subsequent problem.

The ^{31}P NMR spin lattice relaxation time T_1 was measured on the polar lipids of *T. thermophila* dispersed in water and found to be < 10 ms. This result can only be explained by the presence of paramagnetic impurities that cause the phosphorus to relax rapidly, since literature values for phospholipids are usually of the order of a second (5, 38).

Figure 3–3(a) shows the ^{31}P NMR spectrum of the total lipids of *T. thermophila* at 23°C in Tris-EDTA buffer, obtained with a recycling time of 2 s. The value used by Jarrell *et al.* (19) and Deslauriers *et al.* (20) was 1 s. The spectrum is a superposition of two powder patterns, each characteristic of a liquid

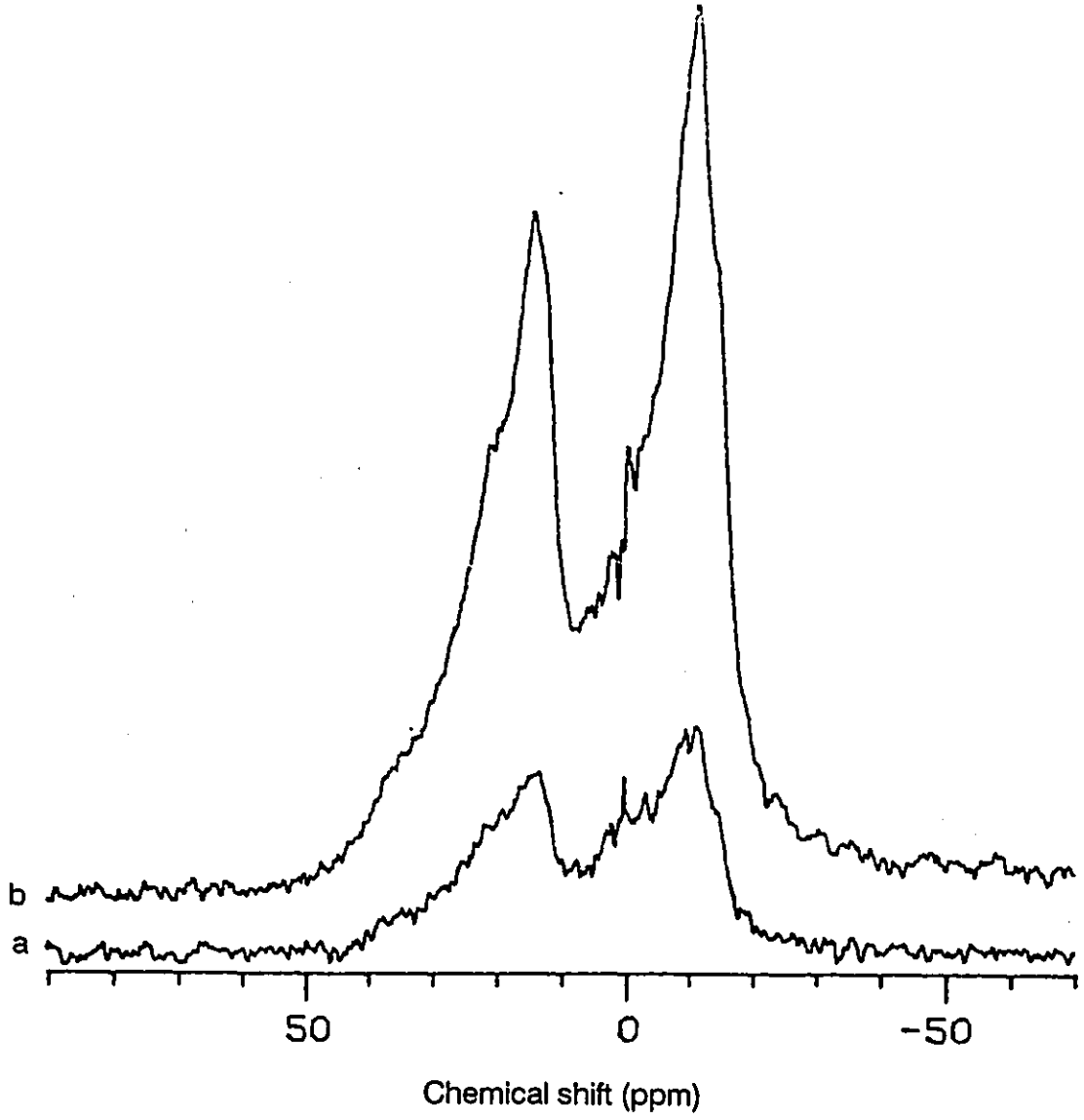

Figure 3–3. ^{31}P NMR spectra (121.5 MHz) of the total lipids of *Tetrahymena thermophila* at 23°C, 320 accumulations. The 90° pulse width was 4.8 μs, and the recycling delay 2 s (a) and 10 s (b).

crystalline phase. The upfield component is attributed to the phospholipids and the other to the phosphonolipids. The signal-to-noise ratio of this spectrum is much lower than that for the same amount of lipids in water. When using a 10-s recycling delay, as shown on Figure 3–3(b), the signal-to-noise ratio improved considerably. The spin-lattice relaxation time T_1 was measured on the same sample and found to be 1.1 s for both components. This determination allowed the setting of a sufficiently long recycling delay for the subsequent ^{31}P NMR experiments.

3.4.2.2 Polar lipids

The phase behavior of *T. thermophila* was studied by ^{31}P NMR. Figure 3–4 presents the spectra of polar lipids dispersed in excess buffer as a function of temperature. The results are quite different from those obtained by Deslauriers *et al.* (20) with total lipids. First, at approximately 15°C, the beginning of a transition from bilayer to hexagonal phase can be observed. As the temperature increases, there is more hexagonal and less bilayer powder pattern. At 45–50°C, only the H_{II} phase is present. Second, there is no evidence for isotropic phase formation. Finally, when decreasing the temperature back to 20°C, the shape of the spectrum is very similar to the previous one at 20°C, showing that the transition is reversible.

Using the DANTE pulse sequence with irradiation on the upfield component corresponding to the phospholipid, the spectrum of only the phosphonolipid can be revealed (Figure 3–5). The phase behavior was found to be the same as described above. A bilayer-type spectrum is observed at low temperature. The spectrum slowly transforms into one characteristic of an hexagonal phase, which is the only phase present at 45°C. Finally, reversibility is apparent when returning to 15°C.

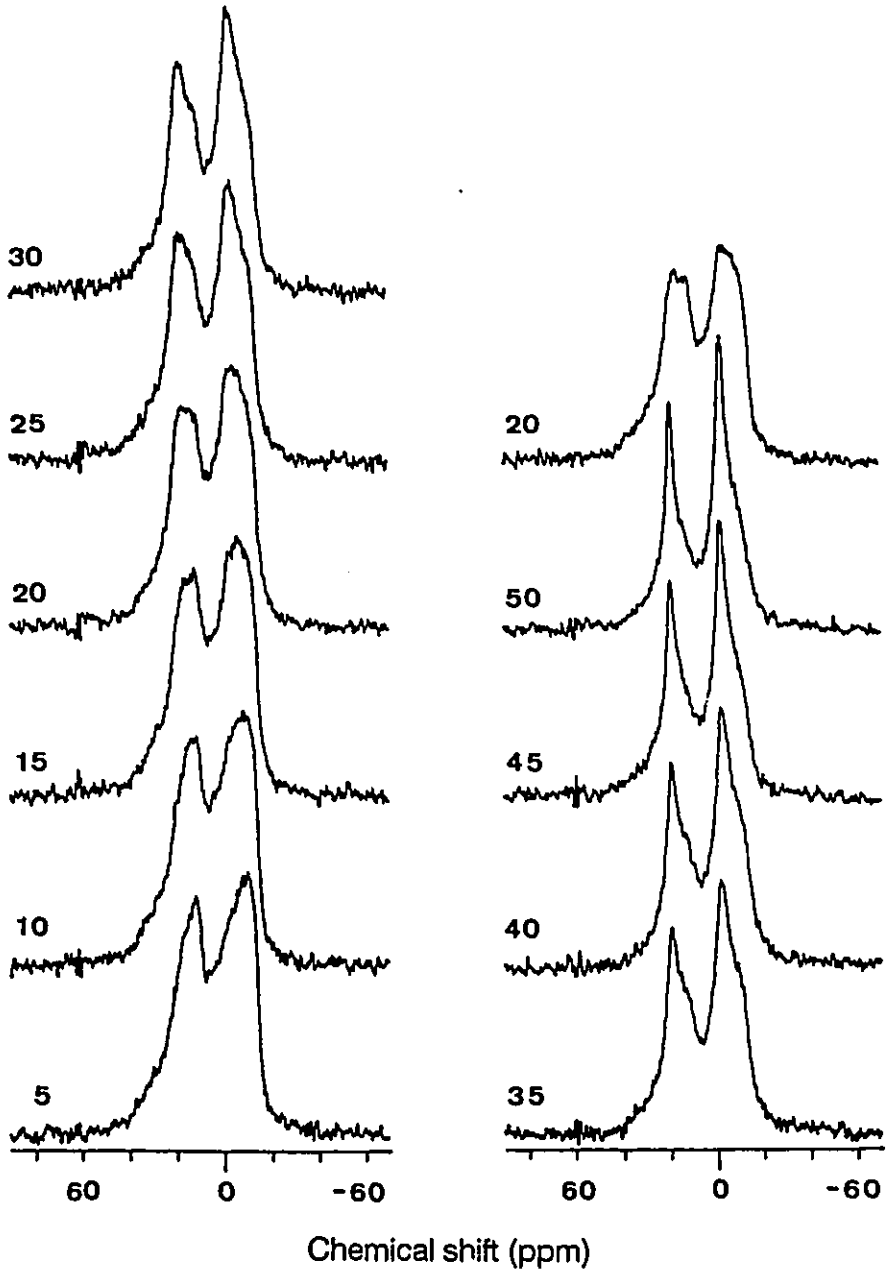

Figure 3-4. ^{31}P NMR spectra (121.5 MHz) of the polar lipids of *T. thermophila* at the indicated temperature, 640 accumulations. The 90° pulse width was 5.8 μs and the recycling delay 4 s.

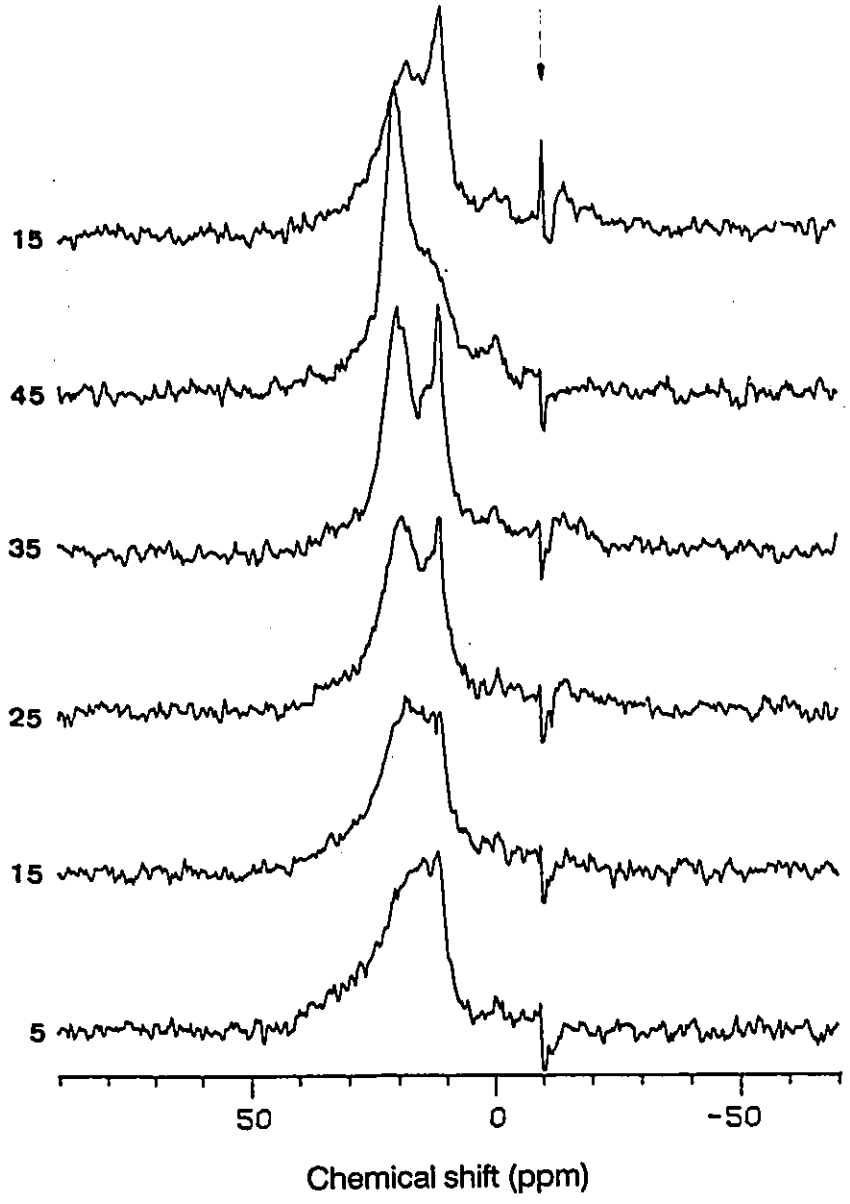

Figure 3–5. 121.5-MHz ^{31}P NMR spectra of the polar lipids of *T. thermophila* at the indicated temperature with selective saturation of the phospholipid resonance using a DANTE pulse sequence. Total number of accumulations: 2000. The 90° pulse width was 6 μs and the recycling delay 4 s. Saturation pulses of 0.5 μs were followed by a 50-μs delay. The number of saturation pulses was 4000 for a total saturation time of 0.2 s. The arrow shows the saturation frequency.

3.4.2.3 Total lipids

The experiment was repeated with total lipids (Figure 3-6). In this case, the behavior is quite different. First, the phase retained bilayer character up to 30°C, the growth temperature. Deslauriers *et al.* (20) have reported a lamellar phase up to 20°C, when the growth temperature was 25°C. Second, there is no evidence for H_{II} phase formation. Finally, at 35°C isotropic peaks begin to appear and at 45–50°C they are the only components visible. When the temperature is decreased back to 20°C, the isotropic peaks are still present and the changes are not easily reversible. The bilayer phase can be brought back by freezing only, therefore the polar lipids show hysteresis in their phase behavior when the neutral lipids are present in the sample.

Similarly, when performing the DANTE experiment on the total lipids to saturate the phospholipid component (Figure 3–7), a transition from a bilayer to an isotropic phase is observed, and it is not easily reversible. The spectra also show a change in time at the same temperature, which is clearly seen at 35°C between the echo and the DANTE spectrum, the former being acquired before the latter at the same temperature. Apparently the transformation of one structure into the other is a slow process. At high temperature, two isotropic peaks are observed because the irradiation point on the phospholipid powder pattern was not placed at the isotropic chemical shift value, but close to the 90° orientation.

Figure 3–8, which shows the echo and the DANTE spectra as well as the subtraction of the latter from the former, allowed the precise measurement of the chemical shielding anisotropy $\Delta\sigma = \sigma_{\parallel} - \sigma_{\perp}$ and isotropic value of the chemical shift tensor $\sigma_i = {}^1/_3(\sigma_{\parallel} + 2\sigma_{\perp})$ for both phospho– and phosphonolipids. The values are $\Delta\sigma = -48$ ppm and $\sigma_i = 1.2$ ppm for the phospholipids and $\Delta\sigma = -31$ ppm and $\sigma_i = -20.1$ ppm for the phosphonolipids. It should be noted

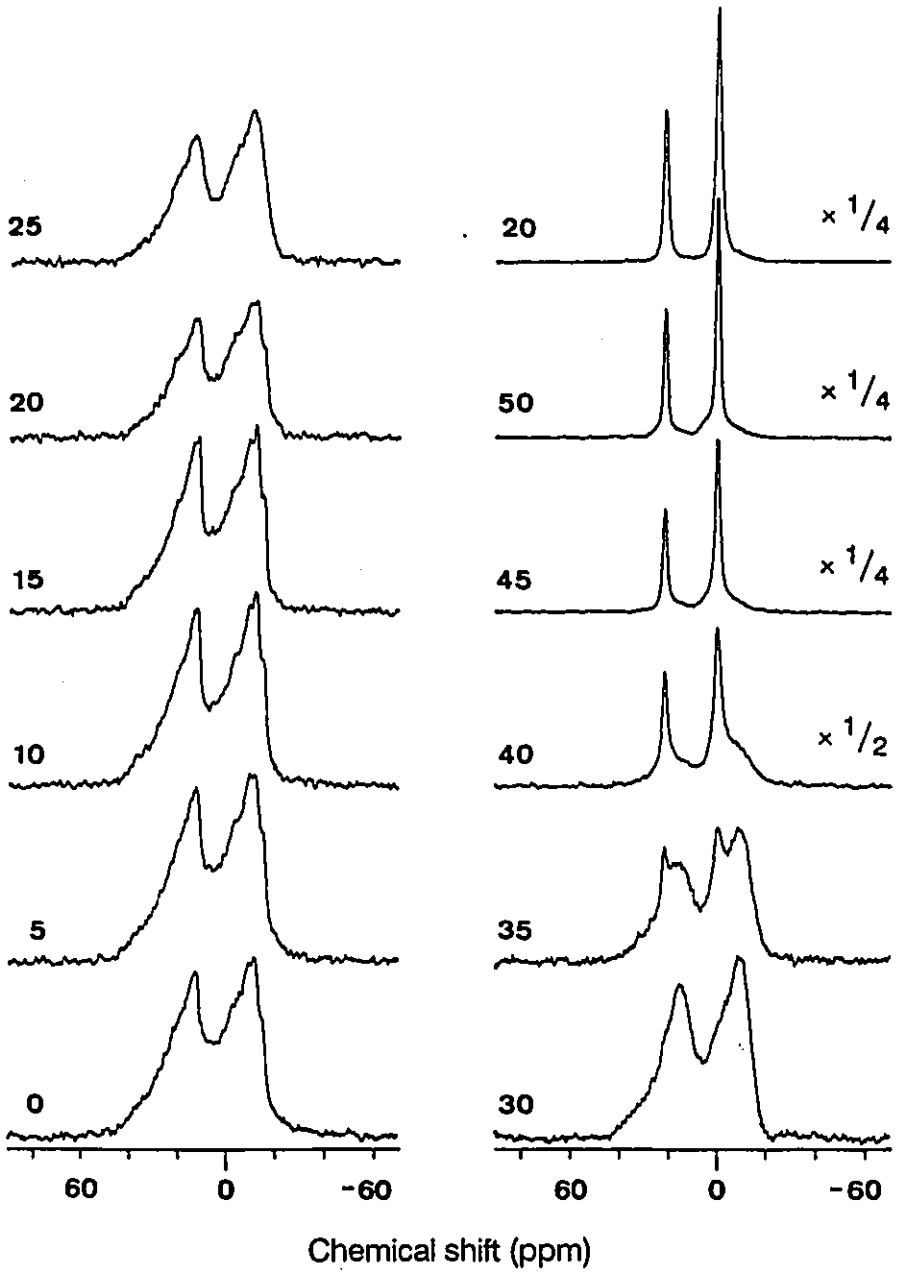

Figure 3–6. 121.5-MHz ^{31}P NMR spectra of the total lipids of *T. thermophila* at the indicated temperature, 400 accumulations. The 90° pulse width was 3.7 μs and the recycling delay 4 s.

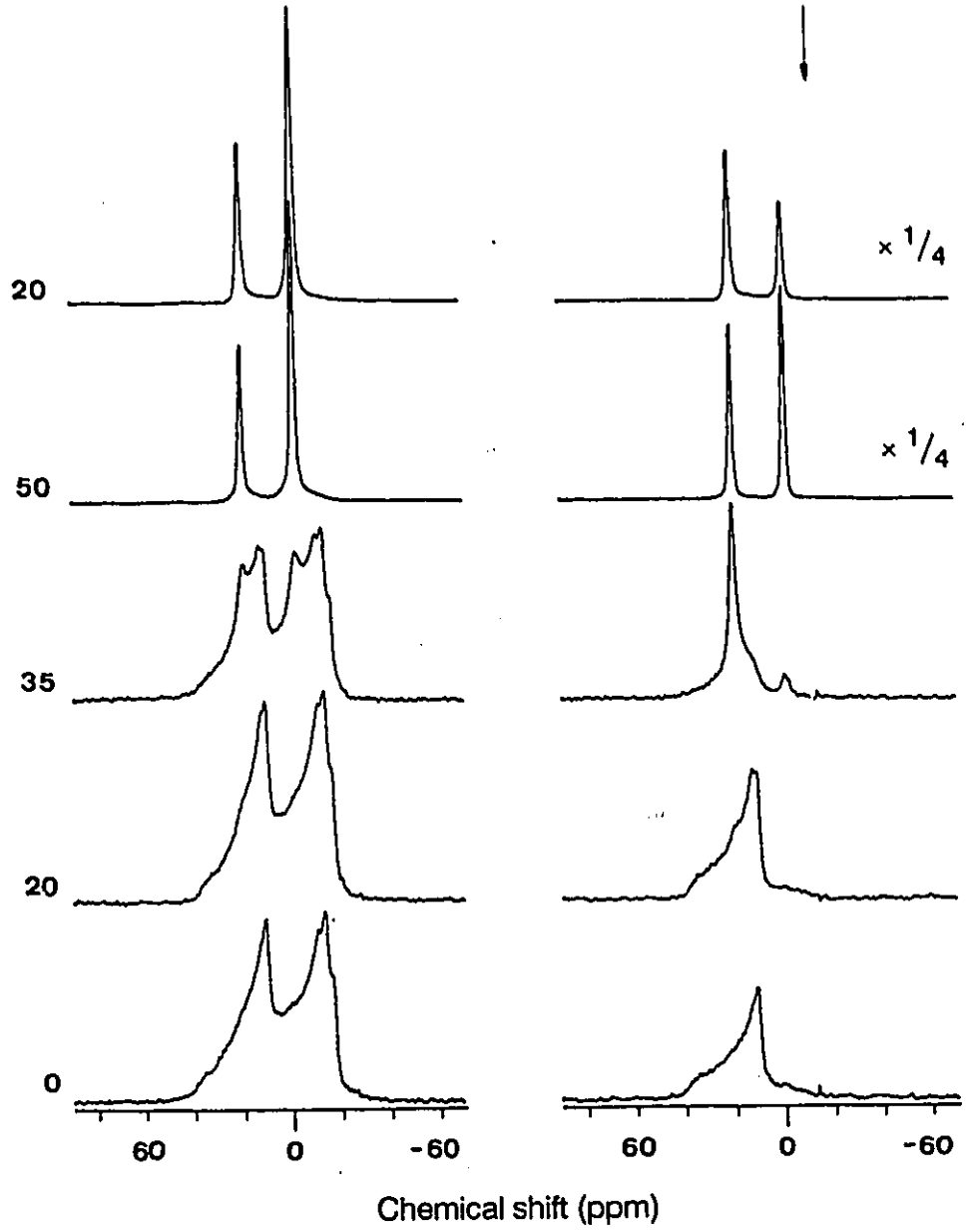

Figure 3–7. ^{31}P NMR spectra (121.5 MHz) of the total lipids of *T. thermophila* at the indicated temperature with a spin echo (left) or with presaturation using the DANTE pulse sequence (right). The total number of accumulations was 1200, the 90° pulse width 6 μs and the recycling delay 4 s. The conditions for the presaturation are those of Figure 3–5. The arrow shows the position of saturation.

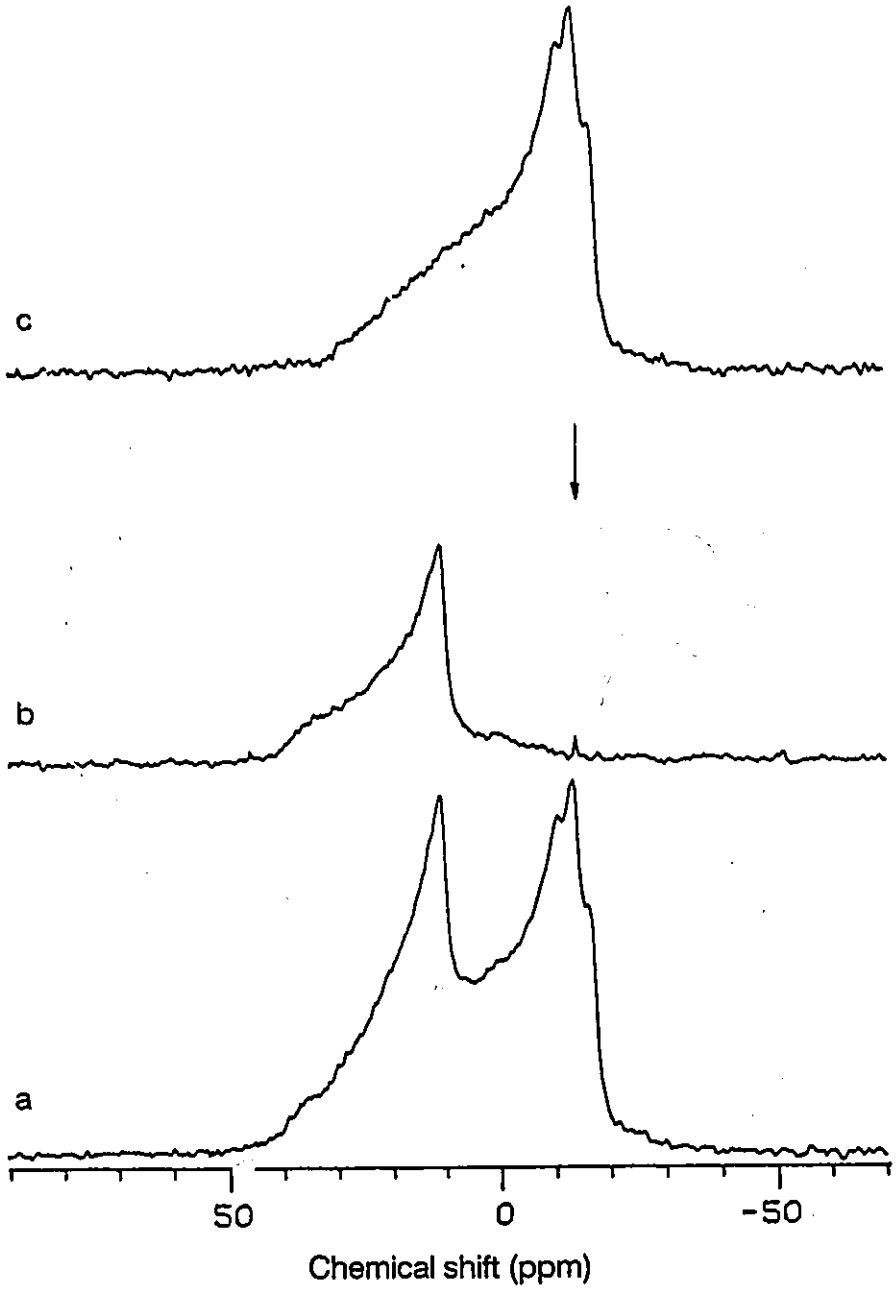

Figure 3–8. 121.5-MHz ^{31}P NMR spectra of the total lipids *T. thermophila* at 0°C with a spin echo (a) or with selective presaturation using a DANTE pulse sequence (b). All conditions are described in Figure 3–7. Spectrum (c) is the subtraction of spectrum (b) from spectrum (a). The saturation frequency is shown by the arrow.

that the absolute value of $\Delta\sigma$ for the phospholipids might be larger than the true value for each individual component, three of them being easily identified on the spectrum (Figure 3–8). On the other hand, only one powder pattern can be distinguished for the phosphonolipid powder pattern. The smaller value for σ_i for the phosphonolipid must be the consequence of a lower electron density around the phosphorus atom in the phosphonate relative to the phosphate. However, there is no possibility to know whether the smaller absolute value of the chemical shift anisotropy $|\Delta\sigma|$ observed for phosphonolipids is due to electronic or structural factors, or a combination of both, if the complete ^{31}P NMR chemical shielding tensor – principal components and orientation of the principal axes – is not known.

Due to the complexity of the system, the exact role of each lipid component cannot be determined. Several studies (19, 21, 39) have shown that PC and sphingolipids can stabilize PE or AEPL in the bilayer form. However, the polar lipids of *Tetrahymena* undergo a bilayer-to-hexagonal phase transition at a relatively low temperature – the transition starts at a temperature lower than the growth temperature. Apparently, the amounts of the above components are not high enough for this stabilization. On the other hand, when neutral lipids are present as well, no hexagonal phase is formed, the bilayer phase being stabilized up to a higher temperature. However, an unknown isotropic component appears, and this transition is partially irreversible.

For reasons indicated above, pure AEPL would be required to determine its own phase behavior, and the effect of other components present in the system could then more easily be determined.

3.4.3 Purification of AEPL

Because of the complexity of total or polar lipid mixtures, purification of AEPL was attempted. The compound could later be studied by ^{31}P NMR, either individually or mixed in different proportions with other polar or neutral lipids.

First attempts at purification of AEPL were done by preparative TLC. The solvent system chloroform–acetic acid–methanol–water 75:25:5:2.2 (7) is suitable to separate AEPL from PE on an analytical scale. However, on a preparative scale, there was overlap of the bands for these two components. In order to be useful as a purification method, the R_f of the two components to separate must differ by at least 0.3, taking into account the large dispersion of the bands caused by different combinations of alkyl and acyl chains. A solvent system that would give such a separation has never been described, and this is easily understood because of the close similarity between the molecular structures of phospho- and phosphonolipids. Therefore, column chromatography was chosen as an alternative.

Silica gel chromatography of total lipids of *Tetrahymena* was carried out to develop a purification method for AEPL. Conventional solvent systems composed of mixtures of chloroform and methanol failed to separate AEPL from PE. Neutral lipids are eluted in the void volume with pure $CHCl_3$. The mixture $CHCl_3$–CH_3OH 9:1 enables the separation of CL. However, AEPL and PE are collected in the same fractions, without separation. Their elution starts with the solvent $CHCl_3$–CH_3OH 7:3, but the polarity must be increased to $CHCl_3$–CH_3OH 6:4 to elute them completely. Elution of more polar lipids starts with $CHCl_3$–CH_3OH 4:6, but resolution of the other components is not good. The method appears useful for the separation of ethanolamine-containing lipids from the other components. The two components of this fraction could be separated by TLC,

since the solvent mixture used is suitable for their separation. However, since the quantities obtainable are low, a column chromatography method would be preferable. A large proportion of acetic acid is required to separate the two classes of lipids (36). Different solvent compositions were tried, without much success.

The solvent systems of Kapoulas (36), containing various proportions of acetic acid in chloroform, were used to purify the AEPL—PE mixture by column chromatography on silica gel. With neither solvent system was it possible to obtain a complete separation of the 2-aminoethylphosphonolipid from its phosphatidylethanolamine analog, although pure PE was obtained in late fractions. It was cumbersome to eliminate all traces of acetic acid, because so much of it had to be used to achieve effective separation.

3.4.4 Hydrolysis with phospholipase D

The last method tried to obtain a pure AEPL fraction was enzymatic hydrolysis of phospholipids with phospholipase D. Since phosphonolipids possess a P—C rather than a P—O bond on the amino side of their headgroup, they are resistant to hydrolysis with this enzyme, whereas phospholipids are transformed to phosphatidic acid (PA), which is believed to be more easily separated from AEPL than PE. With the solvent system used for TLC of the polar lipids, PA migrates close to the solvent front. The results show that, although the amount of PE decreased with time relative to that of AEPL, the reaction never went to completion, even when more enzyme was added. The PE was transformed into a component of R_f sufficiently different from that of AEPL to achieve a good separation by simple column chromatography. However, the method was not satisfactory since the reaction could not be taken to completeness, necessitating separation of residual PE from AEPL.

3.5 Conclusion

Using thin-layer chromatography, the major components of the polar and neutral lipids of *Tetrahymena thermophila* were identified.

^{31}P NMR was used to observe the phase behavior of the polar and total lipids of *Tetrahymena thermophila* dispersed in excess buffer. The results show that a reversible transition from bilayer to hexagonal phase occurs between 15 and 45°C for the polar lipids, whereas for the total lipids the transition temperature is ca. 35°C, but the bilayer is transformed into an unknown isotropic phase. It is suggested that one or more components of the neutral lipids (possibly tetrahymanol) stabilize the bilayer up to higher temperature. However, the formation of the isotropic phase could not be explained. This isotropic phase show hysteresis, and only freeze-thawing can bring back the bilayer spectrum.

Attempts at purification of AEPL having not been successful, it was decided to study phosphonolipids in a more rigorous manner. In order to interpret the above results in terms of headgroup conformation, the ^{31}P NMR chemical shielding tensor is required. By using synthetic compounds, the lipid can be labelled and other nuclei can be used as probes in determining the conformation. Finally, by using model membrane systems of known composition, all the variables can be controlled and the effect of each of them determined individually.

3.6 References

1. M. Horiguchi and M. Kandatsu, *Nature* **184**, 901–902 (1959).

2. C.R. Liang and H. Rosenberg, *Biochim. Biophys. Acta* **125**, 548–562 (1966).

3. G.A. Thompson, Jr., *J. Protozool.* **19**, 231–236 (1972).

4. G.A. Thompson, Jr. and Y. Nozawa, *Biochim. Biophys. Acta* **472**, 55–92 (1977).

5. I.C.P. Smith and I.H. Ekiel, in *Phosphorus–31 NMR, Principles and Applications*, edited by D.G. Gorenstein (Academic Press, Orlando, Florida, 1984), Chap. 15, pp. 447–475.

6. J.D. Smith, W.R. Snyder and J.H. Law, *Biochem. Biophys. Res. Commun.* **39**, 1163–1169 (1970).

7. Y. Nozawa and G.A. Thompson, Jr., *J. Cell Biol.* **49**, 712–721 (1971).

8. G.A. Thompson, Jr., R.J. Bambery and Y. Nozawa, *Biochemistry* **10**, 4441–4447 (1971).

9. T. Hori and Y. Nozawa, in *New Comprehensive Biochemistry*, Volume 4, edited by A. Neuberger and L.L.N. van Deenen (Elsevier Biomedical Press, Amsterdam, 1982), Chap. 3, pp. 95–128.

10. G.A. Thompson, Jr., *Biochemistry* **6**, 2015–2022 (1967).

11. M. Jonah and J.A. Erwin, *Biochim. Biophys. Acta* **231**, 80–92 (1971).

12. H. Berger, P. Jones and D.J. Hanahan, *Biochim. Biophys. Acta* **260**, 617–629 (1972).

13. M. Sugita, Y. Fukunaga, K. Ohkawa, Y. Nozawa and T. Hori, *J. Biochem.* **86**, 281–288 (1979).

14. C.S. Ramesha and G.A. Thompson, Jr., *Biochemistry* **21**, 3612–3617 (1982).

15. J. Erwin and K. Bloch, *J. Biol. Chem.* **238**, 1618–1624 (1963).

16. H. Fukushima, C.E. Martin, H. Iida, Y. Kitajima, G.A. Thompson, Jr. and Y. Nozawa, *Biochim. Biophys. Acta* **431**, 165–179 (1976).

17. T. Watanabe, H. Fukushima and Y. Nozawa, *Biochim. Biophys. Acta* **620**, 133–141 (1980).

18. H. Maruyama, Y. Banno, T. Watanabe and Y. Nozawa, *Biochim. Biophys. Acta* **711**, 229–244 (1982).

19. H.C. Jarrell, R.A. Byrd, R. Deslauriers, I. Ekiel and I.C.P. Smith, *Biochim. Biophys. Acta* **648**, 80–86 (1981).

20. R. Deslauriers, I. Ekiel, R.A. Byrd, H.C. Jarrell and I.C.P. Smith, *Biochim. Biophys. Acta* **720**, 329–337 (1982).

21. K.A. Ferguson, S.W. Hui, T.P. Stewart and P.L. Yeagle, *Biochim. Biophys. Acta* **684**, 179–186 (1982).

22. R.J. Hill, R. Deslauriers, K.W. Butler, R. Colvin and I.C.P. Smith, *Biochemistry* **23**, 2300–2309 (1984).

23. R.J. Hill, *FEBS Lett.* **128**, 278–280 (1981).

24. R.L. Conner, J.R. Landrey, D.H. Burns and F.B. Mallory, *J. Protozool.* **15**, 600–605 (1968).

25. R.E. Wuthier, *J. Lipid Res.* **7**, 558–561 (1966).

26. J. Folch, M. Lees and G.H. Sloane-Stanley, *J. Biol. Chem.* **226**, 497–509 (1957).

27. J.C. Dittmer and M.A. Wells, *Methods Enzymol.* **XIV**, 482–530 (1969).

28. M. Kates, in *Laboratory techniques in biochemistry and molecular biology*, Volume 3, edited by T.S. Work and E. Work (North-Holland, Amsterdam, 1972). pp. 267–610.

29. G. Rouser, G. Kritchevsky, D. Heller and E. Lieber, *J. Amer. Oil Chem. Soc.* **40**, 425–454 (1963).

30. J.C. Dittmer and R.L. Lester, *J. Lipid Res.* **5**, 126–127 (1964).

31. V.E. Vaskovsky and E.Y. Kostetsky, *J. Lipid Res.* **9**, 396 (1968).

32. H. Wagner, L. Hörhammer and P. Wolff, *Biochem. Z.* **334**, 175–184 (1961).

33. M.D. Bischel and J.H. Austin, *Biochim. Biophys. Acta* **70**, 598–600 (1963).

34. M. Rance and R.A. Byrd, *J. Magn. Reson.* **52**, 221–240 (1983).

35. G.A. Morris and R. Freeman, *J. Magn. Reson.* **29**, 433–453 (1978).

36. V.M. Kapoulas, *Biochim. Biophys. Acta* **176**, 324–329 (1969).

37. F.M. Davidson and C. Long, *Biochem. J.* **69**, 458–466 (1958).

38. J. Seelig, *Biochim. Biophys. Acta* **515**, 105–140 (1978).

39. P.R. Cullis and M.J. Hope, *Biochim. Biophys. Acta* **597**, 533–542 (1980).

CHAPTER 4

^{31}P NUCLEAR MAGNETIC RESONANCE CHEMICAL SHIELDING TENSOR OF 2-AMINOETHYLPHOSPHONIC ACID[1]

4.1 Introduction

Solid-state ^{31}P nuclear magnetic resonance (NMR) is a valuable technique for studying phosphorus-containing lipid headgroups, owing to the high natural abundance of ^{31}P, its relatively large gyromagnetic ratio, and the fact that no perturbation need be introduced in the system (2). Phosphonolipids are found in several types of organisms (3), but very little is known about their role or their influence on membrane structure. Like phospholipids, they exhibit polymorphism that can be detected by ^{31}P NMR; in both cases, bilayers and nonbilayer structures give rise to characteristic lineshapes (4).

The information obtained from ^{31}P NMR chemical shift anisotropy of unsonicated phosphorus-containing lipid dispersions can be interpreted in terms of headgroup conformation, molecular motion and lipid polymorphism only if the ^{31}P NMR chemical shielding tensor is known (2). Computational approaches being unfeasible, it is necessary to determine the orientation of the shielding tensor experimentally on suitable model systems. A major problem in the experimental

---

[1] The results presented in this chapter have been published in Reference 1.

determination of the tensor orientation is the difficulty to grow single crystals sufficiently large for NMR investigations. So far, single crystals of phospholipids have been small and of poor quality by normal crystallographic standards (5). The lack of data on the ^{31}P NMR shielding tensor in phosphonates, specifically on its orientation with respect to the molecular frame, precludes any prediction of lineshapes for various phosphonolipid phases. The orientation of the chemical shift tensor is known for several phosphate compounds (6–10); the principal values of the tensor are known for a phosphonolipid (4), but no information is available on its orientation with respect to the molecular framework.

In this work, the ^{31}P NMR chemical shielding tensor was determined in 2-aminoethylphosphonic acid (AEP), a good model for the headgroup component of phosphonolipids. AEP was chosen because it readily forms single crystals, and because it is the phosphonate analog of 2-aminoethyl phosphate, the compound used as a model for phospholipid headgroups (7). Previous works on phosphonates include theoretical calculations of ^{31}P NMR shielding tensors by quantum chemical methods (11, 12), and a report of the principal values of the chemical shift tensor in different phosphonic acid diesters and phosphonic acids (13). This is the first determination of the complete ^{31}P NMR chemical shielding tensor of a phosphonate.

4.2 Theory

As a result of the chemical shift anisotropy and in the absence of other interactions, the NMR spectrum of a sample containing randomly distributed crystallites assumes a characteristic powder pattern, and the principal values of the shielding tensor can be read directly from the spectrum (14). When the sample is a single crystal, narrow resonances are observed; their number depends on the

symmetry of the unit cell and on the number of nonequivalent resonant nuclei in the asymmetric unit. The measured chemical shift σ_{zz} of a particular line corresponds to the *zz* component of the shielding tensor in the laboratory axis system (*xyz*), where *z* is the direction of the magnetic field $\boldsymbol{B_0}$. It is related to the components of the tensor in another axis system according to the equation (15):

$$\begin{aligned}\sigma_{zz} = {} & \sigma_{XX}\sin^2\theta\cos^2\phi + \sigma_{YY}\sin^2\theta\sin^2\phi + \sigma_{ZZ}\cos^2\theta \\ & + \sigma_{XY}\sin^2\theta\sin2\phi + \sigma_{XZ}\sin2\theta\cos\phi \\ & + \sigma_{YZ}\sin2\theta\cos\phi, \end{aligned} \qquad [4\text{–}1]$$

where θ and ϕ are the polar angles of $\boldsymbol{B_0}$ in the axis system (*XYZ*).

In order to determine the six components of the chemical shielding tensor, it is sufficient to measure σ_{zz} in six independent orientations and to solve the resulting six equations (Equation [4–1]). However, when the spectra contain more than one line, it is difficult to determine unambiguously from the spectra in the six orientations which lines arise from the same nucleus, and consequently the following procedure is used. The crystal is mounted on a cube that can be connected to a goniometer in three orthogonal ways. The rotation axis of the goniometer must be perpendicular to $\boldsymbol{B_0}$. An axis system (*x'y'z'*) fixed to the cube is chosen so that *x'*, *y'* and *z'* are perpendicular to the three faces of the cube. For a rotation about the axis *i* of the goniometer cube, it can be shown (16) that:

$$\sigma_{zz}(\rho) = \sigma_{jj}\cos^2\rho + \sigma_{kk}\sin^2\rho + \sigma_{jk}\sin2\rho, \qquad [4\text{–}2]$$

where *i*, *j* and *k* represent the *x'*, *y'* and *z'* cube axes, or other related axes, *i* is the axis perpendicular to and *j* the axis at an angle ρ to the magnetic field direction.

4.3 Experimental part

4.3.1 NMR experiments

^{31}P NMR spectra were obtained at room temperature on a Bruker CXP–300 spectrometer operating at 121.5 MHz. To avoid large first-order phase corrections of the spectra, a spin echo sequence with complete phase cycling is used (17), the first and second pulses being 72 and 144°, respectively, to allow faster recycling. An estimate of the longitudinal relaxation time T_1, obtained using the inversion-recovery method followed by the Hahn echo on powder AEP, allowed the setting of the recycling delay to 15 s, provided the pulse angles used for the echo be shorter than 90 and 180°. Hence, from the Ernst equation (Equation [2–7]): $\alpha = 72°$ when $T = T_1$, where α is the pulse angle and T the recycling delay. The 90° pulse durations ranged from 4.0 to 4.6 μs and the pulse spacing was 42 μs. All spectra were obtained in the presence of gated broadband decoupling; the ^1H decoupling field ($1.4 \cdot 10^{-4}$ T) is applied from the start of the first pulse to the end of the acquisition period. The decoupler frequency was set 3 ppm upfield from the H_2O resonance; at this frequency, the linewidth of the ^{31}P lines of AEP are minimal. Typically, 100 to 300 accumulations were necessary to obtain a good signal-to-noise ratio. In order to improve the signal-to-noise ratio without losing resolution, a double multiplication (Lorentzian broadening, −80 Hz; Gaussian broadening, 200 Hz) is applied to the free induction decays, which are subsequently Fourier transformed from the top of the echo (17).

Chemical shifts are reported in ppm relative to an external reference of 85% H_3PO_4, assuming positive values for resonances at high frequencies. The convention $\sigma_{11} \leq \sigma_{22} \leq \sigma_{33}$ is chosen to label the principal axes.

4.3.2 Goniometer

The single-crystal experiments require that the crystal be rotated about an axis perpendicular to the magnetic field direction. This is accomplished through the use of a specially designed goniometer. A double-tuned ^{31}P–^{1}H home-built probe was modified as diagrammed in Figure 4–1. The goniometer consists of a short horizontal shaft located inside the coil at one end and connected to a 40-tooth worm gear at the other end. The corresponding single-thread worm is itself connected to a long vertical shaft extending to the calibrated dial placed outside the probe. The sample is mounted on a cube that can be attached to the horizontal goniometer shaft in three orthogonal ways. One complete rotation of the vertical shaft corresponds to a 9° rotation of the crystal.

Since the goniometer must be placed inside the magnetic field, it was constructed entirely of nonferromagnetic materials. The worm and worm gear were from Boston Gear Incom International (Quincy, Massachusetts) distributed by MBS Bearing Service (Ottawa, Ontario), and are made of Acetal, with a brass insert for the worm gear. The long vertical shaft is pure aluminum. The sample cube and cube holder are composed of plexiglass. Materials used for the other components include Teflon, Nylon, aluminum and brass.

Using this goniometer, the orientation of the sample could be controlled to within 0.07°. The reproducibility of the system is demonstrated by noting that a spectrum taken at a given orientation is identical to that taken after the crystal is rotated away and then returned to the initial angle.

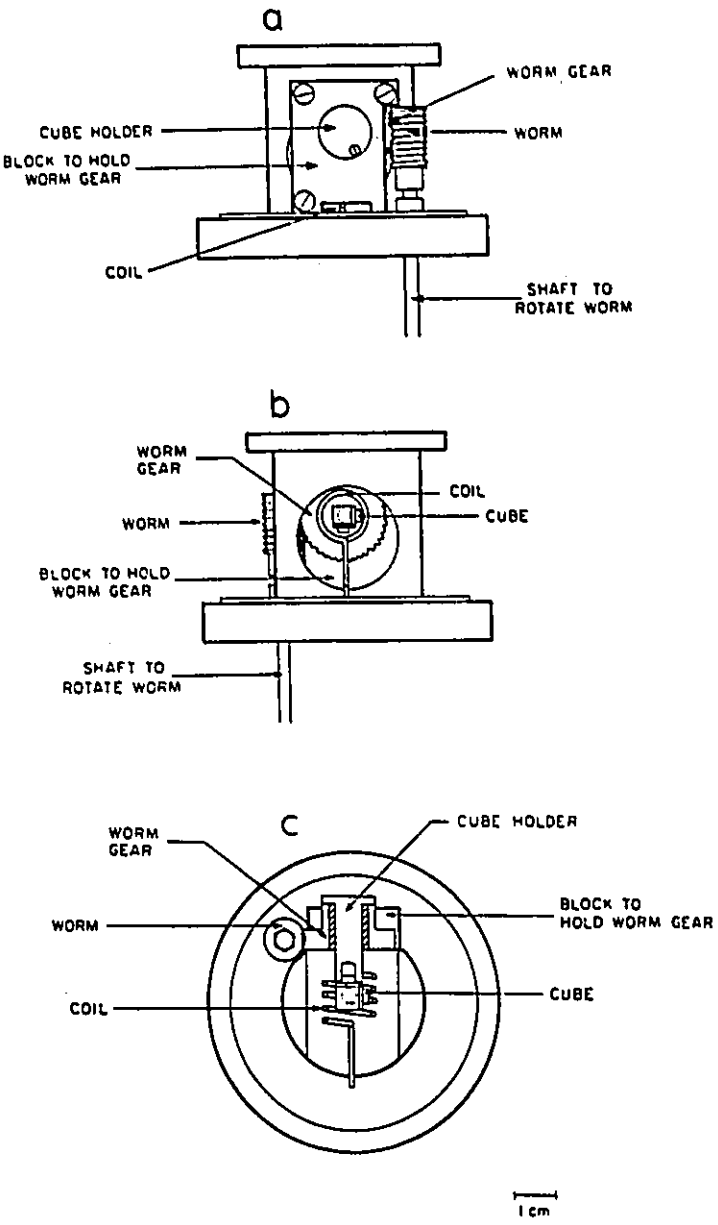

Figure 4–1. Diagram of the top of a double-tuned ^{31}P–^{1}H home-built NMR probe showing the single-axis goniometer modification. (a) Rear view. (b) Front view. (c) Cross section through the middle of the coil.

4.3.3 Sample preparation

AEP was obtained as a powder from Sigma Chemical Company (St. Louis, Missouri), and was used without further purification. Single crystals were grown at room temperature by vapor diffusion of 95% ethanol into a previously filtered 40 mg/ml aqueous solution of AEP, and were harvested after 5 to 10 days. The lengths of the unit cell axes were measured and found to be $\alpha = 10.3593$ (± 0.0012), $\beta = 10.7713$ (± 0.0012) and $\gamma = 8.7738$ (± 0.0011) Å, in agreement with the reported values of $\alpha = 10.35_5$, $\beta = 10.76_7$ and $\gamma = 8.77_2$ Å (18). A crystal measuring approximately $3.0 \times 2.5 \times 1.5$ mm (19 mg) was used for the NMR experiments. The orientation of the crystal axes was determined with a diffractometer. The crystal was transferred from the x-ray goniometer to the NMR goniometer, and the approximate orientation of the unit cell axes with respect to the goniometer cube axes was noted.

4.4 Method and results

4.4.1 NMR measurements

The ^{31}P NMR spectrum of a powder of AEP is shown in Figure 4–2(a). It has the shape characteristic of an asymmetric chemical shielding tensor. This is expected as a result of the low symmetry of the phosphonate group in the AEP molecule. From this spectrum, the principal values are found to be: $\sigma_{11} = -83$, $\sigma_{22} = -15$ and $\sigma_{33} = 45$ ppm, in good agreement with the previously reported values of $\sigma_{11} = -81$, $\sigma_{22} = -11$ and $\sigma_{33} = 47$ ppm (4).

Figure 4–2(b) shows a spectrum from a single crystal of AEP in an arbitrary orientation. Knowledge of the space group and number of resonant nuclei

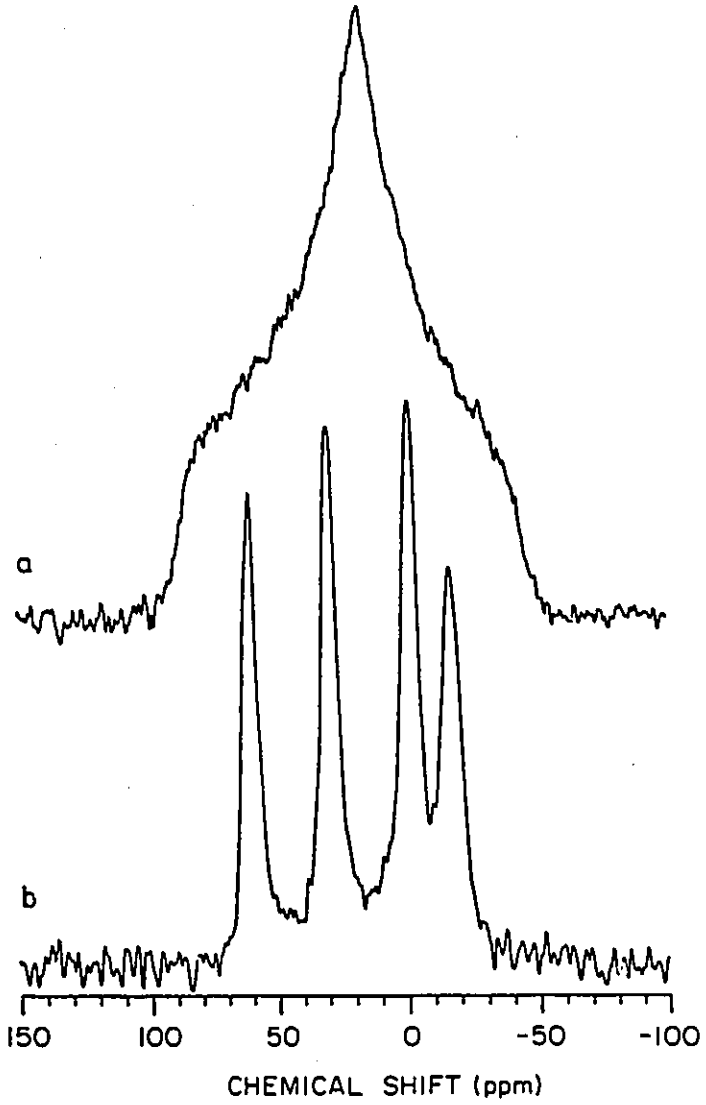

Figure 4–2. ^{31}P NMR spectra of AEP at 121.5 MHz using quadrature detection. The spectral width was 83.3 kHz; free induction decays of 8 K points were transformed to 16 K complex points. (a) Spectrum of a powder sample, 112 accumulations. (b) Spectrum of a single crystal in the orientation indicated by the arrow in Figure 4–5(c), 288 accumulations.

per asymmetric unit allows the prediction of the maximum number of lines that will be seen at any orientation of the crystal. AEP crystallizes in the orthorhombic space group *Pbca* with one molecule per asymmetric unit (18). A stereoscopic illustration of the AEP molecules in the unit cell is shown in Figure 4–3. There are therefore eight molecules per unit cell, occurring in four pairs related by inversion symmetry. Since chemical shielding tensors are invariant under inversion, the presence of four lines results from four magnetically nonequivalent orientations of AEP in the unit cell.

The linewidths in Figure 4–2(b) range from 850 to 1150 Hz, and are orientation-dependent. Increasing the power of the ^{1}H decoupling field does not produce any further line narrowing, indicating that the ^{31}P–^{1}H dipolar interactions are completely removed. Since the shortest distance between two phosphorus atoms in AEP crystals is 4.60 Å, the contribution to the linewidth from P–P dipolar interactions is expected to be about 380 Hz (Equation [2–26]), neglecting the orientation dependence of these interactions. Another contribution to the linewidth is spin-spin (T_2) relaxation. At the magnetic field value used for these measurements (7 T), chemical shift anisotropy is an important relaxation mechanism. The relaxation time T_2, measured on a crystal in an arbitrary orientation, was found to be between 560 and 840 μs, depending on the orientation. These values correspond to linewidths of 380 to 570 Hz (Equation [2–11]). Thus, the combination of T_2 relaxation via the chemical shift anisotropy mechanism and broadening due to intermolecular P–P dipole-dipole interactions accounts for the observed linewidths.

4.4.2 Determination of the tensor

For the computation of the principal components and the orientation angles of the chemical shielding tensor $\underline{\sigma}$ from the three rotation plots, the

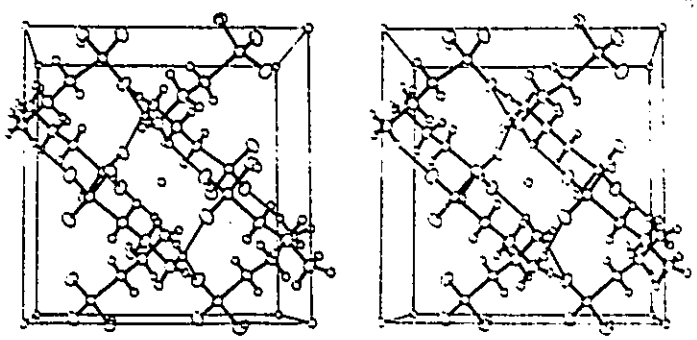

Figure 4–3. ORTEP (19) stereoscopic illustration of the packing of AEP molecules in the *Pbca* unit cell, as viewed down the *c* axis. The *a* axis points to the right and the *b* axis to the top. The stereoscopic image can be observed through a stereoscope with a 9-cm focal length and a 6.5-cm separation between optical centers.

coordinate systems shown in Figure 4–4 are relevant. The experimentally accessible shielding value is given by the matrix element σ_{zz} in the laboratory axis system. The tensor in the cube or sample axis system is obtained from it by applying Equation [4–2]. The desired quantities are eigenvalues of the tensor $\underline{\sigma}$, as well as the orientation of the principal axis system with respect to the crystal or the molecular axis system, expressed by the transformation matrices $R^{(pc)}$ or $R^{(pm)}$ respectively. In the present approach, the tensor $\underline{\sigma}^{(s)}$ is first obtained by a least-squares fit of the shielding values measured for the different orientations of the crystal. The transformation matrix $R^{(cs)}$ is determined exactly from the approximate orientation of the crystal axes with respect to the cube axes and the symmetry of the space group. A molecular axis system related to the symmetry of the phosphonate group is chosen and $R^{(mc)}$ computed from the atom positions in the crystal unit cell. By a subsequent diagonalization, $\underline{\sigma}^{(p)}$ and $R^{(pc)}$ or $R^{(pm)}$ are found.

For the computation, all programs were written in Turbo Pascal 3.0 (Borland International, Scotts Valley, California) and run in CP/M 3.0 (Digital Research, Pacific Grove, California) on a Franklin Ace 100 computer (Apple II+ compatible).

4.4.2.1 Tensors in the cube axis system

The ^{31}P NMR spectra were obtained as a function of the rotation angle about the three orthogonal cube axes. The spectra were taken in 9° intervals over a range of 180°. The experimental points and theoretical curves fitted to Equation [4–2] by the method of least squares are shown in Figure 4–5. The general least-squares method (20) is used to fit a curve that is linear in its coefficients. Matrix inversion following the Gauss-Jordan elimination method with complete pivoting (21, 22) is used to solve a system of linear simultaneous

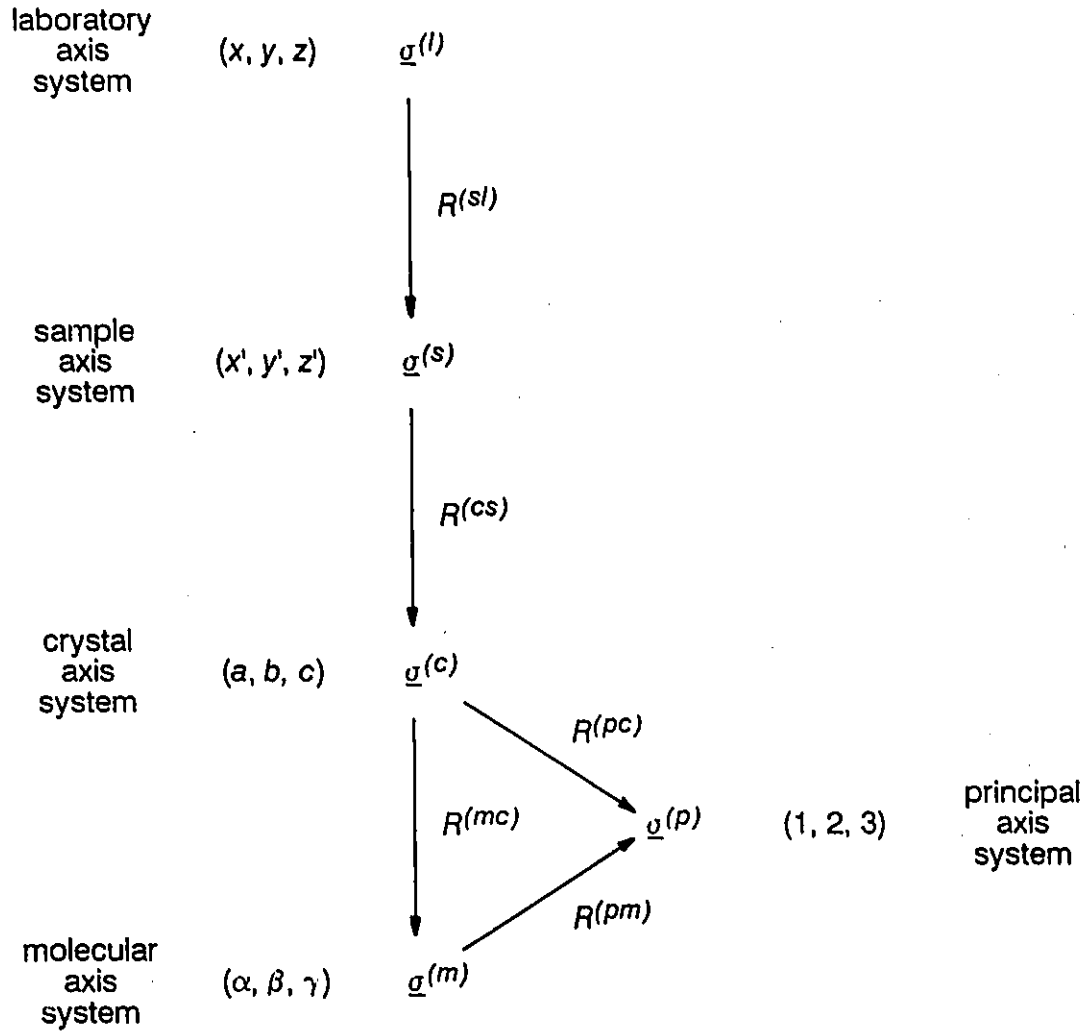

Figure 4–4. Summary of the different coordinate systems used in this study. Also indicated are the rotation matrices transforming the ^{31}P NMR chemical shielding tensor between different axis systems. The superscript of the rotation matrices indicates destination and origin of the transformation, *e.g.* $R^{(sl)}$ is the transformation matrix used to transform the ^{31}P NMR chemical shielding tensor from the laboratory axis system to the sample – or cube – axis system.

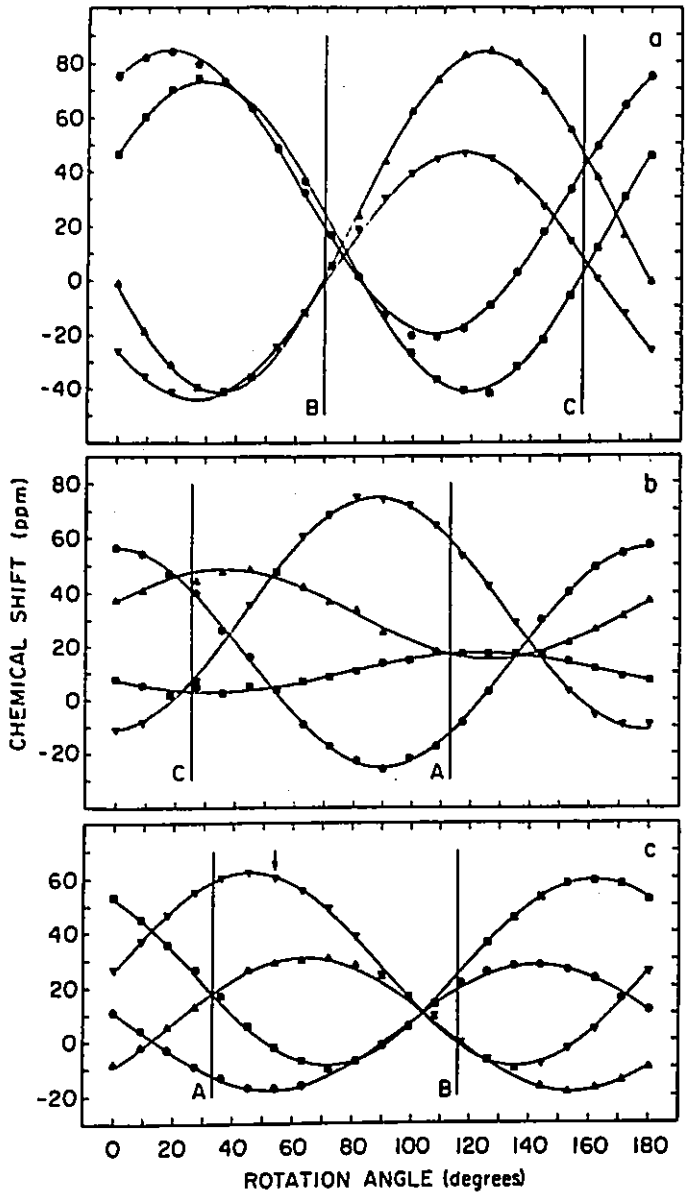

Figure 4–5. Angular dependence of ^{31}P NMR chemical shift for rotation of a crystal of AEP about the x' (a), y' (b) and z' (c) axes of the goniometer cube. The plots include data points and theoretical curves calculated from least-squares analyses. The vertical lines locate equivalent sample orientations, as indicated by the labels A, B and C. The arrow shows the orientation for the spectrum of Figure 4–2(b).

equations. For each rotation curve, the starting position of B_0 is not known. In order to relate the regression coefficients of the curves to the tensor elements in the cube axis system, it is necessary to compare two rotational plots. In fact, for each pair of rotation plots, there are points of equivalent orientation, as shown by the vertical lines in Figure 4–5, which represent the solutions with lowest variance. The intersections are found using Newton's method with Marquardt's modification (23, 24) to solve the least-squares problem. As an example, line A in Figure 4–5(c) corresponds to an orientation in the *x'y'* plane. The equivalent orientation in the *x'z'* plane is given by line A in Figure 4–5(b). In this orientation, the magnetic field is thus exactly along the *x'* axis of the goniometer, which is the intersection of the two planes. After a rotation corresponding to the calculated intersections, the full tensors in the cube axis system are found from the sets of corresponding curves from each of the three rotation plots. In this way, from each set of curves, nine tensor elements are determined, six of them being independent; the diagonal elements are determined twice and the two values averaged (15).

4.4.2.2 Tensors in the crystal axis system

The fact that AEP crystals have an orthorhombic unit cell can be used to transform the tensors to the crystal axis system, using a method that relies on the crystal symmetry (18). Specifically, because they belong to the orthorhombic space group *Pbca*, shielding tensors in the crystal axis system must transform into one another by 180° rotations about the unit cell axes. In this particular axis system, the tensors bear a simple relationship to one another in that the magnitude of the tensor elements are the same and only the sign of the off-diagonal elements can change. This constraint, together with the knowledge of the approximate orientation of the crystal axes with respect to the cube axes, was used in a minimization procedure to determine the exact positions of these crystal axes. The computational method is

the following. A transformation matrix is computed from trial Euler angles determined from the known approximate orientation of the crystal axes with respect to the cube axes. The rotation is performed and the residual sum of squares computed. A modified Simplex method (25–28) is used to solve the nonlinear least-squares problem. Then a quadratic approximation of the function near the minimum (25) is used to get a better solution. The tensors in the crystal axis system are obtained by matrix multiplication and the absolute value of the individual elements averaged for the four tensors.

4.4.2.3 Tensors in the molecular axis system

Since the crystal structure is known, the tensors can then easily be transformed from the crystal axis system to a suitable molecular axis system. Two molecular axis systems are retained. The first one is the same that has been used previously to report tensor data for the phosphate compounds (6–10). The α axis bisects the O(1)−P−O(2) plane, the γ axis is perpendicular to the O(1)−P−O(2) plane and the β axis is perpendicular to the other two to form a right-handed system. The second axis system was used for the computations of the simulations of the ^{31}P NMR chemical shift anisotropy (see Chapter 6). In this system, γ is along the P−C(1) bond, α in the O(3)−P−C(1) plane approximately bisecting the O(1)−P−O(2) angle and the β axis again perpendicular to the other two to form a right-handed system. The atom numbering is that of Ogaya (18).

4.4.2.4 Diagonal tensors

The final step of the procedure is to diagonalize the tensors to obtain the principal elements and their orientations with respect to the particular axis system (29). The method of Jacobi (30–32, 22), which involves planar rotations, is used to diagonalize the tensors.

4.4.2.5 Assignment of the tensors

From the data, four chemical shielding tensors are obtained. The tensors have the same principal elements, but differ in orientation corresponding to the four different orientations of the AEP molecule in the crystal unit cell. This allows four possible assignments of the orientation of the tensor on the molecule. The possible tensor orientations on the AEP molecule were then plotted using the ORTEP program (19). Only the assignment of Figure 4–6 shows definite correlation with the bonds of the phosphonate moiety. Table 4–1 summarizes the data for the ^{31}P NMR shielding tensor, along with the corresponding eigenvectors expressed as their direction cosines both in the crystal and molecular axis systems. The errors of the determined parameters are expressed by their standard deviations calculated by the error propagation laws.

4.5 Discussion

In general, chemical shielding tensors depend on the electronic distributions in both the ground and excited states of a molecule (33–35). No molecular orbital calculation data are available for phosphonic acids. It is however possible to explain the results qualitatively in terms of a modification of the phosphate structure. The ^{31}P NMR chemical shift tensor of AEP can also be compared with that of the phosphate analog, 2-aminoethyl phosphate (7).

The orientations of the tensors are very similar in the two compounds, *i.e.* σ_{22} and σ_{33} are approximately in the plane containing the two short P–O bonds, where there should be multiple-bond character (36), leaving the least shielded element σ_{11} in the perpendicular direction, where only single-bond character is expected (36). The major difference between the tensor orientations in

Figure 4–6. ORTEP (19) representation of the ^{31}P NMR chemical shielding tensor in AEP. These are orthogonal projections of the molecule in the principal axis system of the chemical shielding tensor. The length of each ellipsoid axis is proportional to the shielding in that direction relative to an arbitrary reference (14) defined as $\sigma_{ref} = {}^1/_2(\sigma_{33} - \sigma_{11}) - \sigma_{11}$. The numbering of the atoms corresponds to that used in the original x-ray crystallographic study (18), with primed letters indicating atoms from neighboring molecules.

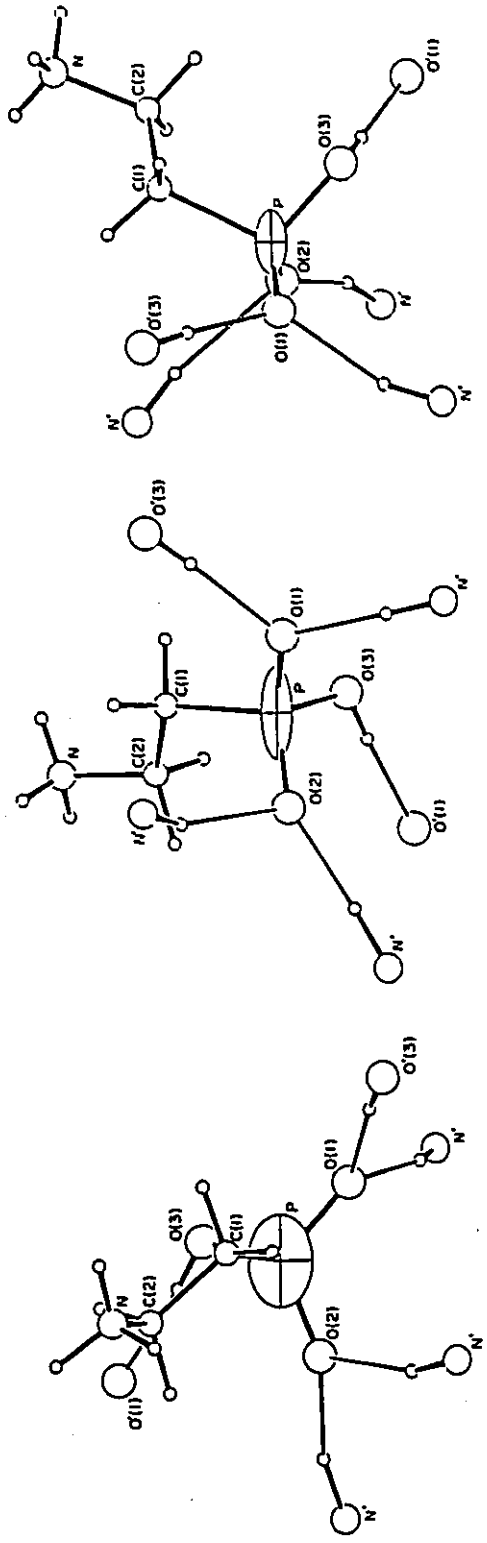
O(1)
O(3)
C(2)
N
C(1)
P
O(2)
N'
O(3)
O(1)
N'
O(3)
O(1)
N'
C(1)
P
O(3)
N
C(2)
O(2)
N'
O(1)
N'
O(3)
O(1)
N'
O(3)
C(1)
P
N
C(2)
O(2)
O(1)
N'
N'

Table 4–1. Principal values and direction cosines of the ^{31}P NMR chemical shielding tensor in AEP relative to the crystallographic axes (*abc*) and the molecular-fixed axes ($\alpha\beta\gamma$)[a].

Principal axis	Principal value[b] (ppm)	Direction cosines with respect to[c]					
		a	*b*	*c*	α	β	γ
1	−87.1 (0.9)	0.3082	0.7324	0.6071	−0.1602	0.0231	0.9868
2	−15.6 (0.4)	−0.9295	0.0959	0.3561	0.9728	0.1731	0.1539
3	47.5 (0.6)	0.2026	−0.6741	0.7103	−0.1673	0.9846	−0.0502

[a] The molecular-fixed axis system was chosen such that the α axis bisects the O(1)−P−O(2) angle, the γ axis is perpendicular to the O(1)−P−O(2) plane − approximately from O(3) to C(1) − and the β axis is perpendicular to the other two to form a right-handed system − approximately from O(2) to O(1) −, the numbering of the atoms being that of Okaya (18).

[b] Values in parentheses represent standard deviations.

[c] Average standard deviation in the direction cosines is ±0.6°.

the two compounds is a shift of σ_{11} in the direction of the P−C bond in AEP. The P−C bond in the phosphonate would have a lower electron density than the corresponding P−O bond in the phosphate; it is thus expected that the 1 axis shifts in the direction of the P−C bond, which is in full agreement with the experimental observations. In fact, the principal axis for σ_{11} is closer by 8° to the P−C(1) bond direction in AEP than to the corresponding P(1)−O(5) bond direction in 2-aminoethyl phosphate (7), the numbering of the atoms being in both cases that of the crystallographic studies (18, 37).

In the AEP crystal, there is no true crystallographic symmetry within the molecule. There is however an approximate local mirror plane at the phosphorus atom, which is spanned by the C(1)−P−O(3) segment. The two tensor elements σ_{11} and σ_{22} are found to lie approximately in this plane, as expected. The deviation from the plane can be explained for σ_{22} by the differences in length of the two short P−O bonds, or by the strength of the hydrogen bonds they make with adjacent molecules. The P−O(1) bond is longer than the P−O(2) bond, because O(1) makes a stronger hydrogen bond with O(3) in an adjacent molecule (18). Therefore, the available electrons are removed from the phosphorus atom in that direction. As a result, σ_{22} is closer to the direction of the P−O(1) bond than to that of the P−O(2) bond, because the former has a lower electron density. Similar observations have been made in phosphate compounds such as 2-aminoethyl phosphate (7), serine phosphate (8), cytidine 3'-phosphate (8), urea phosphoric acid (9), and deoxycytidine 5'-phosphate (10). Also, similar effects of intermolecular hydrogen bonding on ^{13}C NMR chemical shielding tensors in carboxyl (15) and carbonyl (16) carbons have been reported. The most shielded element in the plane perpendicular to the π orbitals is always tilted towards the shortest C−O bond.

When comparing the results obtained for AEP with the theoretical calculations performed on dimethyl methylphosphonate (11), a phosphonic acid diester, the orientations of the tensors are found to be almost coincident, provided the assignment of σ_{22} and σ_{33} is reversed, and the directions of the short and long P–O bonds are exchanged, in one of the two molecules. This has to be done because there are two short P–O bonds in the acid and two long P–O bonds in the diester.

As shown in Table 4–2, the principal values of the ^{31}P NMR chemical shielding tensor of AEP are all smaller than the corresponding values for 2-aminoethyl phosphate (7). In the phosphonate, because a P–C bond replaces a P–O bond, the overall electron density should be lower than in the phosphate. This provides a reason for the shift of the principal values to higher frequencies. Both σ_{11} and σ_{33} are shifted towards lower shielding by at least 20 ppm. A smaller difference is found in the values for σ_{22}. The orientation of this tensor element roughly bisects the O(1)–P–O(2) angle, and it seems that the electron densities in this direction are not very different in the phosphate and the phosphonate. This is explained in the following terms: the overall decrease in electron density is partially compensated in the direction of σ_{22} by a shift of the 2 axis towards the P–O(3) bond direction. The latter shift follows that of σ_{11} towards the P–C(1) bond direction. The same behavior was found in serine phosphate where σ_{22} is tilted towards the protonated P–O(4) bond direction (8), in that case due to a relatively short P–O bond (40).

As a result of the smaller principal values of the shielding tensor for AEP, the isotropic value is also smaller, and correlates well with the larger chemical shift in aqueous solution (Table 4-2). On the other hand, the width of the powder spectrum, expressed as $\sigma_{33} - \sigma_{11}$, is almost the same for AEP and 2-aminoethyl

Table 4–2. Comparison of ^{31}P NMR chemical shielding tensor data for AEP and 2-aminoethyl phosphate[a].

Compound	σ_{AA} (ppm)	σ_{BB} (ppm)	σ_{CC} (ppm)	σ_i (ppm)	δ_{sol}[b] (ppm)	$\Delta\sigma$ (ppm)	η
2-aminoethylphosphonic acid (AEP)	47.5 (σ_{33})	−15.6 (σ_{22})	−87.1 (σ_{11})	−18.4	18.0[c]	−103.1	0.918
2-aminoethyl phosphate[d]	−67 (σ_{11})	−13 (σ_{22})	69 (σ_{33})	−4	3.7[e]	109	0.74

[a] The convention $|\sigma_{AA} - \sigma_{BB}| \leq |\sigma_{BB} - \sigma_{CC}|$ was chosen to label the principal axes. Isotropic chemical shift: $\sigma_i = {}^1/_3(\sigma_{AA} + \sigma_{BB} + \sigma_{CC})$. Chemical shift anisotropy: $\Delta\sigma = \sigma_{CC} - {}^1/_2(\sigma_{AA} + \sigma_{BB})$. Asymmetry parameter: $\eta = (\sigma_{AA} - \sigma_{BB})/(\sigma_i - \sigma_{CC})$.

[b] Chemical shift in aqueous solution at *p*H 7.

[c] Taken from Deslauriers *et al.* (38).

[d] Taken from Kohler and Klein (7).

[e] Taken from Henderson *et al.* (39).

phosphate; similarly, there is not a big difference in the magnitude of the chemical shift anisotropy $\Delta\sigma$ for the two compounds, but the signs are different (Table 4–2). This is attributed to the lower shielding for σ_{11} and σ_{33}, but not for σ_{22}. In other words, the magnitude of σ_{22} is closer to that of σ_{33} in AEP than in 2-aminoethyl phosphate. For the same reason, the asymmetry parameter η for AEP is quite high (Table 4–2). A similar value was also found for dimethylaminomethanediphosphonic acid (η = 0.90), but not for pentanephosphonic acid (η = 0) (13). For the latter phosphonic acid, the result was explained in terms of dynamical processes, which are obviously absent in crystals of AEP because of the strong intermolecular interactions.

As it is the case for 2-aminoethyl phosphate (7), the magnitude and orientation of the ^{31}P NMR chemical shielding tensor of AEP are correlated with the electron density distribution found in the ground state of the phosphonate moiety. Moreover, the principal elements, and especially the principal directions, are very sensitive to the local structure and symmetry around the phosphorus atom.

4.6 Conclusion

The purpose of the present determination was to make possible the interpretation of ^{31}P NMR chemical shift anisotropy data of phosphonolipids. It is believed that the tensor obtained for AEP could be used for phosphonolipids, as that of 2-aminoethyl phosphate was found to be suitable for phospholipids (7). The orientation of the tensor is qualitatively similar in phosphoric acid and its mono- and diesters, but there is a difference in the magnitude of the principal components (6–10). For this reason, despite the rather small differences in the orientation of the tensors, Herzfeld *et al.* (9) have rather used data determined on the phosphate diester barium diethyl phosphate than on 2-aminoethyl phosphate. Although

phosphonolipids are monoesters of AEP, the latter compound is believed to be a good model for this type of lipids, since it is part of the headgroup of both glycerophosphonolipids and ceramide phosphonates (3). In phosphonolipids, the principal directions are assumed to be the same as that for AEP, and the principal values can be determined from a powder spectrum of a phosphonolipid. They have been determined previously for the compound 1,2-dipalmitoyl-*sn*-glycero-3-(2-aminoethyl)phosphonate (4). The principal values are: $\sigma_{11} = -85$, $\sigma_{22} = -27$ and $\sigma_{33} = 65$ ppm. The differences between the figures for AEP and the phosphonolipid are similar to those found between mono- and diesters of phosphoric acid (6–10). The data reported in this study enable a more accurate interpretation of ^{31}P NMR powder spectra of phosphonolipids in model and biological membranes, and ultimately make structural comparisons between phospho- and phosphonolipid headgroups possible.

4.7 References

1. M.-R. Van Calsteren, G.I. Birnbaum and I.C.P. Smith, *J. Chem. Phys.* **86**, 5405–5410 (1987).

2. I.C.P. Smith and I.H. Ekiel, in *Phosphorus–31 NMR, Principles and Applications*, edited by D.G. Gorenstein (Academic Press, Orlando, Florida, 1984), Chap. 15, pp. 447–475.

3. T. Hori and Y. Nozawa, in *New Comprehensive Biochemistry, Phosphonolipids*, edited by J.N. Hawthorne and G.B. Ansell (Elsevier, Amsterdam, 1982), Vol. 4, Chap. 3, pp. 95–128.

4. H.C. Jarrell, R.A. Byrd, R. Deslauriers, I. Ekiel, and I.C.P. Smith, *Biochim. Biophys. Acta* **648**, 80–86 (1981).

5. H. Hauser, I. Pascher, R.H. Pearson and S. Sundell, *Biochim. Biophys. Acta* **650**, 21–51 (1981).

6. S.J. Kohler, J.D. Ellett, Jr., and M.P. Klein, *J. Chem. Phys.* **64**, 4451–4458 (1976).

7. S.J. Kohler and M.P. Klein, *Biochemistry* **15**, 967–973 (1976).

8. S.J. Kohler and M.P. Klein, *J. Am. Chem. Soc.* **99**, 8290–8293 (1977).

9. J. Herzfeld, R.G. Griffin, and R.A. Haberkorn, *Biochemistry* **17**, 2711–2718 (1978).

10. [illegible] Tutunjian, J. Tropp, and J. Waugh, *J. Amer. Chem. Soc.* **105**, 4848–4849 (1983).

11. T. Weller, U. Franck, G. Klose, and R. Lochmann, *Z. Chem.* **22**, 62–63 (1982).

12. T. Weller, U. Franck, G. Klose, and R. Lochmann, *Stud. Biophys.* **93**, 275–276 (1983).

13. G. Klose, L. Trahms, and A. Möps, *Chem. Phys. Lett.* **122**, 545–549 (1985).

14. M. Mehring, *Principles of High-Resolution NMR in Solids*, 2nd ed. (Springer-Verlag, Berlin, 1983), Chap. 2, pp. 8–62.

15. W.S. Veeman, *Prog. NMR Spectrosc.* **16**, 193–235 (1984).

16. K. Takegoshi, A. Naito, and C.A. McDowell, *J. Magn. Reson.* **65**, 34–42 (1985).

17. M. Rance and R.A. Byrd, *J. Magn. Reson.* **52**, 221–240 (1983).

18. Y. Okaya, *Acta Crystallogr.* **20**, 712–715 (1966).

19. C.K. Johnson, ORTEP II, ORNL-5138 (Oak Ridge National Laboratory, Oak Ridge, Tennessee, 1976).

20. W.H. Press, B.P. Flannery, S.A. Tenkolsky and W.T. Vetterling, *Numerical Recipes: The Art of Scientific Computing* (Cambridge University Press, Cambridge, 1986), Chap. 14, pp. 509–515 and 771–774.

21. W.H. Press, B.P. Flannery, S.A. Tenkolsky and W.T. Vetterling, *Numerical Recipes: The Art of Scientific Computing* (Cambridge University Press, Cambridge, 1986), Chap. 2, pp. 24–29 and 682–683.

22. J.W. Cooper, *Introduction to Pascal for Scientists* (John Wiley & Sons, New York, New York, 1981), Chap. 17, pp. 171–184.

23. D.W. Marquardt, *J. Soc. Indust. Appl. Math.* **11**, 431–441 (1963).

24. W.H. Press, B.P. Flannery, S.A. Tenkolsky and W.T. Vetterling, *Numerical Recipes: The Art of Scientific Computing* (Cambridge University Press, Cambridge, 1986), Chap. 14, pp. 523–528 and 774–776.

25. J.A. Nelder and R. Mead, *Comp. J.* **7**, 308–313 (1965).

26. M.S. Caceci and W.P. Cacheris, *Byte* **5**, 340–362 (1984).

27. W.H. Press, B.P. Flannery, S.A. Tenkolsky and W.T. Vetterling, *Numerical Recipes: The Art of Scientific Computing* (Cambridge University Press, Cambridge, 1986), Chap. 10, pp. 289–293 and 739–740.

28. J.W. Cooper, *Introduction to Pascal for Scientists* (John Wiley & Sons, New York, New York, 1981), Chap. 18, pp. 185–197.

29. A. Pines, J.J. Chang, and R.G. Griffin, *J. Chem. Phys.* **61**, 1021–1030 (1974).

30. D.A. Pope and C. Tompkins, *J. Ass. Comp. Mach.* **4**, 459-466 (1957).

31. J. Greenstadt, in *Mathematical Methods for Digital Computers*, edited by A. Ralston and H.S. Wilf (John Wiley & Sons, New York, New York, 1960), Chap. 7, pp. 84–91.

32. W.H. Press, B.P. Flannery, S.A. Tenkolsky and W.T. Vetterling, *Numerical Recipes: The Art of Scientific Computing* (Cambridge University Press, Cambridge, 1986), Chap. 11, pp. 342–349 and 748–750.

33. N.F. Ramsey, *Phys. Rev.* **77**, 567 (1950).

34. N.F. Ramsey, *Phys. Rev.* **78**, 699–703 (1950).

35. N.F. Ramsey, *Phys. Rev.* **83**, 540–541 (1951).

36. D.W.J. Cruickshank, *J. Chem. Soc.* 5486–5504 (1961).

37. J. Kraut, *Acta Crystallogr.* **14**, 1146–1152 (1961).

38. R. Deslauriers, R.A. Byrd, H.C. Jarrell, and I.C.P. Smith, *Eur. J. Biochem.* **111**, 369–375 (1980).

39. T.O. Henderson, T. Glonek, and T.C. Myers, *Biochemistry* **13**, 623–628 (1974).

40. M. Sundaralingam and E.F. Putkey, *Acta Crystallogr.* **B 26**, 790–800 (1970).

CHAPTER 5

CHEMICAL SYNTHESES

5.1 Goals

The major phosphonolipid in *Tetrahymena* membranes is 1-*O*-hexadecyl-2-acyl-*sn*-glycero-3-(2-aminoethyl)phosphonate, where the acyl group is unsaturated (1). The main goal for this study was to synthesize a phosphonolipid that is as close as possible to that found in nature. The study of the differences caused by an ether linkage at position *sn*-1 was also of interest. For this reason, the synthesis of 1-*O*-hexadecyl-2-oleyl-*sn*-glycero-3-(2-aminoethyl) phosphonate as well as 1-palmitoyl-2-oleyl-*sn*-glycero-3-(2-aminoethyl)phosphonate was considered. For comparison purposes, analogous phospho– and phosphonolipids would have to be made. This is best achieved from a single intermediate diradylglycerol by introduction of the appropriate headgroup.

Since solid-state ^{31}P NMR can only give a picture of the conformation of the headgroup up to the phosphorus atom, another nucleus has to be chosen to probe the complete headgroup structure. Labelling is necessary because there are too many hydrogen and carbon atoms on the molecule, the quadrupolar coupling constant of ^{14}N is too large in this type of environment and the natural abundance of the other isotopes of hydrogen, carbon and nitrogen too low. Deuterium is the cheapest and easiest nucleus to introduce; many positions are available, and the

labelling can be made selective. Replacement of hydrogen by deuterium does not introduce any perturbation in the system. ^2H NMR quadrupolar splittings are related to the C$-^2$H bond orientation and motion (see Chapter 2). To obtain a complete picture of the headgroup, the deuterium label would have to be introduced on the hydrophilic part of the molecule, considered to start at position 2 of the chains. Therefore, the positions that could be labelled are: positions 2 and 1 of the hexadecyl chain, position 2 of the palmitoyl and oleyl chains, positions *sn*-1, *sn*-2 and *sn*-3 of the glycerol moiety and positions 1 and 2 of the headgroup.

Natural glycerolipids are chiral molecules. Since it is not known whether the presence of both enantiomers would change the conformation of the individual lipid molecules or the overall structure of the membrane, a stereospecific synthesis was carried out.

5.2 Strategies and discussion

This section presents a literature review pertinent to the goals described above. The possible methods for the preparation of phosphate and phosphonate headgroups, ester and ether chains, and glycerol moiety, as well as for the protection and combination of these individual elements to form the desired final compound will be examined. The major conditions for retaining one method over another are the maximum number of common steps, *i.e.* the introduction of substituents that are different at a later stage of the synthesis, the relative difficulty in introducing the deuterium label and the ease in obtaining and maintaining the desired stereochemistry of the glycerol moiety. In each case, the methods tried and chosen are described, and the reasons for the choices are discussed.

Schemes 5–1 to 5–18 illustrate the chemical reactions retained to synthesize the desired compounds. Because a few reactions failed to give the target compounds in acceptable yields, the strategy had to be modified during the course of the work. In the schemes, only compounds used or successfully synthesized have been given a number.

5.2.1 Headgroups

5.2.1.1 Phosphate

Different methods have been described to synthesize phospholipids from a diradylglycerol. Phosphorylation is usually achieved with phosphorus oxychloride. The second ester bond is introduced by reaction of the resulting dichlorophosphate ester with an alcohol. If the desired compound is a 2-aminoethyl phosphate ester, the alcohol can be 2-aminoethanol itself, 1,2-ethanediol, 2-bromoethanol or 2-aminoethanol protected on the amino group. When 2-aminoethanol is used, a cyclic intermediate oxazaphospholane is formed and the ring can later be opened by acid hydrolysis to give the desired diradylglycero(2-aminoethyl)phosphate (2). If the alcohol is 1,2-ethanediol, a dioxaphospholane cyclic intermediate is opened by treatment with sodium bromide (2). In that case or when 2-bromoethanol is used directly, the resulting diradylglycero(2-bromoethyl)phosphate can be aminated with ammonia (3). Because of the complexity of the latter reaction, namely the low solubility of ammonia in organic solvents and the possibility of formation of undesired secondary amines, it is preferable to use 2-aminoethanol, protected or not (4). Amino protecting groups successfully used include phthalimido (5) and *tert*-butyloxycarbonyl (6–8, 4). The phthalimido protecting group can be removed by hydrazinolysis, but the reaction is not completely selective since esters are

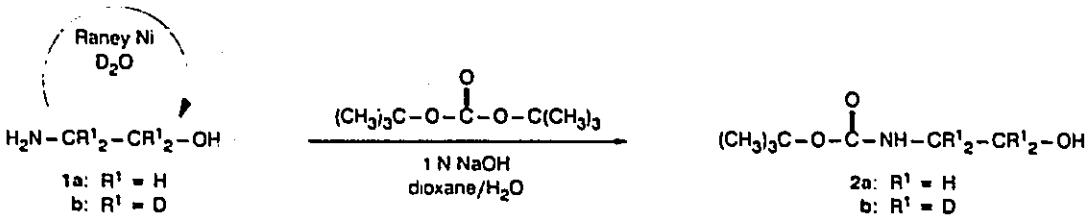

Scheme 5–1. Synthesis of *N-tert*-butyloxycarbonyl-2-aminoethanol **2**.

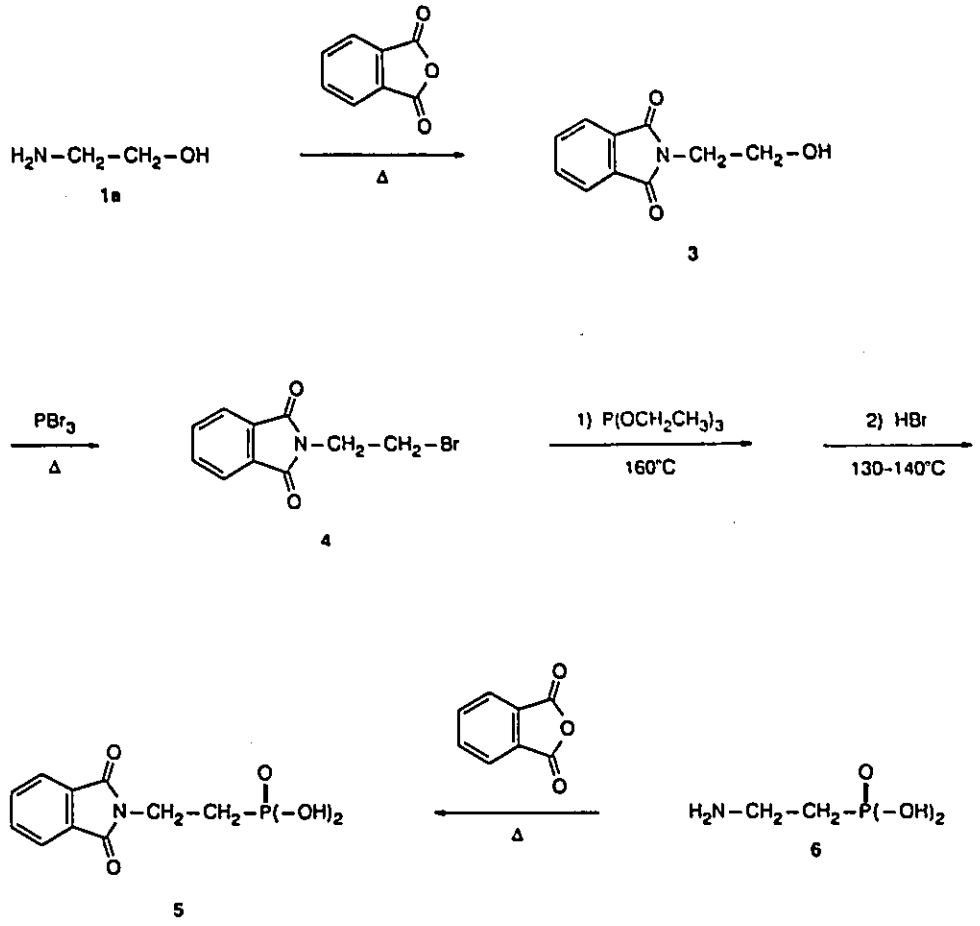

Scheme 5–2. Synthesis of 2-phthalimidoethylphosphonic acid **5**.

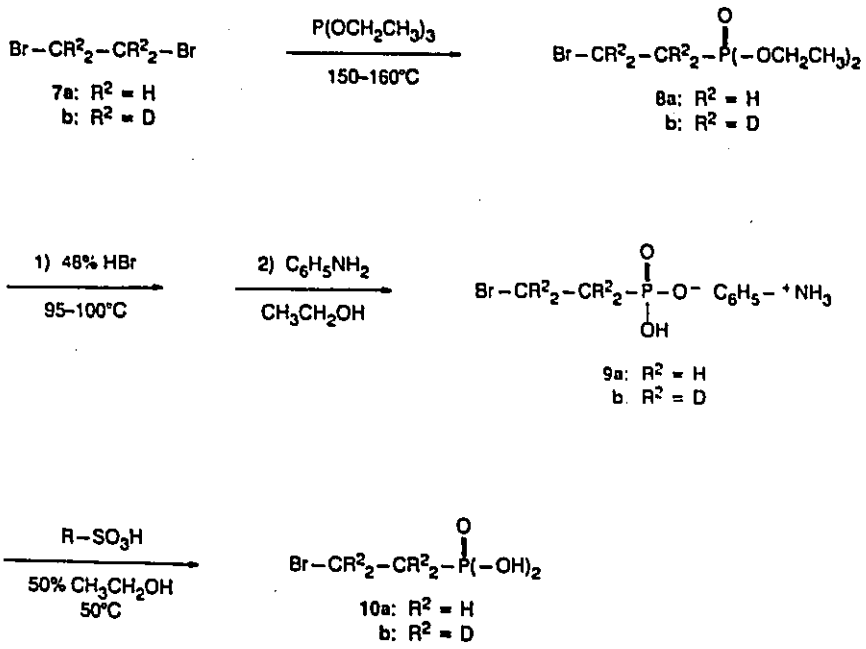

Scheme 5–3. Synthesis of 2-bromoethylphosphonic acid **10**.

Scheme 5–4. Synthesis of 1-*O*-hexadecyl methanesulfonate **13**.

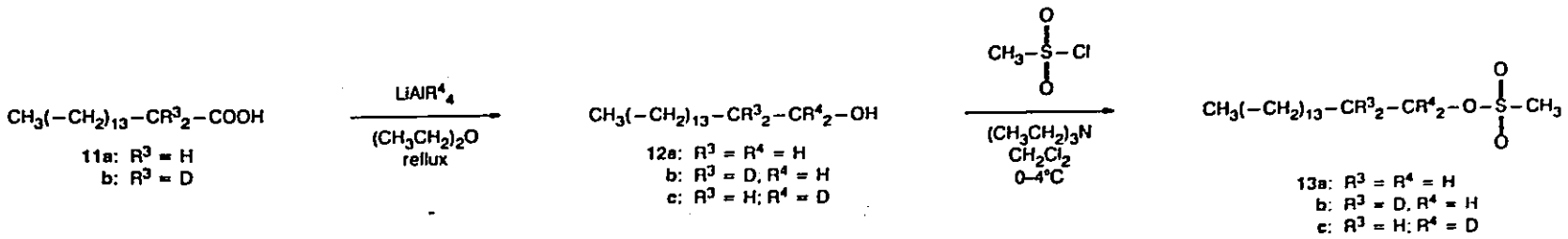
CH3(−CH2)13−CR3 2−COOH
11a: R3 = H
b: R3 = D
LiAlR4 4
(CH3CH2)2O
reflux
CH3(−CH2)13−CR3 2−CR4 2−OH
12a: R3 = R4 = H
b: R3 = D, R4 = H
c: R3 = H; R4 = D
CH3−S−Cl
(CH3CH2)3N
CH2Cl2
0–4°C
CH3(−CH2)13−CR3 2−CR4 2−O−S−CH3
13a: R3 = R4 = H
b: R3 = D, R4 = H
c: R3 = H; R4 = D

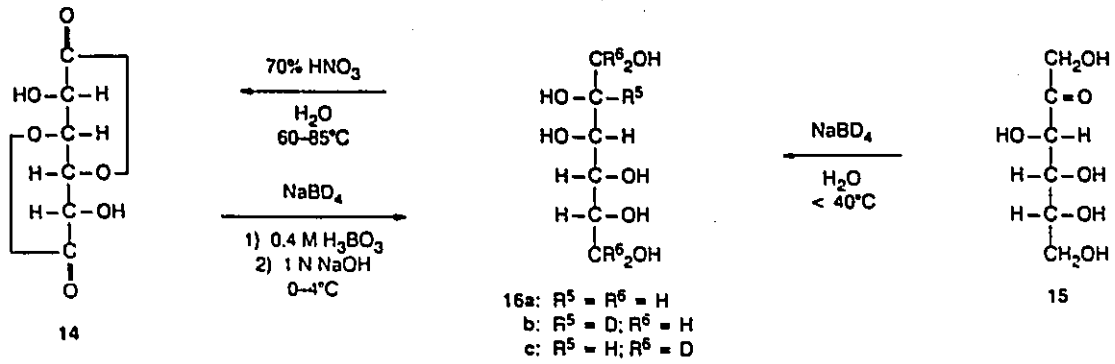

Scheme 5–5. Synthesis of D-mannitol **16**.

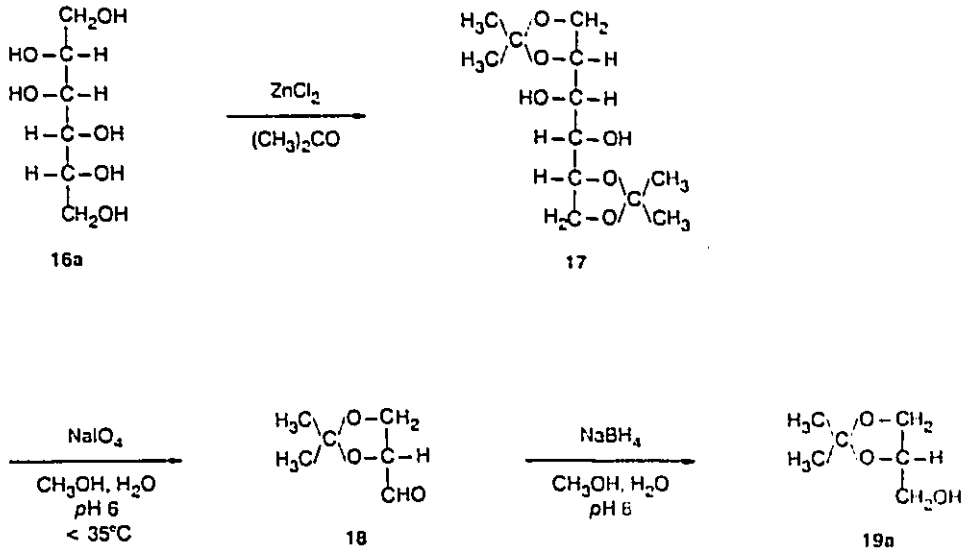

Scheme 5–6. Synthesis of 1,2-*O*-isopropylidene-*sn*-glycerol 19a.

Scheme 5–7. Synthesis of 1-palmitoyl-2-oleyl-*rac*-glycerol.

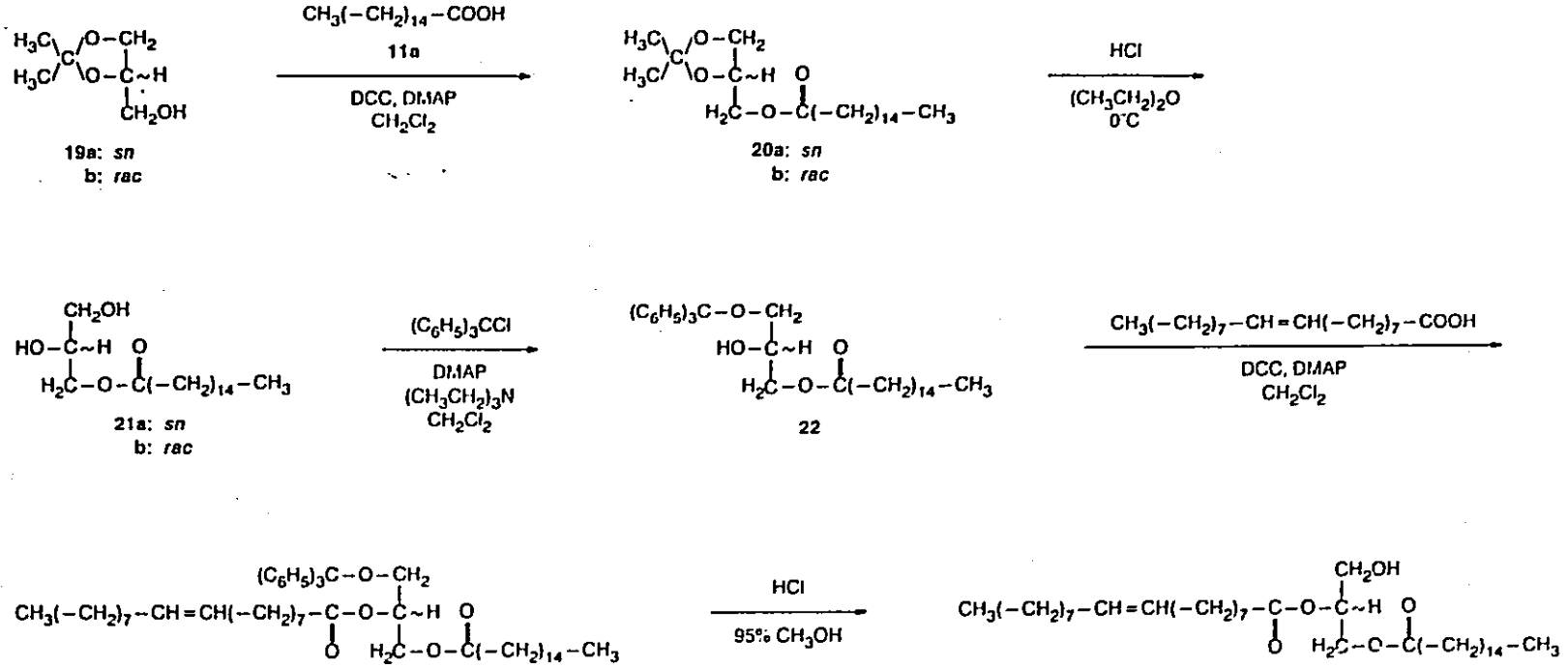
CH3(−CH2)14−COOH
11a
DCC, DMAP
CH2Cl2
19a: sn
b: rac
20a: sn
b: rac
HCl
(CH3CH2)2O
0°C
21a: sn
b: rac
(C6H5)3CCl
DMAP
(CH3CH2)3N
CH2Cl2
22
CH3(−CH2)7−CH=CH(−CH2)7−COOH
DCC, DMAP
CH2Cl2
HCl
95% CH3OH

Scheme 5–8. Synthesis of 3-*O*-hexadecyl-2-oleyl-*sn*-glycerol.

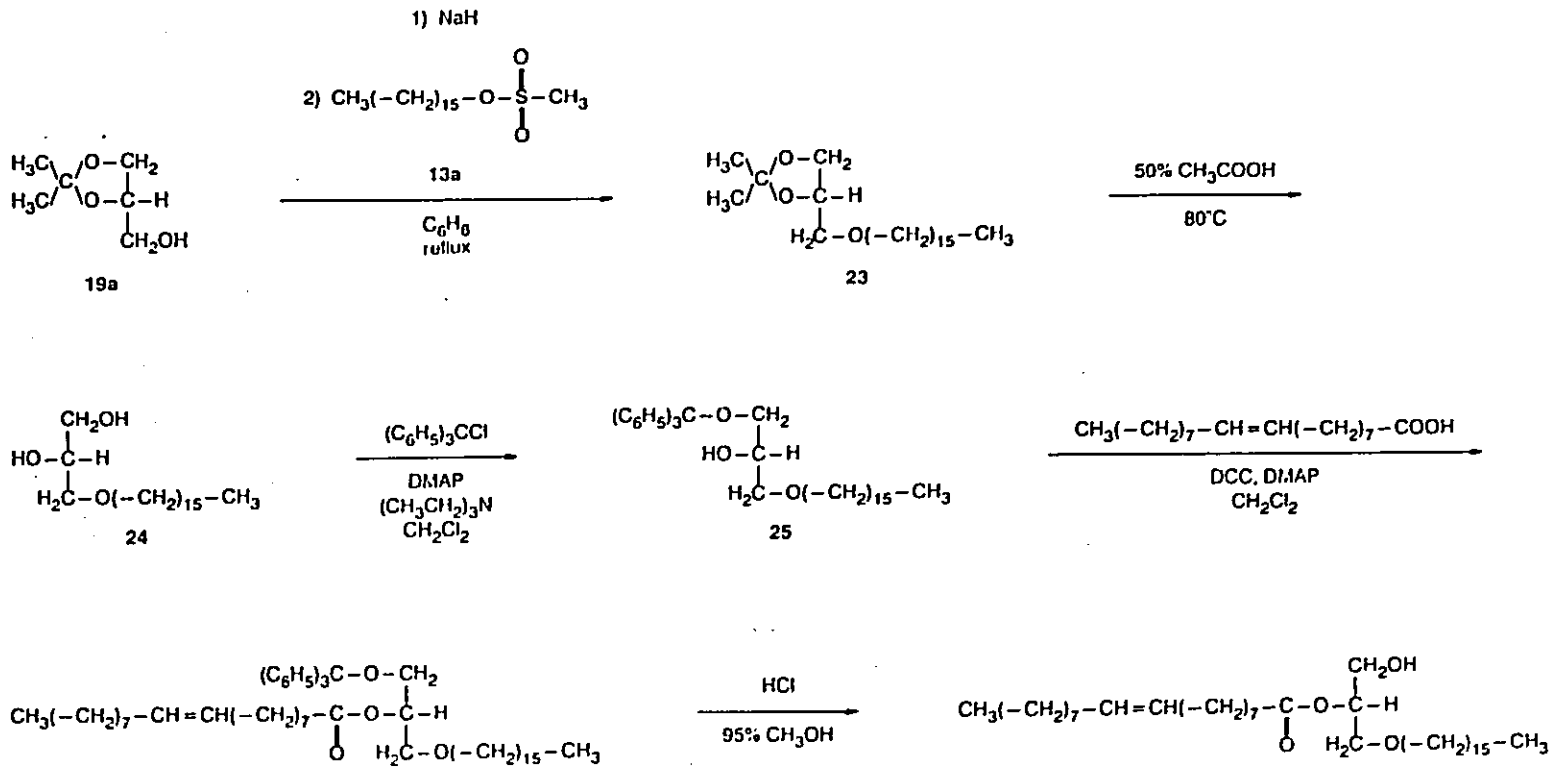
1) NaH
2) CH3(-CH2)15-O-S(=O)2-CH3
13a
C6H6
reflux
19a
23
50% CH3COOH
80°C
24
(C6H5)3CCl
DMAP
(CH3CH2)3N
CH2Cl2
25
CH3(-CH2)7-CH=CH(-CH2)7-COOH
DCC, DMAP
CH2Cl2
HCl
95% CH3OH

Scheme 5–9. Synthesis of 3,4-*O*-isopropylidene-D-mannitol **27**.

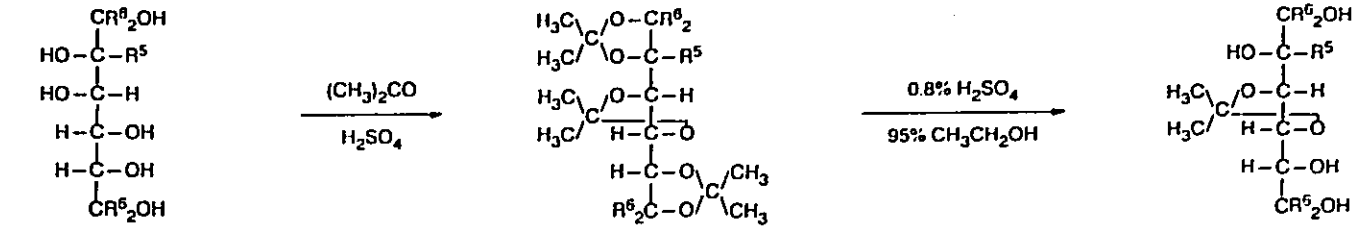

16a: $R^5 = R^6 = H$
b: $R^5 = D; R^6 = H$
c: $R^5 = H; R^6 = D$

26a: $R^5 = R^6 = H$
b: $R^5 = D; R^6 = H$
c: $R^5 = H; R^6 = D$

27a: $R^5 = R^6 = H$
b: $R^5 = D; R^6 = H$
c: $R^5 = H; R^6 = D$

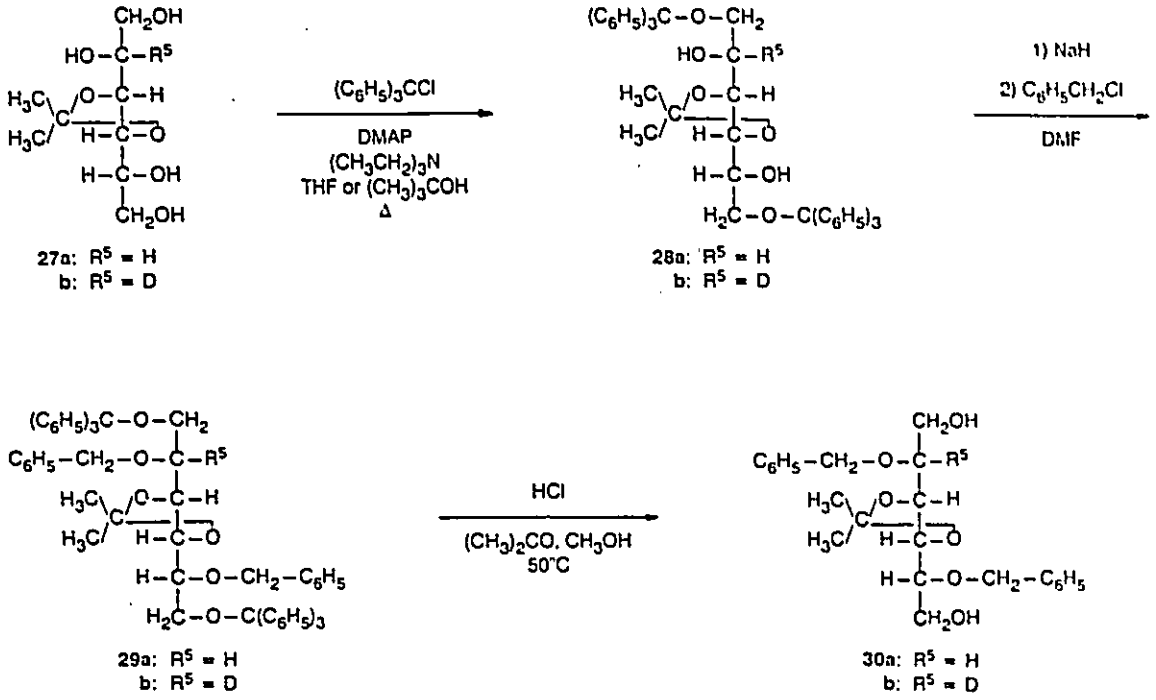

Scheme 5–10. Synthesis of 2,5-di-*O*-benzyl-3,4-*O*-isopropylidene-D-mannitol 30.

Scheme 5–11. Synthesis of 2-*O*-benzyl-1-palmitoyl-*sn*-glycerol **34**.

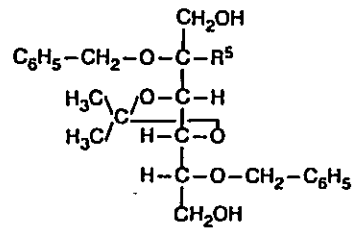

30a: R^5 = H
b: R^5 = D

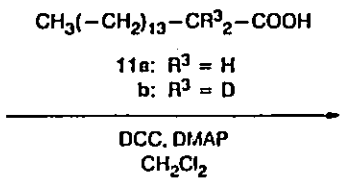

11a: R^3 = H
b: R^3 = D

DCC, DMAP
CH_2Cl_2

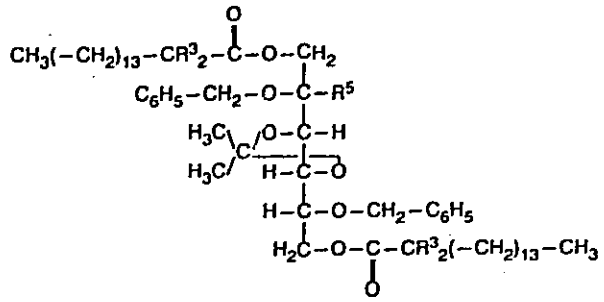

31a: R^3 = R^5 = H
b: R^3 = D; R^5 = H
c: R^3 = H; R^5 = D

90% CF_3COOH
0°C

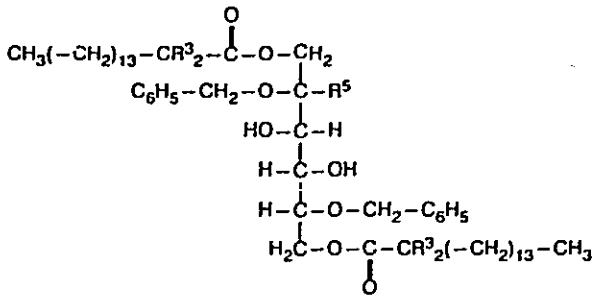

32a: R^3 = R^5 = H
b: R^3 = D; R^5 = H
c: R^3 = H; R^5 = D

H_5IO_6
$(CH_3CH_2)_2O$

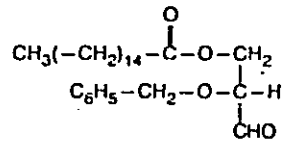

33

$NaBH_4$
CH_3OH
0°C

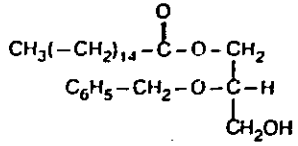

34

Scheme 5–12. Synthesis of 2-oleyl-1-palmitoyl-*sn*-glycero-3-(2-aminoethyl)phosphonate.

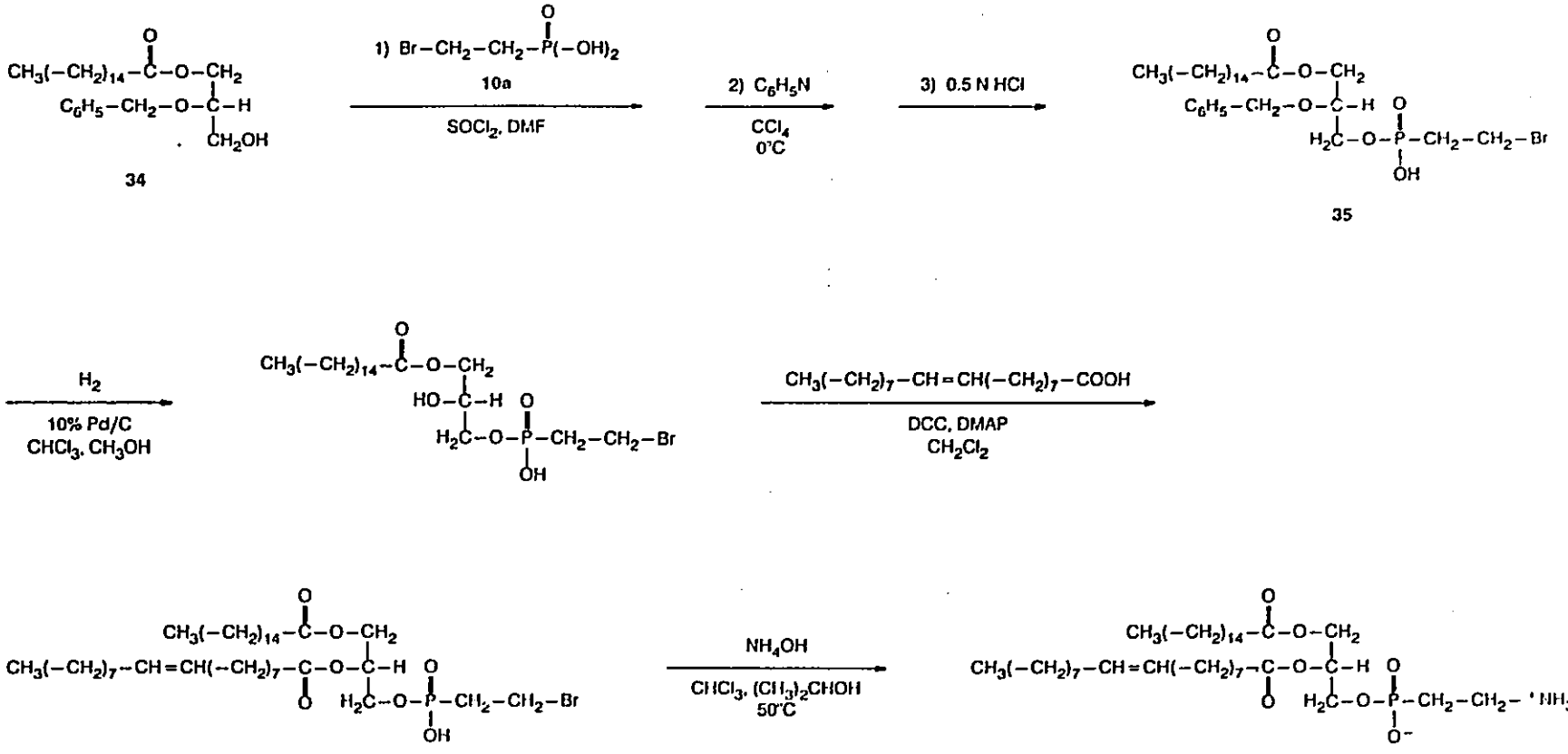
1) Br–CH2–CH2–P(–OH)2
10a
SOCl2, DMF
2) C6H5N
CCl4
0°C
3) 0.5 N HCl
34
35
H2
10% Pd/C
CHCl3, CH3OH
CH3(–CH2)7–CH=CH(–CH2)7–COOH
DCC, DMAP
CH2Cl2
NH4OH
CHCl3, (CH3)2CHOH
50°C

Scheme 5–13. Synthesis of 2-oleyl-1-palmitoyl-*sn*-glycero-3-(2-aminoethyl)phosphate.

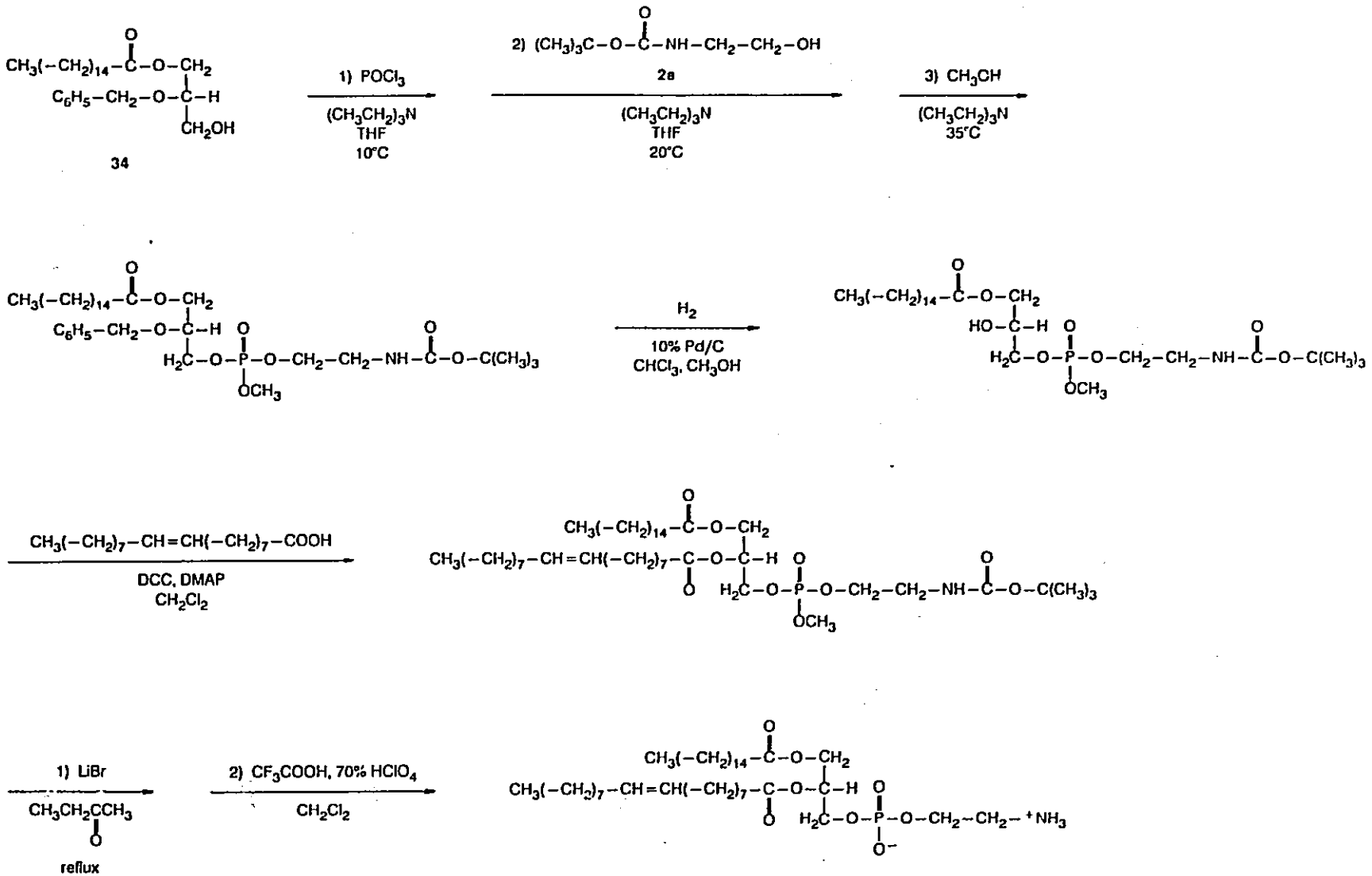
1) POCl3
(CH3CH2)3N
THF
10°C
2) (CH3)3C–O–C(=O)–NH–CH2–CH2–OH
2a
(CH3CH2)3N
THF
20°C
3) CH3CH
(CH3CH2)3N
35°C
34
H2
10% Pd/C
CHCl3, CH3OH
CH3(–CH2)7–CH=CH(–CH2)7–COOH
DCC, DMAP
CH2Cl2
1) LiBr
CH3CH2CCH3
reflux
2) CF3COOH, 70% HClO4
CH2Cl2

Scheme 5–14. Synthesis of 2-*O*-benzyl-1-*O*-hexadecyl-*sn*-glycerol **39**.

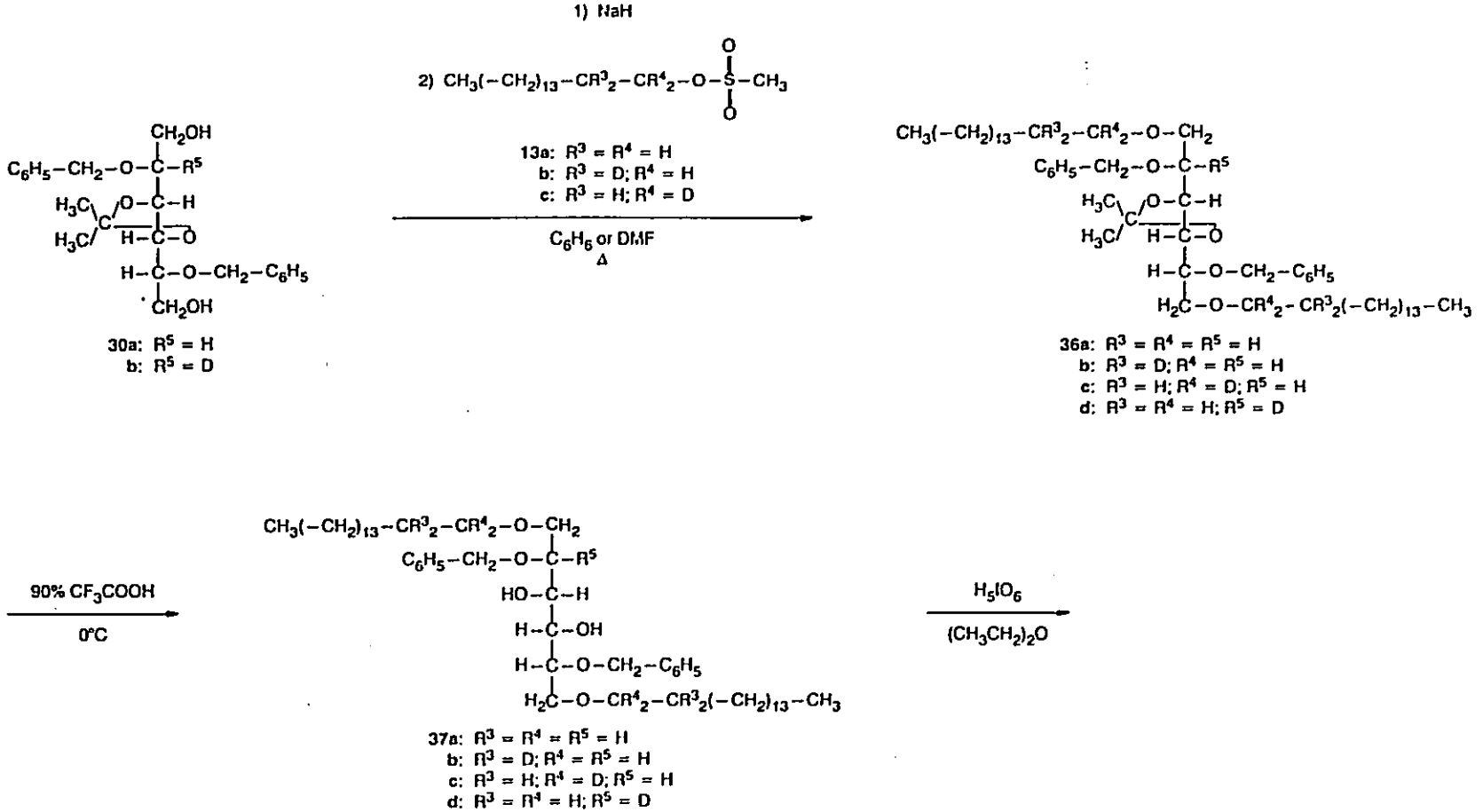
1) NaH
2) CH3(-CH2)13-CR3 2-CR4 2-O-S(=O)(=O)-CH3
13a: R3 = R4 = H
b: R3 = D; R4 = H
c: R3 = H; R4 = D
C6H6 or DMF
Δ
30a: R5 = H
b: R5 = D
36a: R3 = R4 = R5 = H
b: R3 = D; R4 = R5 = H
c: R3 = H; R4 = D; R5 = H
d: R3 = R4 = H; R5 = D
90% CF3COOH
0°C
37a: R3 = R4 = R5 = H
b: R3 = D; R4 = R5 = H
c: R3 = H; R4 = D; R5 = H
d: R3 = R4 = H; R5 = D
H5IO6
(CH3CH2)2O
NaBH4
CH3OH
38
39

Scheme 5–15. Synthesis of 1-*O*-hexadecyl-2-oleyl-*sn*-glycero-3-(2-aminoethyl)phosphonate.

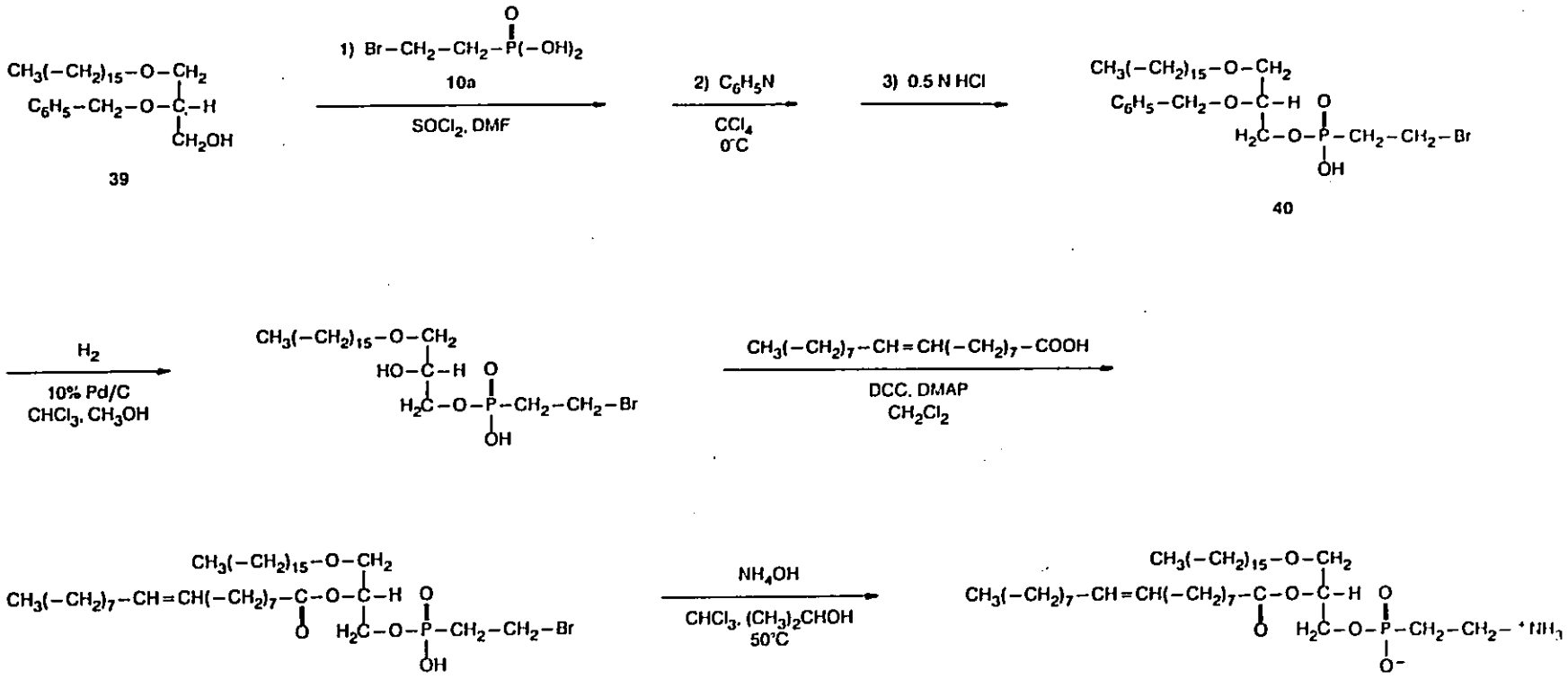
1) Br–CH2–CH2–P(=O)(–OH)2
10a
SOCl2, DMF
2) C6H5N
CCl4
0°C
3) 0.5 N HCl
39
40
H2
10% Pd/C
CHCl3, CH3OH
CH3(–CH2)7–CH=CH(–CH2)7–COOH
DCC, DMAP
CH2Cl2
NH4OH
CHCl3, (CH3)2CHOH
50°C

Scheme 5–16. Synthesis of 1-*O*-hexadecyl-2-oleyl-*sn*-glycero-3-(2-aminoethyl)phosphate.

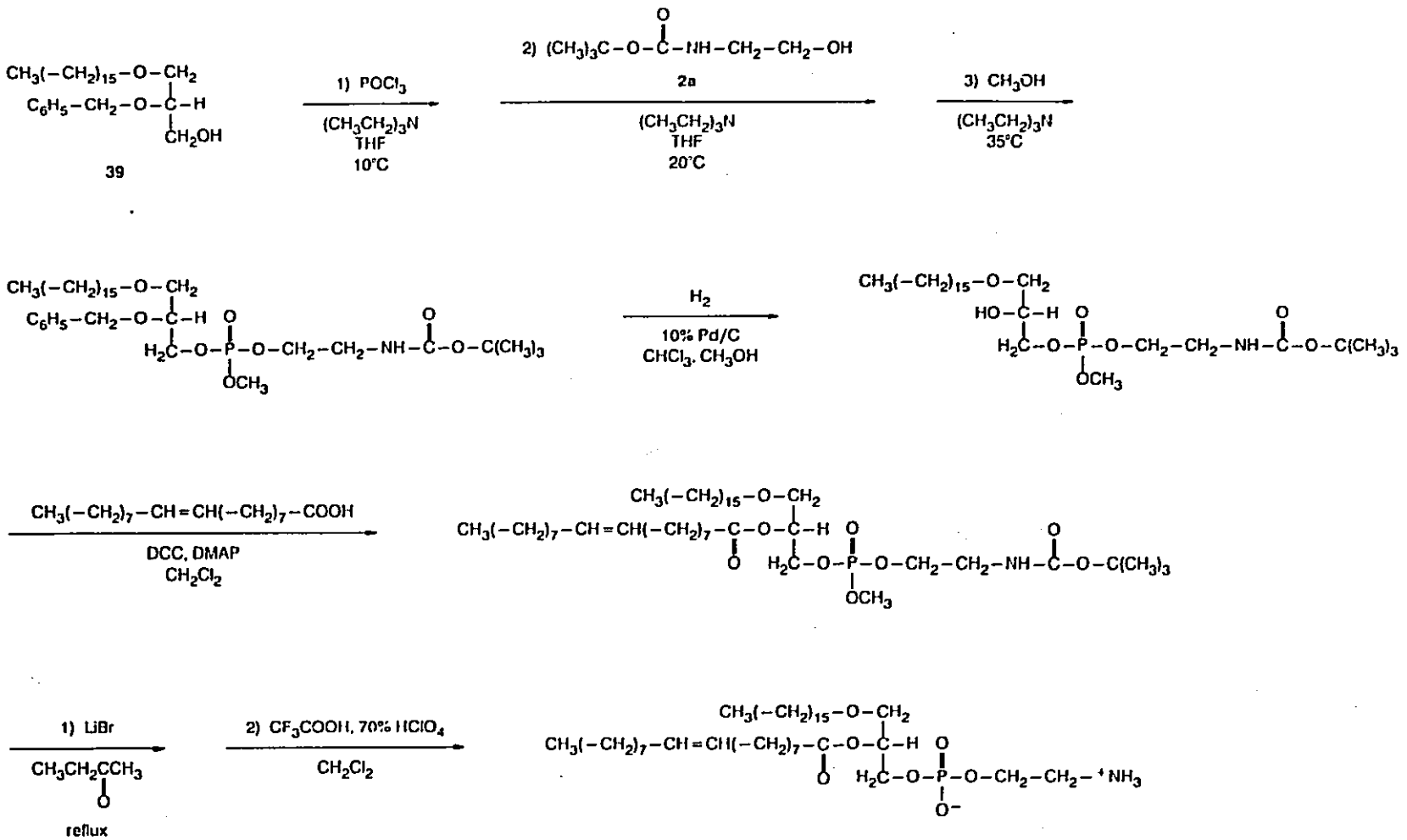
1) POCl3
(CH3CH2)3N
THF
10°C
2) (CH3)3C-O-C(=O)-NH-CH2-CH2-OH
2a
(CH3CH2)3N
THF
20°C
3) CH3OH
(CH3CH2)3N
35°C
39
H2
10% Pd/C
CHCl3, CH3OH
CH3(-CH2)7-CH=CH(-CH2)7-COOH
DCC, DMAP
CH2Cl2
1) LiBr
CH3CH2CCH3
O
reflux
2) CF3COOH, 70% HClO4
CH2Cl2

Scheme 5–17. Synthesis of 1,2-di-*O*-hexadecyl-*sn*-glycerol **44**.

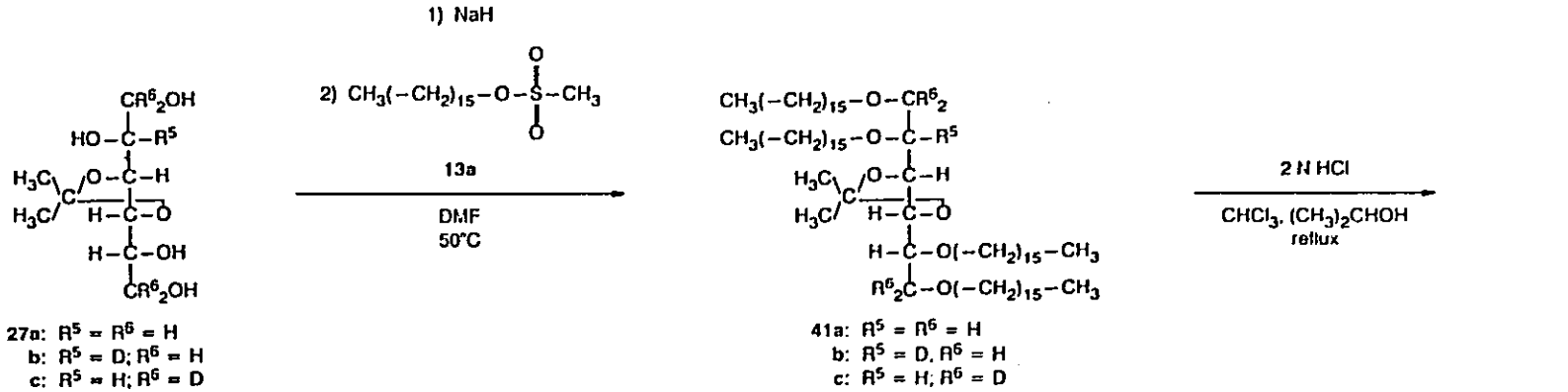

27a: $R^5 = R^6 = H$
b: $R^5 = D$; $R^6 = H$
c: $R^5 = H$; $R^6 = D$

41a: $R^5 = R^6 = H$
b: $R^5 = D$, $R^6 = H$
c: $R^5 = H$; $R^6 = D$

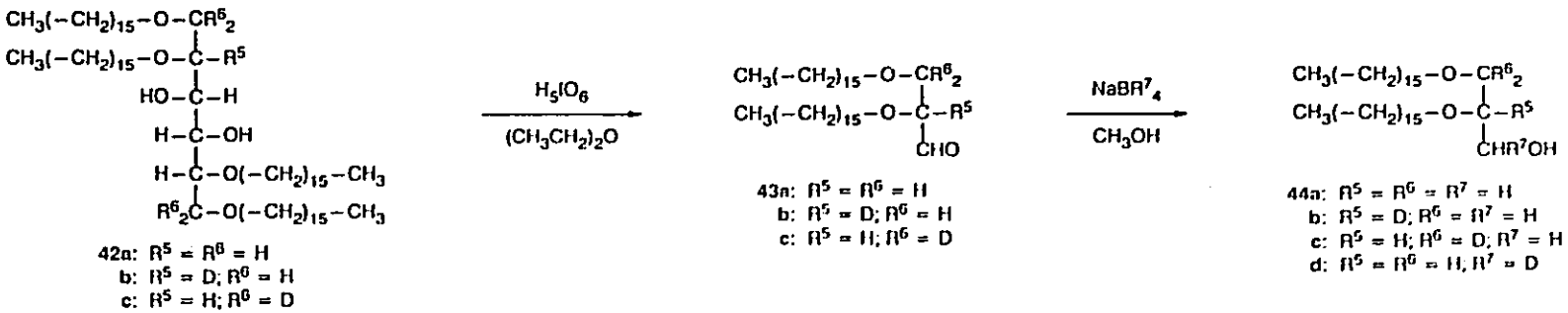

42a: $R^5 = R^6 = H$
b: $R^5 = D$; $R^6 = H$
c: $R^5 = H$; $R^6 = D$

43a: $R^5 = R^6 = H$
b: $R^5 = D$; $R^6 = H$
c: $R^5 = H$; $R^6 = D$

44a: $R^5 = R^6 = R^7 = H$
b: $R^5 = D$; $R^6 = R^7 = H$
c: $R^5 = H$; $R^6 = D$; $R^7 = H$
d: $R^5 = R^6 = H$, $R^7 = D$

Scheme 5–18. Synthesis of 1,2-di-*O*-hexadecyl-*sn*-glycero-3-(2-aminoethyl)phosphonate **46**.

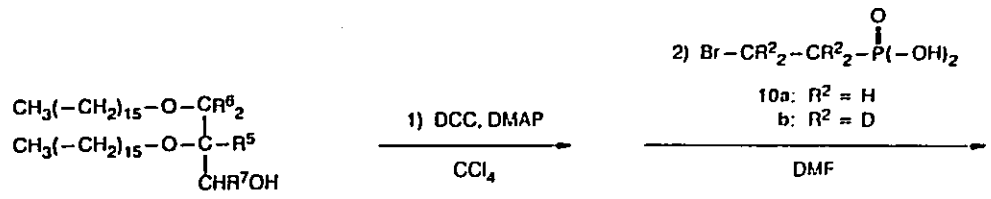

44a: $R^5 = R^6 = R^7 = H$
b: $R^5 = D$; $R^6 = R^7 = H$
c: $R^5 = H$; $R^6 = D$; $R^7 = H$
d: $R^5 = R^6 = H$; $R^7 = D$

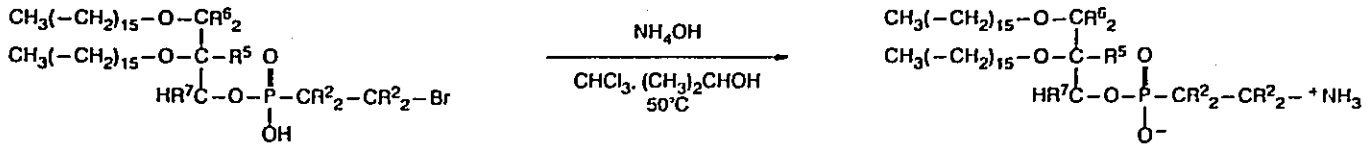

45a: $R^2 = R^5 = R^6 = R^7 = H$
b: $R^2 = D$; $R^5 = R^6 = R^7 = H$
c: $R^2 = H$; $R^5 = D$; $R^6 = R^7 = H$
d: $R^2 = R^5 = H$; $R^6 = D$; $R^7 = H$
e: $R^2 = R^5 = R^6 = H$; $R^7 = D$

46a: $R^2 = R^5 = R^6 = R^7 = H$
b: $R^2 = D$; $R^5 = R^6 = R^7 = H$
c: $R^2 = H$; $R^5 = D$; $R^6 = R^7 = H$
d: $R^2 = R^5 = H$; $R^6 = D$; $R^7 = H$
e: $R^2 = R^5 = R^6 = H$; $R^7 = D$

cleaved as well, and yields are usually low. On the other hand, the *tert*-butyloxycarbonyl group is easily removed under mild acidic conditions. Among the numerous reagents that can be used to introduce this protecting group, di-*tert*-butyldicarbonate was found to be the most convenient, because the only impurities formed are *tert*-butanol and carbon dioxide, *i.e.* volatile compounds. The method is modified after Moroder *et al.* (9), who have successfully used it for the preparation of protected amino acids for peptide synthesis.

The phosphate diester can also be prepared by reversing the order of introduction of the alcohols. The alcohol that will become the headgroup can be phosphorylated with phosphorus oxychloride and the resulting phosphoric acid dichloride allowed to react with the diradylglycerol. Hirt and Berchtold (10) have used this method with 2-phthalimidoethanol, and Diembeck and Eibl (11) with *n*-bromoalkanols for the preparation of phospholipid analogs with an increased P–N distance.

It is possible to obtain 2-aminoethanol deuterated at position 1 by reduction of glycine or one of its esters with lithium aluminum deuteride (12). Similarly, cyanomethanol (prepared from formamide and NaCN) or its esters can be reduced to [1,1–$^2H_2$]ethanolamine (13). However, both positions can be deuterated at once by exchange with Raney nickel in ^2H_2O (14). The extent of deuteration is different for the two positions and this allows the easy identification of their respective signals on solid-state ^2H NMR spectra. 2-Bromoethanol, on the other hand, is not easily available in its deuterated form and has to be prepared from 2-aminoethanol. The preparation of the protected phosphate headgroup is described in Scheme 5–1.

5.2.1.2 Phosphonate

As mentioned in Chapter 3, the headgroup of phosphonolipids is constituted of 2-aminoethylphosphonic acid (AEP), methylated or not. The compound has first been synthesized by Finkelstein (15) starting from diethyl phosphite and ethyl 3-bromopropionate. Since the latter is not available in its deuterated form, it would have to be synthesized. Kosolapoff (16) has used a different approach to synthesize the same compound. With this method, the carbon-phosphorus bond is formed during the so-called Arbuzov reaction, where a trialkyl phosphite reacts with an halogenoalkane, in this case triethyl phosphite and 2-bromoethylphthalimide. The phthalimido group is then hydrolyzed under the same conditions – aqueous HBr – as the diester. Before esterification, the amine function has to be protected. Rosenthal and Pousada (17) have taken advantage of the fact that the phthalimido protecting group was already present during the course of the synthesis of AEP. Instead of aqueous HBr, gaseous HBr has been used for the dealkylation of the ester functions (18), leaving the protecting group intact. This group can be removed by hydrazinolysis at the last step of the synthesis. However, as noted above, the deprotection reaction is not completely specific. Scheme 5–2 describes the preparation of 2-phthalimidoethylphosphonic acid using two different methods. The first one, starting with 2-aminoethanol, could also be used to prepare headgroup-labelled phosphonolipids since the compound can be deuterated by exchange with Raney nickel in ^2H_2O (14). However, it was not possible to isolate the desired compound after dealkylation of the phosphonate diester. The second method, which involves a simple condensation between AEP and phthalic anhydride, gave the desired compound in good yields. It is however not a practical method since the starting compound is not readily available in deuterated form.

The Arbuzov reaction can also be used to prepare 2-bromoethylphosphonic acid from triethyl phosphite and 1,2-dibromoethane (19–21), as shown in Scheme 5–3. An excess 1,2-dibromoethane has to be used in order to obtain monoalkylation only. The latter is available fully deuterated and thus the preparation of a deuterated headgroup is possible. Since both positions will be labelled to the same extent, this might interfere with the determination of their respective ^2H NMR parameters. If it is not possible to assign the quadrupolar splittings on the ^2H NMR spectra, position 2 could be partially deuterated by exchange with Raney nickel in ^2H_2O, as done for 2-aminoethanol (14). The amine function will have to be introduced after esterification by direct amination with ammonia as described by Eibl and Nicksch (3). This method has not been used to prepare 2-aminoethylphosphonate derivatives but only their *N*-methylated analogs. The reaction is more easily effected with methylated amines than with ammonia because of their better solubility in nonpolar solvents. Furthermore, the hydrogen atoms on the α carbon have a marked lability (acidity) that promotes an easy elimination of HBr during the amination reaction. This process is favoured in nonpolar solvents, but a too polar solvent does not dissolve the lipid and the reaction can not take place. However, since no better method is available to obtain the headgroup-deuterated phosphonolipid, it was optimized to give the best possible results. The solvent composition for the reaction has to permit single amination. For this, ammonia has to be readily available to the bromo compound dissolved in an organic solvent, otherwise the amine formed competes with ammonia to produce secondary amines. Ternary mixtures composed of chloroform, water and an alcohol that result in a one-phase system give satisfactory results. The alcohol can not be primary because transesterification of the ester chains could occur, and therefore 2-propanol is used.

For the esterification, 2-phthalimidoethylphosphonic acid has been activated by forming the dichloride with thionyl chloride and a trace of dimethylsulfoxide (DMSO) (17). Esterification of 2-phthalimidoethylphosphonic acid (22–24) or 2-bromoethylphosphonic acid (20, 21, 25) with the diradylglycerol has been achieved by forming the monochloride with phosphorus pentachloride. With the latter method, where phosphorus oxychloride is one of the products of the reaction, care has to be taken to remove it completely or phospholipids will be formed. The thionyl chloride method was tried first (Schemes 5–12 and 5–15), but it was later found that the acid can be efficiently activated with dicyclohexylcarbodiimide (DCC) in the presence of a catalytic amount of *N*,*N*-dimethyl-4-aminopyridine (DMAP), if a dipolar aprotic solvent like *N*,*N*-dimethylformamide (DMF) is used to dissolve the phosphonic acid (Scheme 5–18). This method followed from the successful synthesis of monoesters of nucleoside phosphates and diesters of phosphoric and pyrophosphoric acids (26, 27).

5.2.2 Chains

5.2.2.1 Ester

The most convenient and efficient esterification method uses dicyclohexylcarbodiimide (DCC) as a coupling reagent. The reaction is catalyzed by *N*,*N*-dimethyl-4-aminopyridine (DMAP) to activate the acid (28, 29). No acid chloride nor anhydride need be prepared beforehand, and there is no need for pyridine, the reaction being carried out in dichloromethane.

Since a hydrogen atom at position 2 of a fatty acid chain is more acidic due to the carboxylic acid functional group, deuteration at this position is possible by α-exchange. This is done with NaO^2H in ^2H_2O, as described by Tulloch (30).

5.2.2.2 Ether

Coupling of a long-chain alcohol to the glycerol moiety requires a good leaving group which can be halide, *p*-toluenesulfonate or methanesulfonate. Methods using sodium naphthalene in 1,2-dimethoxyethane (31), potassium in benzene (32) or KOH in xylene (32), and potassium *tert*-butoxide (8, 33–35) have been described. It was found that using NaH as the base gives satisfactory results.

Long-chain alcohols deuterated at position 2 are readily obtained by reduction of the corresponding 2,2–$^2H_2$-labelled fatty acid with $LiAlH_4$; position 1 is labelled by reduction of the unlabelled acid with $LiAl^2H_4$. Since the alcohol has to be used as the starting compound, the methanesulfonate makes an easily introduced leaving group. Tulloch (30) has synthesized alkyl methanesulfonates in CH_2Cl_2 using triethylamine as the base. Good yields are obtained and there is no need for pyridine (36). The preparation of the ether chains is shown in Scheme 5–4.

5.2.3 Glycerol moiety

Different possibilities were considered for the diradylglycerol. The usual starting substance for the synthesis of glycerolipids has been 1,2-*O*-isopropylidene-*sn*-glycerol, which has been synthesized from D-mannitol in three steps (37). D-Mannitol is converted to 1,2:5,6-di-*O*-isopropylidene-D-mannitol by the use of $ZnCl_2$. Its cleavage with lead tetraacetate gives 2,3-*O*-isopropylidene-D-glyceraldehyde, which yields 1,2-*O*-isopropylidene-*sn*-glycerol by catalytic reduction.

Lok *et al.* (38) have synthesized 1,2-*O*-isopropylidene-*sn*-glycerol and 2,3-*O*-isopropylidene-*sn*-glycerol from D- and L-serine. The first step involves a diazotization with $NaNO_2$ in HCl to give the corresponding glyceric acid. The acid is methylated and the diol protected by isopropylidene acetal formation with 2,2-dimethoxypropane in methanol–acetone. Finally, the ester is reduced with lithium aluminum hydride. Although it is claimed that the reaction proceeds with 100% retention of configuration (one inversion for the diazotization followed by another inversion for the reaction with water), methods that do not require bond breakage and formation at the asymmetric carbon atom would give more confidence in the final stereochemistry of the product. Furthermore, deuterium can only be introduced at one position, since optically active and specifically deuterated serine is not readily available.

Tanako *et al.* (39) have published a one-pot method for the preparation of 2,3-*O*-isopropylidene-*sn*-glycerol starting with L-ascorbic acid. The method consists in the preparation of the acetonide of L-ascorbic acid, followed by the reduction of all carbonyl groups with $LiAlH_4$, then the oxidative cleavage of all vicinal diols with sodium periodate and finally the reduction of 2,3-isopropylidene-L-glyceraldehyde. This method was not retained because the possibilities of labelling are limited.

To obtain a glycerol moiety deuterated at positions *sn*-1 or *sn*-2, the starting mannitol has to be labelled. D-[2–$^2H_1$]Mannitol can be obtained by reduction of D-fructose with sodium borodeuteride. Borate complexes formed with polyhydroxy compounds are circumvented by removal of sodium with an ion exchange resin, followed by removal of boric acid as its volatile methyl ester by distilling with an excess methanol under reduced pressure (40). Two epimers are obtained, namely D-[2–$^2H_1$]mannitol and D-[2–$^2H_1$]sorbitol, which are easily

separated based on their different solubility properties. Two crystallizations from methanol–water 1:1 afforded pure labelled D-mannitol. D-Mannitol fully deuterated at positions 1 and 6 can be obtained by reduction of D-mannaric acid with NaB^2H_4. This is possible provided the *p*H is acidic for the reduction of the ester to the aldehyde. The formation of the sodium salt of the acid (in basic conditions), which is nonreactive towards sodium borohydride, is then prevented. The last stage can be done at *p*H 9. The acidic conditions necessary for the first stage can be obtained with boric acid, which is used as a buffer in the second stage (41, 40). D-Mannaric acid itself can be synthesized by oxidation of D-mannose (42) or D-mannitol (42, 43) with nitric acid. The yields are low due to nonspecific oxidation but large scales can be used because the starting materials are inexpensive. The reactions involved for the deuteration of D-mannitol are shown in Scheme 5–5.

Eibl (44) has developed a method that avoids the purification of 1,2:5,6-di-*O*-isopropylidene-D-mannitol, uses sodium metaperiodate for its cleavage into two protected glyceraldehyde molecules and sodium borohydride for the reduction (45). A good optical rotation is obtained by this method and is maintained over months at 5°C in presence of solid potassium hydroxide. The reaction steps involved are illustrated in Scheme 5–6. If sodium borodeuteride is used instead of sodium borohydride, one deuterium atom can be introduced at position 3. Since the reduction is nonstereospecific, both *3R* and *3S* enantiomers will be formed.

Schemes 5–7 and 5–8 describe the synthesis of the diacyl– and alkylacylglycerol respectively. 1-Palmitoyl- (46, 47) and 1-*O*-hexadecyl-*sn*-glycerol (31, 48, 49, 32, 5) have been synthesized from 1,2-*O*-isopropylidene-*sn*-glycerol. For this work, the coupling reactions described above were used. Hydrolysis of the isopropylidene group is performed in ethyl ether–HCl at 0°C (46, 47) in the case of the ester derivative and with aqueous acetic acid for the ether analog (31, 48).

Before introduction of the oleyl chain at position 2 of the glycerol, the primary alcohol functional group has to be protected. The triphenylmethyl protecting group shows a high degree of selectivity for the primary hydroxy groups of polyols. A simplified procedure for its introduction over the classical use of triphenylmethyl chloride in pyridine consists in the activation of the reagent with DMAP (50). The method permits the use of solvents and bases other than pyridine. For no known reason, the reaction gave somewhat low yields and this method of preparation of the diradylglycerol was abandoned at this stage, when a better method was found. As a matter of fact, the use of a diradylglycerol possessing an ester chain at position 2 has been criticized because of the possibility of acyl migration to the free primary alcohol position (35). The resulting phosphorus-containing lipid would be contaminated with the 1,3-diradyl isomer, which is unacceptable.

The problematic storage (racemization) and occasionally unsatisfactory optical purity have been criticized for 1,2-*O*-isopropylidene-*sn*-glycerol (45, 44). New routes have been developed for the synthesis of glycerolipids (8, 34, 35, 4). The starting material is a D-mannitol derivative, 3,4-*O*-isopropylidene-D-mannitol. Although stable and easily prepared, this compound has not often been used in lipid synthesis. It is prepared from D-mannitol by reaction with acetone and H_2SO_4 (51, 52) or with acetone, H_2SO_4 and acetic acid (53), but the former method was more successful. The intermediate compound, 1,2:3,4:5,6-tri-*O*-isopropylidene-D-mannitol, is then converted to the desired compound by mild hydrolysis with ethanolic HCl (54), aqueous acetic acid (52) or methanolic HCl (55). These two reactions are described in Scheme 5–9.

At this stage, two different positions are available for substitution. Since two different chains are desired on the final molecule, the primary position must first be protected with the triphenylmethyl group, as described above.

Because the final substituent at positions 2 and 5 is a fatty acid linked by an ester function, it can not be introduced at this stage, since it will be hydrolyzed under the acidic conditions necessary to deprotect positions 3 and 4. The possibility of acyl migration from position *sn*-2 to *sn*-3 exists after conversion to two glycerol derivatives. The benzyl group is thus used to protect positions 2 and 5 and can be removed at a later stage by hydrogenolysis. A convenient alkylating agent is benzyl chloride. Potassium *tert*-butoxide in *tert*-butanol has been used to form the salt of the alcohol (8, 33–35). Sodium hydride in DMF worked satisfactorily (56). The triphenylmethyl protecting group is removed before purification. Acidic conditions will hydrolyze the triphenylmethyl group but can also attack the isopropylidene group. Methods have been described using the Lewis acid $ZnBr_2$ in an aprotic solvent (57) or BF_3-CH_3OH in CH_2Cl_2 (58). However, the reaction mixture has to be strictly anhydrous, otherwise the acetal is hydrolyzed as well. When acidic conditions in the presence of acetone are used (34, 35), an equilibrium is established and, if an excess acetone is used, it is shifted towards the isopropylidene-protected molecule. Scheme 5–10 illustrates the last three steps described.

The next step involves the introduction of the substituent at positions 1 and 6. These can either be palmitoyl or *O*-hexadecyl. Without purification, the isopropylidene group is removed immediately after under mild acidic conditions with 90% aqueous trifluoroacetic acid (TFA) (59). For the cleavage of the mannitol derivative into two identical substituted glyceraldehyde molecules, several methods have been used. Lead tetraacetate (8, 34, 35) gave unsatisfactory results. If the molecule is water soluble, sodium periodate can be used (45). This is not practical in the case of lipid compounds, although a phase transfer agent, tetrabutylammonium bromide, has been used successfully (56). It was found that using periodic acid in ether gives the most satisfactory results. The reaction

proceeds rapidly in a one-phase system and the workup consists only in filtering the precipitated iodic acid. Reduction of the aldehyde to the corresponding alcohol is easily performed in methanol with sodium borohydride. The preparation of the 1-palmitoyl- and 1-*O*-hexadecyl-*sn*-glycerol is described in Schemes 5–11 and 5–14 respectively.

The headgroup can be introduced at this stage by the methods described above. In the case of the phosphate headgroup, a phosphate triester (8, 4) is formed (Schemes 5–13 and 5–16). Removal of the benzyl group at position 2 has to be done by hydrogenolysis before introduction of the oleyl chain. The final stage consists in the amination (3) of the phosphonate headgroup (Schemes 5–12 and 5–15) and the deprotection of the phosphate headgroup with LiBr in 2-butanone (8, 4) to hydrolyze the triester followed by trifluoroacetic acid – aqueous perchloric acid in CH_2Cl_2 (7, 8, 4) to hydrolyze the *tert*-butyloxycarbonyl group (Schemes 5–13 and 5–16).

Because the catalytic hydrogenation step failed, the synthesis of 1,2-di-*O*-hexadecyl-*sn*-glycerol from 3,4-*O*-isopropylidene-D-mannitol was carried out (Scheme 5–17). Only the phosphonolipid was synthesized via this route (Scheme 5–18).

5.3 Experimental part

5.3.1 Materials and methods

Raney nickel in water at *p*H 10, lithium aluminum deuteride and sodium borodeuteride were from Aldrich Chemical Company (Milwaukee, Wisconsin). Deuterium oxide and 1,2-dibromo[1,1,2,2-$^2H_4$]ethane were obtained

from MSD Isotopes (Montréal, Québec). Di-*tert*-butyldicarbonate and 2-aminoethylphosphonic acid (AEP) were from Sigma Chemical Company (St. Louis, Missouri). [2,2-$^2H_2$]Palmitic acid, prepared by α-exchange with NaO^2H in ^2H_2O (30), was a kind gift of Dr. Harold C. Jarrell. 1,2-*O*-Isopropylidene-*rac*-glycerol was prepared from acetone and glycerol (60) by Dr. Jerzy B. Giziewicz. All other chemicals, solvents and salts were at least reagent grade.

Solvent proportions are given by volume, solid compounds and acids by weight. Melting points are reported uncorrected. Boiling points measured under vacuum are approximate since no manometer was used to determine the pressure. Refractive indices were measured at 20°C with an Erma New Abbe Refractometer (Erma Optical Words, Tokyo). The instrument was calibrated with distilled water which gives η_D^{20} = 1.3329; literature (lit.) η_D^{20} = 1.33299 (61). Densities were determined by weighing a known volume of the liquid at 20 ± 2°C. High-resolution ^1H NMR spectra were taken either on a Bruker AM-300, AM-360 or AM-500 spectrometer using tetramethylsilane (TMS) as an internal or external standard, ^{31}P and ^2H NMR spectra on a Bruker CXP-300, MSL-300 or AM-300 using respectively external 85% H_3PO_4 and the solvent natural abundance signal as references, whereas ^{13}C NMR spectra were obtained on a Bruker CXP-300, MSL-300, AM-300 or AM-360 spectrometer with TMS as internal or external reference.

Petroleum ether (boiling point 35-65°C), benzene, ethyl ether and tetrahydrofuran (THF) are dried by refluxing with petroleum ether-washed sodium and distilled before use. Carbon tetrachloride, chloroform and dichloromethane are dried by reflux and distillation from anhydrous phosphorus pentoxide immediately before use. *N*,*N*-Dimethylformamide (DMF) is distilled under vacuum (water aspirator) from CaH_2 and stored over molecular sieves 5 A (8-12 mesh). Acetone and *tert*-butanol are dried with anhydrous potassium carbonate and distilled before

use. Triethylamine is distilled from CaH_2 and stored over KOH pellets under an argon atmosphere. Pyridine is distilled from KOH under argon and stored on KOH pellets. Water is either doubly distilled or a Milli-Q Water System from Millipore Corporation (Bedford, Massachusetts) is used for its purification. Solvents that are not required perfectly dry are purified by simple distillation.

2-Aminoethanol is distilled under reduced pressure (water aspirator) at 75–80°C before use. Phosphorus tribromide is distilled under vacuum (water aspirator) and the fraction boiling at 45–50°C used for the bromination. Triethyl phosphite is distilled immediately before use, and only the fraction boiling between 156 and 160°C kept for the reaction. Methanesulfonyl chloride is purified by distillation and stored under argon. Thionyl chloride is purified by distillation at 79°C. To purify dicyclohexylcarbodiimide (DCC), the compound is heated above its melting point (34–35°C) and the melted portion is decanted from the solid dicyclohexylurea and used for the reaction. Triphenylmethyl chloride (75 mmol) is purified by dissolving in benzene (10 ml) containing acetyl chloride (3 ml). The mixture is allowed to boil until complete dissolution. Petroleum ether (b.p. 65–110°C) (20 ml) is added and recrystallization is effected at room temperature. Sodium hydride is freed from mineral oil by washing four times with dry petroleum ether and decanting each time.

Rexyn 101 (H) 16–50 mesh (minimum 1.9 meq/ml) is washed with 1 N HCl until the eluate is acidic, then with H_2O until neutral and finally put into the desired solvent. Similarly, Rexyn 201 (OH) 16–50 mesh (minimum 0.95 meq/ml) and Amberlite IRA–400 (OH) 16–50 mesh (1.4 meq/ml) are washed with 1 N NaOH until the eluate is basic, then with H_2O until neutral and finally put into the desired solvent.

Thin-layer chromatography (TLC) was performed on 0.25-mm Silica gel 60 plates (E. Merck, Darmstadt) with no fluorescent indicator. The compounds

are revealed with the following indicators: ninhydrin (62) which gives red spots with primary amino compounds, phosphate spray (63, 64) which gives blue spots with phosphorus-containing compounds, sulfosalycilic acid and $FeCl_3$ (65) which gives white spots on a purple background with the same compounds, and finally a spray composed of 1% cerium sulfate, 1.5% molybdic acid and 10% H_2SO_4 in water which gives blue spots nonspecifically. Column chromatography is performed on Silica gel 60 70–230 mesh (E. Merck, Darmstadt). The column is prepared by suspending the gel in chloroform, waiting until the mixture has cooled down, pouring into the column with a fast flow rate and then equilibrating with the first solvent for elution. A minimum ratio of 10:1 by weight silica gel to mixture to purify is used. The flow rate is kept between 2 and 10 ml/min. Typically, fractions of 20–50 ml are collected.

5.3.2 Synthetic procedures

Compound numbers correspond to those found in Schemes 5–1 to 5–18. Procedures are described with typical scales. When a reaction was performed more than once, the range of yields obtained is given. ^{13}C NMR data are tabulated in Appendix A.

2-Amino[G–^{2}H]ethanol **1b**

A suspension of Raney nickel (50 g) in water is decanted and vortexed twice with 40 ml and twice with 20 ml ^2H_2O and the water decanted each time. To exchange the labile protons, freshly distilled 2-aminoethanol **1a** (0.5 mol) is dissolved in ^2H_2O (20 ml) and the water distilled. This operation is repeated two more times. To exchange the protons attached to carbon atoms, the compound is treated twice with ^2H_2O (50 ml) and Raney nickel (20 g) in ^2H_2O and the water distilled each time. The reaction is followed by ^1H NMR. The deuterated

2-aminoethanol **1b** is purified by distillation under vacuum at 96–97°C (water aspirator). Yield: 42%. Density: 1.060 g/ml; lit. d_4^{20} = 1.0180 (61), d = 1.012 (66), d_4^{25} = 1.0117 (67) for the nondeuterated compound. Refractive index: 1.4523; lit. η_D^{20} = 1.4541 (61), η_D^{20} = 1.4540 (66), η_D^{20} = 1.4539 (67) for the nondeuterated compound. 46.1-MHz ^{2}H NMR (H_2O) δ 3.68 ppm (^{2}H–1), and δ 2.82 ppm (^{2}H–2). ^{2}H NMR was used to measure the extent of deuteration, which gave a ratio of *ca.* 2:1 for the methylene next to the hydroxyl group. It is not possible to determine the absolute value by this method.

N-tert-Butyloxycarbonyl-2-aminoethanol **2a**

A solution containing freshly distilled 2-aminoethanol **1a** (0.1 mol), dioxane (200 ml), water (100 ml) and 1 N NaOH (100 ml) is cooled to 0°C. Di-*tert*-butyldicarbonate (0.11 mol) is added with stirring. The reaction is allowed to proceed at room temperature. The disappearance of 2-aminoethanol is followed with ninhydrin. At the end of the reaction, dioxane is removed by evaporation under reduced pressure. The residual aqueous solution is extracted four times with ethyl acetate. The extracts are dried over Na_2SO_4 and the solvent removed under vacuum. The slightly yellow viscous oil is purified by distillation under reduced pressure at 140–144°C (water aspirator). Yield: 84%. Density: 1.048 g/ml. Refractive index: 1.4486; lit. η_D^{20} = 1.4525 (6).

N-tert-Butyloxycarbonyl-2-amino[G–^{2}H]ethanol **2b**

The same procedure is used with 2-amino[G–^{2}H]ethanol **1b** (0.1 mol). The product is purified by distillation under vacuum at 130–133°C (water aspirator). Yield: 60%. Density: 1.066 g/ml. Refractive index: 1.4468. 46.1-MHz ^{2}H NMR ($CHCl_3$) δ 3.64 ppm (^{2}H–1), and δ 3.24 ppm (^{2}H–2). ^{1}H NMR gave 82% deuteration for the hydroxyl methylene and 39% for the amino methylene.

N-(2-Hydroxyethyl)phthalimide 3

Phthalic anhydride (0.1 mol) and freshly distilled 2-aminoethanol **1a** (0.1 mol) are heated to boiling point for 30 minutes. The product is recrystallized from water (50 ml). Yield: 80%. Melting point (M. p.): 125–127°C; lit. 128°C (68), 129.5°C (61), 126–128°C (66).

N-(2-Bromoethyl)phthalimide 4

Freshly distilled phosphorus tribromide (50 mmol) is added slowly to *N*-(2-hydroxyethyl)phthalimide **3** (75 mmol). The mixture is heated until complete dissolution (30 minutes). The viscous solution is poured onto ice (100 g) with a small amount of 95% ethanol to facilitate the transfer. When the ice has completely melted, the compound is filtered, washed with cold water, dried for a few minutes, and recrystallized from 50% ethanol (200 ml) at 0–4°C. Yield: 50%. M. p.: 79.5–81.5°C; lit. 80–82°C (68), 82–83.5°C (61), 81–84°C (66).

2-Phthalimidoethylphosphonic acid **5**

Phthalic anhydride (8 mmol) and 2-aminoethylphosphonic acid 6 (8 mmol) are heated together for 45 minutes. During that time, the mixture melts slowly, and a new solid crystallizes while cooling. The solid mass is triturated with water and lyophilized. The residue is dissolved in boiling 2-propanol (20 ml), filtered over a Celite mat, and washed twice with warm 2-propanol. Boiling hexane (40 ml) is added to the filtrate. The solution is cooled to 5°C to induce crystallization. Yield: 80%. M. p.: 193–195°C; lit. 196–197 (22), 198.5–199.5°C (17). 121.5-MHz ^{31}P NMR (DMSO-d_6) δ 22.51 ppm.

Diethyl 2-bromoethylphosphonate **8a**

1,2-Dibromoethane **7a** (130 mmol) in a 100-ml 3-neck round-bottom flask equipped with an air condenser, a Stark-Dean trap immersed in an ice-water bath, a reflux condenser and a $CaCl_2$ drying tube is heated with stirring in an oil bath at 150–160°C. Freshly distilled triethyl phosphite (85 mmol) is added dropwise over 6 hours. The reaction mixture is heated for another hour until no more bromoethane condenses in the Stark-Dean trap. The residue is distilled under high vacuum. The first fraction contains the nonreacted 1,2-dibromoethane and triethyl phosphite (24°C). The second fraction is composed of diethyl ethylphosphonate (70–80°C). The desired compound is found in the third fraction (110–115°C). Yield: 34–41%. Density: 1.274 g/ml; lit. 1.275 g/ml (66). Refractive index: 1.4504; lit. η_D^{20} = 1.4600 (66). 121.5-MHz ^{31}P NMR (C^2HCl_3) δ 26.18 ppm.

Diethyl 2-bromo[1,1,2,2-$^2H_4$]ethylphosphonate **8b**

1,2-Dibromo[1,1,2,2-$^2H_4$]ethane **7b** (130 mmol) is heated with stirring in the above-described apparatus. Freshly distilled triethyl phosphite (78 mmol) is added dropwise over 5 hours, and the reaction mixture is heated for 45 more minutes. Distillation with a vacuum pump affords the desired compound. 1,2-Dibromo[1,1,2,2-$^2H_4$]ethane and triethyl phosphite are found in the first fraction (<30°C). In the second fraction (40–70°C) is found diethyl ethylphosphonate. The third fraction, which contains diethyl 2-bromo[1,1,2,2-$^2H_4$]ethylphosphonate **8b**, boils at 77–85°C. Yield: 41%. Density: 1.295 g/ml. Refractive index: 1.4533. 121.5-MHz ^{31}P NMR (C^2HCl_3) δ 26.29 ppm. 46.1-MHz ^2H NMR ($CHCl_3$) δ 3.50 ppm, 2 ^2H (^2H–2), and δ 2.33 ppm, 2 ^2H (^2H–1).

2-Bromoethylphosphonic acid monoanilinium salt **9a**

Diethyl 2-bromoethylphosphonate **8a** (32 mmol) in 48% HBr (40 ml) is heated under reflux in an oil bath at 95–100°C for 20 hours. The reaction mixture is evaporated under reduced pressure at 60°C. The residual yellow oil is dissolved in absolute ethanol (10 ml). Aniline is gradually added until no more precipitate forms. The precipitate is collected and recrystallized from absolute ethanol (150 ml). Yield: 68–71%. M. p.: 148.5–150°C; lit. 150–151.5°C (20, 21).

2-Bromo[1,1,2,2-$^2H_4$]ethylphosphonic acid monoanilinium salt **9b**

Diethyl 2-bromo[1,1,2,2-$^2H_4$]ethylphosphonate **8b** (30 mmol) is hydrolyzed in 48% HBr (35 ml) and treated with aniline as described previously. Yield: 57%. M. p.: 151.5–152°C. 46.1-MHz ^{2}H NMR (H_2O) δ 3.68 ppm, 2 ^2H (^{2}H–2), and δ 2.35 ppm, 2 ^2H (^{2}H–1).

2-Bromoethylphosphonic acid **10a**

2-Bromoethylphosphonic acid monoanilinium salt **9a** (20 mmol) is dissolved in ethanol–water 1:1 (120 ml) at 50°C. The solution is passed three times over Rexyn 101 (H) (35 ml). The column is rinsed with ethanol–water 1:1 until the eluate has a *p*H of 6. The solvents are evaporated to dryness. The thoroughly dried residue is recrystallized in chloroform (75 ml). Yield: 73–87%. M. p.: 90.5–92.5°C; lit. 93–95°C (20, 21).

2-Bromo[1,1,2,2-$^2H_4$]ethylphosphonic acid **10b**

2-Bromo[1,1,2,2-$^2H_4$]ethylphosphonic acid monoanilinium salt **9b** (12 mmol) in ethanol–water 1:1 (70 ml) is passed over Rexyn 101 (H) (30 ml) as

described above. Yield: 91%. M. p.: 91.5–94°C. 46.1-MHz ^2H NMR (H_2O) δ 3.59 ppm, 2 ^2H (^2H-2), and δ 2.33 ppm, 2 ^2H (^2H-1).

1-[2,2-$^2H_2$]Hexadecanol **12b**

[2,2-$^2H_2$]Palmitic acid **11b** (12 mmol) dissolved in dry ethyl ether (100 ml) is added dropwise to maintain a moderate reflux to $LiAlH_4$ (15 mmol) in dry ether (30 ml). Reflux is continued for another 3 hours until TLC (petroleum ether—ethyl acetate 4:1) shows complete conversion. The mixture is cooled in an ice-water bath and H_2O (15 ml) added slowly to destroy the excess $LiAlH_4$. After H_2 evolution has stopped, 10% H_2SO_4 (70 ml) is added slowly to free the alcohol from the lithium and aluminum salts. The phases are separated and the aqueous phase extracted a few times with ethyl ether. The combined ether extracts are washed with water, 5% sodium bicarbonate and water. The solution is dried with sodium sulfate and evaporated to dryness. The product is used directly for the next step.

1-[1,1-$^2H_2$]Hexadecanol **12c**

The reaction is repeated with palmitic acid **11a** (20 mmol) and $LiAl^2H_4$ (22 mmol). The residue is used directly to form the methanesulfonate.

1-Hexadecyl methanesulfonate **13a**

1-Hexadecanol **12a** (0.1 mol) is dissolved in dry CH_2Cl_2 (600 ml) containing dry triethylamine (0.15 mol). The solution is cooled to 0°C. Distilled methanesulfonyl chloride (0.14 mol) dissolved in dry CH_2Cl_2 (50 ml) is added dropwise with stirring. The reaction mixture is kept at 0–4°C overnight. TLC (petroleum ether—ethyl acetate 4:1) shows that all starting material has reacted. The solution is washed four times with water, dried over sodium sulfate and

evaporated to dryness. The residue is recrystallized twice from methanol (200 ml). Yield: 87–93%. M. p.: 50.5–52°C; lit. 54–55°C (32).

1-[2,2-$^2H_2$]Hexadecyl methanesulfonate **13b**

The same procedure is used with the residue of 1-[2,2-$^2H_2$]hexadecanol **12b**. Yield: 85% (2 steps). M. p.: 50–51°C. 46.1-MHz ^2H NMR ($CHCl_3$) δ 1.72 ppm.

1-[1,1-$^2H_2$]Hexadecyl methanesulfonate **13c**

The residue of 1-[1,1-$^2H_2$]hexadecanol **12c** is used in the same procedure. Yield: 50% (2 steps). M. p.: 49.5–51°C; lit. 52–53°C (30). 46.1-MHz ^2H NMR ($CHCl_3$) δ 4.19 ppm.

D-Mannosaccharo-1,4:6,3-dilactone **14**

70% Nitric acid (250 ml) is added by portions with stirring to D-mannitol **16a** (0.5 mol) in water (60 ml). The solution is heated slowly using a water bath. When the temperature reaches 50°C, the reaction becomes vigorous – the solution turns yellow and NO_2 evolves rapidly – and the water bath is replaced by an ice-water bath. When the solution has cooled down, it is heated again to 60°C for 3.5 hours and to 85°C for 30 minutes. The reaction mixture is evaporated under reduced pressure, water being added from time to time to eliminate most of the nitric acid. The residue is dried in a desiccator under vacuum over KOH pellets to eliminate the last traces of HNO_3. The residual gum is triturated with 95% ethanol–ethyl ether 1:1 (200 ml) until all material is suspended. The solid is filtered and recrystallized from 95% ethanol (100 ml). Yield: 8–13%. M. p.: 182–186°C, dec.; lit. 189°C (42), 187°C (43). Calc. for $C_6H_6O_6$: C, 41.39%; H, 3.47%. Found: C,

41.10%; H, 3.44%. 360.1-MHz ^1H NMR (^2H_2O) δ 5.22 ppm, 2 *H* (H–3 + H–4), and δ 4.89 ppm, 2 *H* (H–2 + H–5), $J_{23} = J_{45} = 5.1$ Hz and $J_{34} = 3.2$ Hz, as simulated with the PANIC program supplied with the Bruker software.

D-[2-$^2H_1$]Mannitol **16b**

To a solution of β-D-fructose **15** (0.2 mol) in water (100 ml) under stirring is added dropwise a solution of NaB^2H_4 (75 mmol) in water (100 ml). The temperature is kept below 40°C. The reaction is followed by TLC (acetone–acetonitrile–10% acetic acid 3:5:2) and is complete after one hour. Rexyn 101 (H) (60 ml) is added by small portions. Stirring is continued for another hour. The resin is filtered and washed with water. The filtrate is evaporated at 40°C under reduced pressure to a thick syrup. The residue is co-evaporated four times with methanol to eliminate boric acid as volatile methyl borate. The residual solid is dissolved in water (100 ml) at 50°C. Methanol (100 ml) is added. Crystallization is done at 0–4°C. Two recrystallizations from methanol–water 1:1 afford the pure compound. Yield: 65–73%. M. p.: 162–163°C; lit. 168°C (61), 167–170°C (66), 166–168°C (67) for the nondeuterated compound. 500.1-MHz ^1H NMR (^2H_2O) δ 3.79 ppm, 1 *H*, *dd*, J = 11.8, 2.6 Hz (H–6), δ 3.78 ppm, 1 *H*, *d*, J = 11.8 Hz (H–1), δ 3.73 ppm, 1 *H*, *d*, J = 8.6 Hz (H–4), δ 3.72 ppm, 1 *H*, *s* (H–3), δ 3.69 ppm, 1 *H*, *ddd*, J = 8.6, 5.8, 2.6 Hz (H–5), δ 3.60 ppm, 1 *H*, *dd*, J = 11.8, 5.8 Hz (H–6), and δ 3.59 ppm, 1 *H*, *d*, J = 11.8 Hz (H–1). 46.1-MHz ^2H NMR (H_2O) δ 3.69 ppm.

D-[1,1,6,6-$^2H_4$]Mannitol **16c**

D-Mannosaccharo-1,4:6,3-dilactone **14** (30 mmol) is dissolved in 0.4 M boric acid (150 ml) and the solution cooled in an ice-water bath. NaB^2H_4 (60 mmol) in water (150 ml) previously cooled to 0°C is added to the solution by small portions over 45 minutes. After 15 more minutes at 0°C, the *p*H is adjusted to 9 with 1 N

NaOH. The reaction is allowed to continue overnight at 0–4°C, when TLC (acetone – acetonitrile – 10% acetic acid 3:5:2) shows complete conversion. Rexyn 101 (H) is added until *p*H 4. The mixture is stirred for one hour. The resin is filtered and washed with water. The solvent is evaporated under reduced pressure. The residue is evaporated several times with methanol to remove boric acid as its volatile methyl ester. The residual compound is recrystallized from methanol – water 1:1. Yield: 61–96%. M. p.: 163.5–164°C. 500.1-MHz ^{1}H NMR ($^{2}H_2O$) δ 3.73 ppm, 2 *H*, *d*, J = 8.6 Hz (H–3 + H–4), and δ 3.68 ppm, 2 *H*, *d*, J = 8.6 Hz (H–2 + H–5). 46.1-MHz ^{2}H NMR (H_2O) δ 3.82 ppm, 2 ^{2}H, and δ 3.64 ppm, 2 ^{2}H.

1,2:5,6-Di-*O*-isopropylidene-D-mannitol **17**

Anhydrous $ZnCl_2$ (25 g) is dissolved in dry acetone (150 ml) with stirring for 30 minutes. Powder D-mannitol **16a** (0.1 mol) is added to the decanted solution and stirring continued until TLC (chloroform – methanol 9:1) shows that equilibrium has been reached (4.5 hours). Chloroform (50 ml) and a saturated NaCl solution (50 ml) are added to stop the reaction. The desired compound is extracted in the chloroform – acetone (upper) phase. The aqueous phase is re-extracted with $CHCl_3$ (50 ml). The chloroform extracts are combined and washed with 5% aqueous ammonia (100 ml) to complex traces of Zn^{+2} contaminating the organic phase. The solvent is evaporated to dryness. The residue is used directly in the next step.

2,3-*O*-Isopropylidene-D-glyceraldehyde **18**

The residue of 1,2:5,6-di-*O*-isopropylidene-D-mannitol **17** is dissolved in methanol (20 ml). A solution of $NaIO_4$ (75 mmol) in H_2O (150 ml) adjusted to *p*H 6 with 1 N NaOH is added dropwise, the temperature not being allowed to go above 35°C. Conversion is complete after 10 minutes, as shown by TLC

(chloroform—methanol 9:1 and petroleum ether—ethyl acetate 4:1). Methanol (130 ml) is added and the *p*H adjusted to 8 with KOH. The solution is cooled to 10°C, filtered to remove precipitated $NaIO_3$ and excess $NaIO_4$, and used as is for the reduction.

1,2-*O*-Isopropylidene-*sn*-glycerol **19a**

Sodium borohydride (65 mmol) is added to the solution of 2,3-*O*-isopropylidene-D-glyceraldehyde **18** under magnetic stirring. TLC (petroleum ether—ethyl acetate 4:1) shows that the reduction is complete after 15 minutes. The reaction mixture is extracted with hexane (50 ml) to remove the nonreacted 1,2:3,4:5,6-tri-*O*-isopropylidene-D-mannitol. NaCl is added to saturate the solution, which is extracted with $CHCl_3$ (50 ml). The chloroform extracts are combined and evaporated under vacuum. The residue is purified by distillation under reduced pressure at *ca.* 77°C (water aspirator). Yield: 25% (3 steps). Density: 0.938 g/ml. Refractive index: 1.4336; lit. $\eta_D^{25} = 1.4345$ (38).

1,2-*O*-Isopropylidene-3-palmitoyl-*sn*-glycerol **20a**

To a solution of palmitic acid **11a** (11 mmol) in dry CH_2Cl_2 (100 ml) is added DMAP (0.5 mmol) and 1,2-*O*-isopropylidene-*sn*-glycerol **19a** (10 mmol). The mixture is cooled to 0°C and purified DCC (11 mmol) is added with stirring. Agitation is continued for 5 minutes at 0°C and 3 hours at room temperature until TLC (petroleum ether—ethyl ether 3:2) shows the end of the reaction. The reaction mixture is filtered to remove precipitated dicyclohexylurea. The CH_2Cl_2 phase is washed with 0.5 N HCl (50 ml) and 2% Na_2CO_3 (50 ml), dried over anhydrous Na_2SO_4 and evaporated to dryness. The residue is used as is for the hydrolysis of the isopropylidene protecting group.

2,3-*O*-Isopropylidene-1-palmitoyl-*rac*-glycerol **20b**

The reaction is repeated with palmitic acid **11a** (16 mmol), 1,2-*O*-isopropylidene-*rac*-glycerol **19b** (15 mmol), DMAP (0.75 mmol), and purified DCC (16 mmol). The residue is used directly for the next step.

3-Palmitoyl-*sn*-glycerol **21a**

The residue of 1,2-*O*-isopropylidene-3-palmitoyl-*sn*-glycerol **20a** is dissolved in ethyl ether (30 ml) and cooled in an ice-water bath. Under magnetic stirring, concentrated hydrochloric acid (30 ml) is added slowly. Agitation is continued for 30 minutes, during which time a voluminous precipitate forms. TLC (petroleum ether – ethyl ether 3:2) shows complete conversion. Cold water (130 ml) is added with stirring. After 30 minutes, the precipitate is filtered and dried. Recrystallization is done in petroleum ether. Yield: 45% (2 steps). M. p.: 72–73.5°C; lit. 71–72°C (46, 47).

1-Palmitoyl-*rac*-glycerol **21b**

The hydrolysis of the isopropylidene group of 2,3-*O*-isopropylidene-1-palmitoyl-*rac*-glycerol **20b** is performed as above. Yield: 86% (2 steps). M. p.: 73–75°C.

1-Palmitoyl-3-*O*-triphenylmethyl-*rac*-glycerol **22**

1-Palmitoyl-*rac*-glycerol **21b** (12 mmol), purified triphenylmethyl chloride (13 mmol) and dry triethylamine (18 mmol) are dissolved in dry CH_2Cl_2 (300 ml). DMAP (0.6 mmol) is added and the reaction allowed to proceed overnight at room temperature. TLC (petroleum ether – ethyl ether 3:2) shows that the starting material has completely reacted. The reaction mixture is poured into ice-water. The

organic phase is washed with saturated NH_4Cl and water, and evaporated to dryness. The residue is taken in petroleum ether (100 ml), brought to boiling point and filtered when hot to remove triphenylmethanol. The desired compound crystallizes at room temperature. Yield: 75%. M. p.: 58.5–59.5°C.

3-*O*-Hexadecyl-1,2-*O*-isopropylidene-*sn*-glycerol **23**

To previously washed NaH (9 mmol) in dry benzene (20 ml) is added dropwise over 30 minutes a solution of 1,2-*O*-isopropylidene-*sn*-glycerol **19a** (8 mmol) in dry benzene (10 ml). The mixture is refluxed for 30 minutes to form the salt. 1-Hexadecyl methanesulfonate **13a** (8 mmol) in dry benzene (20 ml) is added dropwise over one hour. The reaction proceeds under reflux overnight after which TLC (petroleum ether – ethyl acetate 4:1) shows complete conversion. The reaction mixture is cooled in an ice-water bath. Ethyl ether (50 ml) and water (50 ml) are added and the phases separated. The aqueous phase is extracted with more ether (25 ml). The combined ether phases are washed with water, dried over anhydrous potassium carbonate and evaporated to dryness. The residue is used directly for the hydrolysis.

3-*O*-Hexadecyl-*sn*-glycerol **24**

The residue of 3-*O*-hexadecyl-1,2-*O*-isopropylidene-*sn*-glycerol **23** from the previous reaction is dissolved in 50% acetic acid (30 ml) and heated to 80°C for 3.5 hours. TLC (petroleum ether – ethyl acetate 4:1) shows that the hydrolysis is complete. The mixture is poured into an excess ice-water (100 ml). The precipitate is collected by filtration and dissolved in ethyl ether. The solution is washed successively with H_2O, 1% potassium carbonate and H_2O, dried with anhydrous sodium sulfate and evaporated to dryness. The desired compound is

recrystallized from petroleum ether at 0°C. Yield: 69% (2 steps). M. p.: 64.5–66°C; lit. 62.5–63.5°C (31), 62–63°C (48), 63°C (49), 65.5°C (32), 65.5–66.5°C (5).

3-*O*-Hexadecyl-1-*O*-triphenylmethyl-*sn*-glycerol **25**

3-*O*-Hexadecyl-*sn*-glycerol **24** (1.8 mmol), purified triphenylmethyl chloride (2 mmol), dry triethylamine (2.5 mmol) and DMAP (0.1 mmol) are dissolved in dry CH_2Cl_2 (40 ml) and allowed to react overnight at room temperature. TLC (petroleum ether—ethyl ether 3:2) shows that the tritylation is complete. The reaction mixture is poured into an ice-water mixture (75 ml). The CH_2Cl_2 phase is separated and the aqueous phase extracted with more CH_2Cl_2. The combined organic phases are washed with a saturated NH_4Cl solution (60 ml) and with water (60 ml), dried with anhydrous Na_2SO_4 and evaporated to dryness. The residue is taken in petroleum ether to crystallize the nonreacted 3-*O*-hexadecyl-*sn*-glycerol and triphenylmethanol. The desired compound is recrystallized from acetone at 0–4°C. Yield: 17%. M. p.: 49.5–50.5°C; lit. 49°C (69).

1,2:3,4:5,6-Tri-*O*-isopropylidene-D-mannitol **26a**

To a suspension of D-mannitol **16a** (0.2 mol) in dry acetone (450 ml) in an ice-water bath concentrated sulfuric acid (4 ml) is added with stirring. The ice-water bath is removed and agitation continued at room temperature until TLC (chloroform—methanol 19:1 or 9:1) shows that equilibrium is reached. The solution is neutralized with saturated potassium bicarbonate or Rexyn 201 (OH). The suspension is filtered and the residue washed on the filter with acetone (2 × 60 ml). The filtrate is concentrated under reduced pressure below 40°C and filtered. The residue is washed with water and dissolved in 95% ethanol (120 ml) at 40–50°C. The solution is cooled to room temperature and water is added dropwise until the

solution becomes turbid. The crystallization is continued at 0–4°C. Yield: 60–76%. M. p.: 66.5–68.5°C; lit. 69–70°C (52), 68–70°C (53), 69–70°C (56).

1,2:3,4:5,6-Tri-*O*-isopropylidene-D-[2-$^2H_1$]mannitol **26b**

D-[2-$^2H_1$]Mannitol **16b** (90 mmol) is submitted to the procedure mentioned above. Yield: 68%. M. p.: 68–68.5°C. 46.1-MHz ^2H NMR ($CHCl_3$) δ 4.17 ppm.

1,2:3,4:5,6-Tri-*O*-isopropylidene-D-[1,1,6,6-$^2H_4$]mannitol **26c**

The same procedure is used with D-[1,1,6,6-$^2H_4$]mannitol **16c** (40 mmol). Yield: 53%. M. p.: 68–68.5°C. 46.1-MHz ^2H NMR ($CHCl_3$) δ 4.03 ppm, 2 ^2H, and δ 3.94 ppm, 2 ^2H.

3,4-*O*-Isopropylidene-D-mannitol **27a**

1,2:3,4:5,6-Tri-*O*-isopropylidene-D-mannitol **26a** (0.1 mol) is dissolved in 95% ethanol (500 ml). 0.8% H_2SO_4 (150 ml) is added and the reaction allowed to proceed until TLC (chloroform–methanol 9:1) shows that all starting material has disappeared (3–4 days). The reaction is stopped by adding solid $BaCO_3$ with saturated $Ba(OH)_2$ or Amberlite IRA-400 (OH) (20 ml). When the *p*H is neutral, the salts or the resin are filtered off and the filtrate is evaporated to dryness. The residue is shaken in acetone for several hours and the undissolved D-mannitol removed by filtration. The filtrate is evaporated and the dry residue recrystallized from benzene–chloroform 1:1. Yield: 59–81%. M. p.: 83.5–84°C; lit. 85°C (54), 86–87°C (52), 85–86°C (70), 86°C (55), 83°C (56).

3,4-*O*-Isopropylidene-D-[2-$^2H_1$]mannitol **27b**

1,2:3,4:5,6-Tri-*O*-isopropylidene-D-[2-$^2H_1$]mannitol **26b** (60 mmol) is used in the same procedure. Yield: 76%. M. p.: 84–84.5°C. 46.1-MHz ^2H NMR (H_2O) δ 3.73 ppm.

3,4-*O*-Isopropylidene-D-[1,1,6,6-$^2H_4$]mannitol **27c**

The same procedure is used with 1,2:3,4:5,6-tri-*O*-isopropylidene-D-[1,1,6,6-$^2H_4$]mannitol **26c** (20 mmol). Yield: 59%. M. p.: 81–82.5°C. 46.1-MHz ^2H NMR (H_2O) δ 3.77 ppm, 2 ^2H, and δ 3.61 ppm, 2 ^2H.

3,4-*O*-Isopropylidene-1,6-di-*O*-triphenylmethyl-D-mannitol **28a**

To 3,4-*O*-isopropylidene-D-mannitol **27a** (20 mmol) dissolved in dry THF (100 ml) are added dry triethylamine (60 mmol), purified triphenylmethyl chloride (45 mmol) and DMAP (2 mmol). The reaction proceeds at room temperature for approximately 5 days until TLC (chloroform–methanol 19:1 or 9:1) shows no more progress. The reaction mixture is poured into ice-water. When the ice has melted, the solution is extracted with $CHCl_3$ and the phases separated. The organic phase is washed twice with saturated NH_4Cl, then with water, dried and evaporated to dryness. The compound is purified by chromatography on silica gel using the solvents petroleum ether–chloroform–ethyl acetate 70:30:1, 70:30:2, 70:30:5 and 70:30:10 for elution. The desired fractions are pooled and evaporated to dryness. The pure product is obtained by recrystallization from petroleum ether–ethyl ether 2:1. The reaction can also be done in the same amount of dry *tert*-butanol under reflux for a few hours. In that case, when the reaction is complete, most of the *tert*-butanol is evaporated under reduced pressure and the

residue dissolved in $CHCl_3$. The purification is performed as above. Yield: 51–75%. M. p.: 165.5–167.5°C.

3,4-*O*-Isopropylidene-1,6-di-*O*-triphenylmethyl-D-[2–H_1]mannitol **28b**

The same amounts of reactants are submitted to the procedure mentioned above using 3,4-*O*-isopropylidene-D-[2–$^2H_1$]mannitol **27b** instead of 3,4-*O*-isopropylidene-D-mannitol **27a**, the solvent being *tert*-butanol. Yield: 83%. M. p.: 167–167.5°C. 46.1-MHz ^2H NMR ($CHCl_3$) δ 3.77 ppm.

2,5-Di-*O*-benzyl-3,4-*O*-isopropylidene-1,6-di-*O*-triphenylmethyl-D-mannitol **29a**

The compound 3,4-*O*-isopropylidene-1,6-di-*O*-triphenylmethyl-D-mannitol **28a** (20 mmol) dissolved in dry DMF (50 ml) is added dropwise over 15 minutes to previously washed NaH (60 mmol) in the same solvent (20 ml) under magnetic stirring. Another 30 to 60 minutes are allowed to form the salt. Benzyl chloride (60 mmol) in dry DMF (20 ml) is added dropwise. The reaction is followed by TLC (petroleum ether–ethyl ether 3:2 or petroleum ether–ethyl acetate 4:1). After the night, water (100 ml) is added dropwise. A white precipitate forms and it is extracted three times with ethyl ether (100 ml each time). The ether phase is washed with water (50 ml), dried over anhydrous sodium sulfate and evaporated to dryness. The residual amorphous solid is used directly for the hydrolysis.

2,5-Di-*O*-benzyl-3,4-*O*-isopropylidene-1,6-di-*O*-triphenylmethyl-D-[2–$^2H_1$]mannitol **29b**

The above procedure is also used with 3,4-*O*-isopropylidene-1,6-di-*O*-triphenylmethyl-D-[2–$^2H_1$]mannitol **28b** (15 mmol). The hydrolysis of the triphenylmethyl protecting group is performed directly on the residue.

2,5-Di-*O*-benzyl-3,4-*O*-isopropylidene-D-mannitol **30a**

The residual compound 2,5-di-*O*-benzyl-3,4-*O*-isopropylidene-1,6-di-*O*-triphenylmethyl-D-mannitol **29a** from the previous reaction is dissolved in acetone (100 ml), methanol (100 ml) and concentrated HCl (1 ml). The solution is heated to 50°C and kept at the same temperature for 1.5 hour, when TLC (petroleum ether—acetone 4:1) shows completion of the reaction. After cooling, dichloromethane (200 ml) is added and the mixture extracted twice with water (200 ml each time). The organic phase is washed with saturated $NaHCO_3$ (100 ml) and water (50 ml), dried over Na_2SO_4 and evaporated to dryness. The compound is freed from triphenylmethanol by chromatography on silica gel using the solvent systems petroleum ether—chloroform—acetone 4:5:1, 3:5:2 and 2:5:3 for elution. The fractions containing the desired product are pooled and the solvent evaporated under vacuum. The pure product is obtained after recrystallization from petroleum ether—ethyl ether 1:1 at 0–4°C. Yield: 47–70% (2 steps). M. p.: 72–73°C.

2,5-Di-*O*-benzyl-3,4-*O*-isopropylidene-D-[2-$^2H_1$]mannitol **30b**

The hydrolysis is performed using the same procedure with the labelled compound 2,5-di-*O*-benzyl-3,4-*O*-isopropylidene-1,6-di-*O*-triphenylmethyl-D-[2-$^2H_1$]mannitol **29b** from the preceding step. Yield: 69% (2 steps). M. p.: 68–69°C. 46.1-MHz ^2H NMR ($CHCl_3$) δ 3.60 ppm.

2,5-Di-*O*-benzyl-3,4-*O*-isopropylidene-1,6-dipalmitoyl-D-mannitol **31a**

2,5-Di-*O*-benzyl-3,4-*O*-isopropylidene-D-mannitol **30a** (2 mmol) and palmitic acid **11a** (4.5 mmol) are dissolved in dry dichloromethane (25 ml). The solution is cooled to 0°C in an ice-water bath. DMAP (0.2 mmol) dissolved in dry CH_2Cl_2 (5 ml) is added, followed slowly by purified DCC (5 mmol) in the same

solvent (20 ml). After 30 minutes, the ice-water bath is removed and agitation continued at room temperature overnight when TLC (petroleum ether—acetone 4:1) shows complete disappearance of the starting material. The precipitated dicyclohexylurea is filtered off and the filtrate evaporated under vacuum. The residue is taken in a small amount of CH_2Cl_2 and residual dicyclohexylurea filtered off. The solution is washed with saturated $NaHCO_3$ and H_2O, dried over anhydrous Na_2SO_4 and evaporated. The residue is used as is for the next step.

2,5-Di-*O*-benzyl-3,4-*O*-isopropylidene-1,6-di[2,2-$^2H_2$]palmitoyl-D-mannitol **31b**

The same procedure is used with the compound 2,5-di-*O*-benzyl-3,4-*O*-isopropylidene-D-mannitol **30a**, replacing palmitic acid **11a** by [2,2-$^2H_2$]palmitic acid **11b**. The hydrolysis is performed directly on the residue.

2,5-Di-*O*-benzyl-3,4-*O*-isopropylidene-1,6-dipalmitoyl-D-[2-$^2H_1$]mannitol **31c**

2,5-Di-*O*-benzyl-3,4-*O*-isopropylidene-D-[2-$^2H_1$]mannitol **30b** (4 mmol) and palmitic acid **11a** (10 mmol) are submitted to the same procedure and the residue used directly for the hydrolysis of the isopropylidene group.

2,5-Di-*O*-benzyl-1,6-dipalmitoyl-D-mannitol **32a**

The residue of 2,5-di-*O*-benzyl-3,4-*O*-isopropylidene-1,6-dipalmitoyl-D-mannitol **31a** from the previous reaction is dissolved in 90% CF_3COOH (20 ml) precooled to 0°C. The reaction is finished after 30 minutes at 0°C, as shown by TLC (petroleum ether—acetone 4:1). Most of the TFA is evaporated under vacuum without heating. The residue is diluted with CH_2Cl_2 and the solution is washed twice with water, then with saturated $NaHCO_3$ and finally with water, dried and evaporated

to dryness. The residue is recrystallized from 95% ethanol at 0–4°C. Yield: 85–93% (2 steps). M. p.: 58.5–60°C.

2,5-Di-*O*-benzyl-1,6-di[2,2-$^2H_2$]palmitoyl-D-mannitol **32b**

The same procedure is used to hydrolyze the isopropylidene group from 2,5-di-*O*-benzyl-3,4-*O*-isopropylidene-1,6-di[2,2-$^2H_2$]palmitoyl-D-mannitol **31b**. Yield: 96% (2 steps). M. p.: 55–57°C. 46.1-MHz ^2H NMR ($CHCl_3$) δ 2.26 ppm.

2,5-Di-*O*-benzyl-1,6-dipalmitoyl-D-[2-$^2H_1$]mannitol **32c**

The compound 2,5-di-*O*-benzyl-3,4-*O*-isopropylidene-1,6-dipalmitoyl-D-[2-$^2H_1$]mannitol **31c** from the previous step is hydrolyzed with 90% CF_3COOH as described above. Yield: 90% (2 steps). M. p.: 58.5–59.5°C. 46.1-MHz ^2H NMR ($CHCl_3$) δ 3.70 ppm.

2-*O*-Benzyl-3-palmitoyl-D-glyceraldehyde **33**

2,5-Di-*O*-benzyl-1,6-dipalmitoyl-D-mannitol **32a** (2 mmol) and H_5IO_6 (2 mmol) are dissolved in ethyl ether (20 ml) and allowed to react at room temperature for one to two hours when TLC (petroleum ether—ethyl acetate 4:1) shows complete conversion. The precipitated HIO_3 is decanted and the ether solution washed successively with water, 10% Na_2SO_3 and water, dried over anhydrous Na_2SO_4 and evaporated to dryness. The residue is used directly for the reduction step.

2-*O*-Benzyl-1-palmitoyl-*sn*-glycerol **34**

The residue of 2-*O*-benzyl-3-palmitoyl-D-glyceraldehyde **33** is dissolved in methanol (30 ml) and cooled in an ice-water bath. $NaBH_4$ (2 mmol)

dissolved in methanol (10 ml) is added by portions. After 1.5 hour, TLC (petroleum ether—ethyl acetate 4:1) shows that reduction is complete. The methanol is evaporated under reduced pressure. The residue is dissolved in ethyl ether, washed several times with water, dried over anhydrous Na_2SO_4 and evaporated to dryness. The compound is recrystallized from methanol at —20°C. Yield: 68–85% (2 steps). M. p.: <22°C.

2-*O*-Benzyl-1-palmitoyl-*sn*-glycero-3-(2-bromoethyl)phosphonate **35**

2-Bromoethylphosphonic acid **10a** (1 mmol), distilled $SOCl_2$ (20 mmol) and dry DMF (1 drop) are allowed to react overnight at room temperature. The residual thionyl chloride is evaporated under argon. Dry CCl_4 (2.5 ml) is added. A solution composed of 2-*O*-benzyl-1-palmitoyl-*sn*-glycerol **34** (0.5 mmol) and dry pyridine (1 mmol) in dry CCl_4 (5 ml) is added dropwise over one hour at 0°C. The reaction is followed by TLC (petroleum ether—acetone 4:1 and chloroform—methanol—water 65:25:4). Ethyl ether (10 ml) and 0.5 N HCl (10 ml) are added to stop the reaction. The phases are separated and the aqueous phase extracted with ether. The combined ether phases are washed with H_2O, dried over anhydrous Na_2SO_4 and evaporated to dryness. The compound is purified on silica gel using chloroform and chloroform—methanol 19:1 for elution. The fractions containing the desired compound are pooled and evaporated to dryness to give an amorphous product. Yield: 37%.

2,5-Di-*O*-benzyl-1,6-di-*O*-hexadecyl-3,4-*O*-isopropylidene-D-mannitol **36a**

To a suspension of previously washed NaH (5 mmol) in dry benzene (10 ml) is added dropwise a solution of 2,5-di-*O*-benzyl-3,4-*O*-isopropylidene-D-mannitol **30a** (2 mmol) in dry benzene (15 ml). The reaction mixture is heated to reflux for one hour. 1-Hexadecyl methanesulfonate **13a** (5 mmol) in dry benzene

(20 ml) is added dropwise under reflux. The reaction is followed by TLC (petroleum ether – ethyl acetate 9:1). After the night, the mixture is brought to room temperature and the reaction is stopped by adding H_2O slowly to destroy the excess sodium hydride. The benzene is evaporated and the water phase extracted twice with CH_2Cl_2. The combined organic phases are washed with water, dried and evaporated to dryness. The residue is used directly for the hydrolysis. If benzene is replaced by *N*,*N*-dimethylformamide, the reaction proceeds faster at a lower temperature (50°C).

2,5-Di-*O*-benzyl-1,6-di-*O*-[2,2-$^2H_2$]hexadecyl-3,4-*O*-isopropylidene-D-mannitol **36b**

Using 2,5-di-*O*-benzyl-3,4-*O*-isopropylidene-D-mannitol **30a** (2 mmol) and 1-[2,2-$^2H_2$]hexadecyl methanesulfonate **13b** (4.5 mmol), the reaction is repeated in C_6H_6 and the hydrolysis performed on the residue.

2,5-Di-*O*-benzyl-1,6-di-*O*-[1,1-$^2H_2$]hexadecyl-3,4-*O*-isopropylidene-D-mannitol **36c**

The reaction is repeated in benzene with the compound 2,5-di-*O*-benzyl-3,4-*O*-isopropylidene-D-mannitol **30a** (2 mmol), replacing 1-hexadecyl methanesulfonate **13a** by 1-[1,1-$^2H_2$]hexadecyl methanesulfonate **13c** (4.5 mmol). The residue is used as is for the next step.

2,5-Di-*O*-benzyl-1,6-di-*O*-hexadecyl-3,4-*O*-isopropylidene-D-[2-$^2H_1$]mannitol **36d**

The procedure described above is used with the compound 2,5-di-*O*-benzyl-3,4-*O*-isopropylidene-D-[2-$^2H_1$]mannitol **30b** (2 mmol) and 1-hexadecyl methanesulfonate **13a** (4.5 mmol) in C_6H_6, and the hydrolysis is performed directly on the residue.

2,5-Di-*O*-benzyl-1,6-di-*O*-hexadecyl-D-mannitol **37a**

The residue of the compound 2,5-di-*O*-benzyl-1,6-di-*O*-hexadecyl-3,4-*O*-isopropylidene-D-mannitol **36a** obtained from the previous reaction is dissolved in 90% CF_3COOH (20 ml) at 0°C and the reaction followed by TLC (petroleum ether – ethyl acetate 4:1). After 30 to 60 minutes, most of the TFA is evaporated under reduced pressure without heating. The residue is dissolved in CH_2Cl_2, washed with H_2O, saturated $NaHCO_3$ and H_2O, dried over Na_2SO_4 and evaporated to dryness. The compound is recrystallized in petroleum ether. Yield: 64–83% (2 steps). M. p.: 54–54.5°C.

2,5-Di-*O*-benzyl-1,6-di-*O*-[2,2-$^2H_2$]hexadecyl-D-mannitol **37b**

The same procedure is repeated with 2,5-di-*O*-benzyl-1,6-di-*O*-[2,2-$^2H_2$]hexadecyl-3,4-*O*-isopropylidene-D-mannitol **36b**. Yield: 72% (2 steps). M. p.: 53–53.5°C. 46.1-MHz ^2H NMR ($CHCl_3$) δ 1.52 ppm.

2,5-Di-*O*-benzyl-1,6-di-*O*-[1,1-$^2H_2$]hexadecyl-D-mannitol **37c**

The labelled compound 2,5-di-*O*-benzyl-1,6-di-*O*-[1,1-$^2H_2$]hexadecyl-3,4-*O*-isopropylidene-D-mannitol **36c** is hydrolyzed using in the same procedure. Yield: 69% (2 steps). M. p.: 52–52.5°C. 46.1-MHz ^2H NMR ($CHCl_3$) δ 3.40 ppm.

2,5-Di-*O*-benzyl-1,6-di-*O*-hexadecyl-D-[2-$^2H_1$]mannitol **37d**

The hydrolysis is repeated with the residue of 2,5-di-*O*-benzyl-1,6-di-O-hexadecyl-3,4-*O*-isopropylidene-D-[2-$^2H_1$]mannitol **36d** in 90% CF_3COOH. Yield: 50% (2 steps). M. p.: 54.5–55°C. 46.1-MHz ^2H NMR ($CHCl_3$) δ 3.69 ppm.

2-*O*-Benzyl-3-*O*-hexadecyl-D-glyceraldehyde **38**

2,5-Di-*O*-benzyl-1,6-di-*O*-hexadecyl-D-mannitol **37a** (2 mmol) and H_5IO_6 (2 mmol) in ethyl ether (100 ml) are allowed to react at room temperature until TLC (petroleum ether—ethyl acetate 4:1) shows complete conversion to the aldehyde. The precipitated HIO_3 is decanted and the ether solution washed with H_2O, 10% Na_2SO_3 and H_2O. The organic phase is dried with anhydrous Na_2SO_4 and evaporated to dryness. The residue is used directly for the reduction step.

2-*O*-Benzyl-1-*O*-hexadecyl-*sn*-glycerol **39**

The 2-*O*-benzyl-3-*O*-hexadecyl-D-glyceraldehyde **38** obtained in the previous reaction is dissolved in methanol (25 ml) at 0°C. A solution of $NaBH_4$ (2 mmol) in methanol (10 ml) cooled to 0°C is added dropwise over 15 minutes. The reaction is continued overnight at room temperature. TLC (petroleum ether—ethyl acetate 4:1) shows completion of the reaction. The methanol is evaporated and the residue taken in CH_2Cl_2. The solution is washed with H_2O, dried over anhydrous Na_2SO_4 and evaporated to dryness. The compound is purified by chromatography on silica gel. Petroleum ether, followed by petroleum ether—ethyl acetate 19:1, 9:1 and 4:1 are used for elution. The fractions containing the pure compound are pooled together and evaporated to dryness. The residue is a colorless amorphous compound. Yield: 58% (2 steps).

2-*O*-Benzyl-1-*O*-hexadecyl-*sn*-glycero-3-(2-bromoethyl)phosphonate **40**

2-Bromoethylphosphonic acid **10a** (1.5 mmol), distilled $SOCl_2$ (20 mmol) and dry DMF (0.1 ml) are allowed to react overnight at room temperature. The residual $SOCl_2$ is evaporated with a stream of argon under vacuum. The residue is cooled to 0°C. Dry CCl_4 (2 ml) is added, followed by dry pyridine

(1 mmol) in dry CCl_4 (5 ml). 2-*O*-Benzyl-1-*O*-hexadecyl-*sn*-glycerol **39** (0.5 mmol) in dry CCl_4 (4 ml) is added dropwise over 30 minutes. The reaction is complete after 2 hours at 0°C as shown by TLC (petroleum ether—ethyl acetate 9:1 and chloroform—methanol—water 65:25:4). To hydrolyze the acid chloride, 0.5 N HCl (5 ml) is added at 0°C. The phases are separated and the organic phase washed with 20% ethanol, saturated $NaHCO_3$ and 10% KCl, dried over anhydrous sodium and magnesium sulfate and evaporated to dryness. The residue is purified on silica gel and eluted successively with chloroform and chloroform—methanol 19:1, 9:1, 4:1 and 2:1. Yield: 44%.

1,2,5,6-Tetra-*O*-hexadecyl-3,4-*O*-isopropylidene-D-mannitol **41a**

To a suspension of previously washed NaH (25 mmol) in dry DMF (10 ml) is added a solution of 3,4-*O*-isopropylidene-D-mannitol **27a** (5 mmol) in the same solvent (50 ml). The sodium salt is formed in 30 minutes at 50°C. 1-Hexadecyl methanesulfonate (21 mmol) dissolved in dry DMF (100 ml) is added dropwise over one hour to the reaction mixture at 50°C. The course of the reaction is followed by TLC (petroleum ether—ethyl acetate 9:1). The reaction mixture is brought to room temperature and water is added slowly to destroy the excess NaH. After cooling, the mixture is extracted three times with petroleum ether. The combined organic phases are washed with 20% aqueous ethanol, dried over Na_2SO_4 and evaporated to dryness. The compound is not isolated but used directly for the hydrolysis.

1,2,5,6-Tetra-*O*-hexadecyl-3,4-*O*-isopropylidene-D-[2-$^2H_1$]mannitol **41b**

3,4-*O*-Isopropylidene-D-[2-$^2H_1$]mannitol **27b** (5 mmol) is submitted to the same procedure and the residue used directly for the next step.

1,2,5,6-Tetra-*O*-hexadecyl-3,4-*O*-isopropylidene-D-[1,1,6,6-$^2H_4$]mannitol **41c**

The procedure is repeated with 3,4-*O*-isopropylidene-D-[1,1,6,6-$^2H_4$]mannitol **27c** (3 mmol). Hydrolysis is performed on the residue without purification.

1,2,5,6-Tetra-*O*-hexadecyl-D-mannitol **42a**

The residue of 1,2,5,6-tetra-*O*-hexadecyl-3,4-*O*-isopropylidene-D-mannitol **41a** is dissolved in $CHCl_3$ (120 ml), 2-propanol (100 ml) and 2 N HCl (10 ml). The solution is refluxed overnight until TLC (petroleum ether–ethyl acetate 9:1) reveals that hydrolysis of the starting material is complete. Water is added to separate the phases. The organic layer is washed with water, saturated aqueous sodium bicarbonate and water, dried over sodium sulfate and evaporated to dryness. The residue is recrystallized from ethyl ether–methanol 1:1 at 0–4°C. Yield: 68% (2 steps). M. p.: 50–51.5°C.

1,2,5,6-Tetra-*O*-hexadecyl-D-[2-$^2H_1$]mannitol **42b**

The same procedure is used with 1,2,5,6-tetra-*O*-hexadecyl-3,4-*O*-isopropylidene-D-[2-$^2H_1$]mannitol **41b**. Yield: 74% (2 steps). M. p.: 55–56°C. 46.1-MHz ^2H NMR ($CHCl_3$) δ 3.66 ppm.

1,2,5,6-Tetra-*O*-hexadecyl-D-[1,1,6,6-$^2H_4$]mannitol **42c**

The compound 1,2,5,6-tetra-*O*-hexadecyl-3,4-*O*-isopropylidene-D-[1,1,6,6-$^2H_4$]mannitol **41c** is submitted to the above procedure. Yield: 60% (2 steps). M. p.: 53.5–54.5°C. 46.1-MHz ^2H NMR ($CHCl_3$) δ 3.56 ppm.

2,3-Di-*O*-hexadecyl-D-glyceraldehyde **43a**

1,2,5,6-Tetra-*O*-hexadecyl-D-mannitol **42a** (1 mmol) and H_5IO_6 (1 mmol) in ethyl ether (60 ml) are allowed to react at room temperature until all starting material is converted to the aldehyde (2–4 hours) as shown by TLC (petroleum ether—ethyl acetate 9:1). The reaction mixture is filtered to remove precipitated HIO_3, which is washed with ether. The filtrate is washed with water, 10% Na_2SO_3 and water, dried over sodium sulfate and evaporated under vacuum. The aldehyde is not purified but used directly for the reduction.

2,3-Di-*O*-hexadecyl-D-[2–$^2H_1$]glyceraldehyde **43b**

1,2,5,6-Tetra-*O*-hexadecyl-D-[2–$^2H_1$]mannitol **42b** (2 mmol) is submitted to the same procedure and the residue used directly for the next step. The oxidation of 1,2,5,6-tetra-*O*-hexadecyl-D-mannitol normally yields two identical 1,2-di-*O*-hexadecyl-D-glyceraldehyde molecules. For this particular case, one of the molecules is labelled, the other not. This corresponds to an isotopic dilution of 50% which will be carried over to subsequent compounds.

2,3-Di-*O*-hexadecyl-D-[3,3–$^2H_2$]glyceraldehyde **43c**

The procedure mentioned above is also used with 1,2,5,6-tetra-*O*-hexadecyl-D-[1,1,6,6–$^2H_4$]mannitol **42c** (1.5 mmol). The reduction is performed directly on the residue.

1,2-Di-*O*-hexadecyl-*sn*-glycerol **44a**

The residue of 2,3-di-*O*-hexadecyl-D-glyceraldehyde **43a** from the previous reaction is dissolved in methanol (25 ml), cooled to 0°C, and sodium borohydride (1 mmol) dissolved in methanol (10 ml) at 0°C is added dropwise over

30 minutes. The reaction is allowed to proceed overnight at room temperature, after which TLC (petroleum ether—ethyl acetate 9:1) reveals complete reaction. The solvent is removed on the rotary evaporator and the residue dissolved in dichloromethane. The solution is washed three times with water, dried over Na_2SO_4 and evaporated to dryness. The pure compound is obtained after recrystallization from ethyl ether—methanol 1:1 at 0°C. Yield: 87–92% (2 steps). M. p.: 48–49°C; lit. 48.5–49.5°C (71), 46–47°C (72).

1,2-Di-*O*-hexadecyl-*sn*-[2–$^2H_1$]glycerol **44b**

Using the procedure described above, 2,3-di-*O*-hexadecyl-D-[2–$^2H_1$]glyceraldehyde **43b** affords the desired compound. Yield: 93% (2 steps). M. p.: 50–50.5°C. 46.1-MHz ^2H NMR ($CHCl_3$) δ 3.66 ppm.

1,2-Di-*O*-hexadecyl-*sn*-[1,1–$^2H_2$]glycerol **44c**

2,3-Di-*O*-hexadecyl-D-[3,3–$^2H_2$]glyceraldehyde **43c** is submitted to the same procedure. Yield: 90% (2 steps). M. p.: 49.5–50°C. 46.1-MHz ^2H NMR ($CHCl_3$) δ 3.50 ppm.

1,2-Di-*O*-hexadecyl-*sn*-(*3RS*)-[3–$^2H_1$]glycerol **44d**

The same two steps (oxidation with periodic acid and reduction with sodium borohydride) are repeated starting with 1,2,5,6-tetra-*O*-hexadecyl-D-mannitol **42a** (1 mmol), replacing $NaBH_4$ by NaB^2H_4 for the reduction. Yield: 82% (2 steps). M. p.: 47–47.5°C. 46.1-MHz ^2H NMR ($CHCl_3$) δ 3.48 ppm.

1,2-Di-*O*-hexadecyl-*sn*-glycero-3-(2-bromoethyl)phosphonate **45a**

2-Bromoethylphosphonic acid **10a** (0.6 mmol) dissolved in dry DMF (1 ml) is added dropwise over 30 minutes to a solution of 1,2-di-*O*-hexadecyl-*sn*-glycerol **44a** (0.5 mmol), purified DCC (0.7 mmol) and DMAP (0.05 mmol) in dry CCl_4 (4 ml) cooled to 0°C. TLC (chloroform – methanol – 30% ammonia 65:30:5) shows that the reaction is complete after 2–4 hours at room temperature. The precipitated dicyclohexylurea is filtered off. The filtrate is washed with 0.5 N HCl and twice with water, dried over anhydrous sodium sulfate and evaporated to dryness. The residue is used directly for the amination step.

1,2-Di-*O*-hexadecyl-*sn*-glycero-3-(2-bromo[1,1,2,2–$^2H_4$]ethyl)phosphonate **45b**

The same amounts of reactants are used, replacing 2-bromoethylphosphonic acid **10a** by 2-bromo[1,1,2,2–$^2H_4$]ethylphosphonic acid **10b**. The residue is used as is for the next step.

1,2-Di-*O*-hexadecyl-*sn*-[2–$^2H_1$]glycero-3-(2-bromoethyl)phosphonate **45c**

2-Bromoethylphosphonic acid **10a** (1 mmol) dissolved in dry DMF (1 ml) at 0°C is added dropwise over 30 minutes to a solution of 1,2-di-*O*-hexadecyl-*sn*-[2–$^2H_1$]glycerol **44b** (0.8 mmol), purified DCC (1.2 mmol) and DMAP (0.08 mmol) in dry CCl_4 (3 ml) in an ice bath. The reaction is continued overnight at room temperature. The workup is done as described previously. The residue is used directly in the next step.

1,2-Di-*O*-hexadecyl-*sn*-[1,1–$^2H_2$]glycero-3-(2-bromoethyl)phosphonate **45d**

The reaction is repeated with 1,2-di-*O*-hexadecyl-*sn*-[1,1–$^2H_2$]glycerol **44c** (0.8 mmol) instead of 1,2-di-*O*-hexadecyl-*sn*-[2–$^2H_1$]glycerol **44b** and

2-bromoethylphosphonic acid **10a** (1 mmol) as described above, and the next step performed on the residue.

1,2-Di-*O*-hexadecyl-*sn*-(3*RS*)-[3-$^2H_1$]glycero-3-(2-bromoethyl)phosphonate **45e**

1,2-Di-*O*-hexadecyl-*sn*-(3*RS*)-[3-$^2H_1$]glycerol **44d** (0.5 mmol) and 2-bromoethylphosphonic acid **10a** (0.6 mmol) are submitted to the above procedure. The amination is performed directly on the residue.

1,2-Di-*O*-hexadecyl-*sn*-glycero-3-(2-aminoethyl)phosphonate **46a**

In a pressure bottle, the residue of 1,2-Di-*O*-hexadecyl-*sn*-glycero-3-(2-bromoethyl)phosphonate **45a** from the previous reaction is dissolved in chloroform (5 ml) at 50°C. 30% Ammonia (5 ml) is added, followed by just enough 2-propanol to obtain a single phase. The mixture is allowed to react at 50°C for 2–3 days, when TLC (chloroform–methanol–30% ammonia 65:30:5) shows no improvement in the course of the reaction. The solvents are evaporated under vacuum. The residue is taken in $CHCl_3$, washed three times with 20% aqueous methanol, dried with sodium sulfate and evaporated to dryness. The product is purified by chromatography on silica gel using for elution the solvent mixtures chloroform–methanol–30% ammonia 100:10:1, 100:15:1, 100:20:1 and 100:30:1. The fractions containing the pure compound are pooled and the solvent evaporated to dryness. Yield: 50–54% (2 steps). M. p.: lit. 159–161°C (23).

1,2-Di-*O*-hexadecyl-*sn*-glycero-3-(2-amino[1,1,2,2-$^2H_4$]ethyl)phosphonate **46b**

The headgroup-deuterated compound 1,2-di-*O*-hexadecyl-*sn*-glycero-3-(2-bromo[1,1,2,2-$^2H_4$]ethyl)phosphonate **45b** is submitted to the same procedure. Yield: 41–53% (2 steps).

1,2-Di-*O*-hexadecyl-*sn*-[2-$^2H_1$]glycero-3-(2-aminoethyl)phosphonate **46c**

Similarly, the above procedure is used again with 1,2-di-*O*-hexadecyl-*sn*-[2-$^2H_1$]glycero-3-(2-bromoethyl)phosphonate **45c** is submitted to the above. Yield: 29% (2 steps).

1,2-Di-*O*-hexadecyl-*sn*-[1,1-$^2H_2$]glycero-3-(2-aminoethyl)phosphonate **46d**

The same procedure is also used with 1,2-di-*O*-hexadecyl-*sn*-[1,1-$^2H_2$]glycero-3-(2-bromoethyl)phosphonate **45d**. Yield: 26% (2 steps).

1,2-Di-*O*-hexadecyl-*sn*-(*3RS*)-[3-$^2H_1$]glycero-3-(2-aminoethyl)phosphonate **46e**

The procedure described above is used with 1,2-di-*O*-hexadecyl-*sn*-(*3RS*)-[3-$^2H_1$]glycero-3-(2-bromoethyl)phosphonate **45e**. Yield: 28–47% (2 steps).

5.4 References

1. H. Berger, P. Jones and D.J. Hanahan, *Biochem. Biophys. Acta* **260**, 617–629 (1972).

2. H. Eibl, *Proc. Natl. Acad. Sci. USA* **75**, 4074–4077 (1978).

3. H. Eibl and A. Nicksch, *Chem. Phys. Lipids* **22**, 1–8 (1978).

4. P. Woolley and H. Eibl, *Chem. Phys. Lipids* **47**, 55–62 (1988).

5. G.K. Chacko and D.J. Hanahan, *Biochim. Biophys. Acta* **164**, 252–271 (1968).

6. F.J.M. Daemen, G.H. De Haas and L.L.M. Van Deenen, *Rec. Trav. Chim.* **82**, 487–496 (1963).

7. H. Eibl, J.O. McIntyre, E.A.M. Fleer and S. Fleischer, *Methods Enzymol.* **98**, 623–632 (1983).

8. H. Eibl, *Angew. Chem. Int. Ed. Engl.* **23**, 257–271 (1984).

9. L. Moroder, A. Hallett, E. Wünsch, O. Keller and G. Wersin, *Hoppe-Seyler's Z. Physiol. Chem.* **257**, 1651–1653 (1976).

10. R. Hirt and R. Berchtold, *Helv. Chim. Acta* **40**, 1928–1932 (1957).

11. W. Diembeck and H. Eibl, *Chem. Phys. Lipids* **24**, 237–244 (1979).

12. A. Weissback and D.B. Sprinson, *J. Biol. Chem.* **203**, 1031–1037 (1953).

13. D.E. Douglas and A.M. Burditt, *Can. J. Chem.* **33**, 1183–1184 (1955).

14. M.G. Taylor and I.C.P. Smith, *Chem. Phys. Lipids* **28**, 119–136 (1981).

15. J. Finkelstein, *J. Amer. Chem. Soc.* **68**, 2397–2398 (1946).

16. G.M. Kosolapoff, *J. Amer. Chem. Soc.* **69**, 2112–2113 (1947).

17. A.F. Rosenthal and M. Pousada, *Rec. Trav. Chim.* **84**, 833–839 (1965).

18. W. Gerrard, W.J. Green and R.A. Nutkins, *J. Chem. Soc.* 1952. 4076–4078.

19. G.M. Kosolapoff, *J. Amer. Chem. Soc.* **70**, 1971–1972 (1948).

20. E. Baer and N.Z. Stanacev, *J. Amer. Chem. Soc.* **87**, 679–680 (1965).

21. E. Baer and N.Z. Stanacev, *J. Biol. Chem.* **240**, 3754–3759 (1965).

22. E. Baer and N.Z. Stanacev, *J. Biol. Chem.* **239**, 3209–3214 (1964).

23. E. Baer and N.Z. Stanacev, *J. Biol. Chem.* **240**, 44–48 (1965).

24. E. Baer and G. Raghypati Sarma, *Can. J. Biochem.* **43**, 1353–1357 (1965).

25. E. Baer and K.V. Jagannadha Rao, *Can. J. Biochem.* **45**, 317–325 (1967).

26. C.A. Dekker and H.G. Khorana, *J. Amer. Chem. Soc.* **76**, 3522–3527 (1954).

27. M. Smith, J.G. Moffatt and H.G. Khorana, *J. Amer. Chem. Soc.* **80**, 6204–6212 (1958).

28. B. Neises and W. Steglich, *Angew. Chem. Int. Ed. Engl.* **17**, 522–524 (1978).

29. A. Hassner and V. Alexanian, *Tet. Lett.* **46**, 4475–4478 (1978).

30. A.P. Tulloch, *Lipids* **12**, 92–98 (1977).

31. E. Baer and H.O.L. Fischer, *J. Biol. Chem.* **140**, 397–410 (1941).

32. W.J. Baumann and H.K. Mangold, *J. Org. Chem.* **29**, 3055–3057 (1964).

33. H. Eibl, *Ger. Offen.* DE 3130867 (Cl. C07C43/164), 21 pp. (1983).

34. H. Eibl, *Ger Offen.* DE 3239858 (Cl. C07C43/02), 52 pp. (1984).

35. H. Eibl and P. Woolley, *Chem. Phys. Lipids* **47**, 47–53 (1988).

36. R.K. Crossland and K.L. Servis, *J. Org. Chem.* 35, 3195–3196 (1970).

37. E. Baer and H.O.L. Fischer, *J. Biol. Chem.* **128**, 463–473 (1939).

38. C.M. Lok, J.P. Ward and D.A. van Dorp, *Chem. Phys. Lipids* **16**, 115–122 (1976).

39. S. Tanako, H Numata and K. Ogasawara, *Heterocycles* **19**, 327–328 (1982).

40. M.L. Wolfrom and A. Thompson, in *Methods in Carbohydrate Chemistry*, Vol. II, edited by R.L. Whistler and M.L. Wolfrom (Academic Press, New York, New York, 1963), pp. 65–68.

41. H.L. Frush and H.S. Isbell, *J. Amer. Chem. Soc.* **78**, 2844–2846 (1956).

42. W.N. Haworth, D. Heslop, E. Salt and F. Smith, *J. Chem. Soc.* **1944**, 217–224.

43. R.P. Linstead, L.N. Owen and R.F. Webb, *J. Chem. Soc.* **1953**, 1225–1231.

44. H. Eibl, *Chem. Phys. Lipids* **28**, 1–5 (1981).

45. J. LeCocq and C.E. Ballou, *Biochemistry* **3**, 976–980 (1964).

46. E. Baer and H.O.L. Fischer, *J. Biol. Chem.* **128**, 475–489 (1939).

47. E. Baer and H.O.L. Fischer, *J. Amer. Chem. Soc.* **67**, 2031–2037 (1945).

48. R.L. Baylis, T.H. Bevan and T. Malkin, *J. Chem. Soc.* **1958**, 2962–2968.

49. T.H. Bevan and T. Malkin, *J. Chem. Soc.* **1960**, 350–353.

50. S.K. Chaudhary and O. Hernandez, *Tet. Lett.* **2**, 95–98 (1979).

51. E. Fischer, *Ber.* **28**, 1167–1170 (1895).

52. L.F. Wiggins, *J. Chem. Soc.* **1946**, 13–14.

53. J. Kuszmann and E. Tomori, *Carbohydr. Res.* **137**, 276–281 (1985).

54. H.O.L. Fischer and H. Appel, *Helv. Chim. Acta* **17**, 1574–1582 (1934).

55. T. Horváth and L. Vargha, *Carbohydr. Res.* **16**, 253–259 (1971).

56. D.A. Mannock, R.N.A.H. Lewis and R.N. McElhaney, *Chem. Phys. Lipids* **43**, 113–127 (1987).

57. M.D. Matteucci and M.H. Caruthers, *Tet. Lett.* **21**, 3243–3246 (1980).

58. A. Hermetter and F. Paltauf, *Chem. Phys. Lipids* **29**, 191–195 (1981).

59. J.E. Christensen and L. Goodman, *Carbohydr. Res.* **7**, 510–512 (1968).

60. R. Wohlgemuth, N. Waespe-Sarcevic and J. Seelig, *Biochemistry* **19**, 3315–3321 (1980).

61. *CRC Handbook of Chemistry and Physics*, 56th Edition, edited by R.C. Weast (CRC Press, Cleveland, Ohio, 1974).

62. H. Wagner, L. Hörhammer and P. Wolff, *Biochem. Z.* **334**, 175–184 (1961).

63. J.C. Dittmer and R.L. Lester, *J. Lipid Res.* **5**, 126–127 (1964).

64. V.E. Vaskovsky and E.Y. Kostetsky, *J. Lipid Res.* **9**, 396 (1968).

65. G. Zweig and J. Sherma, *CRC Handbook of Chromatography, General*, Vol. II (CRC Press, Boca Raton, Florida, 1972), p. 143.

66. *1988–1989 Catalog Handbook of Fine Chemicals* (Aldrich Chemical Company, Milwaukee, Wisconsin, 1988).

67. *The Merck Index*, Eleventh Edition (Merck & Co., Rahway, New Jersey, 1989).

68. T.O. Soine and M.R. Buchdahl, *Org. Syntheses Coll. Vol.* IV, 106–108 (1963).

69. W.J. Baumann and H.K. Mangold, *J. Org. Chem.* **31**, 498–500 (1966).

70. H.F.G. Beving, H.B. Borén and P.J. Garegg, *Acta Chem. Scand.* **21**, 2083–2086 (1967).

71. M. Kates, T.H. Chan and N.Z. Stanacev, *Biochemistry* **2**, 394–397 (1963).

72. P. Michelsen and B. Herslöf, *Chem. Phys. Lipids* **32**, 27–37 (1983).

CHAPTER 6

^{31}P AND ^{2}H SOLID-STATE NUCLEAR MAGNETIC RESONANCE STUDIES OF THE HEADGROUP CONFORMATION OF A SYNTHETIC PHOSPHONOLIPID

6.1 Introduction

Solid-state ^{31}P and ^{2}H nuclear magnetic resonance (NMR) are powerful tools for elucidating the structure and conformation of phosphorus-containing lipid headgroups in model membranes. They also have the advantage of measuring segmental fluctuations quantitatively in terms of order parameters.

In this study, the ^{31}P NMR chemical shielding anisotropy and the ^{2}H NMR quadrupolar splittings were measured as a function of temperature for the specifically headgroup-deuterated phosphonolipid 1,2-di-*O*-hexadecyl-*sn*-glycero-3-(2-aminoethyl)phosphonate dispersed in excess buffer. Then, by analogy with similar studies on different classes of lipids (1–3), possible headgroup conformations were determined in the liquid crystalline and hexagonal phases. A simple model for headgroup reorientation, which involves rapid transitions between two enantiomeric conformations of the headgroup and free rotation about the glycerol C2–C3 bond direction, was used to calculate possible torsion angles. Finally, a comparison is made with the previously determined headgroup conformations of analogous phospholipids.

6.2 Experimental part

6.2.1 Lipid dispersions

To prepare samples for NMR experiments, the synthetic lipids were first purified either by preparative thin-layer chromatography (TLC) on 0.25-mm silica gel 60 plates (E. Merck, Darmstadt) or with the use of a model 7924T Chromatotron (Harrison Research, Palo Alto, California). The system chloroform–methanol–30% ammonia was used for developing TLC plates, the band corresponding to the desired compound scraped off the plates and the lipid eluted with $CHCl_3-CH_3OH$ 1:1. With the Chromatotron, chloroform–methanol–30% ammonia 100:10:1 was used as a solvent system, 2-ml fractions were collected and those that contain the pure compound pooled. After evaporating the solvent with a stream of nitrogen gas, the sample was dried under high vacuum for several hours. The lipid (30–50 mg) was then dispersed in water. This requires several cycles of freezing, thawing and vortexing, and heating above the gel-to-liquid crystal phase transition temperature, cooling and vortexing. The sample was lyophilized and redispersed as above in buffer (25 mM Tris-acetate, 2 mM EDTA, *p*H 7.15). Deuterium-depleted water (Aldrich Chemical Company, Milwaukee, Wisconsin) was used for ^2H NMR. The lipid dispersion is finally transferred to an NMR tube which is sealed with epoxy glue.

6.2.2 Differential scanning calorimetry

Differential scanning calorimetric measurements were performed on 1.2 mg of the nondeuterated lipid dispersed in 1.5 ml of buffer using a Microcal MC-1 differential scanning calorimeter, with a temperature scanning rate of 1°C/min. The temperature scale was calibrated with the gel-to-liquid crystal transition temperature of dipalmitoylphosphatidylcholine (DPPC).

6.2.3 NMR measurements

^{31}P NMR spectra (121.5 MHz) were recorded on a Bruker MSL-300 spectrometer using a home-built probe equipped with a 3.2-mm solenoid coil. A spin echo sequence with full phase cycling was used (4). The ^{31}P $\pi/2$ pulse width was 1.8–2.0 μs. High-power proton decoupling (16 μs ^{1}H $\pi/2$ pulse corresponding to a B_2 field of $3.7 \cdot 10^{-4}$ T) was applied during the pulse sequence and the acquisition period and gated off during the recycling delay. To obtain the powder lipid spectrum, a spectral width of 100 kHz, a recycling time of 20 s, 72 and 144° pulses, and an interpulse spacing of 50 μs were used. For the dispersed lipid, the spectral width was 50 kHz and the recycling time 10 s, the echo used 90 and 180° pulses and the interpulse spacing was 80 μs. In each case, the number of points was 4096. The temperature was regulated to ±1°C by circulating air at the desired temperature around the sample. Chemical shifts are reported in ppm relative to an external reference of 85% H_3PO_4, assuming positive values for resonances at high frequencies.

^{2}H NMR spectra were recorded on a 200-MHz home-built spectrometer operating at 30.7 MHz, using the quadrupolar echo sequence (5). The $\pi/2$ pulse was 2.3–2.4 μs in length (5-mm solenoid coil), and an echo pulse spacing of 60 μs was used. The number of points was 2048. The pulse sequence was repeated every 250 ms for the headgroup-deuterated lipid and every 100 ms for the glycerol-labelled compound. The spectra were acquired by using a spectral width of ±50 and ±100 kHz respectively for the same two compounds. Longitudinal relaxation times T_1 were measured by the inversion-recovery procedure in combination with the quadrupolar echo sequence as described by Perly *et al.* (6). The temperature was regulated electronically to ±0.5°C with a custom-built variable-temperature unit.

Spectra were analyzed on a Nicolet 1180E data processor. The free induction decays were left shifted to the top of the echo before Fourier transformation of the trailing edge. ^{2}H NMR spectra taken above the gel-to-liquid crystal transition temperature were "de-Paked" by the method of Bloom *et al.* (7) to give the 90° oriented sample spectra, from which the quadrupolar splittings were obtained.

6.3 Results

6.3.1 Differential scanning calorimetry

Several studies have demonstrated that ethanolamine lipids can exhibit polymorphic phase behavior in addition to a gel-to-liquid phase transition (8). In order to facilitate the interpretation of ^{31}P and ^{2}H NMR data, the thermal behavior of 1,2-di-*O*-hexadecyl-*sn*-glycero-3-(2-aminoethyl)phosphonate was examined. Differential scanning calorimetry (DSC) thermograms exhibited two endothermic transitions. Jarrell *et al.* (9) have reported a temperature of 63°C for the gel-to-liquid crystal phase transition of 1,2-dipalmitoyl-*sn*-glycero-3-(2-aminoethyl)phosphonate, close to the value of 63.7°C for its phosphate analog 1,2-dipalmitoylphosphatidylethanolamine (DPPE) (10). Apparently, whether the headgroup is a phosphonate or a phosphate does not significantly affect the temperature at which the chains melt. Thus, a temperature close to that of 69.1°C reported for 1,2-di-*O*-hexadecylphosphatidylethanolamine should be expected for the analogous phosphonate. The main transition for 1,2-di-*O*-hexadecyl-*sn*-glycero-3-(2-aminoethyl)phosphonate was centered at 70.2°C. A secondary endothermic transition occurs at 84.5°C. This figure is close to the reported value of 88°C for 1,2-di-*O*-hexadecylphosphatidylethanolamine (DHPE) attributed to the lamellar-to-

hexagonal phase transition (10). The DSC data for 1,2-dipalmitoyl- and 1,2-di-*O*-hexadecyl-*sn*-glycero-3-(2-aminoethyl)phosphonate thus follow the same trend as that for phospholipids, where the temperature of the lamellar-to-hexagonal phase transition was found to increase in the order 1,2-dialkyl < 1-alkyl-2-acyl << 1,2-diacyl, while the temperature of the gel-to-liquid crystal phase transition increased in the reverse order (10).

6.3.2 ^{31}P NMR

Figure 6–1 presents the ^{31}P NMR spectrum of 1,2-di-*O*-hexadecyl-*sn*-glycero-3-(2-aminoethyl)phosphonate in the powder form. From this spectrum, the principal elements of the chemical shielding tensor are found to be: $\sigma_{11} = -94$, $\sigma_{22} = -27$ and $\sigma_{33} = 61$ ppm, in accordance with the reported values of $\sigma_{11} = -85$, $\sigma_{22} = -27$ and $\sigma_{33} = 65$ ppm for the dipalmitoyl analog (9).

The ^{31}P NMR spectra of lipid dispersions (Figure 6–2) show lineshapes characteristic of an effective axially symmetric tensor. The absolute value of the chemical shift anisotropy $|\Delta\sigma|$ slightly decreases from the gel to the liquid crystalline phase (Figure 6–3). At 85.6°C, where the lipid is known to adopt the hexagonal phase, the sign of $\Delta\sigma$ is reversed and its magnitude reduced by a factor of approximately two.

6.3.3 ^{2}H NMR

Figures 6–4 and 6–5 illustrate ^{2}H NMR spectra of aqueous dispersions of the phosphonolipid 1,2-di-*O*-hexadecyl-*sn*-glycero-3-(2-aminoethyl)phosphonate labelled at both headgroup positions and at the position *sn*-3 of the glycerol moiety respectively. Contrary to the chemical shift anisotropy on the phosphorus spectra, the quadrupolar splittings on the deuterium spectra could not be measured below

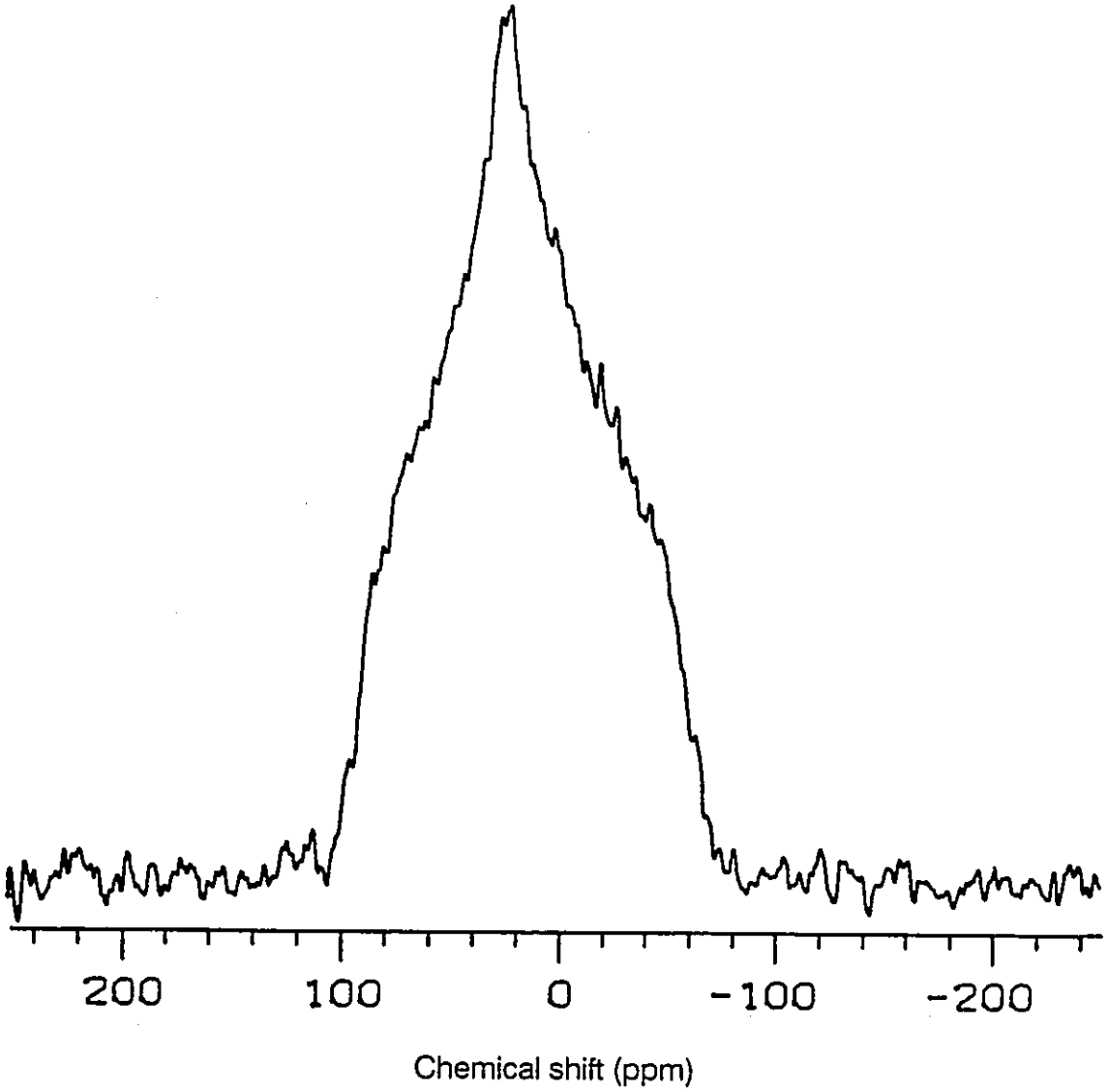

Figure 6–1. ^{31}P NMR spectrum (121.5 MHz) of a 1,2-di-*O*-hexadecyl-*sn*-glycero-3-(2-aminoethyl)phosphonate powder sample at room temperature (22°C), 8000 accumulations.

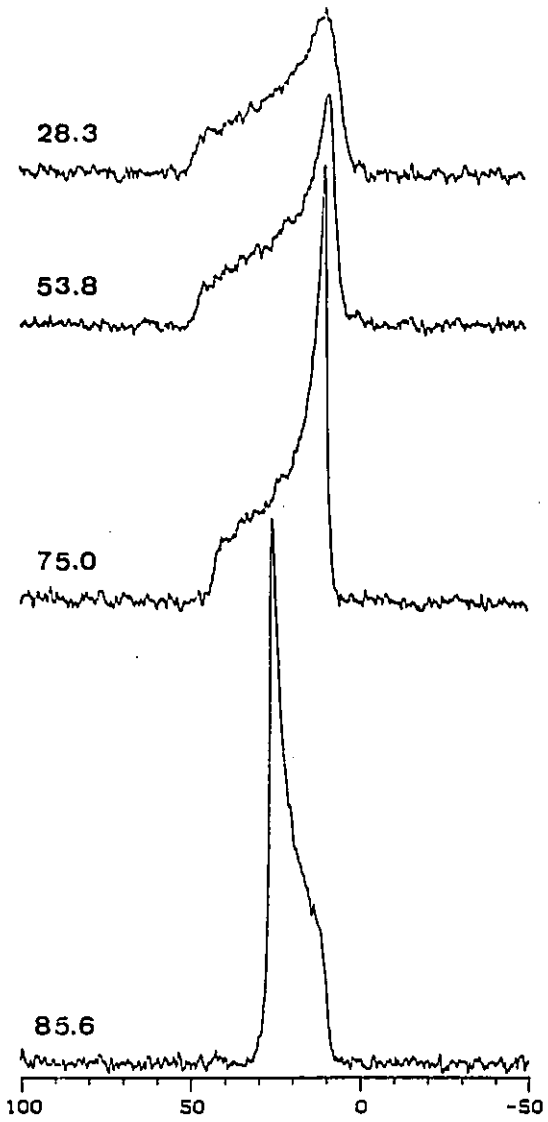

Figure 6–2. ^{31}P NMR spectra (121.5 MHz) of aqueous dispersions of 1,2-di-*O*-hexadecyl-*sn*-glycero-3-(2-aminoethyl)phosphonate at the indicated temperature, 640 accumulations.

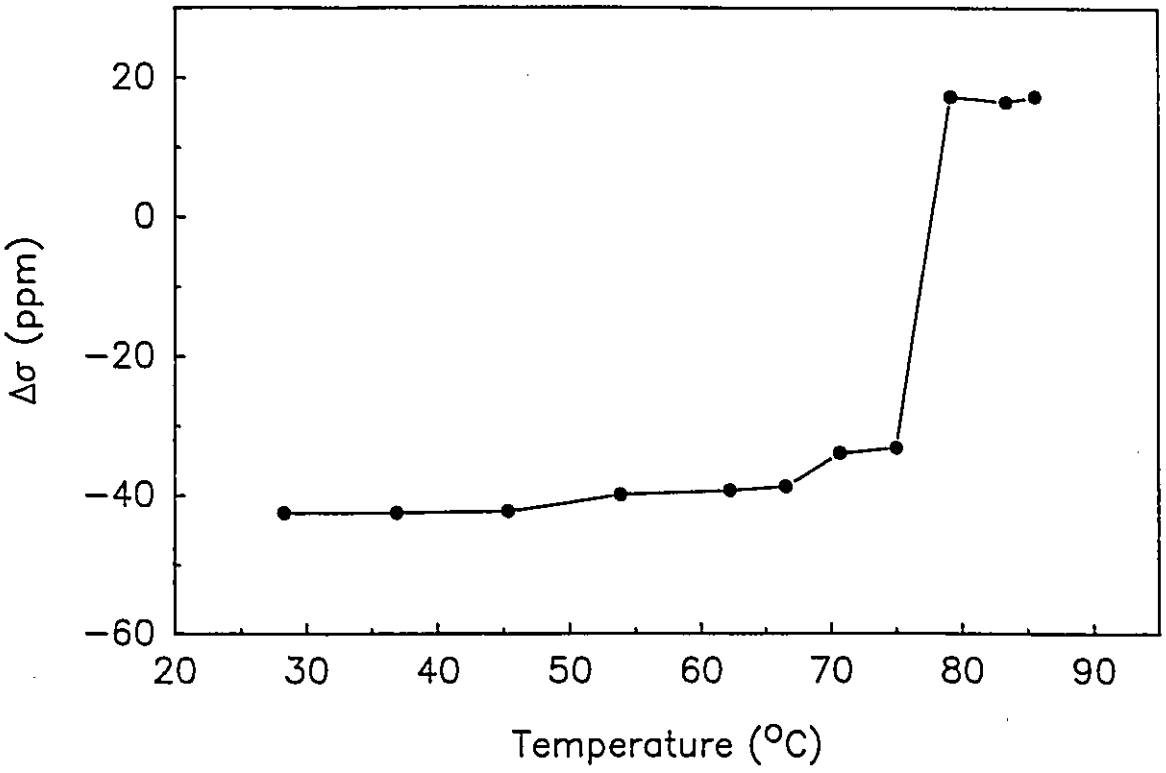

Figure 6–3. Temperature dependence of the ^{31}P NMR chemical shift anisotropy ($\Delta\sigma$) for dispersions of 1,2-di-*O*-hexadecyl-*sn*-glycero-3-(2-aminoethyl)phosphonate in excess buffer.

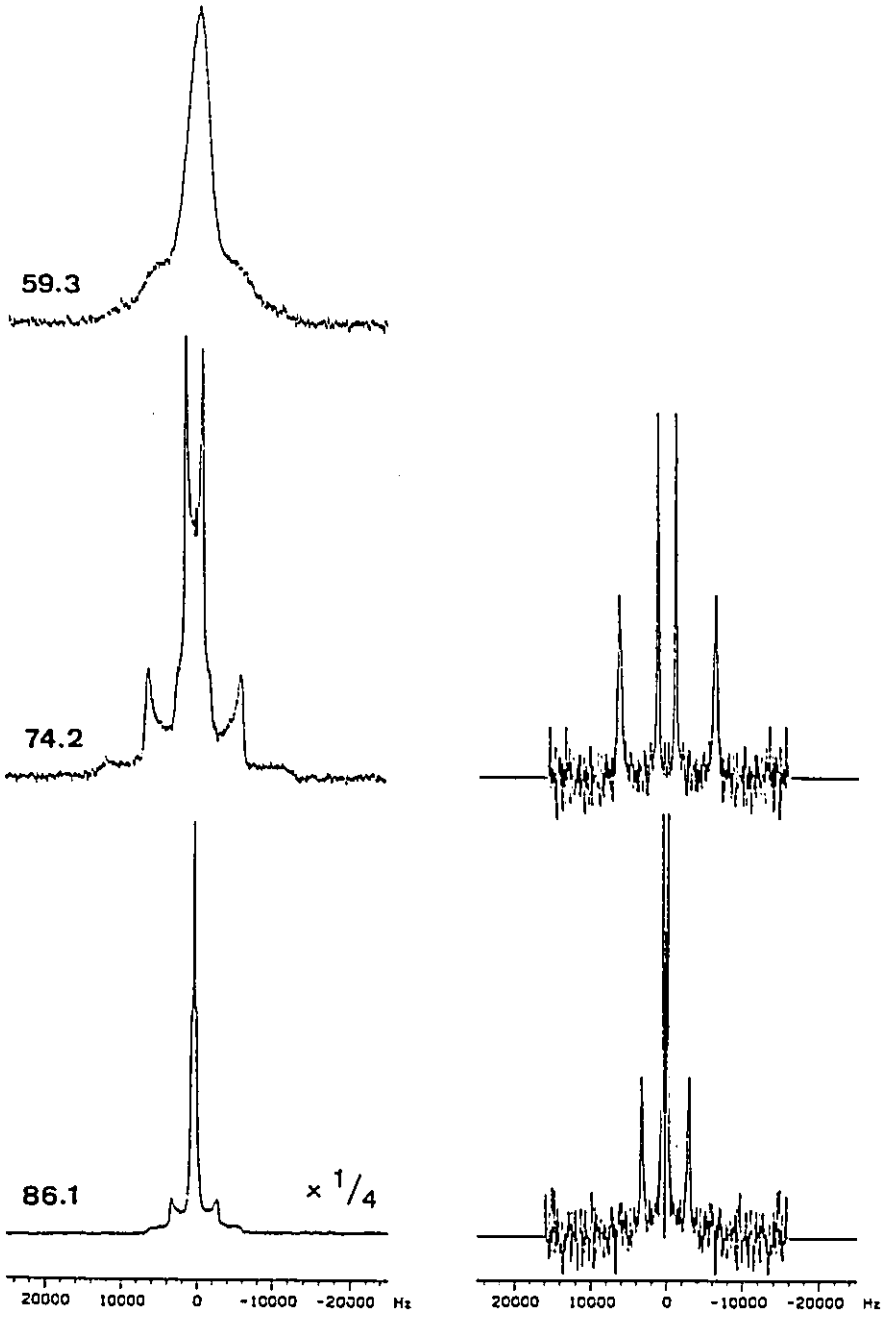

Figure 6–4. ^{2}H NMR spectra (30.7 MHz) of 1,2-di-*O*-hexadecyl-*sn*-glycero-3-(2-amino[1,1,2,2–$^{2}H_4$]ethyl)phosphonate dispersed in excess buffer at the indicated temperature. 20000 accumulations. The spectra on the right correspond to the "de-Paked" version of those on the left for the liquid crystalline and hexagonal phases.

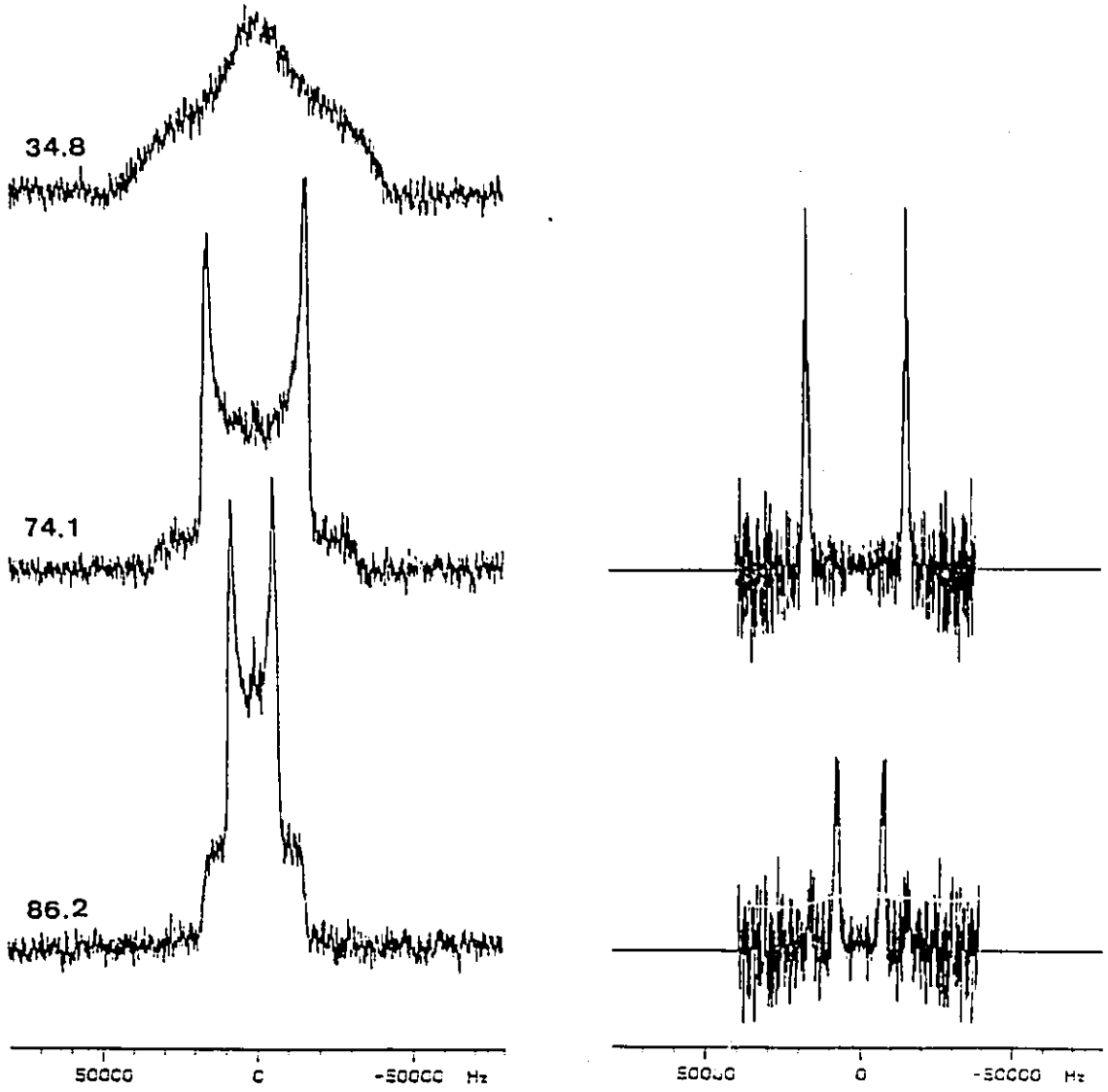

Figure 6–5. ^{2}H NMR spectra (30.7 MHz) of 1,2-di-*O*-hexadecyl-*sn*-[3–^{2}H]glycero-3-(2-aminoethyl)phosphonate dispersed in excess buffer at the indicated temperature, 96000 accumulations. For temperatures above the lamellar-to-hexagonal phase transition, the "de-Paked" spectra are shown on the right.

the gel-to-liquid crystal transition temperature. Below the main transition temperature, the spectra are broad and relatively featureless and are reminiscent of the type of spectra observed for the acyl chains of lipid in the gel state (11, 12). This type of spectrum arises when motions occur with an intermediate rate and/or a low symmetry. Due to similarity to powder spectra observed when the quadrupole splitting tensor is not axially symmetric, this is known as an $\eta = 1$ lineshape (13). Above the main transition temperature, the spectra are axially symmetric, reflecting the onset of rapid axially symmetric motion and the transition from gel to liquid crystal phase. The quadrupolar splittings slowly decrease with temperature in this phase, and then, while still retaining their axially symmetric shape, are reduced to less than one half their value in the hexagonal phase (Figure 6–6).

By analogy to previous studies on ethanolamine lipids, the large splitting in Figure 6–4 is attributed to the deuterium atoms at position 1 of the headgroup and the small splitting to those at position 2. This choice is logical since it is expected that the amplitude of the motions would be larger farther away from the glycerol moiety, and thus the segmental order parameter S would be smaller. Since both positions are C^2H_2 groups, the geometrical parameter and the quadrupolar coupling constant is the same for both and thus the quadrupolar splitting is directly proportional to S.

Table 6–1 reports ^2H NMR spin-lattice relaxation time T_1 data for the three positions in both types of phases. The data shows that the rate of motions increases on going from the glycerol C3 position to a higher position in the headgroup, since T_1 values become larger. In the hexagonal phase, the headgroup motion appears more restricted than in the bilayer phase, as reflected by a smaller relaxation time, although the differences are relatively small.

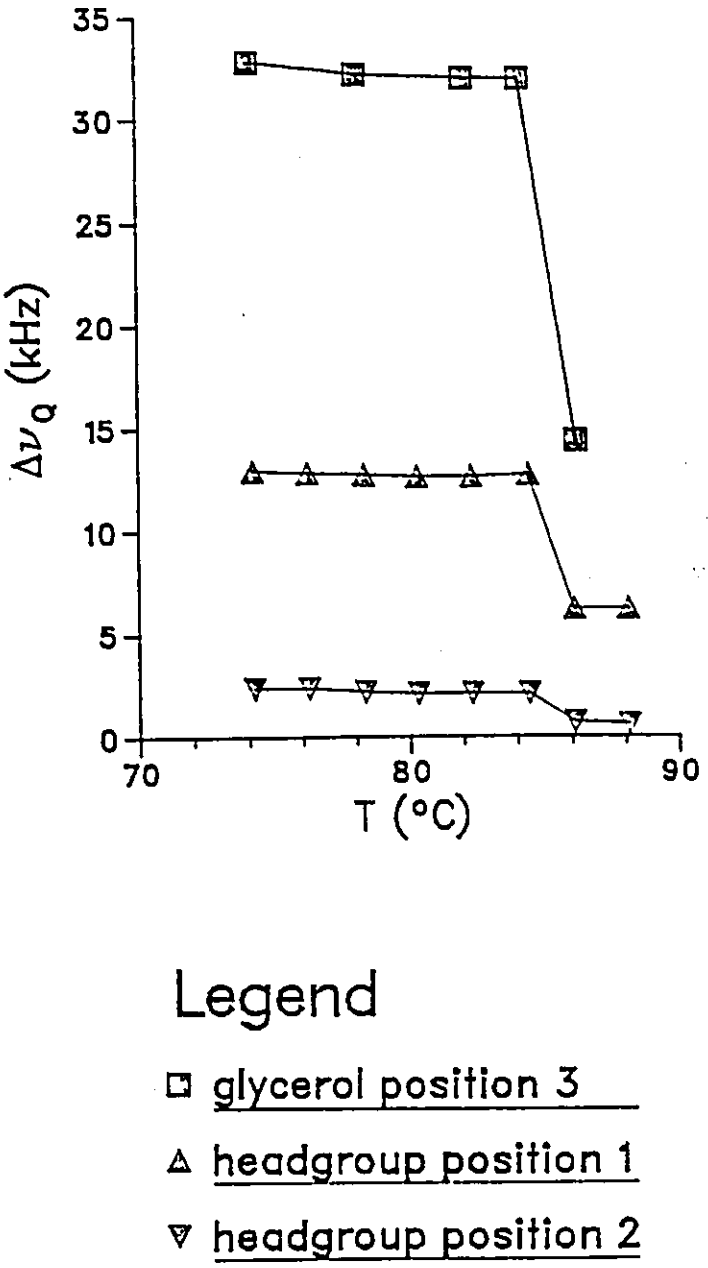

Figure 6–6. Temperature dependence of the ^2H NMR quadrupolar splittings ($\Delta\nu_Q$) for the three different labelled positions of 1,2-di-*O*-hexadecyl-*sn*-glycero-3-(2-aminoethyl)phosphonate in aqueous dispersions above the bilayer-to-hexagonal phase transition temperature.

Table 6-1. ^2H NMR longitudinal relaxation times T_1 data for 1,2-di-*O*-hexadecyl-*sn*-glycero-3-(2-aminoethyl)phosphonate labelled in different positions of the headgroup and the glycerol moiety in the liquid crystalline and hexagonal phases.

Temperature (°C)	Glycerol	Headgroup	
	3	1	2
74	15.2[a]	25.3	42.2
86	14.8	25.0	40.8

[a] T_1 values in ms for the 90° orientation only.

6.3.4 Computational methods

From the ^{31}P NMR spectrum of the powder lipid, the principal values of the chemical shielding tensor for the phosphonolipid could be obtained. The complete ^{31}P NMR chemical shift tensor (the principal values as well as the orientation) of the model compound 2-aminoethylphosphonic acid has been determined previously (see Chapter 4 and Reference 14). It is believed that the orientation of this tensor could be used for phosphonolipids, given that the orientation of the tensor for 2-aminoethanol phosphate was suitable for phospholipids. In the liquid crystalline state, the static ^{31}P NMR shielding tensor is averaged by the headgroup motion and is replaced by an effective tensor which is axially symmetric with respect to the bilayer normal.

Exact axial symmetry is assumed for the ^{2}H NMR quadrupolar coupling tensor, the axis of symmetry being along the C$-^{2}$H bond direction. For that reason, the tensor was replaced by a simple vector in the transformation calculations.

A simple model of headgroup reorientation allowing free rotation about the C2$-$C3 bond of the glycerol is assumed to calculate the headgroup conformation. This bond is approximately parallel to the bilayer normal in crystals of 1,2-dilaurylphosphatidylethanolamine (DLPE) (15, 16). From the ^{2}H NMR quadrupolar splitting for the *sn*-3 glycerol position, it is possible to determine the order parameters of this segment of the glycerol backbone. The order parameter $S_{C-^{2}H}$ of the C3$-^{2}$H bond vector is related to the quadrupolar splitting of the powder-type spectrum according to

$$\Delta\nu_Q(90°) = {}^{3}/_{4}(e^2qQ/4\pi\epsilon_0 h)S_{C-^{2}H}. \qquad [6\text{–}1]$$

At 74.1°C, in the liquid crystalline phase, the quadrupolar splitting is equal to 32.8 kHz, while it is 14.4 kHz in the hexagonal phase at 86.2°C. With a static quadrupolar coupling constant $e^2qQ/4\pi\epsilon_0 h$ of 170 kHz, it follows that $|S_{C-^2H}|$ is equal to 0.257 at 74.1°C and 0.113 at 86.2°C. Assuming exact tetrahedral symmetry, the order parameter of this axis S_{C2-C3}, is given by

$$S_{C2-C3} = S_{C-^2H}/[(3\cos^2 109.5° - 1)/2], \qquad [6\text{–}2]$$

yielding S_{C2-C3} equal to 0.772 and 0.678 for the liquid crystalline and hexagonal phases respectively.

The determination of possible headgroup conformations involves a comparison between the experimental and calculated NMR spectral parameters, *i.e.* the ^{31}P NMR chemical shift anisotropy and the ^2H NMR quadrupolar splittings for the 1 and 2 positions of the headgroup. The respective static tensors are transformed from their principal coordinate systems through intervening bonds into the coordinate system of the glycerol C2–C3 bond, where they are averaged. The result is multiplied by the order parameter for this bond, S_{C2-C3}, to account for the wobbling motion of the segment. The transformations were done by vector and matrix multiplication with a chain-segment transformation matrix,

$$\begin{bmatrix} \cos\alpha & \cos\theta\cos\alpha & \sin\theta\sin\alpha \\ -\sin\alpha & -\cos\theta\cos\alpha & -\sin\theta\cos\alpha \\ 0 & \sin\theta & -\cos\theta \end{bmatrix}$$

the elements of which are functions of the bond (θ) and torsion (α) angles (3).

In order to account quantitatively for the equivalence of the two deuterium atoms at position 1 and the two deuterium atoms at position 2 of the

headgroup, it was assumed that a rapid equilibrium exists between two enantiomeric conformations, one with all torsion angles α_i positive, the other with all torsion angles α_i negative.

A search was performed with $\pm 1°$ increments and 60° torsion angle ranges. Values of α_1 and α_2 that satisfy the chemical shift anisotropy conditions were determined. Similarly, values of α_1, α_2 and α_3 that give the correct quadrupolar splitting for the deuterium atoms at position 1 of the headgroup were kept as possible solutions. Finally, the quadrupolar splittings of the deuterium atoms at position 2 of the headgroup were used to find possible values for α_1, α_2, α_3 and α_4. Table 6–2 summarizes the parameters used for the simulations.

6.3.5 Conformational solutions

Each possible conformational solution found by the search is represented by a dot in Figure 6–7 for the lamellar and hexagonal phases. The results show that the conformations of the headgroup are very similar in both phases. The number of solutions is bigger at 86°C because the magnitudes of the NMR spectral parameters are smaller while the error on it remains constant.

The solutions for α_1 and α_2 are very similar to those found previously for DPPE (3), *i.e.* α_1 is approximately *trans* and α_2 is almost freely variable over the $\pm 30°$ range. This can be explained by the fact that the α_2 axis lies nearly parallel to the bilayer normal in this quasi-conformation. The conformations of the phosphonolipid in the lamellar phase obtained in this manner are very similar to those of DPPE in the same conditions (3). Thus similar conformations for phospho- and phosphonolipid headgroups result in a smaller chemical shift anisotropy for the latter, the value for DPPE in the lamellar phase being 41 ppm (1).

Figure 6–7. Conformational solutions for the headgroup of 1,2-di-*O*-hexadecyl-*sn*-glycero-3-(2-aminoethyl)phosphonate in the lamellar phase at 74°C (left) and in the hexagonal phase at 86°C (right). The torsion angles α_i are given in degrees (°).

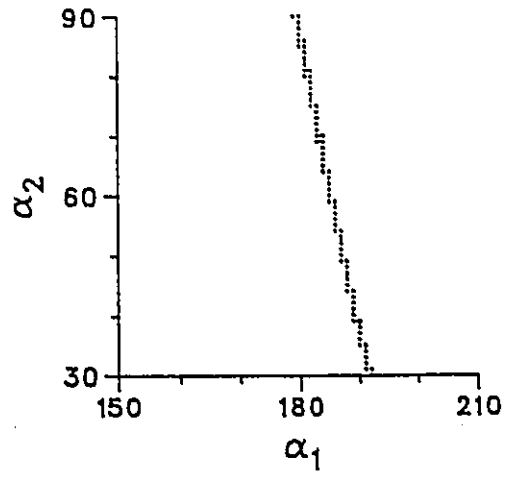
90
60
30
150
180
210
α_2
α_1

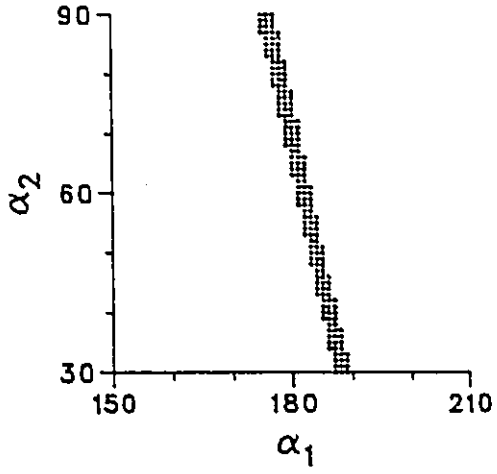
90
60
30
150
180
210
α_2
α_1

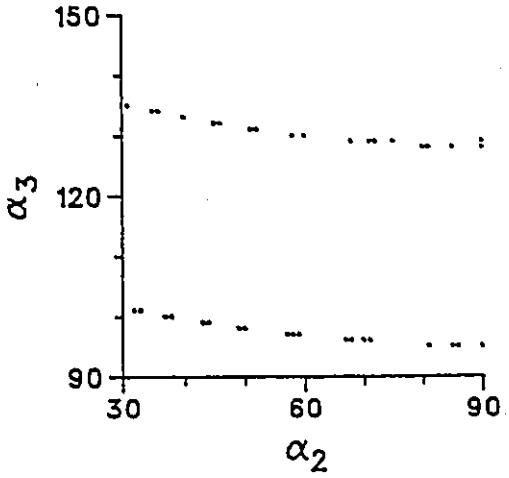
150
120
90
30
60
90
α_3
α_2

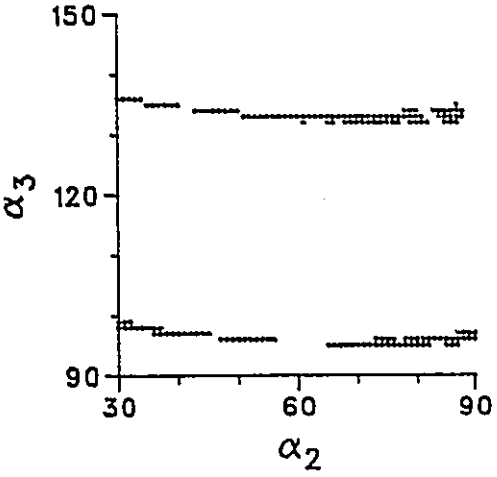
150
120
90
30
60
90
α_3
α_2

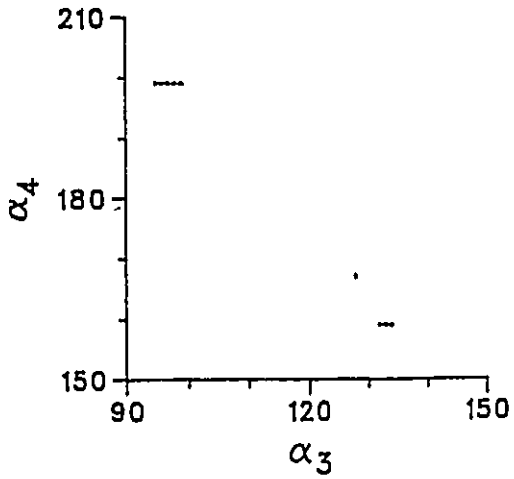
210
180
150
90
120
150
α_4
α_3

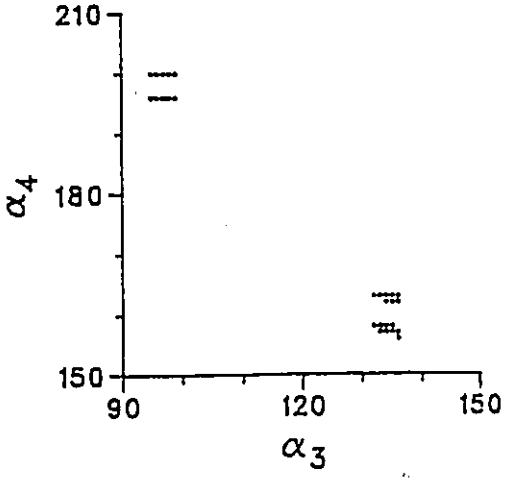
210
180
150
90
120
150
α_4
α_3

Table 6–2. Input data for the determination of possible headgroup conformations of 1,2-di-*O*-hexadecyl-*sn*-glycero-3-(2-aminoethyl)phosphonate dispersed in excess buffer in the liquid crystalline and hexagonal phases by simulation of the ^{31}P NMR chemical shift anisotropy $\Delta\sigma$ and the ^{2}H NMR quadrupolar splittings $\Delta\nu_Q$.

^{31}P NMR data	
$\Delta\sigma$ (± 1.0 ppm)	temperature (°C)
−34.0	70.7
17.3	85.6

^{2}H NMR data		
$\Delta\nu_Q$ (± 0.1 kHz)		temperature (°C)
position 1	position 2	
12.9	2.4	74.2
6.2	0.7	86.1

x-ray diffraction data		
bond angle		value (°)
θ_0	C – C – O	103
θ_1	C – O – P	114
θ_2	O – P – C	105
θ_3	P – C – C	112
θ_4	C – C – N	112

torsion angle ranges investigated		
torsion angle		range (°)
α_0	C – C – C – O	free rotation
α_1	C – C – O – P	150 – 210
α_2	C – O – P – C	30 – 90
α_3	O – P – C – C	30 – 90
		90 – 150
α_4	P – C – C – N	150 – 210

In DPPE, the phosphodiester moiety adopts a gauche-gauche conformation (15, 16, 1, 3). In the case of the phosphonolipid, no solutions were found when α_3 was allowed to vary between 30 and 90°. Two solutions were found however, one around 100° and the other close to 135°. The conformation here is thus different than that of the phospholipid.

For α_4, the search was done for 180 ± 30° because this torsion angle is nearly *trans* in crystals of AEP (17), and a few solutions have been found in this range. The corresponding torsion angle in DPPE, α_5, O–C–C–N, was gauche.

Although the torsion angles are different for phospho– and phosphonolipids, the overall picture is similar, *i.e.* the molecule is bent at the phosphorus atom and the headgroup lies more or less flat at the membrane surface, as shown in Figure 6–8.

6.4 Conclusion

The aim of this study was to determine if the headgroups of phospho– and phosphonolipids adopt different conformations in model membranes. The ^{31}P and ^{2}H NMR parameters were used to calculate possible conformations for the headgroup of 1,2-di-*O*-hexadecyl-*sn*-glycero-3-(2-aminoethyl)phosphonate. The solutions are similar in the liquid crystalline and hexagonal phases, indicating that no major headgroup conformational change is necessary for the lipid to undertake this phase transition.

The geometry adopted by the phosphonate headgroup appears to have the same overall features as that of DPPE, *i.e.* there is a bend at the phosphorus moiety and the rest of the headgroup is nearly parallel to the membrane surface.

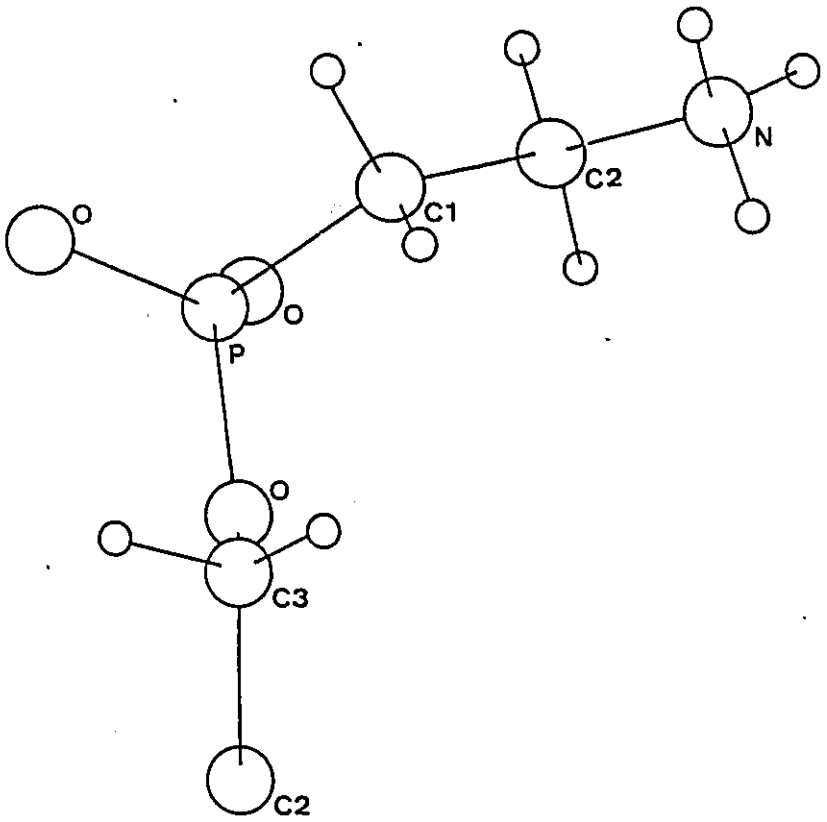

Figure 6–8. Representation of one of the possible headgroup conformations for 1,2-di-*O*-hexadecyl-*sn*-glycero-3-(2-aminoethyl)phosphonate in aqueous dispersions in the liquid crystalline phase (74°C), showing that the headgroup is nearly perpendicular to the C2−C3 bond of glycerol assumed to be parallel to the bilayer normal.

The fact that one less torsion angle has to be determined for the same number of spectral parameters results in a much narrower conformational space for the phosphonate than for the phosphate headgroup.

6.5 References

1. J. Seelig and H.-U. Gally, *Biochemistry* **15**, 5199–5204 (1976).
2. J. Seelig, H.-U. Gally and R. Wohlgemuth, *Biochim. Biophys. Acta* **467**, 109–119 (1977).
3. R. Skarjune and E. Oldfield, **18**, 5903–5909 (1979).
4. M. Rance and R.A. Byrd, *J. Magn. Reson.* **52**, 221–240 (1983).
5. J.H. Davis, K.R. Jeffrey, M. Bloom, M.I. Valic and T.P. Higgs, *Chem. Phys. Lett.* **42**, 390–394 (1976).
6. B. Perly, I.C.P. Smith and H.C. Jarrell, *Biochemistry* **24**, 1055–1063 (1985).
7. M. Bloom, J.H. Davis and L. Mackay, *Chem. Phys. Lett.* **80**, 198–202 (1981).
8. P.R. Cullis and B de Kruijff, *Biochim. Biophys. Acta* **559**, 399–420 (1979).
9. H.C. Jarrell, R.A. Byrd, R. Deslauriers, I. Ekiel and I.C.P. Smith, *Biochim. Biophys. Acta* **648**, 80–86 (1981).
10. J.M. Boggs, D. Stamp, D.W. Hughes and C.M. Deber, *Biochemistry* **20**, 5728–5735 (1981).
11. J.H. Davis, *Biochim. Biophys. Acta* **737**, 117–171 (1983).
12. I.C.P. Smith, *Biomembranes* **12**, 133–168 (1984).

13. H.W. Spiess, in *NMR Basic Principles and Progress*, edited by P. Diehl, E. Fluck and R. Kosfeld (Springer-Verlag, Berlin, 1978), pp. 55–214.

14. M.-R. Van Calsteren, G.I. Birnbaum and I.C.P. Smith, *J. Chem. Phys.* **86**, 5405–5410 (1987).

15. P.B. Hitchcock, R. Mason, K.M. Thomas and G.G. Shipley, *Proc. Natl. Acad. Sci. USA* **71**, 3036–3040 (1974).

16. M. Elder, P. Hitchcock, R. Mason and G.G. Shipley, *Proc. R. Soc. Lond. A* **354**, 157–170 (1977).

17. Y. Okaya, *Acta Crystallogr.* **20**, 712–715 (1966).

CHAPTER 7

CONCLUSIONS

The purpose of this chapter is not only to present the main conclusions of the thesis research, but also to make suggestions for more work in the area of nuclear magnetic resonance (NMR) of membranes in general, and of unusual lipids like phosphonolipids in particular. These future studies could be done at the level of the lipid organization in attempting to explain the phase behavior of natural lipids, from a more chemical physical point of view in the determination of chemical shielding tensors of better models for phosphonolipids, at an organic chemistry level in the synthesis of other phospho– and phosphonolipid analogs possibly with different chain and headgroup compositions labelled in different positions or with other isotopes, and finally from a structural and dynamic point of view in the determination of a picture of headgroup conformation and motions.

7.1 Phase behavior of *Tetrahymena thermophila* lipids

The total lipids of *Tetrahymena thermophila* showed a phase behavior quite different from that of the polar lipids, which is expected when ethanolamine-containing phospho– and phosphonolipids constitute the major molecular species. The polar lipids slowly undergo a phase transition from a lamellar to a hexagonal phase, while the total lipids are stabilized up to a higher temperature in the lamellar phase, before it is transformed into an isotropic phase. This phase showed

hysteresis and freeze-thawing was necessary to restore the bilayer structure. The exact nature of the isotropic phase is unknown, as are the factors responsible for its formation.

This kind of behavior has been shown to occur in other systems. For example, mixtures of soya phosphatidylethanolamine (PE) and egg phosphatidylcholine (PC) adopt either a hexagonal, an isotropic or a bilayer phase depending on relative proportions (1). The same behavior is found when PC is replaced by bovine brain sphingomyelin (SM). Mixtures of soya PE, bovine brain SM and cholesterol in various proportions are highly stabilized into the bilayer phase (2). Equimolar mixtures of polyunsaturated PC and cholesterol or various mixtures of polyunsaturated PC and PE show exactly the same phase behavior as the total lipids of *Tetrahymena*, *i.e.* transformation to an isotropic phase and hysteresis (3).

It would be interesting to study the phase behavior of the individual lipid components of *T. thermophila*, alone or in mixtures of known composition. The effect of the triterpene tetrahymanol as compared with that of cholesterol found in animal cell membranes is of particular interest. Also, the exact role of ceramide phospho- and phosphonolipids deserves attention. This type of study could put some insight into the understanding of how the different lipid components of membranes participate in maintaining the bilayer structure and thus the cell integrity, while still allowing for particular membrane functions such as fusion.

7.2 ^{31}P NMR chemical shielding tensor of phosphonates

The complete ^{31}P NMR chemical shift tensor was measured on a single crystal of 2-aminoethylphosphonic acid (AEP). AEP was chosen as a model for phosphonolipids because it is the constituent of their headgroup. It was found

that the tensor correlates well with the electron distribution around the phosphorus atom expected in the ground state of the molecule. However, phosphonolipids are esters of AEP. Whether this affects only the principal values or also the orientation of the principal axis system is not known. Attempts at the synthesis of a crystalline ester of AEP have been made, but without success, in order to provide a better model for phosphonolipid headgroups. The best model would of course be the phosphonolipid itself, but it would be difficult to obtain sufficiently large single crystals from it. The knowledge of the differences in the chemical shielding tensor between a phosphonic acid and its own ester would give indications on the electron density redistribution induced by esterification.

7.3 Chemical syntheses

In this work, relatively simple procedures have been developed to prepare phospho– and phosphonolipids selectively ^{2}H-labelled in almost any desired position of the molecule. It is well known that small changes in the chemical structure could have important effects on the organization and function of particular lipids. With some more effort, the chain and headgroup composition could be modified to prepare a whole family of analogs. The method is also suitable for labelling with other isotopes; introduction of ^{13}C is somewhat difficult to achieve selectively, but ^{15}N is a good candidate. The procedures described in Chapter 5 could be used to synthesize ^{15}N-labelled phospho– and phosphonolipids, since both [^{15}N]glycine – which can be reduced to [^{15}N]ethanolamine with lithium aluminum hydride – and $^{15}NH_3$ are available commercially.

7.4 Headgroup conformation

The headgroup conformation of a synthetic phosphonolipid was determined using a very simple model for headgroup reorientation. A recent study (4) suggests that this model is not completely adequate, but it was convenient for this particular study, because it allowed a direct comparison with previously determined conformations for analogous phospholipids. The synthesis of analogous phospho- and phosphonolipids with the same chain composition and with deuterium label at equivalent positions would make comparisons possible between the two species using any model.

A better model would take into account the dynamics of the lipid molecule, as determined by relaxation time measurements. For example, if T_1 is shorter for the C2 than for the C1 position of the headgroup, the model should allow for motion, possibly of limited amplitude, of the C1−C2 segment. Similarly, for the glycerol backbone, because of the nonequivalence of the two deuterium atoms on C3, the axis of motional averaging could not be exactly coincident with the C2−C3 bond. Based on the ^{2}H NMR lineshape and spin-lattice relaxation analysis of lipids labelled in the C2 and C3 positions of glycerol (4), the glycerol backbone dynamics can be described in terms of common fast internal motions and a slower whole molecule axial motion. In addition to rotation about the long axis of the molecule, a model involving a fast-limit three-site jump about the C2−C3 bond of the glycerol moiety was used to simulate lineshape and relaxation features in the gel state. Such a model could be used to simulate the ^{31}P and ^{2}H NMR parameters obtained for the headgroup of phospho- and phosphonolipids. It would probably narrow down the number of possible conformational solutions and give a better confidence into the determined headgroup conformation, without requiring unreasonable assumptions to be made.

The ultimate goal would of course be to obtain a picture of the conformation of the whole lipid molecule, together with the time dependence of this conformation, *i.e.* the motions of each individual segment, and the motion of the molecule as a whole and with respect to its neighbors. The larger the number of NMR parameters obtained for a particular lipid system, the better this goal could be achieved. For this, studies of lipids labelled in other positions or with other isotopes than deuterium would be required. ^{2}H NMR studies of the phosphonolipid labelled in the *sn*-1 and *sn*-2 positions are now in progress and will allow a more precise definition of the conformation of the glycerol backbone. An additional NMR parameter, the dipolar coupling between ^{2}H and ^{1}H or between ^{2}H and ^{2}H in the case of nonequivalent $C-^{2}H_{2}$ groups, could be measured and used in the calculations. The model of molecular motion described above could also be refined and extended with lineshape and relaxation data obtained for these positions. Finally, ^{15}N NMR could be used advantageously to narrow down the number of possible headgroup conformations by providing an additional NMR parameter at the very end of the headgroup (5).

The results presented in this thesis have not answered all the questions concerning the differences in the headgroup conformations of phospho- and phosphonolipids; they have only given an indication that, despite noticeable differences in the torsion angle ranges adopted by their headgroups, the overall spatial arrangement for the lipids of these two species are very similar. In fact, using a vast array of techniques, the only important difference found between the two molecular species is the added resistance to enzymatic and chemical degradation conferred to phosphonolipids by the presence of the carbon-phosphorus bond.

Finally, the more is known about a particular system, the more there is still to know, since new questions arise during the course of the studies, and the

greater the level of complexity that could be investigated. The complexity of life and of the universe probably has no limits and there will always be something to investigate further. This statement makes science even more attractive.

7.5 References

1. P.R. Cullis and B. de Kruijff, *Biochim. Biophys. Acta* **507**, 207–218 (1978).

2. P.R. Cullis and M.J. Hope, *Biochim. Biophys. Acta* **597**, 533–542 (1980).

3. C.J. Dekker, W.S.M. Geurts van Kessel, J.P.G. Klomp, J. Pieters and B. de Kruijff, *Chem. Phys. Lipids* **33**, 93–106 (1983).

4. M. Auger, M.-R. Van Calsteren, I.C.P. Smith and H.C. Jarrell, *Biochemistry*, **29**, 5815–5821 (1990).

5. S. Akoka, C. Tellier and S. Poignant, *Biochemistry* **25**, 6972–6977 (1986).

APPENDIX A

^{13}C NUCLEAR MAGNETIC RESONANCE DATA OF SYNTHETIC COMPOUNDS

A.1 Explanation of the tables

Tables A–1 to A–10 report the ^{13}C NMR chemical shifts of the compounds whose synthesis is described in Chapter 5, expressed in ppm downfield from tetramethylsilane (TMS), either external when the solvent is $^{2}H_2O$ or internal with all other solvents. Multiplicities were determined either from nondecoupled spectra, using the attached proton test (APT) (1) or the distortionless enhancement by polarization transfer (DEPT) pulse sequences (2). They are reported with P for primary, S for secondary, T for ternary and Q for quaternary carbons. For aromatic rings, the symbol ϕ is used, together with *i* for *ipso*, *o* for *ortho*, *m* for *meta*, and *p* for *para* carbons. Primed numbers represent chains substituted on carbons 1 and 6 of mannitol or on carbon 1 of glycerol. Similarly, double primed numbers are used for chains on carbons 2 and 5 of mannitol or on carbon 2 of glycerol. Triple primed numbers designate the headgroup carbons positioned on carbon 3 of glycerol.

Peaks were assigned to particular carbons using the following considerations: relative intensity, multiplicity, coupling to other nuclei, disappearance of a carbon due to deuteration, and isotope shift. In addition, lipid chains were assigned according to Batchelor *et al.* (3), whereas Bremser *et al.* (4)

Table A–1. 75.5-MHz ^{13}C NMR chemical shifts in ppm of compounds **2a**, **2b**, **3**, **4**, **5** and **6**.

Carbon	**2a** C^2HCl_3	**2b** C^2HCl_3	**3** C^2HCl_3	**4** C^2HCl_3	**5** DMSO-d_6	**6** ^2H_2O
CH_2-O	62.58 S	–	61.21			
CH_2-Br				28.21		
CH_2-P					26.69 (132.)[a]	26.11 (132.)
CH_2-N	43.16 S	–	40.90	39.28	32.61	35.53
C=O	156.86 Q	156.86 Q				
$C(-CH_3)_3$	79.66 Q	79.65 Q				
CH_3	28.38 P	28.39 P				
C=O			168.89	167.85	167.46	
ϕ_i			132.00	131.81	131.68	
ϕ_o			123.46	123.53	122.88	
ϕ_m			134.20	134.27	134.20	

[a] $^1J_{C-P}$ values in Hertz are given in parentheses.

Table A–2. 75.5-MHz ^{13}C NMR chemical shifts in ppm of compounds **7a**, **7b**, **8a**, **8b**, **9a**, **9b** and **10a**.

Carbon	**7a** C^2HCl_3	**7b** C^2HCl_3	**8a** C^2HCl_3	**8b** C^2HCl_3	**9a** ^2H_2O	**9b** ^2H_2O	**10a** ^2H_2O
C–1	29.57 S	28.83 Q (24.)[b]	30.82 (134.)[a]	30.03 (132.) (20.)	32.94 (127.)	–	31.51 (127.)
C–2	29.57 S	28.83 Q (24.)	23.85	23.30 (24.)	26.79	–	25.11
CH_2			62.04 (7.)	62.01 (7.)			
CH_3			16.45 (7.)	16.44 (5.)			
ϕ_i					128.97	129.03	
ϕ_o					122.76	122.79	
$\phi_m + \phi_p$					130.13	130.17	

[a] J_{C-P} values in Hertz are given in parentheses in normal script.

[b] $^1J_{C-^2H}$ values in Hertz are given in parentheses in italic script.

Table A–3. 75.5-MHz ^{13}C NMR chemical shifts in ppm of compounds **11a**, **11b**, **12a**, **13a**, **13b** and **13c** in C^2HCl_3.

Carbon	**11a**	**11b**	**12a**	**13a**	**13b**	**13c**
C–1	179.70	180.11 Q	63.09	70.15	70.08	–
C–2	33.97	–	32.87			
C–3	24.72	24.56 S	25.79	25.46	25.56	25.40
C–14	31.90	31.94 S	31.97	31.94	31.90	31.94
C–15	22.71	22.71 S	22.75	22.71	22.71	22.71
C–16	14.11	14.14 P	14.14	14.11	14.11	14.14
CH_3				37.44	37.40	37.40

Table A–4. 75.5-MHz ^{13}C NMR chemical shifts in ppm of compounds **14**, **16a**, **16b** and **16c** in ^2H_2O.

Carbon	**14**	**16a**	**16b**	**16c**
C–1	175.30	63.22 S	63.30 S	–
C–2	69.37	70.86 T	–	70.98
C–3	76.46	69.24 T	69.42 T	69.50
C–4	76.46	69.24 T	69.48 T	69.50
C–5	69.37	70.86 T	71.05 T	70.98
C–6	175.30	63.22 S	63.38 S	–

Table A–5. 75.5-MHz ^{13}C NMR chemical shifts in ppm of compounds **19a**, **21a**, **21b** and **24** in C^2HCl_3.

Carbon	**19a**	**21a**	**21b**	**24**
C–1	65.84 S (148.)[a]	65.16	65.16[b]	64.36
C–2	76.30 T (147.)	70.28	70.28	70.44
C–3	62.86 S (143.)	63.35	63.35[b]	72.54
$C(-CH_3)_2$	109.40 Q			
CH_3 *cis*[c]	26.68 P (127.)			
CH_3 *trans*[c]	25.26 P (127.)			
C–1'		174.40	174.36	71.89
C–2'		34.20	34.17	
C–3'		24.95	24.91	26.11
C–14'		31.94	31.94	31.94
C–15'		22.71	22.71	22.71
C–16'		14.14	14.14	14.11

[a] $^1J_{C-H}$ values in Hertz are given in parentheses.

[b] Assigned as if it were 3-*O*-palmitoyl-*sn*-glycerol **21a**.

[c] Assigned according to References 5 and 6.

Table A-6. 75.5-MHz ^{13}C NMR chemical shifts in ppm of compounds **26a**, **26b**, **26c**, **27a**, **27b** and **27c**.

Carbon	**26a** C^2HCl_3	**26b** C^2HCl_3	**26c** C^2HCl_3	**27a** ^2H_2O	**27b** ^2H_2O	**27c** ^2H_2O
C-1	66.33 S	66.20 S	-	62.80 S	62.51 S	-
C-2	76.39 T	-	76.24 T	72.51 T	-	72.18
C-3	79.50 T	79.38 T	79.42 T	78.92 T	78.62 T	78.67
C-4	79.50 T	79.38 T	79.42 T	78.92 T	78.62 T	78.67
C-5	76.39 T	76.38 T	76.24 T	72.51 T	72.31 T	72.18
C-6	66.33 S	66.31 S	-	62.80 S	62.61 S	-
$C(-CH_3)_2$ 3,4	110.17 Q	110.19 Q	110.15 Q	110.66 Q	110.53 Q	110.51
CH_3 *cis* + *trans*	27.50 P	27.49 P	27.45 P	26.40 P	26.24 P	26.23
$C(-CH_3)_2$ 1,2:5,6	109.59 Q	109.59 Q	109.56 Q			
CH_3 *cis*[a]	26.53 P	26.53 P	26.52 P			
CH_3 *trans*[a]	25.37 P	25.35 P	25.34 P			

[a] Assigned according to References 5 and 6.

Table A–7. 75.5-MHz ^{13}C NMR chemical shifts in ppm of compounds **28a**, **28b**, **30a** and **30b** in C^2HCl_3.

Carbon	**28a**	**28b**	**30a**	**30b**
C–1	65.23 S	65.10 S	61.26 S	61.17 S
C–2	72.41 T	–	79.91 T	–
C–3	79.92 T	79.85 T	79.00 T	78.77 T
C–4	79.92 T	79.85 T	79.00 T	78.77 T
C–5	72.41 T	72.38 T	79.91 T	79.94 T
C–6	65.23 S	65.20 S	61.26 S	61.17 S
$C(-CH_3)_2$	109.30 Q	109.10 Q	109.99 Q	109.94 Q
CH_3	26.89 P	26.89 P	27.17 P	27.15 P
$C(-\phi)_3$	86.87 Q	86.84 Q		
ϕ_i	143.92 Q	143.92 Q		
ϕ_o	127.84 T[a]	127.80 T[a]		
ϕ_m	128.74 T[a]	128.71 T[a]		
ϕ_p	127.03 T	127.03 T		
$CH_2-\phi$			72.38 S	72.34 S
ϕ_i			137.76 Q	137.78 Q
ϕ_o			128.55 T	128.74 T
ϕ_m			127.92 T[a]	128.00 T
ϕ_p			127.98 T[a]	128.00 T

[a] Assignments in the same column may be reversed.

Table A–8. 75.5-MHz ^{13}C NMR chemical shifts in ppm of compounds **32a**, **32b**, **32c**, **37a**, **37b**, **37c** and **37d** in C^2HCl_3.

Carbon	**32a**	**32b**	**32c**	**37a**	**37b**	**37c**	**37d**
C–1	62.89 S	62.81 S	62.86	71.05 S	71.07 S	70.92 S	71.00
C–2	78.17 T	78.08 T	–	78.96 T	78.97 T	78.93 T	–
C–3	68.84 T	68.75 T	68.82	70.26 T	70.29 T	70.24 T	70.19
C–4	68.84 T	68.75 T	68.82	70.26 T	70.29 T	70.24 T	70.19
C–5	78.17 T	78.08 T	78.14	78.96 T	78.97 T	78.93 T	78.90
C–6	62.89 S	62.81 S	62.86	71.05 S	71.07 S	70.92 S	71.00
$CH_2-\phi$	72.88 S	72.84 S	72.89	73.04 S	73.03 S	73.03 S	73.01
ϕ_i	137.74 Q	137.71 Q	137.74	138.34 Q	138.38 Q	138.33 Q	138.31
ϕ_o	128.53 T	128.53 T	128.57	128.37 T	128.37 T	128.39 T	128.38
ϕ_m	128.05 T	128.05 T	128.08	127.95 T	127.93 T	127.98 T	127.95
ϕ_p	128.05 T	128.05 T	128.08	127.71 T	127.69 T	127.74 T	127.70
C–1'	173.98 Q	174.05 Q	174.06	71.86 S	71.76 S	–	71.86
C–2'	34.28 S	–	34.31				
C–3'	24.98 S	24.81 S	25.00	26.14 S	25.93 S	26.08 S	26.12
C–14'	31.95 S	31.92 S	31.97	31.95 S	31.94 S	31.94 S	31.92
C–15'	22.71 S	22.71 S	22.75	22.71 S	22.70 S	22.70 S	22.69
C–16'	14.12 P	14.13 P	14.17	14.14 P	14.12 P	14.12 P	14.11

Table A–9. ^{13}C NMR chemical shifts in ppm of compounds **34**, **35**, **39** and **40**.

Carbon	**34**	**35**	**39**	**40**
	90.6 MHz	75.5 MHz	75.5 MHz	90.6 MHz
	C^2HCl_3	$C^2HCl_3 - C^2H_3O^2H$	C^2HCl_3	$C^2HCl_3 - C^2H_3O^2H$
C–1	62.88 S[a]	63.57 S	71.17	70.55 S
C–2	77.36 T	76.20 T (7.)[b]	77.96	77.74 T (6.)
C–3	61.95 S[a]	63.30 S (1.)	63.08	64.28 S (1.)
CH_2-	72.15 S	72.34 S	72.15	72.68 S
ϕ_i	137.98 Q	137.66 Q	138.42	–
ϕ_o	128.49 T	128.52 T	128.47	128.73 T
ϕ_m	127.85 T	127.98 T	127.43	128.28 T
ϕ_p	127.85 T	127.98 T	127.43	128.15 T
C–1'	173.81 Q	174.18 Q	71.91	72.23 S
C–2'	34.21 S	34.29 S		
C–3'	24.94 S	24.98 S	26.17	26.47 S
C–14'	31.95 S	32.01 S	31.96	32.28 S
C–15'	22.70 S	22.77 S	22.73	23.03 S
C–16'	14.13 P	14.15 P	14.12	14.23 P
C–1'''		32.20 S (129.)		32.60 S (131.)
C–2'''		27.03 S		27.26 S

[a] Assignments in the same column may be reversed.

[b] J_{C-P} values in Hertz are given in parentheses.

Table A–10. ^{13}C NMR chemical shifts in ppm of compounds **42a**, **42b**, **42c**, **44a**, **44b**, **44c** and **44d** in C^2HCl_3.

Carbon	**42a**	**42b**	**42c**	**44a**	**44b**	**44c**	**44d**
	75.5 MHz	75.5 MHz	75.5 MHz	90.6 MHz	75.5 MHz	75.5 MHz	75.5 MHz
C–1	70.84 S	70.77 S	–	70.93 S	70.89 S 70.96 S	–	70.94 S 70.99 S
C–2	79.75 T	–	79.62 T	78.26 T	78.27 T	78.13 T	78.22 T
C–3	70.18 T	70.13 T	70.17 T	63.13 S	63.09 S 63.15 S	63.12 S	62.79 T[a]
C–4	70.18 T	70.18 T	70.17 T				
C–5	79.75 T	79.75 T	79.62 T				
C–6	70.84 S	70.83 S	–				
C–1'	71.84 S	71.85 S	71.78 S	71.88 S	71.89 S	71.82 S	71.89 S
C–3'	26.15 S	26.15 S	26.15 S	26.13 S	26.13 S	26.12 S	26.13 S
C–14'	31.95 S	31.95 S	31.95 S	31.95 S	31.95 S	31.95 S	31.95 S
C–15'	22.71 S	22.71 S	22.71 S	22.72 S	22.71 S	22.70 S	22.71 S
C–16'	14.12 P	14.13 P	14.13 P	14.15 P	14.13 P	14.13 P	14.13 P
C–1"	71.39 S	71.35 S 71.39 S	71.38 S	70.42 S	70.39 S 70.43 S	70.41 S	70.43 S
C–2"	30.13 S	30.13 S	30.13 S	30.10 S	30.11 S	30.11 S	30.11 S
C–3"	26.23 S	26.23 S	26.15 S	26.13 S	26.13 S	26.12 S	26.23 S
C–14"	31.95 S	31.95 S	31.95 S	31.95 S	31.95 S	31.95 S	31.95 S
C–15"	22.71 S	22.71 S	22.71 S	22.72 S	22.71 S	22.70 S	22.71 S
C–16"	14.12 P	14.13 P	14.13 P	14.15 P	14.13 P	14.13 P	14.13 P

[a] Triplet due to coupling to ^2H.

was used as a general reference. Carbons of lipid chains which occur between 29 and 30 ppm, *i.e.* those of carbons 4 to 13 and in some cases carbon 2 of alkyl chains, are not reported in the tables because of partial overlap and difficulties in assigning the individual lines properly.

A.2 References

1. S.L. Patt and J.N. Shoolery, *J. Magn. Reson.* **46**, 535–539 (1982).

2. D.M. Doddrell, D.T. Pegg and M.R. Bendall, *J. Magn. Reson.* **48**, 323–327 (1982).

3. J.G. Batchelor, R.J. Cushley and J.H. Prestegard, *J. Org. Chem.* **39**, 1698–1705 (1974).

4. W. Bremser, B. Franke and H. Wagner, in *Chemical Shift Ranges in Carbon–13 NMR Spectroscopy*, edited by H.F. Ebel (Verlag Chemie, Weinheim, 1982).

5. Y. Senda, J. Ishiyama and S. Imaizumi, *Bull. Chem. Soc. Japan* **50**, 2813–2814 (1977).

6. J.G. Buchanan, A.R. Edgar, D.I. Rawson, P. Shahidi and R.H. Wightman, *Carbohydr. Res.* **100**, 75–86 (1982).